CURRENT STATE AND FUTURE DIRECTIONS OF CRANIAL FOCUSED ULTRASOUND THERAPY

EDITED BY: Vibhor Krishna, Francesco Sammartino, J. Levi Chazen and Aristide Merola

PUBLISHED IN: Frontiers in Neurology

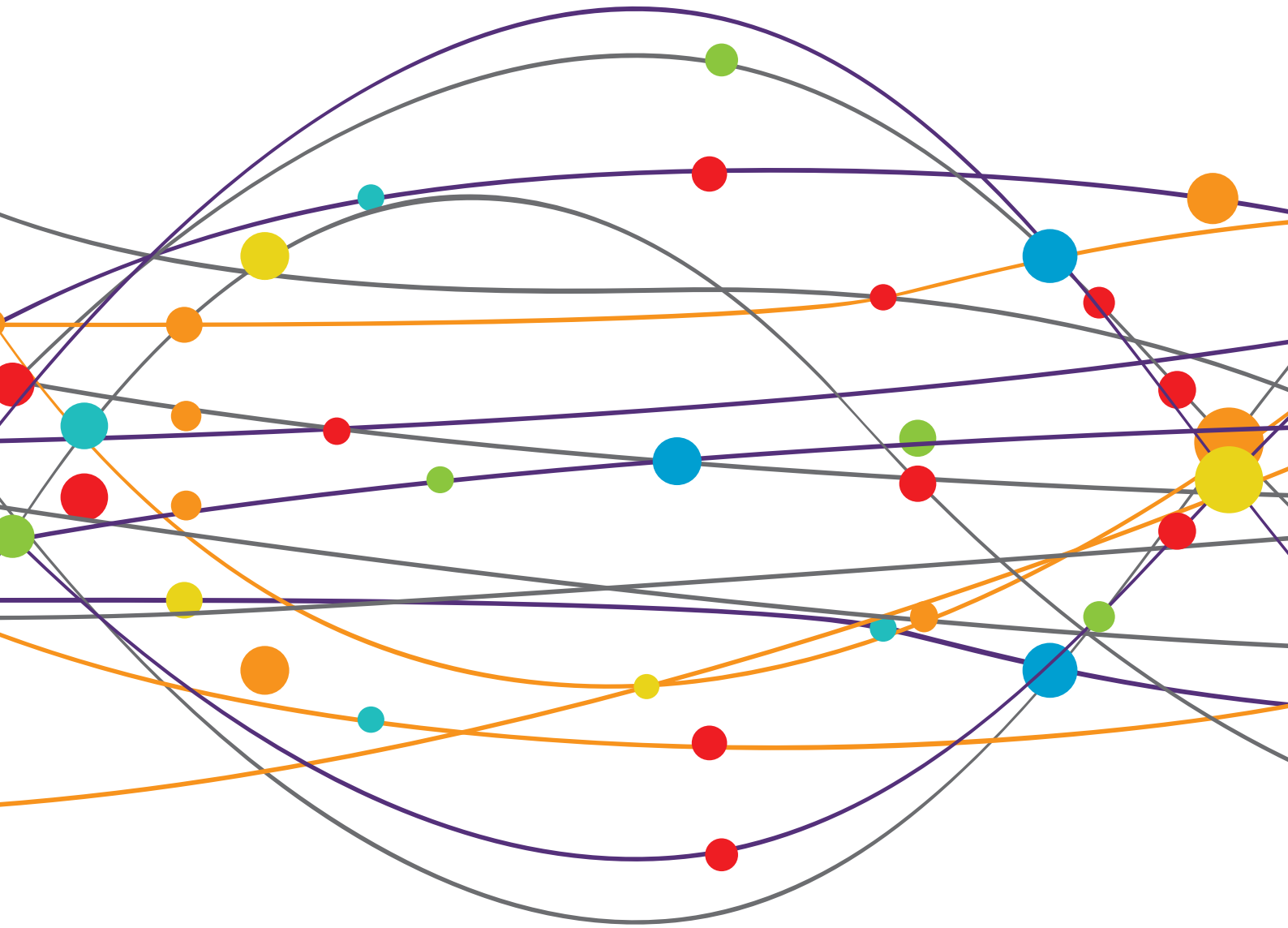

frontiers Research Topics

frontiers

ISSN 1664-8714
ISBN 978-2-83250-828-2
DOI 10.3389/978-2-83250-828-2

About Frontiers

Frontiers is more than just an open-access publisher of scholarly articles: it is a pioneering approach to the world of academia, radically improving the way scholarly research is managed. The grand vision of Frontiers is a world where all people have an equal opportunity to seek, share and generate knowledge. Frontiers provides immediate and permanent online open access to all its publications, but this alone is not enough to realize our grand goals.

Frontiers Journal Series

The Frontiers Journal Series is a multi-tier and interdisciplinary set of open-access, online journals, promising a paradigm shift from the current review, selection and dissemination processes in academic publishing. All Frontiers journals are driven by researchers for researchers; therefore, they constitute a service to the scholarly community. At the same time, the Frontiers Journal Series operates on a revolutionary invention, the tiered publishing system, initially addressing specific communities of scholars, and gradually climbing up to broader public understanding, thus serving the interests of the lay society, too.

Dedication to Quality

Each Frontiers article is a landmark of the highest quality, thanks to genuinely collaborative interactions between authors and review editors, who include some of the world's best academicians. Research must be certified by peers before entering a stream of knowledge that may eventually reach the public - and shape society; therefore, Frontiers only applies the most rigorous and unbiased reviews.
Frontiers revolutionizes research publishing by freely delivering the most outstanding research, evaluated with no bias from both the academic and social point of view. By applying the most advanced information technologies, Frontiers is catapulting scholarly publishing into a new generation.

What are Frontiers Research Topics?

Frontiers Research Topics are very popular trademarks of the Frontiers Journals Series: they are collections of at least ten articles, all centered on a particular subject. With their unique mix of varied contributions from Original Research to Review Articles, Frontiers Research Topics unify the most influential researchers, the latest key findings and historical advances in a hot research area! Find out more on how to host your own Frontiers Research Topic or contribute to one as an author by contacting the Frontiers Editorial Office: frontiersin.org/about/contact

CURRENT STATE AND FUTURE DIRECTIONS OF CRANIAL FOCUSED ULTRASOUND THERAPY

Topic Editors:
Vibhor Krishna, The Ohio State University, United States
Francesco Sammartino, The Ohio State University, United States
J. Levi Chazen, Hospital for Special Surgery, United States
Aristide Merola, The Ohio State University, United States

Topic Editors Vibhor Krishna and J. Levi Chazen have received grants for research purposes from Insightec Inc. The other Topic Editors declare no competing interests with regard to the Research Topic subject.

Citation: Krishna, V., Sammartino, F., Chazen, J. L., Merola, A., eds. (2022). Current State and Future Directions of Cranial Focused Ultrasound Therapy. Lausanne: Frontiers Media SA. doi: 10.3389/978-2-83250-828-2

Table of Contents

04 ***Editorial: Current State and Future Directions of Cranial Focused Ultrasound Therapy***
J. L. Chazen, Francesco Sammartino and Vibhor Krishna

07 ***Outcome and Complications of MR Guided Focused Ultrasound for Essential Tremor: A Systematic Review and Meta-Analysis***
Mohit Agrawal, Kanwaljeet Garg, Raghu Samala, Roopa Rajan, Vikas Naik and Manmohan Singh

24 ***MRI Guided Focused Ultrasound-Mediated Delivery of Therapeutic Cells to the Brain: A Review of the State-of-the-Art Methodology and Future Applications***
Nabid Ahmed, Dheeraj Gandhi, Elias R. Melhem and Victor Frenkel

40 ***Peripheral Nerve Focused Ultrasound Lesioning—Visualization and Assessment Using Diffusion Weighted Imaging***
Matthew R. Walker, Jidan Zhong, Adam C. Waspe, Karolina Piorkowska, Lananh N. Nguyen, Dimitri J. Anastakis, James M. Drake and Mojgan Hodaie

52 ***Focused Ultrasound Mediated Opening of the Blood-Brain Barrier for Neurodegenerative Diseases***
Paul S. Fishman and Johnathan M. Fischell

57 ***Resting State Functional Connectivity Signatures of MRgFUS Vim Thalamotomy in Parkinson's Disease: A Preliminary Study***
Mario Stanziano, Nico Golfrè Andreasi, Giuseppe Messina, Sara Rinaldo, Sara Palermo, Mattia Verri, Greta Demichelis, Jean Paul Medina, Francesco Ghielmetti, Salvatore Bonvegna, Anna Nigri, Giulia Frazzetta, Ludovico D'Incerti, Giovanni Tringali, Francesco DiMeco, Roberto Eleopra and Maria Grazia Bruzzone

74 ***Technical Comparison of Treatment Efficiency of Magnetic Resonance-Guided Focused Ultrasound Thalamotomy and Pallidotomy in Skull Density Ratio-Matched Patient Cohorts***
Abdul-Kareem Ahmed, Sijia Guo, Nathaniel Kelm, Ryan Clanton, Elias R. Melhem, Rao P. Gullapalli, Alexander Ksendzovsky, Howard M. Eisenberg, Timothy R. Miller and Dheeraj Gandhi

82 ***Magnetic Resonance Image Guided Focused Ultrasound Thalamotomy. A Single Center Experience With 160 Procedures***
Asad M. Lak, David J. Segar, Nathan McDannold, Phillip Jason White and Garth Rees Cosgrove

89 ***Somatotopic Organization of Hyperdirect Pathway Projections From the Primary Motor Cortex in the Human Brain***
Sonia Pujol, Ryan P. Cabeen, Jérôme Yelnik, Chantal François, Sara Fernandez Vidal, Carine Karachi, Eric Bardinet, G. Rees Cosgrove and Ron Kikinis

100 ***Low-intensity Transcranial Ultrasound Stimulation Facilitates Hand Motor Function and Cortical Excitability: A Crossover, Randomized, Double Blind Study***
Meng-Fei Zhang, Wei-Zhou Chen, Fub-Biao Huang, Zhi-Yong Peng, Ying-Chan Quan and Zhi-Ming Tang

frontiers | Frontiers in Neurology

TYPE Editorial
PUBLISHED 18 July 2022
DOI 10.3389/fneur.2022.946634

OPEN ACCESS

EDITED AND REVIEWED BY
Leonard Verhagen Metman,
Rush University, United States

*CORRESPONDENCE
J. L. Chazen
chazenjl@hss.edu

SPECIALTY SECTION
This article was submitted to Experimental Therapeutics, a section of the journal Frontiers in Neurology

RECEIVED 17 May 2022
ACCEPTED 01 July 2022
PUBLISHED 18 July 2022

CITATION
Chazen JL, Sammartino F and Krishna V (2022) Editorial: Current state and future directions of cranial focused ultrasound therapy. *Front. Neurol.* 13:946634. doi: 10.3389/fneur.2022.946634

Editorial: Current state and future directions of cranial focused ultrasound therapy

J. L. Chazen[1]*, Francesco Sammartino[2] and Vibhor Krishna[3]

[1]Department of Radiology, Hospital for Special Surgery, New York, NY, United States, [2]Department of Neurosurgery, The Ohio State University, Columbus, OH, United States, [3]Department of Neurosurgery, University of North Carolina, Chapel Hill, NC, United States

KEYWORDS

MRgFUS, focused ultrasound (MRgFUS), HIFU, magnetic resonance-guided focused ultrasound surgery (MRgFUS), focused ultrasound (FUS)

Editorial on the Research Topic
Current State and Future Directions of Cranial Focused Ultrasound Therapy

Transcranial focused ultrasound (FUS) is a transformative technology to treat neurological and psychiatric disorders. Following pre-clinical development for decades, FUS ablation received FDA approval for essential tremor (ET) treatment in July 2016 (1). The field has undergone rapid development with innovations in image guidance (2, 3), technique optimization (4), and expansion of target selection beyond the thalamus (5–7). In addition to cranial ablation, focused ultrasound can transiently open the transient blood-brain barrier (BBB) in targeted locations and is being actively tested for applications in Alzheimer's disease and brain tumors for targeted drug delivery (8–10).

The current collection of articles highlights the recent innovations in clinical and investigational applications of FUS. Walker et al. discuss the application of DWI and diffusion tractography to visualize the sciatic nerve in piglets They demonstrate reliable sciatic nerve visualization and disruption following MRgFUS ablation in an animal model with histopathologic correlation. This research expands the reach of MRgFUS ablation to the peripheral nervous system and may lead to clinical applications for pain relief with durable nerve conduction blocks (11, 12).

Ahmed A-K et al. explore the impact of ablation location (thalamotomy vs. pallidotomy) on treatment efficiency in a cohort of 40 patients with matched skull density ratios (SDR). Acoustic and thermal simulations were performed at each target, and the findings confirm that globus pallidus interna ablation, located further from the geometric center of the skull, was associated with a higher energy requirement when compared with thalamic ablation. This data has important implications for patient selection for pallidotomy and other off-center ablation targets.

Ahmed N et al. present a thorough review of MRgFUS applications for therapeutic cell delivery in the brain through BBB opening techniques. The authors review the existing methodology of intracerebral cell delivery, including vascular, intrathecal, and stereotactic delivery techniques. Current and future potential for clinical translation

is reviewed with applications in neurodegenerative disease, malignancy, autoimmune disorders, and stroke therapy.

Stanziano et al. present data on the resting-state functional MRI connectome in patients with tremor-dominant Parkinson's disease undergoing FUS thalamotomy. Baseline, 1-month, and 3-month connectome data were evaluated for differences in connectivity using a comparative region of interest analysis. The results shed light on changes in functional connectivity between primary motor cortices, supplementary motor cortices, cingulate cortex, and lobe VI of the cerebellar hemispheres. In addition, correlative changes in functional connectivity were observed to a different extent in patients who had a positive clinical response.

Pujol et al. present DTI tractography parcellation of the hyperdirect pathway projections from the M1 cortex and reveals a somatotopic organization by the trunk, arm, hand, face, and tongue. This study analyzed the Human Connectome Project data and should have important implications for patient-specific tractography. By defining patient-specific somatotopy, practitioners could better define ablation targets and avoid off-target effects from FUS ablation.

Agrawal et al. present a systemic review and meta-analysis pooling results from 29 studies of the clinical outcomes and complications of MRgFUS ventral intermediate (Vim) thalamic nucleus ablation for ET patients. Importantly, the analysis revealed a statistically significant reduction in postprocedural ataxia when DTI-based targeted was employed. This review not only supports robust clinical outcomes from Vim ablation in ET patients but reinforces the benefits of diffusion tractography in target selection.

Fishman and Fischell present a review of existing and future techniques for BBB opening to treat neurodegenerative disease. Pre-clinical studies on the delivery of growth factors, antibodies, viral vectors, and nanoparticles into the brain with targeted BBB opening are reviewed. Safety data on the BBB opening technique is presented with a thoughtful reflection on future directions.

Lak et al. present a single-center experience with 160 thalamic FUS ablations in patients with ET or tremor-dominant Parkinson's disease, the largest experience published thus far. They report MRgFUS thalamotomy is a safe and effective procedure with a mean 78% tremor reduction at 2 years. In addition, the most observed side effects at 2 years were imbalance followed by sensory disturbance. This data further bolsters existing literature on the safety and efficacy of MRgFUS thalamotomy.

We anticipate this collection will be of great interest to seasoned and new practitioners of cranial MRgFUS. The field has undergone rapid innovation with exciting future horizons.

Author contributions

JC, FS, and VK: manuscript preparation and editing. All authors contributed to the article and approved the submitted version.

Conflict of interest

The authors declare that the research was conducted in the absence of any commercial or financial relationships that could be construed as a potential conflict of interest.

Publisher's note

References

1. Elias WJ, Lipsman N, Ondo WG, Ghanouni P, Kim YG, Lee W, et al. A randomized trial of focused ultrasound thalamotomy for essential tremor. *N Engl J Med*. (2016) 375:730–9. doi: 10.1056/NEJMoa1600159

2. Chazen JL, Sarva H, Stieg PE, Min RJ, Ballon DJ, Pryor KO, et al. Clinical improvement associated with targeted interruption of the cerebellothalamic tract following MR-guided focused ultrasound for essential tremor. *J Neurosurg*. (2018) 129:315–23. doi: 10.3171/2017.4.JNS162803

3. Krishna V, Sammartino F, Agrawal P, Changizi BK, Bourekas E, Knopp MV, et al. Prospective tractography-based targeting for improved safety of focused ultrasound thalamotomy. *Neurosurgery*. (2019) 84:160–8. doi: 10.1093/neuros/nyy020

4. Sammartino F, Snell J, Eames M, Krishna V. Thermal neuromodulation with focused ultrasound: implications for the technique of subthreshold testing. *Neurosurgery*. (2021) 89:610–6. doi: 10.1093/neuros/nyab238

5. Gallay MN, Moser D, Rossi F, Magara AE, Strasser M, Bühler R, et al. MRgFUS pallidothalamic tractotomy for chronic therapy-resistant Parkinson's disease in 51 Consecutive patients: single center experience. *Front Surg*. (2019) 6:76. doi: 10.3389/fsurg.2019.00076

6. Eisenberg HM, Krishna V, Elias WJ, Cosgrove GR, Gandhi D, Aldrich CE, et al. MR-guided focused ultrasound pallidotomy for Parkinson's disease: safety and feasibility. *J Neurosurg*. (2020) 135:1–7. doi: 10.3171/2020.6.JNS192773

7. Martinez-Fernandez R, Manez-Miro JU, Rodriguez-Rojas R, Del Álamo M, Shah BB, Hernández-Fernández F, et al. randomized trial of focused ultrasound subthalamotomy for Parkinson's disease. *N Engl J Med*. (2020) 383:2501–13. doi: 10.1056/NEJMoa2016311

8. Rezai AR, Ranjan M, D'Haese PF, Haut MW, Carpenter J, Najib U, et al. Noninvasive hippocampal blood-brain barrier opening in Alzheimer's

disease with focused ultrasound. *Proc Natl Acad Sci USA*. (2020) 117:9180–2. doi: 10.1073/pnas.2002571117

9. Lipsman N, Meng Y, Bethune AJ, Huang Y, Lam B, Masellis M, et al. Blood–brain barrier opening in Alzheimer's disease using MR-guided focused ultrasound. *Nat Commun*. (2018) 9:2336. doi: 10.1038/s41467-018-04529-6

10. Mainprize T, Lipsman N, Huang Y, Meng Y, Bethune A, Ironside S, et al. Blood-brain barrier opening in primary brain tumors with non-invasive MR-guided focused ultrasound: a clinical safety and feasibility study. *Sci Rep*. (2019) 9:321. doi: 10.1038/s41598-018-36340-0

11. Foley JL, Little JW, Vaezy S. Image-guided high-intensity focused ultrasound for conduction block of peripheral nerves. *Ann Biomed Eng*. (2007) 35:109–19. doi: 10.1007/s10439-006-9162-0

12. Choi EJ, Choi YM, Jang EJ, Kim JY, Kim TK, Kim KH. Neural ablation and regeneration in pain practice. *Korean J Pain*. (2016) 29:3–11. doi: 10.3344/kjp.2016.29.1.3

frontiers in Neurology

SYSTEMATIC REVIEW
published: 07 May 2021
doi: 10.3389/fneur.2021.654711

Outcome and Complications of MR Guided Focused Ultrasound for Essential Tremor: A Systematic Review and Meta-Analysis

Mohit Agrawal[1†], *Kanwaljeet Garg*[2*†], *Raghu Samala*[2], *Roopa Rajan*[3], *Vikas Naik*[4] *and Manmohan Singh*[2]

[1] Department of Neurosurgery, All India Institute of Medical Sciences, Jodhpur, India, [2] Department of Neurosurgery, All India Institute of Medical Sciences, New Delhi, India, [3] Department of Neurology, All India Institute of Medical Sciences, New Delhi, India, [4] Department of Neurosurgery, Bangalore Medical College, Bangalore, India

OPEN ACCESS

Edited by:
Vibhor Krishna,
The Ohio State University,
United States

Reviewed by:
Bhavya Shah,
University of Texas Southwestern Medical Center, United States
Jin Woo Chang,
Yonsei University Health System, South Korea
Dheeraj Gandhi,
University of Maryland, United States

***Correspondence:**
Kanwaljeet Garg
kanwaljeet84@gmail.com

[†] *These authors have contributed equally to this work*

Specialty section:
This article was submitted to Experimental Therapeutics, a section of the journal Frontiers in Neurology

Received: *21 January 2021*
Accepted: *12 April 2021*
Published: *07 May 2021*

Citation:
Agrawal M, Garg K, Samala R, Rajan R, Naik V and Singh M (2021) Outcome and Complications of MR Guided Focused Ultrasound for Essential Tremor: A Systematic Review and Meta-Analysis. Front. Neurol. 12:654711. doi: 10.3389/fneur.2021.654711

Background: Magnetic resonance guided focused ultrasound (MRgFUS) is a relatively novel technique to treat essential tremor (ET). The objective of this review was to analyze the efficacy and the safety profile of MRgFUS for ET.

Methods: A systematic literature review was done. The post procedure changes in the Clinical Rating Scale for Tremor (CRST) score, hand score, disability and quality of life scores were analyzed.

Results: We found 29 studies evaluating 617 patients. DTI based targeting was utilized in six cohorts. A significant difference was observed in the pooled standard mean difference between the pre and postoperative total CRST score (p-value < 0.001 and 0.0002), hand score (p-value 0.03 and 0.02); and the disability at 12 months (p-value 0.01). Head pain and dizziness were the most in procedure complications. The immediate pooled proportion of ataxia was 50%, while it was 20% for sensory complications, which, respectively, declined to 31 and 13% on long term follow up. A significant reduction ($p = 0.03$) in immediate ataxia related complications was seen with DTI targeting.

Conclusion: MRgFUS for ET seems to be an effective procedure for relieving unilateral tremor. Use of DTI based targeting revealed a significant reduction in post procedure ataxia related complications as compared to traditional targeting techniques. Analysis of other complications further revealed a decreasing trend on follow up.

Keywords: cerebellothalamic tract, diffusion tensor imaging, essential tremor, magnetic resonance guided focused ultrasound, targeting technique comparison, ventral intermediate nucleus

INTRODUCTION

Essential tremor (ET) is the most common form of adult movement disorder (1, 2), with an estimated prevalence of 4–6% (3, 4). Although not life threatening, it carries significant morbidity due to functional impairment from loss of hand function (5). Medications such as propranolol and primidone are the first line therapy, but many patients with ET become drug refractory (5). These patients can be good candidates for surgical treatments such as deep brain stimulation, radiofrequency thalamotomy, focused ultrasound thalamotomy, or gamma knife thalamotomy (GKT).

FIGURE 1 | (A) PRISMA flow diagram outlining the literature search process. **(B)** Bar chart depicting the type and number of studies with year of publication. **(C)** Bar chart depicting the country where the study was conducted. **(D)** Bar chart depicting the trend in targeting technique over the years.

Stereotactic radiofrequency ablation of basal ganglia and thalamic structures, including the VIM nucleus was one of the first surgical interventions to be offered to ET patients (6). The higher risk of side effects eventually led clinicians to consider DBS as a choice for surgical treatment of ET (7–9). However, there are several drawbacks related to its use, such as implant related complications and the requirement of frequent hospital visits for programming (10, 11). GKT was developed as a relatively less invasive thalamotomy method, but suffered from unpredictable lesion size limitation and time taken for the clinical benefit to become apparent (12). MRgFUS integrates ultrasonic waves with magnetic resonance imaging for therapeutic transcranial ablation (13). MRgFUS thalamotomy is an image guided procedure with no incision. It is a precision thalamotomy, in other words. Advantages of MRgFUS include non-invasiveness, real time real-time visualization of the thermal spot, and temperature monitoring while testing for a clinical response during lesion creation. Moreover, there are no hardware-related complications, and the patients do not require repeated hospital visits for programming. New advances are being made to improve the results of MRgFUS. Diffusion tensor imaging, which allows the delineation of the CTT, has been incorporated in recent times in an effort to improve the target of the ultrasonic waves (14).

An earlier review published on the topic included only nine studies (15). Many errors were pointed out in the article, including an insufficient number of studies to draw relevant conclusions (16). Additionally, no long-term data were available at that time. Since then, several centers around the world have embraced this technique. This review summarizes the latest available evidence in literature in terms of efficacy and complications of MRgFUS for ET. Owing to the paucity of Class

Abbreviations: MRgFUS, magnetic resonance guided focused ultrasound; ET, essential tremor; RFA, radiofrequency ablation; VIM, ventral intermediate; DBS, deep brain stimulation; GKT, gamma knife thalamotomy; MRI, magnetic resonance imaging; DTI, diffusion tensor imaging; CTT, cerebello thalamic tract; PRISMA, Preferred Reporting Items for Systematic Reviews and Meta Analyses; CRST, clinical rating scale for tremor; QOL, quality of life; QUEST, quality of life in essential tremor; SDR, skull density ratio; RCT, randomized controlled trial; PSA, posterior subthalamic area; CST, corticospinal tract; ML, medial lemniscus; SMD, standardized mean difference; SDC, supplementary digital content.

I evidence and the unlikelihood of prospective studies comparing the various surgical techniques available for treating ET, this meta-analysis strives to provide pooled results of a number of smaller studies on the topic.

METHODS

Literature Search

A search for published literature till May 2020 was done on PubMed, Google Scholar, Cochrane library database and Medline using the keywords "MR guided," "focused ultrasound," "essential tremor," "thalamotomy," "ventral intermediate nucleus," "cerebellothalamic," and "diffusion imaging" in various combinations. References of the relevant studies and other review articles on the subject were also studied to supplement the initial search. Only English language articles were considered. Two authors manually and independently reviewed all publications encountered during the search. Disagreements, if any, were resolved with the opinion of a third independent observer. PRISMA guidelines were followed throughout (**Figure 1A**).

Inclusion and Exclusion Criteria

Studies describing the use of MRgFUS for the treatment of medically refractory ET (unilateral or bilateral) in the adult population were selected for this review. The exclusion criteria were studies that reported outcomes on patients with tremors secondary to any other causes, such as drug-induced tremor, history of preceding trauma within 3 months, psychogenic tremor, or co-morbid Parkinson disease and dystonia were excluded. For studies with mixed diagnoses, we only included outcomes reported for ET patients. To keep the focus primarily on MRgFUS, we excluded cases where a previous procedure such as DBS, radiosurgery or stereotactic ablation was done. To avoid duplication of results, we only included outcomes from a single publication where multiple publications reported outcomes from the same study cohort.

Data Extraction

Data were extracted by two authors independently. Clinical data collected included the maximum reported period of follow up, the total Clinical Rating Scale for Tremor score (maximum score 160) (17, 18), hand score – a subset of CRST Part A and B (maximum score 32), disability as CRST Part C (maximum score 32) and quality of life as determined by the Quality of Life in Essential Tremor Questionnaire score (0–100%). All the data points were collected using a standardized data collection instrument developed in Microsoft Excel (Microsoft Inc., Redmond, WA) template.

TABLE 1 | Methodological index for non-randomized studies (MINORS) scores for included studies*.

References	Clearly stated aim	Inclusion of consecutive patients	Prospective collection of data	Endpoints appropriate to aim of study	Unbiased assessment of the study endpoint	Follow up period appropriate to aim of study	Loss to follow up < 5%	Prospective calculation of study size	Total score
Lipsman et al. (24)	2	2	2	2	1	1	2	0	12
Elias et al. (25)	2	2	2	2	1	1	2	0	12
Chang et al. (26)	2	2	2	2	1	1	2	0	12
Gallay et al. (27)	2	2	2	2	1	1	1	0	11
Zaroor et al. (28)	2	2	2	2	1	1	2	0	12
Schreglmann et al. (29)	2	2	2	2	2	1	2	0	13
Kim et al. (30)	2	2	0	2	1	1	2	0	10
Chazen et al. (31)	2	2	2	2	1	0	0	0	9
Federau et al. (32)	2	2	0	2	1	1	2	0	9
Jung et al. (33)	2	2	2	2	1	1	2	0	12
Iacopino et al. (34)	2	2	2	2	1	1	1	0	11
Krishna et al. (35)	2	2	2	2	2	1	2	0	13
Boutet et al. (36)	2	2	0	2	1	1	2	0	10
Park et al. (37)	2	2	2	2	2	2	1	0	13
Hori et al. (38)	2	2	0	2	1	1	2	0	10
Pineda-Pardo et al. (39)	2	1	2	2	1	1	1	0	10
Jones et al. (40)	2	2	0	2	2	1	1	0	10
Sinai et al. (41)	2	2	2	2	1	1	1	0	11
Chang et al. (42)	2	2	1	2	1	1	2	0	11
Miller et al. (43)	2	2	0	2	1	1	1	0	8
Krishna et al. (44)	2	2	0	2	1	1	2	0	10
Gallay et al. (45)	2	2	2	2	1	1	2	0	12
Fukutome et al. (46)	2	2	0	2	1	1	2	0	10

Score per criterion: 0, not reported; 1, reported but inadequate; 2, reported and adequate. Ideal global score for non-comparative study is 16.

The *primary outcome* variable was the change in CRST score pre and postoperatively at 3 and 12 months. The *secondary outcomes* were the difference in disability and QOL scores. For the meta-analysis, studies that reported the outcome as a mean value (with standard deviation) of the total CRST score, hand score, CRST Part C score and QUEST score were included. Studies reporting outcome as median or percentage improvement in outcome scores, studies that reported the hand score out of 12/16 were excluded from that part of the analysis. Case reports were excluded from the meta-analysis.

Complications attributed to the procedure were recorded as immediate (occurring during the procedure to within 48 h after the procedure), short-term (from the third day onwards till 3 months), and long-term (persisting/appearing more than 3 months later). The complications were divided into two broad categories - neurologic and minor/treatment related. The neurological complications were further divided into four subcategories – sensory (paresthesia, taste disturbance, dysesthesia, tinnitus), motor (facial or limb weakness), ataxia (dizziness, gait ataxia, dysmetria/hand ataxia) and speech & swallowing. The minor/treatment related complications were categorized as headache and fatigue, sonication, MRI, frame related and others.

Statistical Analysis

Statistical analysis of the pooled data was performed using R software (R Foundation for Statistical Computing, Vienna, Austria) employing the "meta" and "metaphor" packages (19–21). We first performed the analysis using fixed-effect modeling and later, with random-effect methods (after assessing heterogeneity with fixed modeling). Thus, all values reported in the current analysis were from random-effect modeling (was heterogeneity significant for all analyses). The extent of heterogeneity between the studies was quantified using the I^2 statistic. Values of $I^2 < 25\%$, 25–75%, and >75% were defined as low, moderate and high heterogeneity, respectively (22). The results were expressed as a standardized mean difference with a 95% confidence interval. A negative SMD indicates improvement in the relevant score postoperatively. P-value < 0.05 was considered as statistically significant. Linear regression analysis was performed to detect any significant correlation between parameters.

Risk of Bias Assessment

Studies were assessed for a possible publication bias initially using a funnel plot, which was later quantified using Egger's test. Publication bias was evaluated for reporting of CRST total score at 3 months. Egger's regression test showed that the X-axis intercept occurred at −1.587 with p-value (two-tailed) being 0.04315 (**Supplementary Material 1**).

Study Quality Assessment

The MINORS criteria were used to assess the methodological quality of non-randomized surgical studies (23) (**Table 1**).

RESULTS

A total of 29 studies (24–52), evaluating a total of 617 patients (156 female) fulfilled the inclusion criteria for the systematic review. Out of these 29 studies, there was only one RCT (47), with the rest being observational studies. There were fourteen prospective and eight retrospective studies and three case reports (**Figure 1B**). At present, the procedure has been performed in eight countries (**Figure 1C**). Three studies were reporting long term follow-up (37, 48, 49) of the patients in the RCT. Mean age of the patients ranged from mean 61.7 ± 8.1 to 78 ± 6 years in the studies, except a case report which reported the use of MRgFUS in treating nonagenarians (51). Mean disease duration ranged from 15.4 ± 13.3 to 34.3 ± 22.1 years. The maximum follow-up reported was 5 years by Sinai et al. in two patients (41). The baseline characteristics of the studies are summarized in **Table 2**.

Targeting Method and Operative Parameters

Majority of the studies followed atlas-based targeting which was further refined by direct targeting based on MRI. DTI based targeting was reported by six studies, two of whom were case reports (**Table 2**, **Figure 1D**). Treatment parameters used by various centers have been summarized in **Table 3**. The skull density ratio (SDR) was more than a mean of 0.45 for all studies, except one which reported a median value of 0.38 (38). The mean number of sonications ranged from 11 ± 3.2 to 22.5 ± 7.6. All studies reported maximum temperature attained as >55°C for the lesioning except Chang et al. (26), who reported 53 ± 3.3°C as the mean temperature attained, and Jones et al. (40), who described a series of 19 patients in whom multiple low-temperature sonications were used to create a lesion. The maximum energy delivered ranged from a mean of 10,320 ± 4,537 to 16,910 ± 8,340 J. The sonication time ranged from a mean of 82.8 ± 30.8 to 105 ± 55 min. A recent case report mentioned 80 min as the sonication time (51). Four centers utilized a 1.5T MRI for the procedure (34, 46, 50, 52) while the rest performed it on a 3T machine.

Tremor Outcome

Tremor outcomes, in the form of CRST scores and its subsets, for all studies have been summarized in **Table 4**. Total CRST scores 3 months after the procedure were reported by nine studies. The pooled standard mean difference between postoperative and preoperative total CRST score at 3 months was −1.93 (95% CI: −2.32 to −1.54, p-value < 0.001). The studies showed moderate heterogeneity with I^2 of 33% (**Figure 2A**).

Seven studies reported total CRST scores at 12 months after the procedure. The pooled standard mean difference was −2.07 (95% CI: −2.70 to −1.44). P-value was found to be significant at <0.01. The studies showed high heterogeneity with I^2 of 68%. Sensitivity analysis was done, and 2 studies (33, 47) were found to be contributing to heterogeneity. Analysis was redone after removing these 2 studies. Hence, the final analysis for total CRST scores at 12 months after the procedure included five studies. The pooled standard mean difference was −2.12 (95% CI: −2.57 to

TABLE 2 | Study details arranged chronologically by the month and year of publication along with follow up and outcome scores [*For descriptive purposes, the cohort of patients reported by Krishna et al. (35) and Elias et al. (47) were split into two groups, each with its own distinct characteristics].

References	Study design	Period of recruitment of patients	Place where conducted	No. of patients	Mean age ± SD (range) (in years)	Sex (male, female)	Mean disease duration ± SD (range) (in years)	Target	Localization method	Maximum follow up (range)	Mean total CRST score		CRST part A		Hand score		CRST part C		QUEST	
											Preoperative	Postoperative (follow up – number of patients)	Preoperative	Postoperative (follow up – number of patients)	Preoperative (maximum score)	Postoperative (follow up – number of patients)	Preoperative	Postoperative (follow up – number of patients)	Preoperative	Postoperative (follow up – number of patients)
Lipsman et al. (24)	Prospective, uncontrolled	May 2012–January 2013	Toronto, Canada	4	70.8 ± 7.8 (58–77)	4, 0	17.8 ± 8.2 (6–25)	VIM	Standard	3 month	70.75 ± 17.0	35.25 ± 9.5	NA	NA	7.25 ± 1.9 (out of 12)	1.25 ± 0.82 (3 m)	20.75 ± 3.9	10.25 ± 2.8	NA	NA
Elias et al. (25)	Prospective, uncontrolled	February–December 2011	Virginia, USA	15	66.6 ± 8.0 (53 to 79)	10, 5	32.0 ± 21.3 (4–60)	VIM	Standard	1 year	54.9 ± 14.4	24.3 ± 14.8	NA	NA	20.4 ± 5.2 (out of 32)	4.3 ± 3.5 (3 m), 5.2 ± 4.8 (1 yr)	18.2 ± 4.1	2.8 ± 3.4	NA	NA
Chang et al. (26)	Prospective, uncontrolled	March–November 2012	Seoul, Korea	8	66.1 ± 5.3 (61–78)	7, 1	32.1 ± 16.1 (15–57)	VIM	Standard	6 month	NA	NA	5.1 ± 1.2	1.4 ± 1.4	NA	NA	13.5 ± 3.7	2.8 ± 2.8	NA	NA
Gallay et al. (27)	Prospective, uncontrolled	NA	Solothurn and Bern, Switzerland	21	69.1 ± 9.2	15, 6	29.9 ± 15	CTT	Standard	1 year	57.6 ± 13.2	25.8 ± 17.6 (1 yr−10)	NA	NA	NA	NA	NA	NA	NA	NA
Elias et al. (47) (Treatment group)*	Randomized Control Trial	August 2013–September 2014	Multicentric-8	56	70.8 ± 8.7	37, 19	28.3 ± 16.4	VIM	Standard	1 year	50.1 ± 14.0	29.6 ± 13 (3 m); 32.4 ± 14.5 (12 m)	NA	NA	18.1 ± 4.8 (out of 32)	9.6 ± 5.1 (3 m), 10.9 ± 4.5 (1 yr)	16.5 ± 4.6	6.2 ± 5.6 (3 m), 6.3 ± 6.2 (1 yr)	42.6 ± 18.3	23.1 ± 16.9 (3 m), 41.4 ± 19.4 (1 yr)
Elias et al. (47) (Sham Crossover)*	Randomized Control Trial	August 2013–September 2014	Multicentric-8	21 (19 crossover, 2 retreat)	71.4 ± 7.3	15, 5	27.9 ± 14.9	VIM	Standard	1 year	45.43 ± 12.55	23.48 ± 10.95 (3 m); 25.00 ± 11.11 (6 m); 18.67 ± 16.02 (1 yr−9)	NA	NA	16.5 ± 4.21 (out of 32)	7.43 ± 3.88 (3 m),8.00 ± 3.86 (6 m), 6.71 ± 4.7 (1 yr−9)	NA	NA	NA	NA
Chang et al. (48)	2 year follow up of patients in RCT by Elias et al. (47)	August 2013–September 2014	Multicentric-8	76 (67 followed till 2 years)	71.0 ± 8.3 (47–89)	52, 24	16.8 ± 12.3	VIM	Standard	2 year	NA	NA	NA	NA	19.8 ± 4.9 (out of 32)	8.9 ± 4.8 (1 yr−70), 8.8 ± 5.0 (2 yr−67)	16.4 ± 4.5	5.4 ± 5.3 (1 yr −70) 6.5 ± 5.0 (2 yr−67)	NA	NA
Halpern et al. (49)	3 year follow up of patients in RCT by Elias et al. (47)	August 2013–September 2014	Multicentric-8	76 (52 followed till 3 years)	71.0 ± 8.3 (47–89)	52, 24	16.8 ± 12.3	VIM	Standard	3 year	NA	NA	NA	NA	20.1 ± 4.7 (out of 32)	9.5 ± 5.4	16.4 ± 4.5	7.5 ± 6.1	43.1 ± 18.3	23.8 ± 19.6
Zaroor et al. (28)	Prospective, uncontrolled	November 2013–January 2016	Haifa, Israel	18	73.1 ± 6.2 (64–87)	12, 6	15.5 ± 9.3 (5–30)	VIM	Standard	12.5 ± 7.0 (3–24) month	40.7 ± 11.6	9.3 ± 7.1 (1 m); 8.2 ± 5.0 (6 m)	NA	NA	NA	NA	NA	NA	44.8 ± 12.9	13.1 ± 13.2 (1 m); 12.3 ± 7.2 (6 m)
Schreglmann et al. (29)	Prospective, uncontrolled	NA	St. Gallen, Switzerland	6	70.7 ± 8.5 (58–82)	2, 4	24.5 ± 22.5 (2–56)	CTT	Standard	6 month	43.8 ± 9.8	19.8 ± 6.8	NA	NA	14.3 ± 4.9 (out of 32)	2.5 ± 2.6	NA	NA	NA	52% improvement
Kim et al. (30)	Retrospective	2012–2014	Seoul, South Korea	23	64.7 (47–77)	20, 3	20.5 (5–54)	VIM	Standard	1 year	NA	NA	NA	NA	NA	(>90% improvement was taken as success) 21 patients (91.3%) at 1 m, 18 (78.3%) at 12 m	NA	NA	NA	NA
Chazen et al. (31)	Prospective, uncontrolled	NA	New York, USA	4	64.25 ± 11.7	3, 1	NA	CTT	DTI based	NA	NA	NA	NA	NA	3.75 ± 1.0 (out of 15)	0.25 ± 0.50 (Immediate post treatment)	NA	NA	NA	NA

(Continued)

TABLE 2 | Continued

References	Study design	Period of recruitment of patients	Place where conducted	No. of patients	Mean age ± SD (range) (in years)	Sex (male, female)	Mean disease duration ± SD (range) (in years)	Target	Localization method	Maximum follow up (range)	Mean total CRST score		CRST part A		Hand score		CRST part C		QUEST	
											Preoperative	Postoperative (follow up – number of patients)	Preoperative	Postoperative (follow up – number of patients)	Preoperative (maximum score)	Postoperative (follow up – number of patients)	Preoperative	Postoperative (follow up – number of patients)	Preoperative	Postoperative (follow up – number of patients)
Federau et al. (32)	Retrospective	August 2013–May 2014	Stanford, USA	7	78 ± 6	5, 2	NA	VIM	Standard	1 year	NA	NA	6.5 ± 1.3	2.3 ± 1.1	21.5 ± 2.0 (out of 32)	9.7 ± 5.2	NA	NA	NA	NA
Jung et al. (33)	Prospective, uncontrolled	March 2012–September 2014	Seoul, South Korea	20	64.1 (47–77)	17, 3	21.2 (5–54)	VIM	Standard	1 year	44.75 ± 9.57	14.65 ± 9.19	12.60 ± 3.80	2.75 ± 3.18	18.15 ± 3.96 (out of 32)	5.80 ± 4.53	12.80 ± 3.17	5.75 ± 4.25	64.16 ± 17.75	27.38 ± 13.96
Iacopino et al. (34)	Prospective, uncontrolled	January 2015–September 2017	Palermo, Italy	13	65.22 ± 11.87	10, 3	22.38 (3–70)	VIM	Standard	6 month	40.2 ± 11.8	17.3 ± 7.31 (3 m); 17.7 ± 8.80 (11 pts−6 m)	NA	NA	6.4 ± 2.97 (out of 16)	2.1 (3 m), 2.2 (6 m−11)	NA	NA	35.09± 12.25	17.09 ± 10.67(3 m), 18.44 ± 13.76 (6 m−11)
Krishna et al. (35)	Prospective, uncontrolled	July 2015–September 2016	Ohio, USA	10	70.8 ± 9.7	6, 4	34.3 ± 22.1	VIM	DTI based	6 month	59.3 ± 17.3	29 ± 16 (3 m), 32 ± 15.9 (6 m−9)	20.7 ± 8	11.6 ± 6.5 (3m)	17.4 ± 4.5 (out of 32)	6.5 ± 3.7 (3 m)	18.1 ± 5.1	4.3 ± 4.4 (3 m)	81.7 ± 17.7	45.3 ± 11.6 (3 m), 45.6 ± 10.8 (6 m−9)
Boutet et al. (36)	Retrospective	May 2012–August 2017	Toronto, Canada	66	72.4 ± 8.4	47, 19	23.0 ± 14.4	VIM	NA	3 month	59.7 ± 17.4	34.8 ± 14.4	NA	NA	NA	NA	NA	NA	NA	NA
Park et al. (37)	Prospective, uncontrolled [4 year follow up of patients reported in RCT by Elias et al. (47)]	October 2013–August 2014	Seoul, South Korea	12	61.7 ± 8.1 (47–72)	10, 2	17.8 ± 13.03 (7–54)	VIM	Standard	4 year	NA	NA	NA	NA	17.4 ± 3.8 (out of 32)	5.3 ± 3.4 (1 yr), 6.9 ± 5.9 (2 yr), 7.5 ± 5.3 (3 yr), 7.7 ± 4.1 (4 yr)	12.7 ± 3.0	2.9 ± 2.4 (1 yr), 5.1 ± 3.6 (2 yr), 4.4 ± 3.3 (3 yr), 4.7 ± 3.0 (4 yr)	NA	NA
Hori et al. (38)	Retrospective	April 2015–October 2017	Tokyo, Japan	12	76.5 ± 3.8 (67–82)	9, 3	Median 15 (10–70)	VIM	Standard	1 year	NA	NA	NA	NA	NA	NA	NA	NA	NA	NA
Pineda-Pardo et al. (39)	Prospective, uncontrolled	NA	Madrid, Spain	24	68.0 ± 10.1	17, 7	18.6 ± 12.8	VIM + CTT	Atlas + DTI based (to extend the target)	1 year	52.9 ± 13.0	23.8 ± 8.3 (3 m); 26.4 ± 11.3 (1 yr−19)	5.6 ± 1.8	1.0 ± 0.9 (3 m), 1.5 ± 1.3 (1 yr−19)	NA	NA	17.3 ± 4.8	4.2 ± 4.1 (0–15) (3 m), 5.4 ± 4.9 (0–19) (1 yr−19)	NA	NA
Yang et al. (50)	Case Report	NA	Philadelphia, USA	1	74	1, 0	1	CTT	DTI based	3 month	25	5 (3 m)	NA	NA	10 (out of 32)	1 (3 m)	9	0 (3 m)	NA	NA
Jones et al. (40)	Retrospective	July 2015–July 2018	Toronto, Canada	19 low temperature (LT), 30 high temperature (HT)	NA	NA	NA	VIM	Standard	1 year	NA	NA	NA	NA	20.5 ± 5.8 (Low Temperature - LT), 20.3 ± 5.0 (Hight Temperature - HT) (out of 32)	Improvement by 53% ± 32 and 51% ± 22% at 3 m, 45% ± 55% and 44% ± 22% (1 yr−9 LT, 27 HT)	NA	NA	NA	NA
Sinai et al. (41)	Prospective, uncontrolled	Nov 2013–Nov 2018	Haifa, Israel	44	Median 70.5 (63–87)	27, 17	16.3 ± 10.4 (1–30)	VIM	Standard	Median 12 month	Median 46.0	Median 12.0 (1 m−44); 18.0 (1 yr−24); 11.0 (2 yr−15); 16.0 (3 yr−10); 14.0 (4 yr−6); 8.0 (5 yr−2)	NA	NA	Median 19 (out of 32)	Median 0.0 (1 m−44); 4.0 (1 yr−24); 4.0 (2 yr−15); 3.5 (3 yr−10); 5.0 (4 yr−6); 3.0 (5 yr−2)	NA	NA	41.5	Median 5.5 (1 m−44); 14.0 (0–89) (1 yr−24); 15.0 (2 yr−15); 15.5 (3 yr−10); 14.5 (4 yr−6); 11.0 (5 yr−2)
Chang et al. (42)	Prospective, uncontrolled	since 2013	Seoul, South Korea	50	66.65 ± 9.95 (45–80)	42, 8	NA	VIM	Standard	17.8 ± 19.8 (1–60) month	NA	NA	NA	NA	12.12 ± 0.51 (out of 32)	5.88 ± 0.52	12.52 ± 0.52	3.64 ± 0.47	NA	NA

(Continued)

TABLE 2 | Continued

References	Study design	Period of recruitment of patients	Place where conducted	No. of patients	Mean age ± SD (range) (in years)	Sex (male, female)	Mean disease duration ± SD (range) (in years)	Target	Localization method	Maximum follow up (range)	Mean total CRST score		CRST part A		Hand score		CRST part C		QUEST	
											Preoperative	Postoperative (follow up – number of patients)	Preoperative	Postoperative (follow up – number of patients)	Preoperative (maximum score)	Postoperative (follow up – number of patients)	Preoperative	Postoperative (follow up – number of patients)	Preoperative	Postoperative (follow up – number of patients)
Miller et al. (43)	Retrospective	July 2014–August 2016	Baltimore, USA	4	NA	NA	NA	VIM + CTT	Atlas + DTI based (to extend the target)	3 month (1 patient died of unrelated cause after 3 months. For the rest, benefit was sustained till 1 year follow up, no scores mentioned)	57.5 ± 16.8	29.5 ± 6.4	NA	NA	6.5 ± 1.0 (out of 16)	0.75 ± 0.9	NA	NA	NA	NA
Krishna et al. (44) (Pivotal)*	Retrospective	2013–2015	Multicentric - 8	75 (treatment + sham crossover)	71.3 ± 8.4	51, 24	16.8 ± 12.3	VIM	Standard	1 year	NA	NA	NA	NA	19.9 ± 5 (out of 32)	Improvement: 56.3 ± 25.5% (3 m), 52.1 ± 24.9% (1 yr)	NA	Improvement : 68.3 ± 27.6% (3 m), 65.9 ± 30.9% (1 yr)	NA	NA
Krishna et al. (44) (Post Pivotal)*	Retrospective	2015–2016	Multicentric - 18	114	71 ± 9.5	80, 34	15.4 ± 13.3	VIM	Standard	1 year	NA	NA	NA	NA	19.3 ± 5 (out of 32)	Improvement: 63.6 ± 26.1% (3 m), 61.9 ± 24.9% (1 yr)	NA	Improvement: 72.3 ± 25.9% (3 m), 66.1 ± 32.1% (1 yr)	NA	NA
Gallay et al. (45)	Prospective, uncontrolled	After 2016	Solothurn & Bern, Switzerland	10	66 ± 8 years	8, 2	31 ± 14	CTT (3 patients also had a contralateral centrum medianum thalamotomy)	Standard	1 year	48 ± 12	16 ± 7 (3 m); 17 ± 8 (1 yr)	11.8 ± 3.9	3.6 ± 1.5 (3m), 4.3 ± 1.9 (1 yr)	NA	NA	14.2± 3.4	2.6 ± 2.0 (3 m), 3.4 ± 2.6 (1 yr)	NA	NA
Paff et al. (51)	Case Report	NA	Toronto, Canada	1	93	1, 0	40	VIM	Standard	1 year	NA	52% improvement	NA	NA	NA	64% improvement in hand score	NA	NA	NA	NA
Buch et al. (52)	Case Report	NA	Philadephia, USA	1	80	1, 0	NA	VIM + CTT	DTI based	6 week	NA	NA	NA	NA	20 (out of 32)	2	21	2	NA	NA
Fukutome et al. (46)	Retrospective	May 2016–August 2017	Nara, Japan	15	62.9 ± 11.3 (41–82)	11, 4	21.5 ± 14.0 (2–47)	VIM	Standard	1 year	NA	NA	NA	NA	18.5 ± 5.8 (out of 32)	4.6 ± 5.7	NA	NA	NA	NA

RCT, randomized controlled trial; SD, standard deviation; VIM, ventral intermediate nucleus; CTT, cerebello-thalamic tract; DTI, diffusion tensor imaging; NA, not available; m, month; yr, year.

TABLE 3 | Treatment parameters [*For descriptive purposes, the cohort of patients reported by Krishna et al. (35) and Elias et al. (47) were split into two groups, each with its own distinct characteristics].

References	Mean skull density ratio ± SD (range)	No. of sonications ± SD (range)	Maximum energy delivered ± SD (range) (in Joules)	Peak temperature ± SD (range) (in °C)	Mean operative time ± SD (range) (in minutes)	MRI
Lipsman et al. (24)	NA	22.5 ± 7.6 (12–29)	NA	59.3 ± 2.9 (56–63)	NA	3T
Elias et al. (25)	NA	17.9 ± 4.6 (11–26)	10,320 ± 4,537 (6,500–20,800)	58.5 ± 2.5 (54–63)	NA	3T
Chang et al. (26)	NA	NA	NA	53 ± 3.3 (48–61)	227.5 (169–293) (No vertigo group) to 260.6 (160–354) (Vertigo group)	3T
Gallay et al. (27)	NA	NA	16,073 ± 6,037	NA	285 ± 66	3T
Elias et al. (47) (Treatment group)*	NA	18.5 ± 5.2	14,497.0 ± 6,695.7 (3,500–34,860)	55.6 ± 2.3 (50.0–60.7)	NA	3T
Elias et al. (47) (Sham Crossover)*	NA	NA	NA	NA	NA	3T
Chang et al. (48)	NA	18.5 ± 5.2	14,497.0 ± 6,695.7 (3,500–34,860)	55.6 ± 2.3 (50.0–60.7)	NA	3T
Halpern et al. (49)	NA	18.5 ± 5.2	14,497.0 ± 6,695.7 (3,500–34,860)	55.6 ± 2.3 (50.0–60.7)	NA	3T
Zaroor et al. (28)	NA	20.8 ± 6.4	12,231.5 ± 3,189.8	56.88 ± 2.5	NA	3T
Schreglmann et al. (29)	NA	11 ± 3.2 (8–17)	12,008 ± 4,441 (7,800–19,950)	62.0 ± 2.5 (58–64)	271.6 ± 40 (215–305)	3T
Kim et al. (30)	NA	NA	NA	NA	NA	3T
Chazen et al. (31)	NA	NA	NA	NA	NA	3T
Federau et al. (32)	NA	18.6 ± 5.7 (12–28)	NA	NA	NA	3T
Jung et al. (33)	NA	16.8 (13–20)	15,910 ± 5,702.7	57.9	NA	3T
Iacopino et al. (34)	NA	NA	NA	NA	NA	1.5T
Krishna et al. (35)	0.54 ± 0.1	13.9 ± 4.5	NA	NA	174.3 ± 41.6 (Sonification time : 82.8 ± 30.8)	3T
Boutet et al. (36)	0.48 ± 0.1	NA	NA	56.6 ± 2.3	NA	3T
Park et al. (37)	0.49 ± 0.08 (0.26–0.6)	17.3 ± 1.6 (15–20)	15,552.4 ± 6,574.1 (7,150–25,488)	NA	NA	3T
Hori et al. (38)	Median 0.38 (0.27–0.61)	Median 17 (9–26)	Median 23,054 (5,849–38,658)	Median 56 (52–59)	NA	3T
Pineda-Pardo et al. (39)	NA	NA	NA	NA	NA	3T
Yang et al. (50)	NA	14	16,080	64	NA	1.5T
Jones et al. (40)	NA	NA	NA	NA	NA	3T
Sinai et al. (41)	Median 0.47 (0.31–0.67)	Median 19.5 (9–36)	Median 12,077 (6,000–35,500)	NA	NA	3T
Chang et al. (42)	0.51 ± 0.08 (0.26–0.72)	15.12 ± 3.88	NA	58.76±2.89	NA	3T
Miller et al. (43)	NA	NA	NA	NA	NA	3T
Krishna et al. (44) (Pivotal)*	0.55 ± 0.1 (unreported for 17 pts)	17.4 ± 4.3	14,410 ± 7,390	55.6 ± 2.8	88 ± 40	3T
Krishna et al. (44) (Post Pivotal)*	0.5 ± 0.1 (unreported for 4 pts)	17.1 ± 5.3	16,910 ± 8,340	56.7 ± 2.5	105 ± 55	3T
Gallay et al. (45)	0.54 ± 0.06 (0.33–0.62)	NA	13,720 (5,850–36,000)	NA	NA	3T
Paff et al. (51)	0.65	13	18,302	59	80	3T
Buch et al. (52)	0.46	16	22,559	60	NA	1.5T
Fukutome et al. (46)	0.45 ± 0.11 (0.30–0.80)	NA	16,275 ± 8,610 (4,791–33,018)	57.3 ± 1.9 (54–60)	NA	1.5T

TABLE 4 | Summary of outcomes after meta-analysis.

Outcome variables	Standard mean difference between pre & postoperative score (95% CI)	No. of participants (studies)	*p*-value	Heterogeneity (I^2)
Total CRST score (at 3 months)	−1.93 (−2.32 to −1.54)	208 (9)	**<0.001***	Moderate (33%)
Total CRST score (at 12 months)	−2.12 (−2.57 to −1.67)	63 (5)	**0.002***	Low (0%)
Hand score (at 3 months)	−2.36 (−3.56 to −1.15)	102 (4)	**0.03***	Moderate (67%)
Hand score (at 12 months)	−2.35 (−2.83 to −1.86)	204 (8)	**0.02***	Moderate (57%)
CRST Part C score (at 3 months)	−2.66 (−3.53 to −1.79)	104 (5)	0.08	Moderate (52%)
CRST Part C score (at 12 months)	−2.57 (−3.33 to −1.80)	202 (7)	**0.01***	Moderate (64%)
QUEST score (at 3 months)	−1.49 (−2.93 to −0.04)	79 (3)	0.13	Moderate (51%)
QUEST score (at 6 months)	−2.20 (−3.40 to −1.00)	58 (4)	0.07	Moderate (57%)

CI, confidence interval; NA, not applicable.
**Significant. Bold denote significant values.*

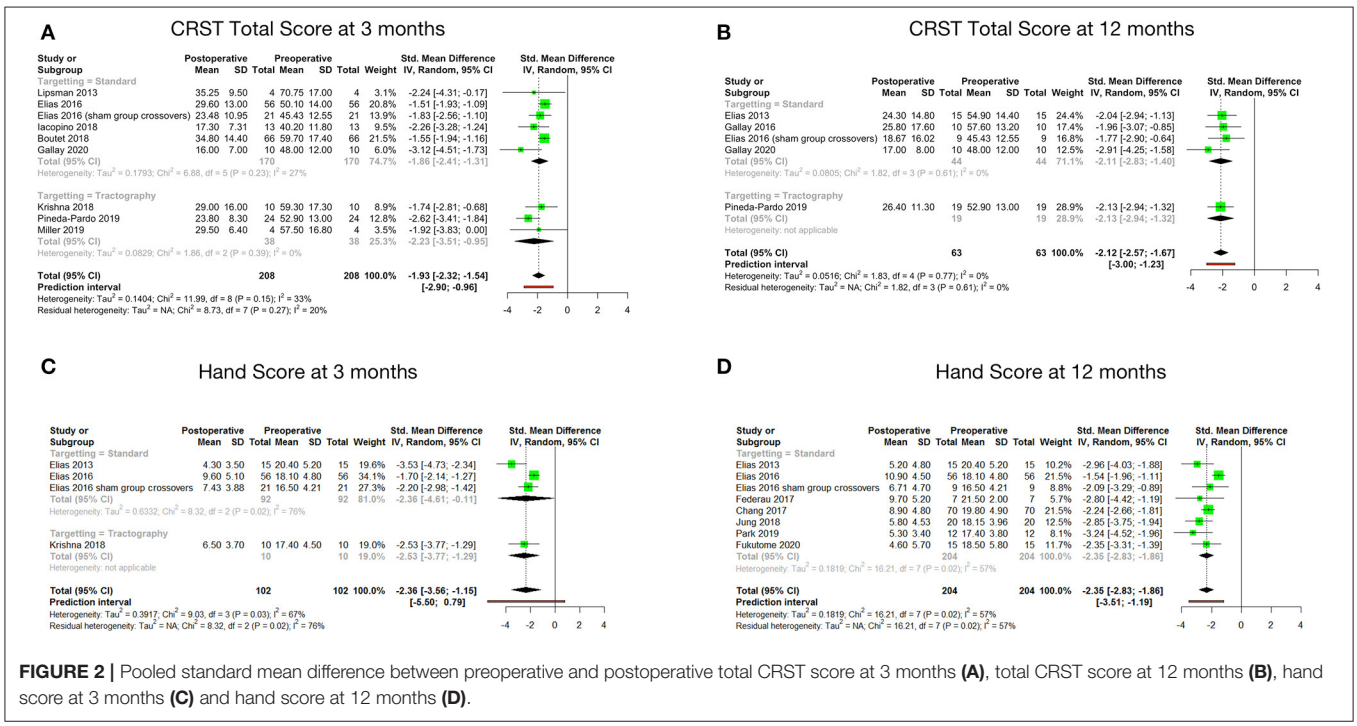

FIGURE 2 | Pooled standard mean difference between preoperative and postoperative total CRST score at 3 months **(A)**, total CRST score at 12 months **(B)**, hand score at 3 months **(C)** and hand score at 12 months **(D)**.

−1.67). *P*-value was found to be significant at 0.002. The studies showed low heterogeneity with I^2 of 0% (**Figure 2B**).

Four cohorts reported hand scores (out of a total of 32) at 3 months. The pooled standard mean difference was −2.36 (95% CI: −3.56 to −1.15; *p*-value - 0.03). The studies showed high heterogeneity with I^2 of 67% (**Figure 2C**). Eight cohorts reported hand scores at 12 months. The pooled standard mean difference was −2.35 (95% CI: −2.83 to −1.86; *p*-value - 0.02). The studies showed moderate heterogeneity with I^2 of 57% (**Figure 2D**).

The standard mean difference between the preoperative and postoperative total CRST score and hand scores was found to be significant at 3 and 12 months following the procedure. Subgroup analysis of the mean changes in CRST scores according to the targeting technique (standard vs. DTI based) revealed that the difference was not statistically significant between the two groups.

Disability and QOL Outcome

Disability, as per the CRST Part C score at 3 months after MRgFUS, was reported by five studies. The pooled standard mean difference was −2.66 with 95% CI: −3.53 to −1.79 (*p*-value - 0.08). The studies showed moderate heterogeneity with I^2 of 52% (**Figure 3A**). Disability at 12 months after MRgFUS was reported by eight cohorts. The pooled standard mean difference was −4.54 with 95% CI: −8.95 to −0.12 (*p*-value < 0.01). The studies showed considerable heterogeneity with I^2 of 96%. Sensitivity analysis was done, and 1 study (42) was found to be contributing to heterogeneity. Analysis was redone after removing this study. Hence, the final analysis for disability at 12 months after MRgFUS included seven studies. The pooled standard mean difference was −2.57 with 95% CI: −3.33 to −1.80 (*p*-value - 0.01). The studies showed moderate heterogeneity with I^2 of 64% (**Figure 3B**).

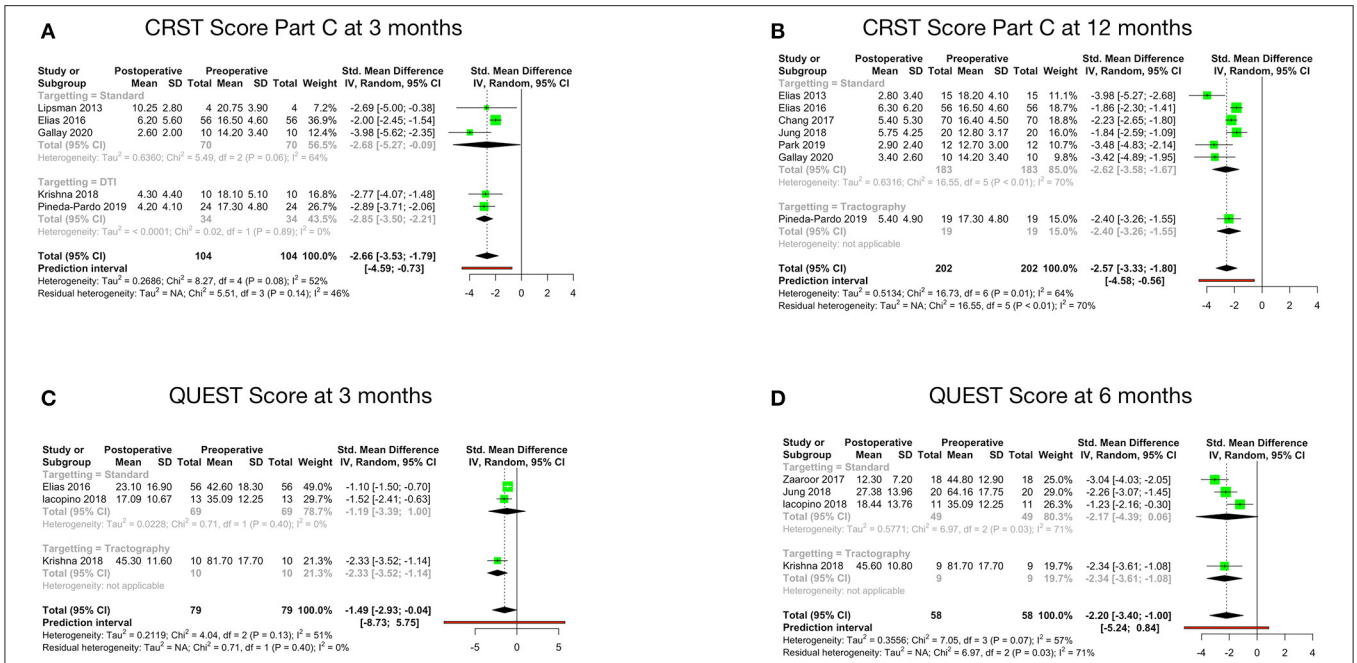

FIGURE 3 | Pooled standard mean difference between preoperative and postoperative disability scores at 3 months **(A)**, disability scores at 12 months **(B)**, QUEST scores at 3 months **(C)** and QUEST scores at 6 months **(D)**.

QOL, as per the QUEST score at 3 months, was reported by three cohorts. The pooled standard mean difference was −1.49 (95% CI: −2.93 to −0.04; *p*-value - 0.13). The studies showed moderate heterogeneity with I^2 of 51% (**Figure 3C**). Four cohorts reported QOL at 6 months. The pooled standard mean difference was −2.20 (95% CI: −3.40 to −1.00; *p*-value - 0.07). The studies showed moderate heterogeneity with I^2 of 57% (**Figure 3D**).

The comparison between preoperative and postoperative disability revealed statistically significant difference in the Part C score at 12 months (*p*-value: 0.01) (**Table 4**). Further subgroup analysis disclosed no statistically significant difference.

Complications

Details regarding the immediate, short term, and long-term complications are provided in the supplementary data (**Supplementary Materials 2–4**). The total complications were arranged according to the targeting method – standard vs. DTI based (**Table 5**) The pooled proportion of sensory, motor, ataxia and speech & swallowing related complications was calculated for immediate, early and late (occurring or persisting after 3 months) complications (**Table 6**, **Figure 4**, **Supplementary Material 5**).

Ataxia was the most common postoperative complication. All complications showed a decreasing trend over time. Subgroup analysis revealed significantly less immediate post procedure ataxia related complications in the DTI group, although no significant difference was noted over long term analysis.

DISCUSSION

The first reports of the use of MRgFUS in medically refractory ET were published in 2013 (24, 25). Standard atlas-based targeting was utilized to create a lesion in the contralateral VIM nucleus of the thalamus. The USFDA approved the use of MRgFUS in ET in 2016 after a randomized sham-controlled trial showed favorable results in the MRgFUS group (47). In a short time period, there has been a significant amount of research on the subject. However, most of these studies have small sample size. Our review article summarizes the latest available evidence in literature in terms of efficacy and complications of MRgFUS for ET. Owing to the paucity of studies involving large number of patients, this meta-analysis strives to provide pooled results of a number of smaller studies on the topic. We did an updated systematic review and meta-analysis of the studies describing the outcomes and adverse events following the use of MRgFUS in essential tremor. Though reviews have been published in the past on this topic, but there were significant shortcomings (15, 16). Our review article summarizes the latest available evidence in literature in terms of efficacy and complications of MRgFUS for ET. The primary outcome analyzed was the change in total CRST score and hand score (out of 32) after treatment, while the secondary outcomes measured were the quality of life and the complication rates. We have also tried to find whether any difference in efficacy and complication rate exists according to the area targeted - VIM nucleus of thalamus or CTT in the PSA.

Clinical Efficacy

All studies have reported good postoperative outcomes. We found a significant difference in the pooled SMD between the postoperative and preoperative primary outcome variables, at 3- and 12-months post-procedure. This shows MRgFUS to be an effective surgical modality for the treatment of ET. Additionally, there was a statistically significant improvement in the disability

TABLE 5 | Total number of complications (grouped according to the targeting method).

References	Neurological												Minor/Treatment Related											
	Sensory			Ataxia/gait disturbance			Motor			Speech and swallowing			Headache and fatigue			Sonication related			Frame and MRI related			Other		
	A	B	C	A	B	C	A	B	C	A	B	C	A	B	C	A	B	C	A	B	C	A	B	C
Atlas based targeting																								
Lipsman et al. (24)	2	1	NA	0	0	NA	0	0	NA	0	0	NA	0	0	NA	0	0	NA	0	0	NA	1 Deep Vein Thrombosis	1 Deep Vein Thrombosis	NA
Elias et al. (25)	15	4	4	10	5	0	1 (Grip)	1 (5 days)	0	1	0	0	0	0	0	33	0	0	12	0	0	0	0	0
Chang et al. (26)	0	0	0	1	1	0	0	0	0	0	0	0	0	0	0	5	0	0	0	0	0	3 failed to attain temperature above 50 °C	0	0
Gallay et al. (27)	0	0	0	5	5	1	0	0	0	0	0	0	0	0	0	0	0	0	0	0	0	0	0	0
Elias et al. (47) (Treatment group)	27	17	10	32	17	8	2 (Grip)	2 (Grip)	1 (Grip)	2	2	2	11	3	2	54	0	0	17	0	0	0	0	0
Elias et al. (47) (Sham Crossover)	13	8	8	14	7	4	3 (Grip)	2 (Grip)	1 (Grip)	3	2	2	11	2	2	16	0	0	7	0	0	0	0	0
Chang et al. (48)	NA	NA	1	NA	NA	12	NA	NA	1	NA	NA	0	NA	NA	0	NA	NA	0	NA	NA	0	NA	NA	0
Halpern et al. (49)	NA	NA	12	NA	NA	10	NA	NA	2	NA	NA	1	NA	NA	1	NA	NA	0	NA	NA	0	NA	NA	1-slow movements
Zaroor et al. (28)#	4	4	0	9	9	0	0	0	0	0	0	0	4	0	0	39	0	0	8	8	0	0	0	0
Schreglmann et al. (29)	0	0	0	3	3	0	0	0	0	0	0	0	0	0	0	4	0	0	0	0	0	0	0	0
Kim et al. (30)	1	1	0	1	1	0	2 (Facial)	2 (Facial- one resolved in 1 month)	1 (Facial)	0	0	0	0	0	0	0	0	0	0	0	0	0	0	0
Federau et al. (32)	NA	NA	NA	NA	NA	NA	NA	NA	NA	NA	NA	NA	NA	NA	NA	NA	NA	NA	NA	NA	NA	NA	NA	NA
Jung et al. (33)	0	0	0	1	1	0	0	0	0	0	0	0	0	0	0	10	0	0	3	0	0	0	0	0
Iacopino et al. (34)#	2	0	0	6	3	2	1 (Grip)	1 (Grip - 1 week)	0	0	0	0	0	0	0	10	0	0	6	0	0	4 ET patients - aborted treatment due to severe headache; 1 ET patient - failed to attain ablative temperature	0	0
Boutet et al. (36)	12	5	NA	62	20	NA	13	6	NA	3	3	NA	0	0	NA	NA	NA	NA	NA	NA	NA	0	0	NA
Park et al. (37)	1	1	0	1	1	1	0	0	0	0	0	0	0	0	0	2	0	0	0	0	0	0	0	0
Hori et al. (38)	NA	NA	NA	NA	NA	NA	NA	NA	NA	NA	NA	NA	NA	NA	NA	NA	NA	NA	NA	NA	NA	NA	NA	NA
Jones et al. (40)	NA	NA	NA	NA	NA	NA	NA	NA	NA	NA	NA	NA	NA	NA	NA	NA	NA	NA	NA	NA	NA	NA	NA	NA
Sinai et al. (41)	11	11	5	24	24	2	0	0	0	0	0	0	4	4	0	65	0	0	1	1	0	0	0	0
Chang et al. (42)	NA	NA	NA	NA	NA	NA	NA	NA	NA	NA	NA	NA	NA	NA	NA	NA	NA	NA	NA	NA	NA	NA	NA	NA
Krishna et al. (44) (Pivotal)	NA	NA	42	NA	NA	59	NA	NA	4 mild, 2 moderate	NA	NA	5	NA	NA	0	NA	NA	0	NA	NA	0	NA	NA	6 mild, 3 moderate

(Continued)

TABLE 5 | Continued

References	Neurological												Minor/Treatment Related											
	Sensory			Ataxia/gait disturbance			Motor			Speech and swallowing			Headache and fatigue			Sonication related			Frame and MRI related			Other		
	A	B	C	A	B	C	A	B	C	A	B	C	A	B	C	A	B	C	A	B	C	A	B	C
Krishna et al. (44) (Post Pivotal)	NA	NA	56	NA	NA	89	NA	NA	16 mild	NA	NA	17	NA	NA	0	NA	NA	0	NA	NA	0	NA	NA	16 mild, 2 moderate
Gallay et al. (45)	1	1	1	7	5	5	0	0	0	5	1	1	0	0	0	4	0	0	1	1	0	0	0	0
Paff et al. (51)	0	0	0	1	1	0	1 (c/l lower limb)	1 (c/l lower limb) (1 m)	0	0	0	0	0	0	0	0	0	0	0	0	0	0	0	0
Fukutome et al. (46)	1	1	1	1	1	1	0	0	0	0	0	0	0	0	0	9	0	0	0	0	0	0	0	0
Total	**90**	**54**	**140**	**178**	**104**	**194**	**23**	**15**	**28**	**14**	**8**	**28**	**30**	**9**	**5**	**251**	**0**	**0**	**55**	**10**	**0**	**9**	**1**	**28**
DTI based targeting																								
Chazen et al. (31)	NA	NA	NA	NA	NA	NA	NA	NA	NA	NA	NA	NA	NA	NA	NA	NA	NA	NA	NA	NA	NA	NA	NA	NA
Krishna et al. (35)	0	1	0	4	3	1	0	0	0	0	0	0	0	0	0	0	0	0	0	0	0	0	0	0
Pineda-Pardo et al. (39)	4	4	4	7	7	1	0	0	0	1	1	1	0	0	0	0	0	0	0	0	0	0	0	0
Yang et al. (50)	0	0	0	0	0	0	0	0	0	0	0	0	0	0	0	0	0	0	0	0	0	0	0	0
Miller et al. (43)	NA	NA	NA	NA	NA	NA	NA	NA	NA	NA	NA	NA	NA	NA	NA	NA	NA	NA	NA	NA	NA	NA	NA	NA
Buch et al. (52)	NA	NA	NA	NA	NA	NA	NA	NA	NA	NA	NA	NA	NA	NA	NA	NA	NA	NA	NA	NA	NA	NA	NA	NA
Total	**4**	**5**	**4**	**11**	**10**	**2**	**0**	**0**	**0**	**1**	**1**	**1**	**0**	**0**	**0**	**0**	**0**	**0**	**0**	**0**	**0**	**0**	**0**	**0**

Studies reporting zero complications are marked as "0." Studies in which no complication data was reported for respective time period are marked as "NA."

A, immediate (during treatment to within 48 h); B, short term (48 h–3 months); C, long term (persisting for more than 3 months). Period in brackets denotes time until when the complication persisted.

[#]*Complications not mentioned separately for ET patients.*

TABLE 6 | Summary of complications after meta-analysis.

Outcome variables	Pooled proportion (95% CI)	No. of participants (studies)	Heterogeneity (I^2)	*p*-value after subgroup analysis (standard vs. DTI based targeting)
Immediate				
Sensory	20% (12–31%)	386 (18)	High (72%)	0.46
Motor	10% (7–14%)	386 (18)	Low (11%)	0.20
Ataxia	50% (44–56%)	386 (18)	High (79%)	**0.03***
Speech & Swallowing	7% (5–11%)	386 (18)	Moderate (33%)	0.47
Short-term				
Sensory	16% (11–23%)	386 (18)	Moderate (43%)	0.93
Motor	6% (4–9%)	386 (18)	Low (0%)	0.46
Ataxia	29% (22–38%)	386 (18)	Moderate (49%)	0.95
Speech and swallowing	4% (3–7%)	386 (18)	Low (0%)	0.96
Long-term				
Sensory	13% (7–23%)	368 (16)	High (76%)	0.88
Motor	5% (3–7%)	391 (17)	Low (0%)	0.86
Ataxia	31% (24–38%)	378 (16)	High (87%)	0.09
Speech and swallowing	5% (3–8%)	391 (17)	Low (0%)	0.77

CI, confidence interval.
**Significant. Bold denote significant values.*

of the patients at 12 months postoperatively, as evaluated by the CRST Part C score. Only one study had a control group; hence between-group comparison was not possible.

For any other surgical technique to replace DBS as the procedure of choice for refractory ET, it has to prove itself as at-par, if not better than DBS. Comparative studies between RFA and DBS have reported better improvement in function and fewer adverse effects with DBS (53). Gamma knife thalamotomy for ET was first described in the 1990s. It's a non-invasive procedure, however, the inability to monitor real-time clinical response, variation in the size of the lesion produced, unpredictable radiation effects, and a delay in clinical response have resulted in GKT being reserved for patients who are otherwise unfit for DBS (12).

Non-invasiveness of the MRgFUS is an advantage of MRgFUS over DBS. Class I evidence in the form of an RCT gave a big impetus to MRgFUS (47). In a retrospective analysis of RFA, DBS, and MRgFUS for ET, outcomes of the procedures between the three groups were not statistically different (30). Another retrospective analysis showed comparable efficacy and QOL between unilateral DBS and MRgFUS (54). A recent study compared a trial on the use of VIM DBS for ET, with the RCT done by Elias et al. (47, 55, 56). They found a greater percentage improvement with DBS, although the patients in the DBS group had worse baseline tremor scores.

Long Term Outcome

Sustained improvement in tremor scores has been demonstrated on long term follow up of patients (37, 41, 48, 49). At 3 years of follow up, the patients enrolled in the RCT had a reduction of 56% in hand score, 63% in disability score and a 50% improvement in the QOL (49). At 4 years of follow up in 12 patients, a 56% reduction in hand score and 63% reduction in the disability scores was seen (37). The maximum available follow up of 5 years in two patients revealed a total CRST score of 8.0 (6–10) and QUEST score of 11.0 (6–16), as compared to a baseline score of 46.0 (16–74) and 41.5 (15–93) respectively (41).

A decline in efficacy over time, in the form of a small increase in the hand tremor and disability scores at 3 years as compared to the scores at 6 months has been noted (49). Four patients out of 76 underwent DBS (49). Sinai et al. observed a return of tremor in 11% of their patients (5/44) (41). Further studies with a greater number of patients are needed to refute this observation. The decline in the efficacy over time may be due to the progressive nature of the disease (57). In such cases, it is feasible to treat the patients again and this is certainly a big strength of MRgFUS.

Treatment Parameters

A meta-analysis of the mentioned treatment parameters could not be done due to the unavailability of adequate data for analysis. Some studies in literature have tried to correlate various treatment parameters with the clinical outcome. SDR was significantly associated with the outcome at 1 and 6 months by Sinai et al. (41), while no such relationship was found in other studies (42, 44, 46). The study which included patients with SDR < 0.4 found no statistically significant difference in the mean SDR of patients who had sustained improvement in symptoms and those who had recurrence of symptoms in this study. Traditionally, a SDR value of <0.40 has been associated with higher energy requirements. But recent clinical series investigating this topic have found no significant difference in the clinical outcome or the complication rate in this subgroup as compared to the patients with SDR value > 0.40 (58, 59).

The higher maximal temperature has been found to significantly influence the percentage change in tremor scores (41, 45). Intraoperative tremor reduction has not been found

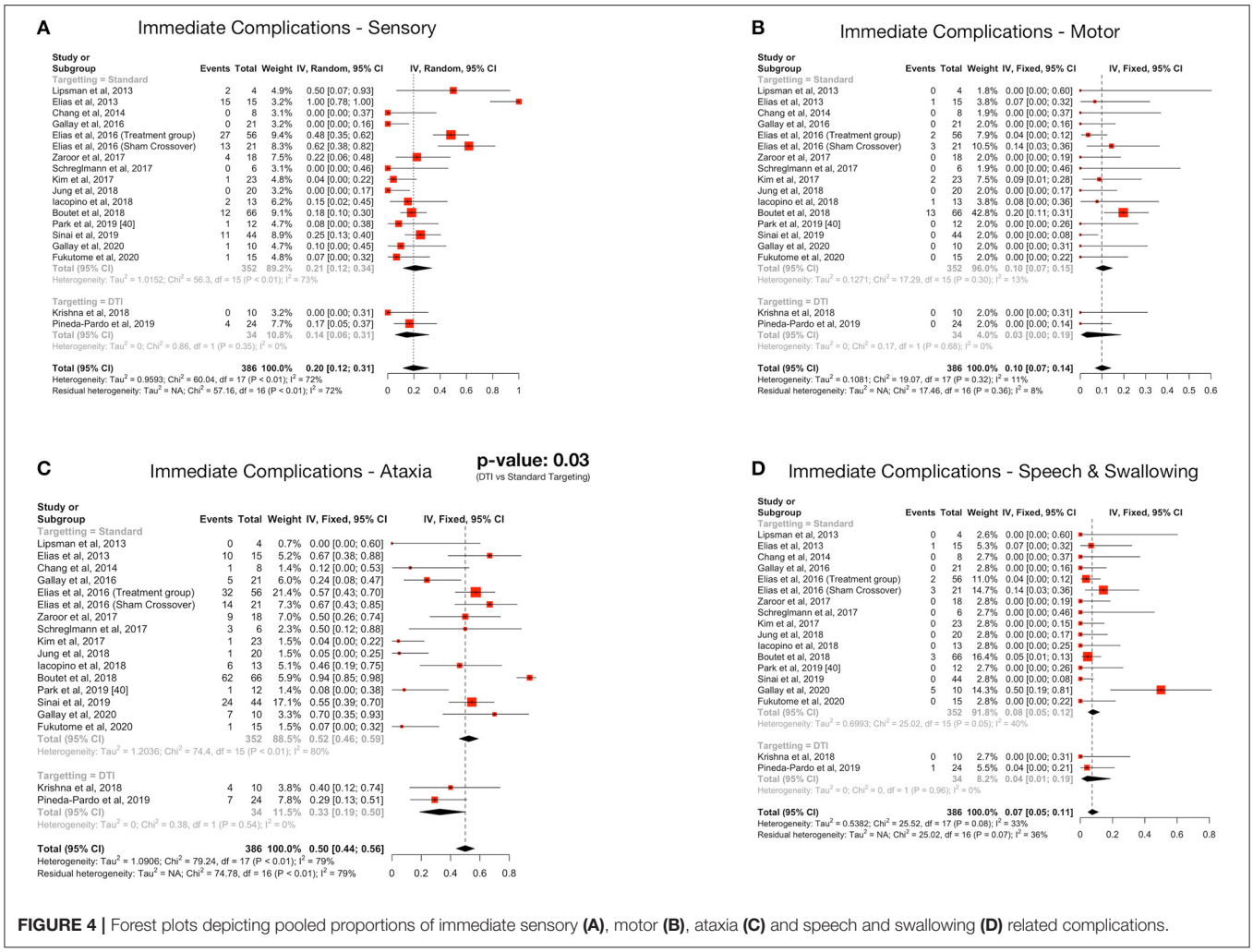

FIGURE 4 | Forest plots depicting pooled proportions of immediate sensory **(A)**, motor **(B)**, ataxia **(C)** and speech and swallowing **(D)** related complications.

to correlate to outcome at 3 months, while procedure duration and number of sonications have been shown to be significantly less with the use of DTI (35). Studies have previously found an association between younger age, short disease duration, better baseline tremor scores, fewer number of sonications and a higher maximal temperature during treatment to a better outcome (35, 44, 46). Experience acquired with the technique has also been found to have a positive impact on the outcome positively (44). It has been recommended by some that the procedure should be restricted to a few specialized centers only (41). Barring three patients who underwent bilateral procedures 1 year apart (27), all FUS procedures have been performed unilaterally. ET is a progressive disease, with most patients having bilateral symptoms (57). Thus, more experience with bilateral procedures is required.

Complications

More than 1/3rd of patients developed sonication related complications, amongst which head pain and dizziness were the most common. This seems to be a significant source of discomfort for the patient. Iacopino et al. (34) reported four patients in whom treatment had to be aborted due to severe head pain. None of the sonication or frame related complications persisted beyond 3 months.

Ataxia, which included gait disturbance and hand ataxia, was the most common neurological side effect, followed by sensory deficits. The immediate pooled proportion of ataxia was 50%, while it was 20% for sensory complications, which is considerable. The high complication rate has been postulated to be due to the small size of the VIM nucleus and non-visibility on MRI resulting in the potential overlap of the lesion with the surrounding structures like the ML and CST. The reason why ataxia is the most common acute complication was suggested to be due to the objective nature of assessment (36). Further, it was demonstrated that the area responsible for postoperative ataxia overlapped significantly with the area associated with clinical benefit (36). Fortunately, data suggests that these complications partially resolve with time as evident by the decreased incidence of late complications (**Table 4**). Furthermore, no additional side effects were observed in each subsequent year of follow up amongst the patients enrolled in the RCT (37, 48, 49). But a major limitation in assessing the long-term complications of the patients undergoing MRgFUS is the high dropout rate (48, 49).

Halpern et al. found it to be as high as 31% in 3 years (49). Thus, a true picture of the permanence of the complications is hard to assess.

No hemorrhage, seizure or trajectory related complications have been noted till now with MRgFUS for ET, making it a uniquely safe procedure in this aspect as compared to DBS or RFA (11, 30, 59).

Role of DTI in Target Localization Technique

VIM nucleus of the thalamus, which has traditionally been used as the target for MRgFUS, is not visible on the 3T MRI and surgeons have to target it based on an atlas or an estimate based on their experience. Microelectrode recording is not possible intra-operatively as the procedure is incisionless. A series of low power sonications, delivered before creating the actual lesion, are usually used to observe the resolution of tremor or the appearance of side effects. However, this method of confirming target accuracy has not been scientifically validated. On the other hand, CTT fibers localized to the PSA have been shown to have a high density of clinically relevant fibers for targeting (53, 60, 61). Gallay et al. were the first to target the CTT using atlas-based co-ordinates (27). Boutet et al. identified distinct areas in the thalamus associated with clinical benefit and complications (36).

Advances in DTI have allowed surgeons to visualize the CTT and individualize surgical targeting accordingly. Both the CST and ML can also be localized, thus clearly demarcating the target according to the unique anatomy of each patient (31, 35, 39, 43). The surgical target thus identified has been found to be anterior and lateral to the atlas-based target (62). This should theoretically lead to better postoperative outcomes. Our analysis revealed a significant reduction in ataxia immediately after DTI based targeting. This is noteworthy as post procedure ataxia has been observed to be an important source of patient discomfort. Thus, use of DTI could decrease patient distress and lead to better acceptability of the procedure. A significant benefit was not apparent on analysis of the other complications. This could be due to the smaller number of studies utilizing DTI. Moreover, it must be emphasized that DTI based targeting is not yet standardized. Differences exist in the number of tracts generated for localization. All the centers have generated the ipsilateral CTT tract (one track) for target localization in the VIM region of the thalamus. Many studies have additionally utilized the ipsilateral CST and ML tracts (three tracks) and adjusted the surgical target accordingly to avoid significant motor and sensory side effects. Anatomical considerations of the CTT tract which originates from the contralateral dentate projections and then decussates in the superior cerebellar peduncle to reach the ipsilateral motor cortex via the thalamus, have led some centers to generate the contralateral CTT tract (four track) in addition to the previously defined three tracks, for refining the target localization (62, 63). Thus, there are differences between the various surgical teams performing DTI based MRgFUS and there is no consensus on what are the best practices although there seems to be an increasing trend to the DTI usage (62–65). The utility of DTI in this regard remains to be definitely proven with additional numbers and long-term data.

Limitations

Observational studies formed the majority basis for the analysis as there is only one clinical trial on the subject. These two types of studies are assessed differently in terms of bias and the strength of evidence, and thus recommendations, that they can offer are markedly different. Authors have used various subsets of the CRST scale to report the outcomes, thus precluding standardized comparison. Few studies included patients who underwent bilateral MRgFUS, which is associated with higher rates of complication. However, the data of these patients was not provided separately and could not be excluded from our analysis. The possibility of some overlap between subsets of patients reported from the same center cannot be completely ruled out. DTI based targeting is a novel procedure, and the number of studies utilizing it are quite low in number. A high level of heterogeneity in between studies needs to be kept in mind.

CONCLUSION

MRgFUS for ET is an effective procedure for relieving unilateral tremor. Use of DTI based targeting revealed a significant reduction in post procedure ataxia related complications as compared to traditional targeting techniques. Analysis of other complications further revealed a decreasing trend on follow up. As of now, it seems to be the procedure of choice for patients unable to tolerate an invasive procedure. For it to replace established surgical options like DBS, further research will be required to prove long term clinical efficacy in both unilateral and bilateral procedures.

DATA AVAILABILITY STATEMENT

The original contributions presented in the study are included in the article/**Supplementary Material**, further inquiries can be directed to the corresponding author/s.

AUTHOR CONTRIBUTIONS

MA and KG: conceptualization, data curation, formal analysis, investigation, methodology, resources, software, roles/writing - original draft, and writing - review and editing. RS, RR, and VN: data curation, visualization, and writing - review and editing. MS: project administration, supervision, and writing - review and editing. All authors contributed to the article and approved the submitted version.

SUPPLEMENTARY MATERIAL

The Supplementary Material for this article can be found online at: https://www.frontiersin.org/articles/10.3389/fneur.2021.654711/full#supplementary-material

REFERENCES

1. Deuschl G, Bain P, Brin M. Consensus statement of the movement disorder society on tremor. Ad Hoc Scientific Committee. *Mov Disord.* (1998) 13 (Suppl. 3):2–23. doi: 10.1002/mds.870131303
2. Bhatia KP, Bain P, Bajaj N, Elble RJ, Hallett M, Louis ED, et al. Consensus statement on the classification of tremors. from the task force on tremor of the International Parkinson and Movement Disorder Society. *Mov Disord.* (2018) 33:75–87. doi: 10.1002/mds.27121
3. Louis ED, Ferreira JJ. How common is the most common adult movement disorder? Update on the worldwide prevalence of essential tremor. *Mov Disord.* (2010) 25:534–41. doi: 10.1002/mds.22838
4. Kamble N, Pal PK. Tremor syndromes: a review. *Neurol India.* (2018) 66 (Suppl. S1):36–47 doi: 10.4103/0028-3886.226440
5. Deuschl G, Raethjen J, Hellriegel H, Elble R. Treatment of patients with essential tremor. *Lancet Neurol.* (2011) 10:148–61. doi: 10.1016/S1474-4422(10)70322-7
6. Schreglmann SR, Krauss JK, Chang JW, Martin E, Werner B, Bauer R, et al. Functional lesional neurosurgery for tremor: back to the future? *J Neurol Neurosurg Psychiatry.* (2018) 89:727–35. doi: 10.1136/jnnp-2017-316301
7. Benabid AL, Pollak P, Gervason C, Hoffmann D, Gao DM, Hommel M, et al. Long-term suppression of tremor by chronic stimulation of the ventral intermediate thalamic nucleus. *Lancet.* (1991) 337:403–6. doi: 10.1016/0140-6736(91)91175-T
8. Benabid AL, Pollak P, Gao D, Hoffmann D, Limousin P, Gay E, et al. Chronic electrical stimulation of the ventralis intermedius nucleus of the thalamus as a treatment of movement disorders. *J Neurosurg.* (1996) 84:203–14. doi: 10.3171/jns.1996.84.2.0203
9. Zesiewicz TA, Elble RJ, Louis ED, Gronseth GS, Ondo WG, Dewey RB Jr, et al. Evidence-based guideline update: treatment of essential tremor: report of the quality standards subcommittee of the American Academy of Neurology. *Neurology.* (2011) 77:1752–5. doi: 10.1212/WNL.0b013e318236f0fd
10. Sankhe M, Churi O. Newer advances in lesional surgery for movement disorders. *Neurol India.* (2018) 66 (Suppl. S1):113–21 doi: 10.4103/0028-3886.226463
11. Wong JK, Hess CW, Almeida L, Middlebrooks EH, Christou EA, Patrick EE, et al. Deep brain stimulation in essential tremor: targets, technology, and a comprehensive review of clinical outcomes. *Expert Rev Neurother.* (2020) 20:319–31. doi: 10.1080/14737175.2020.1737017
12. Schreglmann SR, Krauss JK, Chang JW, Bhatia KP, Kägi G. Functional lesional neurosurgery for tremor: a systematic review and meta-analysis. *J Neurol Neurosurg Psychiatry.* (2018) 89:717–26. doi: 10.1136/jnnp-2017-316302
13. Harary M, Segar DJ, Huang KT, Tafel IJ, Valdes PA, Cosgrove GR. Focused ultrasound in neurosurgery: a historical perspective. *Neurosurg Focus.* (2018) 44:E2. doi: 10.3171/2017.11.FOCUS17586
14. Ranjan M, Elias GJB, Boutet A, Zhong J, Chu P, Germann J, et al. Tractography-based targeting of the ventral intermediate nucleus: accuracy and clinical utility in MRgFUS thalamotomy. *J Neurosurg.* (2019) 1–8. doi: 10.3171/2019.6.JNS19612. [Epub ahead of print].
15. Mohammed N, Patra D, Nanda A. A meta-analysis of outcomes and complications of magnetic resonance-guided focused ultrasound in the treatment of essential tremor. *Neurosurg Focus.* (2018) 44:E4. doi: 10.3171/2017.11.FOCUS17628
16. Schreglmann SR, Bhatia KP, Hägele-Link S, Werner B, Martin E, Kägi G. Letter to the Editor. Errors in the meta-analysis of outcomes and complications of MRgFUS. *Neurosurg Focus.* (2018) 45:E15. doi: 10.3171/2018.3.FOCUS1898
17. Fahn S, Tolosa E, Marin C. Clinical rating scale for tremor. In: Jankovic J, Tolosa E, editors. *Parkinson's Disease and Movement Disorders*. Baltimore, MD: Urban and Schwarzenberg (1988). p. 225–34.
18. Stacy MA, Elble RJ, Ondo WG, Wu SC, Hulihan J. Assessment of interrater and intrarater reliability of the Fahn-Tolosa-Marin tremor rating scale in essential tremor. *Mov Disord.* (2007) 22:833–8. doi: 10.1002/mds.21412
19. Viechtbauer W. Conducting meta-analyses in R with the metafor package. *J Stat Softw.* (2010) 36:1–48. doi: 10.18637/jss.v036.i03
20. Balduzzi S, Rücker G, Schwarzer G. How to perform a meta-analysis with R: a practical tutorial. *Evid Based Ment Health.* (2019) 22:153–60. doi: 10.1136/ebmental-2019-300117
21. Wickham H. *ggplot2: Elegant Graphics for Data Analysis*. New York, NY: Springer-Verlag (2016).
22. Higgins JP, Thompson SG, Deeks JJ, Altman DG. Measuring inconsistency in meta-analyses. *BMJ.* (2003) 327:557–60. doi: 10.1136/bmj.327.7414.557
23. Slim K, Nini E, Forestier D, Kwiatkowski F, Panis Y, Chipponi J. Methodological index for non-randomized studies (minors): development and validation of a new instrument. *ANZ J Surg.* (2003) 73:712–6. doi: 10.1046/j.1445-2197.2003.02748.x
24. Lipsman N, Schwartz ML, Huang Y, Lee L, Sankar T, Chapman M, et al. MR-guided focused ultrasound thalamotomy for essential tremor: a proof-of-concept study. *Lancet Neurol.* (2013) 12:462–8. doi: 10.1016/S1474-4422(13)70048-6
25. Elias WJ, Huss D, Voss T, Loomba J, Khaled M, Zadicario E, et al. A pilot study of focused ultrasound thalamotomy for essential tremor. *N Engl J Med.* (2013) 369:640–8. doi: 10.1056/NEJMoa1300962
26. Chang WS, Jung HH, Kweon EJ, Zadicario E, Rachmilevitch I, Chang JW. Unilateral magnetic resonance guided focused ultrasound thalamotomy for essential tremor: practices and clinicoradiological outcomes. *J Neurol Neurosurg Psychiatry.* (2015) 86:257–64. doi: 10.1136/jnnp-2014-307642
27. Gallay MN, Moser D, Rossi F, Pourtehrani P, Magara AE, Kowalski M, et al. Incisionless transcranial MR-guided focused ultrasound in essential tremor: cerebellothalamic tractotomy. *J Ther Ultrasound.* (2016) 4:5. doi: 10.1186/s40349-016-0049-8
28. Zaaroor M, Sinai A, Goldsher D, Eran A, Nassar M, Schlesinger I. Magnetic resonance-guided focused ultrasound thalamotomy for tremor: a report of 30 Parkinson's disease and essential tremor cases. *J Neurosurg.* (2018) 128:202–10. doi: 10.3171/2016.10.JNS16758
29. Schreglmann SR, Bauer R, Hägele-Link S, Bhatia KP, Natchev P, Wegener N, et al. Unilateral cerebellothalamic tract ablation in essential tremor by MRI-guided focused ultrasound. *Neurology.* (2017) 88:1329–33. doi: 10.1212/WNL.0000000000003795
30. Kim M, Jung NY, Park CK, Chang WS, Jung HH, Chang JW. Comparative evaluation of magnetic resonance-guided focused ultrasound surgery for essential tremor. *Stereotact Funct Neurosurg.* (2017) 95:279–86. doi: 10.1159/000478866
31. Chazen JL, Sarva H, Stieg PE, Min RJ, Ballon DJ, Pryor KO, et al. Clinical improvement associated with targeted interruption of the cerebellothalamic tract following MR-guided focused ultrasound for essential tremor. *J Neurosurg.* (2018) 129:315–23. doi: 10.3171/2017.4.JNS162803
32. Federau C, Goubran M, Rosenberg J, Henderson J, Halpern CH, Santini V, et al. Transcranial MRI-guided high-intensity focused ultrasound for treatment of essential tremor: a pilot study on the correlation between lesion size, lesion location, thermal dose, and clinical outcome. *J Magn Reson Imaging.* (2018) 48:58–65. doi: 10.1002/jmri.25878
33. Jung NY, Park CK, Chang WS, Jung HH, Chang JW. Effects on cognition and quality of life with unilateral magnetic resonance-guided focused ultrasound thalamotomy for essential tremor. *Neurosurg Focus.* (2018) 44:E8. doi: 10.3171/2017.11.FOCUS17625
34. Iacopino DG, Gagliardo C, Giugno A, Giammalva GR, Napoli A, Maugeri R, et al. Preliminary experience with a transcranial magnetic resonance-guided focused ultrasound surgery system integrated with a 1.5-T MRI unit in a series of patients with essential tremor and Parkinson's disease. *Neurosurg Focus.* (2018) 44:E7. doi: 10.3171/2017.11.FOCUS17614
35. Krishna V, Sammartino F, Agrawal P, Changizi BK, Bourekas E, Knopp MV, et al. Prospective tractography-based targeting for improved safety of focused ultrasound thalamotomy. *Neurosurgery.* (2019) 84:160–8. doi: 10.1093/neuros/nyy020
36. Boutet A, Ranjan M, Zhong J, Germann J, Xu D, Schwartz ML, et al. Focused ultrasound thalamotomy location determines clinical benefits in patients with essential tremor. *Brain.* (2018) 141:3405–14. doi: 10.1093/brain/awy278
37. Park YS, Jung NY, Na YC, Chang JW. Four-year follow up results of magnetic resonance-guided focused ultrasound thalamotomy for essential tremor. *Mov Disord.* (2019) 34:727–34. doi: 10.1002/mds.27637
38. Hori H, Yamaguchi T, Konishi Y, Taira T, Muragaki Y. Correlation between fractional anisotropy changes in the targeted ventral intermediate nucleus and clinical outcome after transcranial MR-guided focused ultrasound thalamotomy for essential tremor: results of a pilot study. *J Neurosurg.* (2019) 132:568–73. doi: 10.3171/2018.10.JNS18993

39. Pineda-Pardo JA, Martínez-Fernández R, Rodríguez-Rojas R, Del-Alamo M, Hernández F, Foffani G, et al. Microstructural changes of the dentato-rubro-thalamic tract after transcranial MR guided focused ultrasound ablation of the posteroventral VIM in essential tremor. *Hum Brain Mapp.* (2019) 40:2933–42. doi: 10.1002/hbm.24569
40. Jones RM, Kamps S, Huang Y, Scantlebury N, Lipsman N, Schwartz ML, et al. Accumulated thermal dose in MRI-guided focused ultrasound for essential tremor: repeated sonications with low focal temperatures. *J Neurosurg.* (2019) 132:1802–9. doi: 10.3171/2019.2.JNS182995
41. Sinai A, Nassar M, Eran A, Constantinescu M, Zaaroor M, Sprecher E, et al. Magnetic resonance-guided focused ultrasound thalamotomy for essential tremor: a 5-year single-center experience. *J Neurosurg.* (2019) 1–8. doi: 10.3171/2019.3.JNS19466. [Epub ahead of print].
42. Chang KW, Park YS, Chang JW. Skull factors affecting outcomes of magnetic resonance-guided focused ultrasound for patients with essential tremor. *Yonsei Med J.* (2019) 60:768–73. doi: 10.3349/ymj.2019.60.8.768
43. Miller TR, Zhuo J, Eisenberg HM, Fishman PS, Melhem ER, Gullapalli R, et al. Targeting of the dentato-rubro-thalamic tract for MR-guided focused ultrasound treatment of essential tremor. *Neuroradiol J.* (2019) 32:401–7. doi: 10.1177/1971400919870180
44. Krishna V, Sammartino F, Cosgrove R, Ghanouni P, Schwartz M, Gwinn R, et al. Predictors of outcomes after focused ultrasound thalamotomy. *Neurosurgery.* (2020) 87:229–37. doi: 10.1093/neuros/nyz417
45. Gallay MN, Moser D, Jeanmonod D. MR-guided focused ultrasound cerebellothalamic tractotomy for chronic therapy-resistant essential tremor: anatomical target reappraisal and clinical results. *J Neurosurg.* (2020) 1–10. doi: 10.3171/2019.12.JNS192219. [Epub ahead of print].
46. Fukutome K, Kuga Y, Ohnishi H, Hirabayashi H, Nakase H. What factors impact the clinical outcome of magnetic resonance imaging-guided focused ultrasound thalamotomy for essential tremor? *J Neurosurg.* (2020) 1–6. doi: 10.3171/2020.2.JNS192814. [Epub ahead of print].
47. Elias WJ, Lipsman N, Ondo WG, Ghanouni P, Kim YG, Lee W, et al. A randomized trial of focused ultrasound thalamotomy for essential tremor. *N Engl J Med.* (2016) 375:730–9. doi: 10.1056/NEJMoa1600159
48. Chang JW, Park CK, Lipsman N, Schwartz ML, Ghanouni P, Henderson JM, et al. A prospective trial of magnetic resonance-guided focused ultrasound thalamotomy for essential tremor: results at the 2-year follow-up. *Ann Neurol.* (2018) 83:107–14. doi: 10.1002/ana.25126
49. Halpern CH, Santini V, Lipsman N, Lozano AM, Schwartz ML, Shah BB, et al. Three-year follow-up of prospective trial of focused ultrasound thalamotomy for essential tremor. *Neurology.* (2019) 93:e2284–93. doi: 10.1212/WNL.0000000000008561
50. Yang AI, Chaibainou H, Wang S, Hitti FL, McShane BJ, Tilden D, et al. Focused ultrasound thalamotomy for essential tremor in the setting of a ventricular shunt: technical report. *Oper Neurosurg.* (2019) 17:376–81. doi: 10.1093/ons/opz013
51. Paff M, Boutet A, Neudorfer C, Elias GJB, Germann J, Loh A, et al. Magnetic resonance-guided focused ultrasound thalamotomy to treat essential tremor in nonagenarians. *Stereotact Funct Neurosurg.* (2020) 98:182–6. doi: 10.1159/000506817
52. Buch VP, McShane BJ, Beatson N, Yang A, Blanke A, Tilden D, et al. Focused ultrasound thalamotomy with dentato-rubro-thalamic tractography in patients with spinal cord stimulators and cardiac pacemakers. *Stereotact Funct Neurosurg.* (2020) 98:263–9. doi: 10.1159/000507031
53. Schuurman PR, Bosch DA, Bossuyt PM, Bonsel GJ, van Someren EJ, de Bie RM, et al. A comparison of continuous thalamic stimulation and thalamotomy for suppression of severe tremor. *N Engl J Med.* (2000) 342:461–8. doi: 10.1056/NEJM200002173420703
54. Huss DS, Dallapiazza RF, Shah BB, Harrison MB, Diamond J, Elias WJ. Functional assessment and quality of life in essential tremor with bilateral or unilateral DBS and focused ultrasound thalamotomy. *Mov Disord.* (2015) 30:1937–43. doi: 10.1002/mds.26455
55. Harary M, Segar DJ, Hayes MT, Cosgrove GR. Unilateral thalamic deep brain stimulation versus focused ultrasound thalamotomy for essential tremor. *World Neurosurg.* (2019) 126:e144–52. doi: 10.1016/j.wneu.2019.01.281
56. Wharen RE Jr, Okun MS, Guthrie BL, Uitti RJ, Larson P, Foote K, et al. Thalamic DBS with a constant-current device in essential tremor: a controlled clinical trial. *Parkinsonism Relat Disord.* (2017) 40:18–26. doi: 10.1016/j.parkreldis.2017.03.017
57. Louis ED, Agnew A, Gillman A, Gerbin M, Viner AS. Estimating annual rate of decline: prospective, longitudinal data on arm tremor severity in two groups of essential tremor cases. *J Neurol Neurosurg Psychiatry.* (2011) 82:761–5. doi: 10.1136/jnnp.2010.229740
58. D'Souza M, Chen KS, Rosenberg J, Elias WJ, Eisenberg HM, Gwinn R, et al. Impact of skull density ratio on efficacy and safety of magnetic resonance-guided focused ultrasound treatment of essential tremor. *J Neurosurg.* (2019) 132:1392–7. doi: 10.3171/2019.2.JNS183517
59. Boutet A, Gwun D, Gramer R, Ranjan M, Elias GJB, Tilden D, et al. The relevance of skull density ratio in selecting candidates for transcranial MR-guided focused ultrasound. *J Neurosurg.* (2019) 132:1785–91. doi: 10.3171/2019.2.JNS182571
60. Gallay MN, Jeanmonod D, Liu J, Morel A. Human pallidothalamic and cerebellothalamic tracts: anatomical basis for functional stereotactic neurosurgery. *Brain Struct Funct.* (2008) 212:443–63. doi: 10.1007/s00429-007-0170-0
61. Blomstedt P, Sandvik U, Fytagoridis A, Tisch S. The posterior subthalamic area in the treatment of movement disorders: past, present, and future. *Neurosurgery.* (2009) 64:1029–38. Discussion 1038–1042. doi: 10.1227/01.NEU.0000345643.69486.BC
62. Sammartino F, Krishna V, King NK, Lozano AM, Schwartz ML, Huang Y, et al. Tractography-based ventral intermediate nucleus targeting: novel methodology and intraoperative validation. *Mov Disord.* (2016) 31:1217–25. doi: 10.1002/mds.26633
63. Yamada K, Akazawa K, Yuen S, Goto M, Matsushima S, Takahata A, et al. MR imaging of ventral thalamic nuclei. *AJNR Am J Neuroradiol.* (2010) 31:732–5. doi: 10.3174/ajnr.A1870
64. Soares JM, Marques P, Alves V, Sousa N. A hitchhiker's guide to diffusion tensor imaging. *Front Neurosci.* (2013) 7:31. doi: 10.3389/fnins.2013.00031
65. O'Donnell LJ, Westin CF. An introduction to diffusion tensor image analysis. *Neurosurg Clin N Am.* (2011) 22:185–96. doi: 10.1016/j.nec.2010.12.004

Conflict of Interest: The authors declare that the research was conducted in the absence of any commercial or financial relationships that could be construed as a potential conflict of interest.

frontiers in Neurology

SYSTEMATIC REVIEW
published: 17 June 2021
doi: 10.3389/fneur.2021.669449

MRI Guided Focused Ultrasound-Mediated Delivery of Therapeutic Cells to the Brain: A Review of the State-of-the-Art Methodology and Future Applications

*Nabid Ahmed, Dheeraj Gandhi, Elias R. Melhem and Victor Frenkel**

Department of Diagnostic Radiology and Nuclear Medicine, and Department of Neuroradiology, University of Maryland School of Medicine, Baltimore, MD, United States

OPEN ACCESS

Edited by:
Vibhor Krishna,
The Ohio State University,
United States

Reviewed by:
Roberto Eleopra,
Fondazione IRCCS Istituto Neurologio Carlo Besta, Italy
Francesco Di Lorenzo,
Santa Lucia Foundation (IRCCS), Italy
Yuexi Huang,
Sunnybrook Research Institute (SRI), Canada

****Correspondence:***
Victor Frenkel
vfrenkel@som.umaryland.edu

Specialty section:
This article was submitted to Experimental Therapeutics, a section of the journal Frontiers in Neurology

Received: *18 February 2021*
Accepted: *14 May 2021*
Published: *17 June 2021*

Citation:
Ahmed N, Gandhi D, Melhem ER and Frenkel V (2021) MRI Guided Focused Ultrasound-Mediated Delivery of Therapeutic Cells to the Brain: A Review of the State-of-the-Art Methodology and Future Applications. Front. Neurol. 12:669449. doi: 10.3389/fneur.2021.669449

Stem cell and immune cell therapies are being investigated as a potential therapeutic modality for CNS disorders, performing functions such as targeted drug or growth factor delivery, tumor cell destruction, or inflammatory regulation. Despite promising preclinical studies, delivery routes for maximizing cell engraftment, such as stereotactic or intrathecal injection, are invasive and carry risks of hemorrhage and infection. Recent developments in MRI-guided focused ultrasound (MRgFUS) technology have significant implications for treating focal CNS pathologies including neurodegenerative, vascular and malignant processes. MRgFUS is currently employed in the clinic for treating essential tremor and Parkinson's Disease by producing precise, incisionless, transcranial lesions. This non-invasive technology can also be modified for non-destructive applications to safely and transiently open the blood-brain barrier (BBB) to deliver a range of therapeutics, including cells. This review is meant to familiarize the neuro-interventionalist with this topic and discusses the use of MRgFUS for facilitating cellular delivery to the brain. A detailed and comprehensive description is provided on routes of cell administration, imaging strategies for targeting and tracking cellular delivery and engraftment, biophysical mechanisms of BBB enhanced permeability, supportive proof-of-concept studies, and potential for clinical translation.

Keywords: central nervous system diseases, cellular therapy, MRI-guided focused ultrasound, blood-brain barrier, cellular tracking

INTRODUCTION

Neurologic Cellular Therapies

Treating CNS disorders with cells were trialed first in the late 1980s, when patients with Parkinson's disease (PD) and Huntington's disease (HD) underwent intrastriatal injections of fetal mesencephalic tissue. Modest improvements in motor and cognitive function were noted in PD patients, but survival of transplanted fetal dopaminergic cells was low, and a cohort of patients also developed post-engraftment dyskinesias, possibly due to patchy reinnervation (1). Engraftment was verified via increased PET signaling in HD patients (2), but one patient was noted to have graft tissue overgrowth in a 5-year follow-up, demonstrating a potential risk of fetal tissue implantation

(3). Despite these limitations, the pilot trials motivated future research into using exogenous cells to treat CNS disease, especially from sources that did not raise the ethical concerns involved with fetal tissue. Over time, the consensus on the mechanistic goal of this strategy shifted from outright cell replacement toward the inclusion of more complex functions, including local immunomodulation, inducing differentiation of endogenous stem cells, or encapsulating small molecular drugs for controlled release. Compared to other therapeutic vehicles (liposomes and nanoparticles), the biological machinery of a therapeutic cell can be exploited for their natural signaling networks, migration behaviors, and endosomal compartmentalization. Moreover, cells can be genetically engineered *in vitro* to express neurotrophic factors (4), enzymes to convert innocuous prodrugs into active forms for targeted therapies (5), or chimeric antigen ligands designed to target specific pathologic cell markers for more targeted therapy (6). They can also be designed to contain built-in suicide genes to ensure that they are not retained longer than intended or undergo mutation (7).

Stem Cells

Research probing the biochemical and mechanical underpinnings of stem cell differentiation continues to grow with ever increasing preclinical and clinical studies. Stem cells maintain their definition as undifferentiated cells with self-renewal capacity that are mainly classified based on "potency," or capacity to develop into one or all of the three germ layers; further classification schemes are based on sourcing technique or location. Human Embryonic Stem Cells (hESCs) and induced Pluripotent Stem Cells (iPSCs) exhibit pluripotency i.e., capacity to differentiate into somatic cells of all three embryonic germ layers. Applications employing hESCs, which are derived from the embryonic inner cell mass, are limited due to ethical constraints and the risk of tumorigenicity if not fully differentiated into the tissue of interest. iPSCs are created via transfecting somatic cells (e.g., from the skin or peripheral blood) with reprogramming transcriptional factors (8). Clinical grade, human PSCs (hPSCs) for direct differentiation into midbrain dopamine neurons, for example, are currently being developed for the treatment of PD (9). While patient-derived lines that circumvent immune rejection is promising, challenges still include maximizing reprogramming efficiency and overcoming costs of expansion and safety testing (10, 11). Adult stem cells (neural, mesenchymal, hematopoietic, colonic epithelial) exhibit multipotency i.e., capacity to differentiate into a somatic cell of their respective germ layer. These reside within "stem cell niches" that have been identified in several organ tissues and either continuously proliferate and differentiate (e.g., colonic stem cells) or lie dormant until receiving molecular cues after injury (12).

Neural stem cells (NSCs) and Mesenchymal stem cells (MSCs) are common stem cell types under study for neurologic cell therapies. NSCs were discovered to reside within the subventricular zone of the lateral ventricles and subgranular zone of the dentate gyrus, two areas of adult neurogenesis which have been implicated in learning, memory and mood regulation (13, 14). The NSC migratory and differentiation functions are influenced by a network of supportive cells that provide synaptic input, transcriptional signals, and epigenetic cues (15). NSCs have been therapeutically exploited for their cell replacement potential in becoming neuronal or glial progenitor cells, producing neurotrophic factors that promote neuronal growth, and for delivering a variety of anticancer payloads (16). Isolating large therapeutic quantities of autologous NSCs directly from a patient, however, is challenging. Two recently developed harvesting techniques are being evaluated comparatively. One involves directly transforming adult somatic cells into a NSC (i.e., "transdifferentiation") (17), while the other differentiates iPSCs to create "induced" NSCs (iNSCs) (18). MSCs reside in multiple areas in the body including bone marrow, dental pulp, adipose tissue, umbilical cord blood and amniotic fluid, conferring their ability to be sourced relatively easier than NSCs. MSCs have been shown to cross the BBB and home to primary and metastatic tumors of the brain through chemokine signaling (19, 20). The pleiotropic functions of MSCS (growth factor secretion, immunomodulation, neuroprotection, angiogenesis, anti-apoptosis, inducing differentiation) (21) are undergoing rigorous study for therapeutic intent, shifting the focus from MSC mediated regeneration potential toward exploiting MSC "medicinal signaling" (22). Another promising component of MSC therapy involves its natural cell-cell communication ability via exosomes, nanometer-sized lipid membrane bound vesicles that secrete a variety of cargo molecules to maintain tissue homeostasis (23). Drug encapsulation using exosomes can extend the agent's half-life, and maximize targeted and controlled delivery with minimal effects on healthy tissues (24). This can be beneficial in cases where a biologic therapeutic (e.g., cytokines, miRNA, growth factors) may either have difficulty reaching the pathologic cerebral area, or cause systemic side effects if delivered on their own (e.g., inflammatory reactions from systemic IL-2).

Immune Cells

Immune cell delivery is the other arm of CNS cellular therapies currently being investigated, mainly in the context of treating malignancy, but more recently also being explored for neurodegenerative conditions (25). One of the primary findings of small animal studies, which established the new experimental domain of natural killer (NK) cell therapeutics, was their ability to recognize and kill human glioblastoma (GBM) cells through direct cell-mediated cytotoxicity (26). As NK cells account for only ∼3% of circulating immune cells, autologous harvesting would not be able to reach therapeutic levels, and expansion *ex vivo* would be required. Many clinical trials use the immortalized NK-92 cell line, due to relative ease of expansion and implementation (compared to autologous harvesting). To circumvent the immunosuppressive environment of brain tumors, which downregulates NK activity, NK cells can be engineered *ex vivo* to overexpress activating cytokines (Il-12 or IL-15) to form "activated" NK cells, which increases tumor cell killing efficacy (27). The clinical success of chimeric antigen receptors in T-cells (CAR-T cells) for treating lymphoblastic leukemias shows promise toward implementing a

similar strategy using NK cells, a lymphoid relative of T-cells, for solid brain malignancies (28). The use of CAR-T cells is an evolving form of cancer immunotherapy, in which autologously or allogeneic derived T-cells are genetically modified to target and attack specific cancer cells via chimeric antigen receptor binding (29, 30).

ROUTES OF ADMINISTRATION FOR CELLULAR THERAPY

The route of administering therapeutic cells into pathologic intracerebral regions plays a critical role toward successful implantation. The BBB is a multicellular capillary network that protects the brain parenchyma from intrusion of foreign pathogens and neurotoxins, and regulates cerebral perfusion and flux of ions, hormones, and glucose to ensure normal functioning of neuronal circuits. Therapeutic cells must either circumvent the BBB or be functionalized to utilize one of many transmigratory pathways of the BBB for access to the target site (31).

Intracerebral injections offer the most direct access for cellular implantation, by bypassing the BBB. However, the stereotactic technique can carry increased risk of hemorrhage and infection (32). This method is also less appealing due to the limited effective volume of delivery, especially for larger agents (33). Intrathecal administration bypasses the BBB via injection of the therapeutic agent or cell directly into the subarachnoid space and the CSF. This approach is mainly utilized for treating leptomeningeal disease, delivering chemotherapeutics for leptomeningeal disease (34), and baclofen for analgesia (35). For parenchymal disease, intrathecal administration of cells may have limitations due to the rapid turnover of CSF (i.e., minimizing interaction time between the cell therapy and brain-CSF barrier) (31).

Vascular routes of administration include intra-arterial (IA) and intravenous (IV) administration, and are commonly employed for procedural simplicity. There was initial concern for the IV route being a potential nidus for pulmonary thromboembolism (36), but a recent systematic review of 47 randomized clinical trials utilizing intravascular administration of MSCs found no statistically significant risk of embolic complications compared to controls (37). Nevertheless, studies report injected cells accumulating within the microvasculature of the lung, i.e., a "pulmonary trapping" effect (38), leading to decreased cell engraftment at the treatment target. Intracarotid (i.e., IA) injections can bypass filtering organs and allow cells to reach the CNS to a greater degree than by IV (39).

Hyperosmolar BBB disruption involves intravascular delivery of an agent, typically mannitol, that increases oncotic pressure and drives fluid outside of microvascular epithelial cells, causing shrinkage and thus paracellular passage of therapeutics, including stem cells, into the brain (40). A drawback of this procedure is that it may lead to increases in BBB permeability in off-target brain regions. This would for example, allow greater exposure to endogenous neurotoxins (i.e., albumin), which may result in adverse effects that include vaso-vagal responses and focal seizures (31). Due to the risk of compounding vasogenic edema, using this approach to treat an entire multifocal CNS disorder that presides over separate cerebrovascular regions may not be feasible to complete in a single treatment session and may have to be divided over multiple periods (41).

Intranasal delivery is a developing administration approach that is not yet fully understood but thought to bypass the BBB by relying on migration along olfactory and trigeminal nerve tracts and into CSF flow tracts (42). Many studies have demonstrated higher CSF levels of chemotherapeutics, small molecular drugs, and nanoparticles using this innovative approach, relative to conventional intravenous routes. However, this strategy may be limited by clearance from the ciliated mucosal epithelium (43).

Implantable devices such as the Ommaya reservoir have successfully been used for delivering growth factors, analgesics and chemotherapy directly into CSF circulation. This approach has notable drawbacks that would preclude the delivery of cells due to clogging and pump failure (44). Collectively, limitations encountered by these routes may include invasiveness, low rates of engraftment, and low target region specificity. The common cell administration routes implemented in preclinical and clinical trials, each with their specific advantages and disadvantages, are summarized in **Table 1**.

MRgFUS TECHNOLOGY AND CLINICAL APPLICATIONS

Choosing one of the aforementioned delivery routes is governed by specific preferences such as the required accuracy of targeting or minimizing the degree of invasiveness. The choice can also be dictated by characteristics of the CNS pathology, such as focality. A condition like PD for example has lesions typically occurring in one region compared to Multiple Sclerosis (MS) where lesions are in multiple regions. Engraftment rates of cells in some studies have not been encouraging. For example, one study investigating IV injection of MSCs into a traumatic brain injury (TBI) rat model yielded $<4\%$ of cells reaching arterial circulation (51). Therefore, a growing number of researchers have been investigating the use of focused ultrasound (FUS) under MRI guidance (MRgFUS) to pre-treat focal pathologic regions for enhancing cell delivery. MRgFUS is a non-invasive modality that is advantageous for its spatial specificity and minimal off-target effects. MRgFUS technology is gaining substantial interest for its ability to provide controlled, non-invasive, and targeted therapeutic ultrasound energy, which can be adjusted to create a variety of beneficial biological effects for treatments in the brain (52). These specific effects include destructive thermal ablation (53, 54), radiosensitization (55), immune activation (56, 57), BBB opening for therapeutic delivery (58, 59), and stem cell homing (60, 61).

The variation in induced effects is controlled by the mode of application, which can be continuous or pulsed (i.e., non-continuous), and further modified by varying the duration and intensity of the applied ultrasound energy. Thermal tissue effects predominate with continuous exposures, and temperatures can rise to 60°C in the focal region within seconds, leading to tissue

TABLE 1 | Administration routes for intracerebral cellular therapy.

Technique		Advantages/Disadvantages	Ref
Intraparenchymal (Stereotactic injection)	**ADV:**	Bypasses BBB; most direct access to CNS region of pathology, high engraftment rate	(45)
	DIS:	Invasive (risk of hemorrhage, infection, injury to normal tissue), glial scar formation, not feasible in poor surgical candidates	
Intrathecal (Injection)	**ADV:**	Bypasses BBB	(46)
	DIS:	Invasive, high CSF turnover	
Intrathecal Device	**ADV:**	Bypasses BBB	(47)
	DIS:	Invasive, device failure (improper dosage, cell death inside reservoir, clogging)	
Intranasal	**ADV:**	Bypasses BBB, Least invasive	(48)
	DIS:	Poor engraftment rates, targeting, cells required to migrate long distances	
Systemic (IA)	**ADV:**	Higher cell engraftment compared to IV	(39)
	DIS:	Embolism risk, non-specific targeting	
Systemic (IV)	**ADV:**	Relatively less invasive than IA	(49)
	DIS:	Pulmonary trapping effect Reticuloendothelial trapping (liver, spleen)	
Hyperosmotic BBB disruption	**ADV:**	Higher cell engraftment compared to IV	(50)
	DIS:	Embolism risk, non-specific targeting	

destruction by the process of coagulative necrosis. With pulsed FUS (pFUS) exposures, mechanical tissue effects predominate, and temperature elevations are minimal (within the range 4–5°C) (62–64). Globally, focused ultrasound ablative therapies have been approved and implemented for thyroid nodules, bone metastases, uterine fibroids, and tumors of the liver, pancreas, kidney, prostate, and breast. With regards to intracranial applications, the FDA approved MRgFUS ablation for essential tremor in 2016, and recently tremor-dominant PD in 2018[1] These two milestones have provided the motivation for more preclinical and clinical studies to be proposed and developed. To date, up to 2000 patients in the US have undergone MRgFUS treatments for either the aforementioned FDA-approved indications or in new clinical studies for the treatment of neuropathic pain (NCT03111277), AD (NCT04118764), epilepsy (NCT02804230), obsessive compulsive disorder (NCT03156335), ALS (NCT03321487), and brain malignancies (NCT00147056).

FUS Mediated BBB Opening

Reliable BBB opening (BBBO) is achieved with the combination of MRgFUS and IV injection of ultrasound contrast agents (i.e., microbubbles, MBs) which are typically 1–10 micron lipid or albumin based spheres containing a bio-inert gas. Early pFUS studies without using MBs demonstrated that meaningful mechanical effects, such as those required for permeabilizing the BBB, could not be generated without the presence of tissue damage (65). A landmark study by Hynynen et al. found that incorporating MBs significantly improved the clinical feasibility of the technique. It allowed for finer control of BBB permeability and required lower intensities, lessening the risk of skull heating and damage (66). After injection, the MBs travel throughout the circulatory system and eventually reach the capillaries within the target volume of the FUS transducer.

Acoustic cavitation is one of the non-thermal pFUS based mechanisms for generating bioeffects. This occurs in the form of expansion of the MBs during the negative pressure part of the ultrasound cycle and contraction during the positive pressure part. Upon pFUS exposure, the MBs transmit these mechanical oscillations onto the endothelial cells, which can alter BBB permeability. Low pressure amplitudes, in which MB oscillations remain stable (i.e., non-inertial cavitation), are employed to induce transient BBB opening through a number of proposed paracellular and transcellular mechanisms. If the pressure amplitude becomes too high, the MBs undergo unstable oscillations (i.e., inertial cavitation) where they expand and eventually collapse. This is undesirable in BBBO where shock waves generated can damage cells of the microvasculature. Hence, monitoring for cavitation is crucial for this application of MRgFUS (67).

Most human MRgFUS treatments in the brain are performed using a hemispherical 1,024-element ultrasound transducer array that communicates with the MRI system (**Figure 1**). Each of the contiguous transducer elements is driven by an individual power source. Depending on the treatment target, specific individual elements will be activated, where the beams converge (i.e., at the "focus"), which is electronically steered in 3-dimensional space within the brain. Important to note is that the acoustic power applied to each element is typically incapable of inducing a deleterious biological effect. However, the additive power at the focus is sufficient to thermally ablate tissue, or conversely, generate the mechanical effects designed for opening the BBB. Real-time acoustic monitoring of cavitation determines optimal sonication parameters during the procedure. The transducer is fitted to the patient's head via a stereotactic frame affixed to the scalp under local anesthetic. The patient's head is coupled to the transducer via a flexible silicone membrane. The closed membrane contains degassed water for effective transmission of the ultrasound energy. The patient lies awake on the MRI table throughout the procedure and is able to respond to questions to ensure no adverse symptoms are being experienced.

Pre-procedural T1, T2 and T2* images are obtained from the MRI scanner and transferred to the MRgFUS graphic user

[1]https://www.fusfoundation.org/.

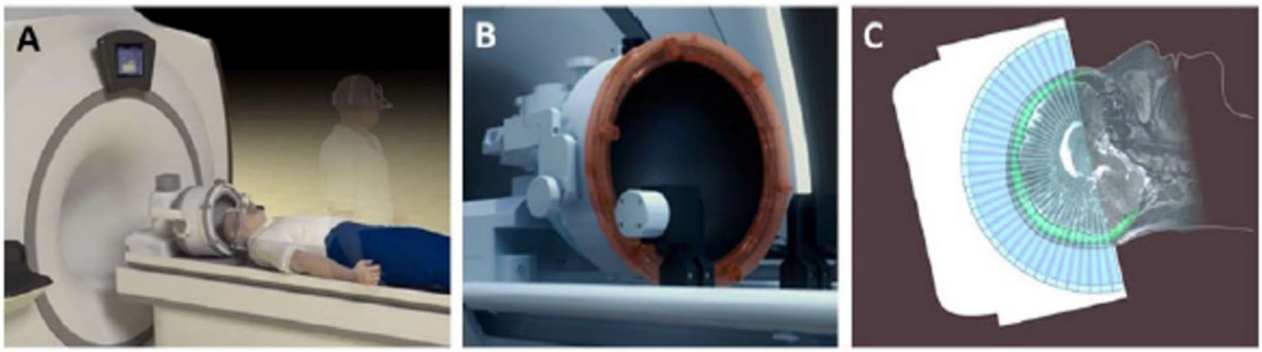

FIGURE 1 | Set-up of MRgFUS patient treatment. **(A)** A schematic representation of patient lying supine on MR table being fitted with FUS phased-array transducer array; **(B)**, Close up of the 1,024 ultrasound element array for electronic steering of the ultrasound beam. **(C)** A schematic 2-dimensional representation of the multiple ultrasound beams focused non-invasively through the skull (bright green) to a single target. The image of the skull is obtained from a prior computed tomographic scan that is mechanically registered to the MR image. Information from the skull is used by the planning software to correct for aberrations to the beam paths and accurately position the focus at the desired target. Adapted from *Fishman and Frenkel, Journal of Central Nervous System Disease 2017* (68). Reprinted with permission from SAGE Publishing.

interface (GUI). The target treatment volume is identified using an overlay on the MR images. The location of the region of treatment will determine which of the 1,024 ultrasound transducer elements will be activated during treatment. The beam is then steered electronically, automatically rastering (i.e., moving from point to point) through the treatment volume with user defined spacing (69).

Immediately prior to the beginning of treatment, a suspension of MBs is then injected intravenously. Before administering full sonication treatments, a "power-ramp" test is done at each region to determine the minimal power output that opens the BBB for that specific patient. Short sonications to the region are applied incrementing in power at 5% intervals until cavitation is detected with the use of an acoustic feedback controller via hydrophone measurement. The full sonications are then delivered at 50% power of the determined cavitation threshold (70). Real time MR thermometry is employed to ensure tissue temperatures that create irreversible change in surrounding tissues are not reached during BBBO (71). After sonication treatments are complete, gadolinium enhanced T1 imaging, which has been shown to correlate to the degree of BBBO and therapeutic delivery, is obtained for verification (72). Transient BBBO with MRgFUS was successfully verified and determined to be safe in patients with Glioblastoma (NCT03551249; NCT03616860), Alzheimer's Disease (AD) (NCT04118764), and more recently Amyotrophic Lateral Sclerosis (ALS) (NCT03321487). Trials for PD (NCT04370665) and HER2 amplified brain metastases (NCT03714243) are currently underway (73–75). Additional clinical trials exploring other direct effects of BBB opening (e.g., glial cell activation, amyloid beta plaque clearance, neurogenesis) for neurodegenerative diseases (NCT03739905) are planned (76). As effects of BBB-opening have been shown to last from 4–8 h, (67) therapeutic cells could then be administered intravenously or intra-arterially within this window.

MRgFUS-MEDIATED CELL DELIVERY

Preclinical Studies of MRgFUS-Mediated Cell Delivery

Successful MRgFUS assisted cell delivery was first demonstrated using a combined approach of intracarotid injection of dual GFP/Iron Oxide-labeled NSCs and MRgFUS targeted to the striatum and hippocampus. The goal of this study was to demonstrate the feasibility, reversibility, and safety of this approach over conventional methods (i.e., injection and hyperosmolar BBBO). Histological analysis showed limited damage and red blood cell extravasation in non-target areas, and 32 viable NSCs per square millimeter of sonicated brain tissue, with neuronal specific biomarkers present 4–24 h after treating (77). Another study using bone marrow MSCs administered IV with FUS treatments to the lateral hippocampal area, demonstrated a 2-fold increase in engraftment rate compared to IV injection alone. FUS treatments also show increased expression of the cell adhesion molecules (CAM), including ICAM and VCAM, which is thought to improve targeting of the cells (78).

In addition to stem cells, immune cells have also been investigated using MRgFUS BBBO. CAR NK-92 cells were administered IV in a murine model of HER2-amplifed brain metastasis. Interestingly, IV injection of the NK cells immediately before BBBO resulted in a 5-fold increase in the number of cells observed to be delivered compared to injecting cells after BBBO (79). A follow-up study investigated survival in this model using temporally different pFUS treatment protocols. A "front-loaded" group, which concentrated pFUS treatments in the 1st week of treatment, was found to have greater survival relative to controls, whereas the group that had more equally distributed treatments did not show improvement (80). This finding introduced more questions to be investigated, such as how treatment frequency affects therapeutic cell delivery, or

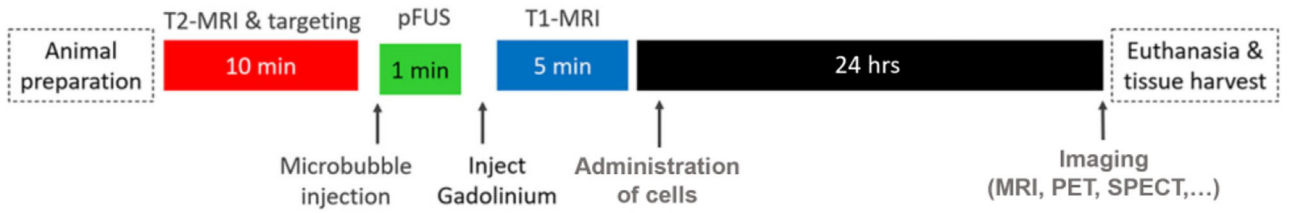

FIGURE 2 | Typical timeline for an MRgFUS preclinical study investigating cellular delivery. Adapted from *Shen et al. Cell Transplantation 2017* (81). Reprinted with permission from SAGE Publishing.

if these treatments become inefficacious as intracranial tumor burden passes a certain threshold.

Investigations evaluating the potential of magnetic enhancement of MRgFUS for cellular delivery were also conducted. Dual labeled, fluorescent/super paramagnetic iron-oxide nanoparticle (SPION), human NPCs (hNPCs) were administered following MRgFUS BBBO. The procedural timeline for this study is shown in **Figure 2**. Three different magnets were then evaluated, positioned in the head region of the treated rats following the injections. Increasing magnet strength was found to be correlated with higher ratios of SPION labeled hNPCs to non-SPION labeled hNPCs observed in the treated brains (**Figure 3**) (81). This procedure, using MRgFUS and an external magnet, was previously demonstrated for brain delivery of magnetic nanoparticles on their own (82). Whether the addition of magnetic cell labeling and targeting to a pFUS approach provides a clinically significant improvement will have to be determined.

More recently, BBBO via low intensity ultrasound was evaluated in a brain-ischemia rat model, induced by middle-cerebral artery occlusion. Although this study was limited by using unfocused low intensity ultrasound and not pFUS, the results are noteworthy in that they demonstrated significant increases in IV-administered MSC engraftment and slight improvement in neurological outcomes, compared to IV injection of the MSCs alone. The authors acknowledged that using a focused beam would allow better spatial control of delivery and treatment (83).

The results described above provide important proof-of-concept validation using MRgFUS for enhancing cellular delivery, as well as first insights into the mechanisms involved in in this process. The general consensus is that physical/structural alterations generated (i.e., gaps), such as those facilitating smaller agent delivery, are less likely to be involved due to the relatively larger size of cells, which can be orders of magnitude greater. Other potential mechanisms involved are presented in the following section ("FUS effects on cell homing"). Preclinical studies of MRgFUS assisted cell delivery for other CNS pathologies are underway. Established animal models of MS (84) or AD (76) are considered to be good candidates for future investigations. The preclinical studies employing ultrasound for enhancing cellular delivery to the brain are summarized in **Table 2**.

FUS Effects on Cell Homing

Vascular extravasation of stem cells to sites of injury is analogous with endogenous immune cell behavior (leukocytes, monocytes, t-cells, dendritic cells) in that stem cells also follow a sequence of chemoattraction, margination, rolling, adhesion, and diapedesis. This is due to similar expression profiles of integrins, cytokine and chemokine receptors (e.g., VCAM-1, B1 integrins) (85, 86). Many preclinical studies have demonstrated in multiple organ tissues, including the CNS, that pretreatment with pulsed focused ultrasound (pFUS) non-destructively alters the vascular endothelial microenvironment, evidenced by an upregulation of chemokines, cytokines, trophic factors (CCTFs) and cell adhesion molecules (CAM). This pattern of pFUS mediated mechanical effects and biological changes permit significant increases of stem cell/immune cell homing and transmigration compared to simple vascular injection, i.e., referred to as enhanced homing, permeability & retention (EHPR) (87). In a murine skeletal muscle model, Burks et al. showed that pFUS exposures increased infiltration and presence of dual fluorescent/super paramagnetic iron oxide nanoparticles (SPION)-labeled macrophages, MSCs and endothelial progenitor cells (EPCs) relative to untreated controls. FUS exposures were shown to result an upregulation of cytokines (notably Il-1, TNF-a, IFN-y), growth factors (VEGF, SDF-1α) and cell adhesion molecules (ICAM-1 and VCAM-1) (88, 89). Similar outcomes were noted in a murine kidney model, where an 5-fold increase in bone marrow stromal cell count was noted 3 days post-treatment compared to the contralateral untreated kidney, aided by visual confirmation via T2* weighted MRI and histology (87).

In subsequent studies, the same group showed how pFUS mediated delivery of MSCs improved disease outcomes. This included improved survival in a model of cisplatin induced acute kidney injury (AKI) (90), and improvement in reperfusion and a reduction in fibrosis in a model of critical limb ischemia (**Figure 4**) (91). Most recently, this procedure was shown to also be successful for enhancing homing to the myocardium in the left ventricle in a rat model, indicating the potential of this approach for cardiac regeneration (92). It has been proposed that FUS induces Ca influx via mechanosensitive calcium channels (TRPC1), leading to activation of the NFkβ pathway and transient expression of TNFα. The increase in TNFα then drives COX2 canonical pathways that generate cell homing signals (93, 94).

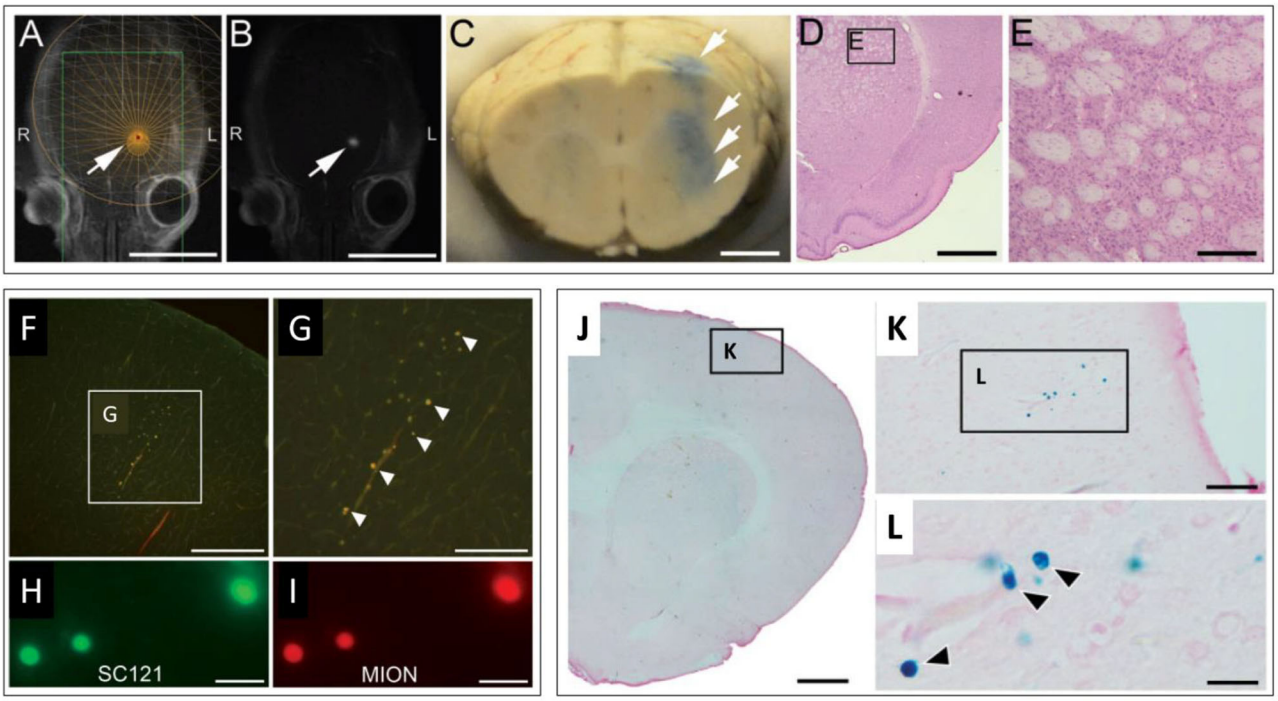

FIGURE 3 | MRgFUS mediated delivery of dual labeled (fluorescence & SPION) NPCs in the rodent brain. **(A,B)** Representative screen captures from an MRgFUS system graphic user interface. **(A)** T2 weighted axial MRI image of a rat brain showing treatment target (arrow) overlay. **(B)** T1 contrast MRI image showing hyperintense signal from gadolinium extravasation at location of treatment (arrow), indicating successful BBBO. Signal coincides with treatment target in "A". **(C)** Whole brain coronal section indicating successful BBBO, evidenced by Evans blue dye (arrows) that extravasated in the region of the focal zone. **(D)** H&E stained brightfield histological section demonstrating unaffected tissue in the region of MRgFUS treatment. **(E)** higher magnification region from "D" (inset). **(F–I)** Fluorescence microscopy images of fluorescently labeled NPCs in the brain. **(F)** Fluorescently labeled NPCs in the dorsal cortex. **(G)** higher magnification of inset in "F". **(H)** Fluorescent signals detected from labeled human cytoplasmic antigen (SC121). **(I)** Higher magnification of fluorescently labeled NPCs. Co-localization of fluorescent signals in "H" and "I" provide evidence that labeled cells are NPCs (human). **(J–L)** Brightfield microscopy images of Prussian blue stained histological sections (for SPION) indicating the presence of NPCs. **(J)** Low magnification image. **(K)** Inset in "J." **(L)** Inset in "K." Individual cells (blue) are seen (arrows). Scale bars: A, B = 10 mm; C = 2 mm; D = 2 mm; E = 200 μm; F = 400 μm; G = 200 μm; H, I = 20 μm; J = 1 mm; K = 50 μm; L = 5 μm. Adapted from *Shen et al. Cell Transplantation 2017* (81). Reprinted with permission from SAGE Publishing.

The studies described above were carried out using pFUS treatments without the use of microbubbles. Instead, higher acoustic pressures were used, being approximately 5-fold greater than those used for BBB opening. These treatments also targeted the parenchyma as opposed to the vasculature. In previous studies, the mechanical effects generated by these treatments appeared as widening of intercellular spaces and were shown to enhance interstitial transport of a range of therapeutic formulations (e.g., nanoparticles, monoclonal antibodies, plasmid DNA) in skeletal muscle (63, 95), solid tumors (96), and the brain (97). The proposed ultrasound mechanism for creating these effects is the generation of unidirectional radiation forces, which if large enough can displace tissue locally in the region of the focal zone. Through repetitive pulsing, it is thought that this movement of tissue acts on the relatively weak structural elements in the tissue, being the interfaces between individual cells (95).

MRgFUS studies have also been conducted in the brain to investigate the generation of CCTFs and CAMs for the purpose of enhancing cell homing. Kovacs et al. mapped the proteomic and transcriptomic time course of MRgFUS mediated BBBO in a murine model. Within 5 min of exposure, expression of (TNF-α, IL1α/β, IL18, IFN-γ) and CAM was observed, as well as stromal derived factor (SDF1-α), a significant chemokine utilized by lymphocytes and mesenchymal stem cells, within 2 h (61). These results observed in the brain were transient and consistent with those observed in earlier studies in the kidney and skeletal muscle and underlying mechanism of NFkβ activation, indicating that the effects could potentially be beneficial for stem cell homing (87, 88, 91, 98). The molecular effects in the brain were confirmed in a recent study where similar factors over the same time course were found to be upregulated by MRgFUS (60). Overall, MRgFUS effects for BBBO have been shown to be transient and safe, without producing neuronal apoptosis or inflammation (99). To date however, these specific effects were not shown to be associated with enhanced cell homing to the brain.

TRACKING CELLULAR ENGRAFTMENT

The ability to monitor activity of exogenous cells (migration to target region, viability, differentiation), as well as potential

TABLE 2 | Preclinical studies investigating ultrasound for cellular delivery to the brain.

Study design and highlights	Year	Ref
IA administration and MRgFUS increased NSC engraftment into rat striatum and hippocampus. Safety and reversibility of the treatments were also demonstrated.	2011	(77)
IV administration and MRgFUS improved delivery of NK92 cells in rat breast cancer brain metastasis model. More cells were delivered when administered prior to MRgFUS compared to afterward.	2013	(79)
Follow-up study in this model demonstrated that enhanced cellular delivery translates to improved survival. Front loading treatments compared to even temporal distribution also improved outcomes.	2016	(80)
IV administration and MRgFUS improved delivery of dual labeled NPCs in rat brain. Magnetic targeting of SPION labeled cells with external magnet improved retention of cells compared to non-labeled cells.	2017	(81)
IV administration and FUS pretreatment in rat brain resulted in a 2-fold increase in MSC transplantation in the lateral hippocampus. Improved delivery was apparently associated with increased expression of CAMs.	2020	(78)
Low intensity, non-FUS improved MSC engraftment 2-fold in rat brain ischemia model. Enhanced engraftment was associated with improved neurological outcomes.	2020	(83)

immunogenic or tumorigenic complications, is essential for evaluating the efficacy of CNS cellular therapies, in addition to monitoring engraftment response in the patient. Clinically relevant intracranial cell tracking modalities involve structural (MRI) and tracer-based (PET/SPECT) imaging, each of which have their own specific direct and indirect methods of cell tracking *in vivo*. Experimental studies evaluating cell labeling techniques for the purpose of tracking must verify that they do not negatively affect cell viability and/or key cellular functions (migration, division, differentiation, cytokine release). The duration and modality of monitoring will depend on a multitude of factors such as the therapeutic application (i.e., short-term immunomodulation vs. long-term cell replacement/regeneration).

Direct and Indirect Cell Labeling Techniques

Direct cell labeling involves cells that are treated with an agent before administration, allowing them to be detectable upon reaching a threshold concentration. Direct techniques places emphasis on nanoparticle fabrication, as their large surface area and other tunable characteristics allow for greater contrast or uptake of imaging agents (100). Despite relatively simple implementation, nanoparticle cell labeling may not be able to detect viability or distinguish the labeled cells from the local cells in the milieu. Furthermore, nanoparticles can either leak out, reducing engraftment resolution, or be taken up by macrophages that ingest dead labeled cells. In a clinical context, direct techniques may be suitable for short-term tracking purposes, such as verifying engraftment post-administration (101).

Indirect cell labeling requires viral or non-viral transfection of a gene transcript into the cell that encodes a reporter protein that generates a detectable signal based off of its interactions with an administered contrast/tracer agent (e.g., molecular trapping, enzymatic cleavage, or cell surface receptor interaction) (102). Since the reporter persists as long as the engrafted cells are alive, indirect techniques can distinguish cell viability, and grafted cells can be imaged repeatedly when the need arises for follow-up imaging. Since viral transfection of reporter genes carry a mutagenic risk, other genetic engineering methods such as non-viral vectors (e.g., cationic nanoparticles), or site-specific genome editing (i.e. CRISPR-cas9 delivery) could be potential viable alternatives.

MRI-Based Techniques

High soft-tissue resolution of MRI allows cellular grafts to be identified precisely within intracerebral regions. SPION-based cell tracking, which demarcates engrafted cells through changes in T2 relaxivity, is a common direct labeling method. The 1st generation of SPIONS (Feridex, Endorem), currently only available for preclinical studies in the US, was first reported in a brain trauma patient for tracking cell migration for a temporal lobe injection of autologous NSCs labeled with Feridex (103). Second generation agents (Ferumoxytol, Ferumoxtran) require cell transfection techniques (e.g., magnetoporation, magnetoelectroporation) due to less efficient uptake by cells (102). Accurate signal quantification from this iron-based labeling agent can be compromised by a number of factors, including resident macrophages engulfing SPION containing cell fragments, dilution of SPION concentration as the therapeutic cells divide, and not being able to be distinguish the cell signals from areas of hemorrhage or trauma (104). Advanced dynamic image processing techniques, such as pixel-to-pixel analysis, have demonstrated how labeling cells with SPIONs can enable monitoring cellular delivery in real-time (**Figure 5A**) (105).

19F MRI is another direct method which involves direct spin detection of the biologically safe isotope fluorine-19, enabling highly sensitive and quantitative "hot-spot" imaging as seen with PET/SPECT studies. One study demonstrated labeling of intracerebrally administered natural killer cells with fluorine-19, which importantly showed no cytotoxicity and change in NK cell therapeutic efficacy (109). In another study, 19F labeling of glial-progenitor cells transplanted into an ALS animal model was not found alter capacity for astrocyte differentiation (**Figure 5B**) (106). Indirect cell labeling for MRI has been explored preclinically, however to a lesser extent than with PET/SPECT. Overexpression of ferritin transporters can increase iron-based signaling of transplanted cells, however sensitivity in the setting of inflammation may be low (110). One group looked

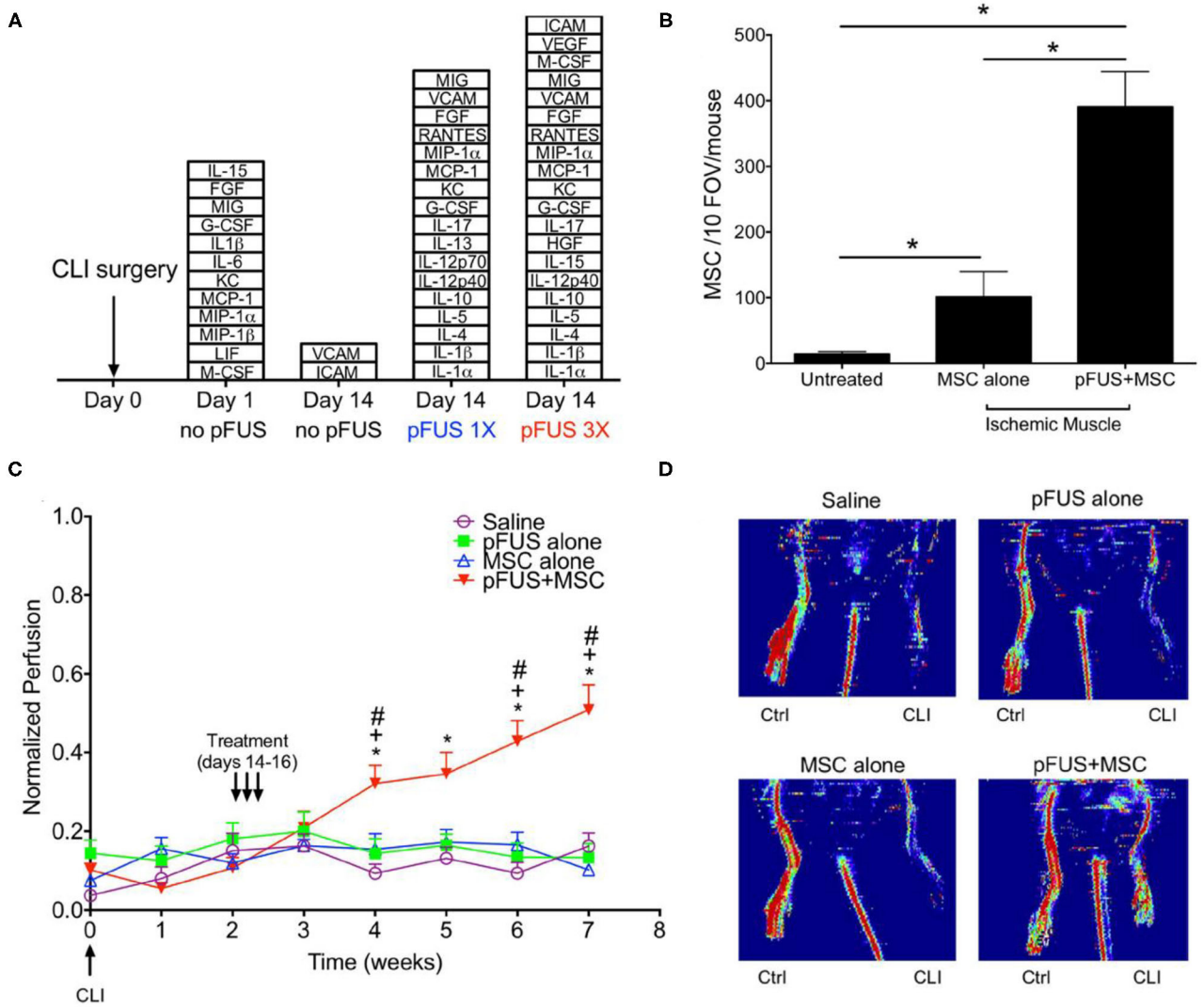

FIGURE 4 | FUS mediated delivery of MSCs in murine model of CLI in skeletal muscle **(A)** Stacked box plots comparing proteomic responses of CLI muscle between FUS treatment and untreated controls. The chemokines, cytokines, trophic factors, and cell adhesion molecules listed are those have significantly higher levels than those in normal muscle after CLI alone ($n = 6$). **(B)** SPION labeled MSCs in control and FUS treated skeletal muscle in CLI mice. Significantly greater numbers of MSCs were observed in FUS treated animals, based on Prussian blue staining of cells ($n = 5$). **(C)** Temporal changes in normalized perfusion comparing control and FUS treated CLI mice. Results are based on laser Doppler perfusion imaging (LDPI) indicating reperfusion that occurred in FUS treated animals only ($n = 7$). **(D)** Representative LDPI images at week 5 in the study for each experimental group. Adapted from Tebebi et al. *Sci Rep 2017* (91). Reprinted with permission from *Nature Research*.

at transfecting a biotinylated cell surface receptor that can produce detectable MRI signal upon exposure to magnetic nanoparticle- or Gadolinium-labeled streptavidin molecules (111).

PET/SPECT-Based Techniques

Highly sensitive "hot spot" signaling in Positron Emission Tomography (PET) and Single-Photon Emission Computed Tomography (SPECT) imaging, ensures that visualized signals are coming from the cells that were delivered. The half-lives (HL) of radionuclide agents available for direct labeling should be taken into consideration when specifying the required duration of tracking of the delivered cells. Indium-Tropolone labeling of MSCs has been shown to have no effect on proliferation or differentiation (112), but this was not the case when using Indium-Oxine (113). Technitium-99, with a HL of 6 h, was used to label neural progenitor cells that carried gene delivery products to a mouse glioma model (114). Another SPECT study tracking NSC homing to glioblastoma tumors in mice used mesoporous silica nanoparticles conjugated with Indium-111 (HL: 67 h). The use of this agent formulation lowered the required dosage of the radionuclide and thus lessened chances of cellular damage (**Figure 5C**) (107). In PET imaging, fluorine-18 radioisotope (HL: 110 min) was used to track MSCs and

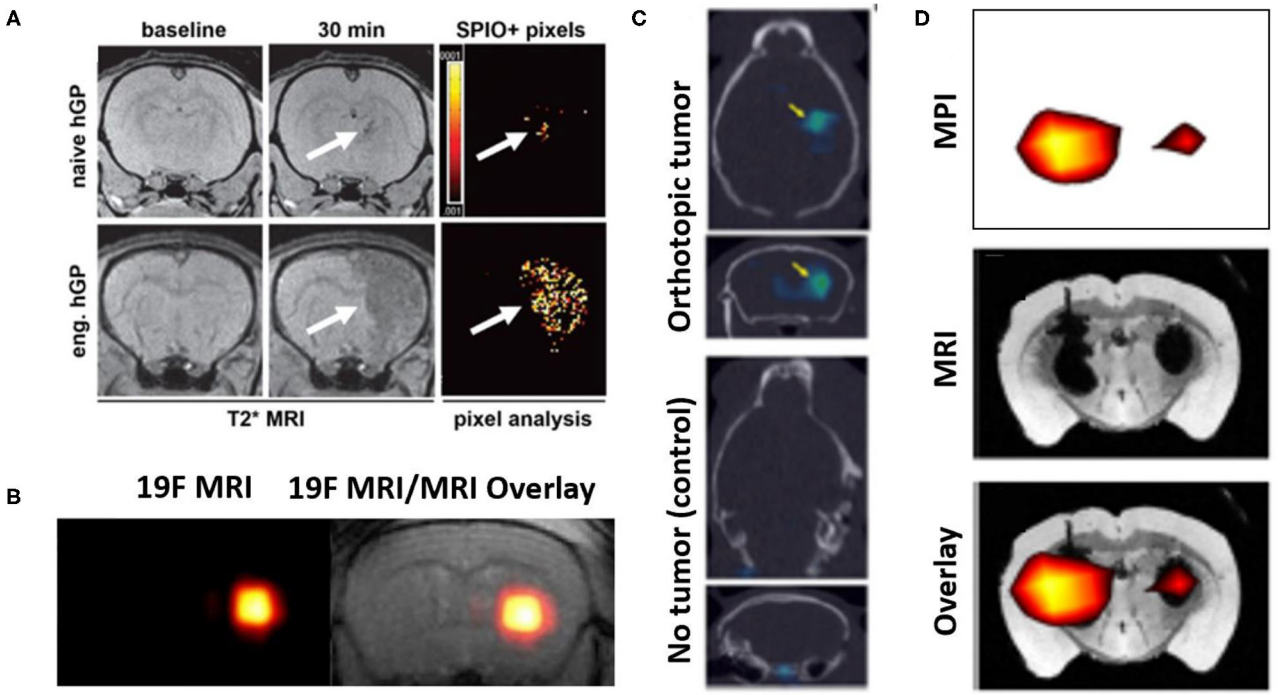

FIGURE 5 | Representative examples of image-based cell tracking methods in the brain. **(A)** T2* MR images of rat brains with experimentally induced inflammation and infused with SPION-labeled human glial precursor cells (hGP). At 30 min. post-infusion, greater numbers of targeted (eng.) cells are observed in the inflamed tissue compared to naïve cells (arrows, hypointense signal). The results are supported by pixel-by-pixel analysis, comparing pre- and post-infusion MR images, which can be quantitatively compared. Modified, with permission, from "*Gorelik et al.* Use of MR cell tracking to evaluate targeting of glial precursor cells to inflammatory tissue by exploiting the very late antigen-4 docking receptor. *Radiology* 2012; 265: 175-185" (105). **(B)** (left) 19F MRI and (right) 19F MRI & T2 weighted MR images of fluorine-19 labeled glial progenitor cells injected into a mouse brain striatum. "Hot spot" in each image is clearly identified, indicating the presence of the labeled cells. Figure adapted from *Richard et al. Stem Cells Translational Medicine 2019.* Reprinted under creative commons license (106). **(C)** SPECT signals (arrows) from 111-In labeled NSCs administered into control mice (lower) and those with a glioma model (upper), to which the cells have homed. In both panels, SPECT images are overlayed on CT scans. Figure adapted from *Cheng et al. 2016* (107). This research was originally published in the Journal of Nuclear Medicine. **(D)** MPI imaging of SPION labeled MSCs in the left hemisphere (1×10^5 cells) and right hemisphere (5×10^4 cells) transplanted in a mouse brain. Lower panel shows MPI signals (upper panel) superimposed on T2* MR image (middle panel). Figure adapted from *Bulte et al. Tomography 2015* (108). Reprinted under creative commons license.

multipotent adult progenitor cells (MAPCs) and were shown not affect the main cell characteristics (115). Bioluminescent and fluorescent imaging methods have also been used in rodent studies to track NSCs to study neurodegenerative disease, where results of these agents corroborated the results of the PET/SPECT imaging (116).

Magnetic Particle Imaging

Magnetic particle imaging (MPI) is a developing modality that involves applying external magnetic fields (i.e., MRI) to directly detect exogenously administered SPIONs (**Figure 5D**) (108). SPIONs in the context of MPI behave as tracer agents, producing "hot spot" signaling as seen with F-19 MRI or PET/SPECT. While still in its infancy, MPI technology potentially has additional applications in guiding hyperthermia therapy, making physiological measurements in cerebral and cardiac vasculature, and assisting with diagnosis of acute stroke (117). Intracerebrally injected MSCs labeled with 1st generation SPIO agents (Feridex) and MSCs labeled with 2nd generation agents (Ferumoxytol, Ferucarbotran) injected into mouse calvarial defects were tracked using MPI as initial proof-of concept investigations (108, 118). This technique has been shown, for example, to produce excellent correlation between the "hot spot" signal generated and the number of cells being imaged (108). Instrumentation suitable for human use is currently in development. MRgFUS cell delivery could potentially benefit from the use of a hybrid MRI/MPI scanner, where MRI would delineate areas of FUS exposure and MPI-cell tracking verify that the cells have reached their target region (119, 120).

POTENTIAL FOR CLINICAL TRANSLATION

CNS pathologies throughout the diagnostic spectrum may vary in their progression, effects on BBB integrity, and subsequent cellular and inflammatory responses. Clinical presentations may overlap and involve mass effect symptoms (headache/nausea), excitotoxicity (seizure, akathisia), neuropathy, focal deficits in cognition, motor, sensory, gait, coordination, possible behavioral changes, and at its worst, the inability to perform life-sustaining functions. For a given CNS condition, the selection and modification of the therapeutic cell type is informed by the symptoms presented and the desired mechanism of

action (i.e., cell-mediated cytotoxicity, recruiting other cells, differentiation, replacement, immunomodulation, secretion, prodrug conversion). By employing the advantages of increased target specificity and cell homing and retention using pFUS, cellular therapy applications in the brain may obtain better clinical outcomes. The following section will outline potential benefits of employing MRgFUS delivery approaches for certain CNS disorders.

Neurodegenerative Diseases

Neurodegenerative conditions are expected to become more prevalent in the years to come as life expectancy continues to increase. PD alone is projected to affect 14 million people world-wide by 2040 (121). Pharmacological therapies may only treat or temporarily delay severe symptoms (e.g., acetylcholinesterase inhibitors for AD, riluzole for ALS). New cell therapy strategies are under consideration for treating underlying pathology, through mechanisms such as functional cell replacement, enhancing immune system functions to clear aggregated proteins, or modifying microenvironments through growth factor delivery (4–7). Strategies for PD that employ cell replacement therapies are considered promising for restoring dopaminergic neurotransmission in order to functionally rescue the dopamine-depleted striatum (122). Functional recovery has been achieved in murine models of Huntington's Disease via MSCs overexpressing brain-derived neurotrophic growth factor (BDNF) injection (4). as well as in ALS models using glial cell derived neurotrophic factor (GDNF)-secreting NPCs via intracranial injection (123). Clinical investigations involving intra-putaminal injections of ESC-derived dopaminergic neurons are currently ongoing (124). MRgFUS can be used to accurately target pathological regions associated with this class of diseases (i.e., the striatum in PD, caudate nucleus in HD, motor cortex in ALS) in lieu of stereotactic injection and increase therapeutic cell homing. MRgFUS has been shown to be safe for repeated treatment; an obvious advantage over direct stereotactic injections (125).

Malignancies

MRgFUS cell therapies can potentially play a role in post-glioma resection consolidation therapy and treatment of brain metastases. Recurrence remains a significant issue in the management of glioblastoma (GBM), a devastating condition with a 12–18-month median survival (126). This may be due to residual tumor cells developing resistance to chemotherapeutics, one mechanism which involves efflux transporter upregulation of the BBB surrounding the glial tumor (127). iNSCs expressing tumoricidal molecules (128), and MSCs that release exosomes containing anti-cancer miRNA (129), both have been shown to reduce glioma growth rates and prolong median survival in mouse models. NSCs overexpressing cytosine deaminase, the enzyme converter of prodrug 5-FC to 5-FU, was demonstrated to be safe in a study of 15 patients with high-grade gliomas post-resection (130). FUS-mediated delivery of NK-92 cells for a HER2-amplified brain metastases rat model showed increased survival (80). Repeated MRgFUS BBBO treatments in GBM patients was deemed safe in a recent 2020 study (131). This highlights the potential that anti-cancer cell therapies delivered this way can be done using multiple treatments.

Autoimmune Diseases

Multiple Sclerosis involves autoimmune destruction of the white matter tracts throughout the CNS which follows an unpredictable spatiotemporal progression. Because of its multifocal nature, the therapeutic approach of a MRgFUS stem-cell delivery regiment may be beneficial for disease modifying therapies of MS or for treating acute flares, while other routes such as direct injection may be less optimal (132). Since the clinical management of an MS flare already involves MRI scanning to detect new lesions of immune hyperactivity, an MRgFUS procedure to deliver immunomodulatory MSCs or NSCs to these regions could be seamlessly integrated (133). By combining cell therapies with standard of care, which involve systemic high potency corticosteroids and a tapered course of oral corticosteroids, the high burden of these medications that confer adverse effects (i.e., Cushing's syndrome symptoms of weight gain, impaired wound healing, muscle breakdown) may be reduced (134). Multiple clinical trials examining MSC administration via intrathecal (46) or intravenous routes (135, 136) have demonstrated functional improvement. Intrathecal MSC administration was tested in 10 patients with medication refractory MS showed increased proportion of regulatory T-cells within 24 h and mean Expanded Disability Status Scale (EDSS) scores dropping from 6.7 to 5.9 at 3 months (137).

Acute CNS Pathologies

Overlapping cell signaling pathways and mechanisms that activate cell death and neuroprotective mechanisms exist between ischemic stroke and TBI (138). In ischemic stroke, prolonged hypoxia of a CNS region secondary to either thrombotic or embolic occlusion, or global hypoperfusion, leads to necrotic and apoptotic cell death and edema following protease-mediated breakdown of the BBB (127). TBI, while acute in onset, imparts a poor prognosis from its chronic sequelae, characterized by mitochondrial dysfunction, metabolic disturbances, glial cell over-activation, excitotoxicity, and vasospasm. Cell therapies for these conditions are aimed at preventing further neuronal death through promoting angiogenesis, downregulating inflammation, and increasing synaptic plasticity. Recent results from an open-label phase IIa trial of stereotactic injection of the SB623 line (genetically modified allogeneic MSCs expressing an intracellular domain of the notch signaling pathway, involved in neuronal differentiation), showed that 16 of 18 patients with a 6–60 month stroke history exhibited significant improvements in European Stroke Scale and NIH Stroke Scale scoring (139). Using an MRgFUS BBBO approach to pretreat the ischemic penumbral region or the mechanically impacted parenchyma before intravascular delivery of cells could potentially be beneficial. Currently, only one preclinical study examining this approach for either stroke or TBI has been conducted (83).

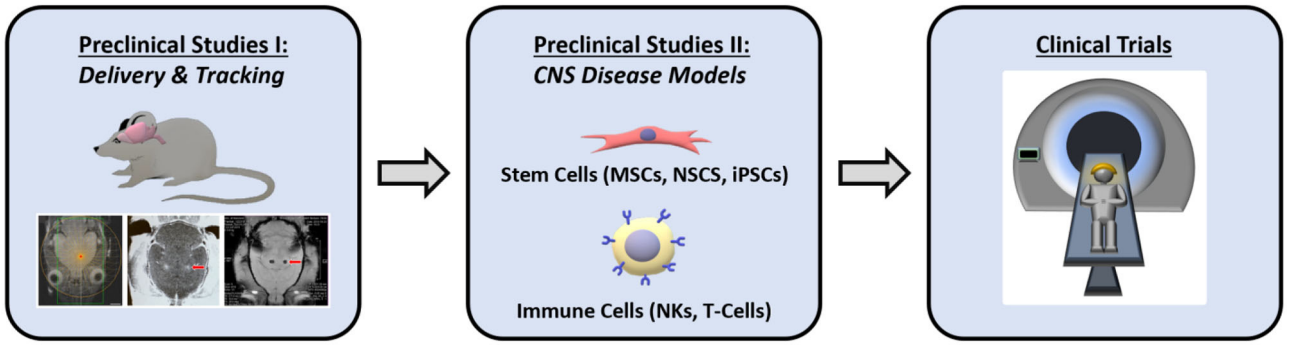

FIGURE 6 | Schematic representation of the anticipated preclinical and clinical stages involved for clinical translation in using MRgFUS for enhancing cellular therapy.

CONCLUSIONS

With significant improvements in FDA-approved cell manufacturing practices, rapidly accumulating clinical trial results supporting the safety of MRgFUS-mediated BBBO, and the report of studies demonstrating the potential of delivering chemotherapeutics, antibodies, drug-loaded-NPs across the BBB with this modality, it is foreseeable that neuro-interventionalists will be interested in the delivery of therapeutic cells using this method as the best next step (140). Before adapting this cell delivery approach for clinical trials, ongoing animal studies will need to continue to explore both practical and mechanistic questions that probe the process of MRgFUS assisted cell delivery. Although it has been shown that IA routes can be more effective than IV routes (141), experimental groups in future studies should include both methods of cell administration with MRgFUS to provide greater translational insight. The distribution and iteration of pFUS exposures, as well as many other sonication parameters, should be further explored and tailored to each CNS disease for safety and efficacy purposes. For instance, Alkins et al. showed that front-loading pFUS-mediated NK-92 cell treatments to the HER2 amplified brain tumor mouse, rather than distributing them over time, improved survival outcomes (80).

In conclusion, the question of whether an MRgFUS assisted cell delivery approach can significantly reduce neurological disease morbidity/mortality, and hospital costs (e.g., surgically re-intervening on patients with recurrent GBM), is being discussed as FUS technology undergoes widespread adoption. The continued investigation of MRgFUS technology for this specific therapeutic purpose will be aided by many more preclinical studies combining different cell types with tracking methods. Overall, the results from these studies are encouraging and provide motivation to further pursue this application and evaluate its feasibility for clinical translation (**Figure 6**).

More recently, it was announced that MRgFUS ablation for tremor-dominant Parkinson's will receive Medicare coverage. Intracranial MRgFUS treatments can be carried out with any MRI with a modified table to house the hemispherical transducer array and currently, there are 800 systems in the US in operation (See footnote 1), and many more worldwide. As clinical trials exploring one-time stereotactic injections of stem cell therapies are ongoing and show promise, the aspects of repeatability and non-invasiveness of MRgFUS delivery will enable greater inclusion of patients who may be poor surgical candidates. The combination of cellular therapeutics and MRgFUS mediated delivery shows great potential for helping to usher in the next generation of treatment paradigms for CNS disorders.

AUTHOR CONTRIBUTIONS

NA, DG, EM, and VF contributed to the conception and design of the manuscript. NA wrote the first completed draft. DG, EM, and VF provided critical reviews of the first, second, and third versions of the manuscript. All authors read and approved the final submitted version of the manuscript.

FUNDING

This review was supported in part by the Department of Diagnostic Radiology and Nuclear Medicine, University of Maryland School of Medicine, Baltimore, MD.

REFERENCES

1. Piccini P, Brooks DJ, Bjorklund A, Gunn RN, Grasby PM, Rimoldi O, et al. Dopamine release from nigral transplants visualized *in vivo* in a Parkinson's patient. *Nat Neurosci.* (1999) 2:1137–40. doi: 10.1038/16060

2. Bachoud-Lévi A-C, Rémy P, Nguyen J-P, Brugières P, Bourdet C, Baudic S, et al., Motor and cognitive improvements in patients with Huntington's disease after neural transplantation. *Lancet.* (2000) 356:1975–9. doi: 10.1016/S0140-6736(00)03310-9

3. Keene CD, Chang RC, Leverenz JB, Kopyov O, Perlman S, Hevner RF, et al. A patient with Huntington's disease and long-surviving fetal neural transplants that developed mass lesions. *Acta Neuropathol.* (2009) 117:329–38. doi: 10.1007/s00401-008-0465-0
4. Pollock K, Dahlenburg H, Nelson H, Fink KD, Cary W, Hendrix K, et al. MSCs genetically engineered to overexpress BDNF improve outcomes in Huntington's disease mouse models. *Mol Ther.* (2016) 24:965–77. doi: 10.1038/mt.2016.12
5. Aboody KS, Najbauer J, Metz MZ, D'Apuzzo M, Gutova M, Annala AJ, et al. Neural stem cell-mediated enzyme/prodrug therapy for glioma: preclinical studies. *Sci Transl Med.* (2013) 5:184ra159. doi: 10.1126/scitranslmed.3005365
6. Burger MC, Zhang C, Harter PN, Romanski A, Strassheimer F, Senft C, et al. CAR-engineered NK cells for the treatment of glioblastoma: turning innate effectors into precision tools for cancer immunotherapy. *Front Immunol.* (2019) 10:2683. doi: 10.3389/fimmu.2019.02683
7. Greco R, Oliveira G, Stanghellini MT, Vago L, Bondanza A, Peccatori J, et al. Improving the safety of cell therapy with the TK-suicide gene. *Front Pharmacol.* (2015) 6:95. doi: 10.3389/fphar.2015.00095
8. Takahashi K, Tanabe K, Ohnuki M, Narita M, Ichisaka T, Tomoda K, et al. Induction of pluripotent stem cells from adult human fibroblasts by defined factors. *Cell.* (2007) 131:861–72. doi: 10.1016/j.cell.2007.11.019
9. Kim TW, Koo SY, Studer L. Pluripotent stem cell therapies for Parkinson disease: present challenges and future opportunities. *Front Cell Dev Biol.* (2020) 8:729. doi: 10.3389/fcell.2020.00729
10. Staerk J, Dawlaty MM, Gao Q, Maetzel D, Hanna J, Sommer CA, et al. Reprogramming of human peripheral blood cells to induced pluripotent stem cells. *Cell Stem Cell.* (2010) 7:20–4. doi: 10.1016/j.stem.2010.06.002
11. Chang EA, Jin SW, Nam MH, Kim SD. Human induced pluripotent stem cells: clinical significance and applications in neurologic diseases. *J Korean Neurosurg Soc.* (2019) 62:493–501. doi: 10.3340/jkns.2018.0222
12. Mitsiadis TA, Barrandon O, Rochat A, Barrandon Y, De Bari. C. Stem cell niches in mammals. *Exp Cell Res.* (2007) 313:3377–85. doi: 10.1016/j.yexcr.2007.07.027
13. Takagi Y. History of neural stem cell research and its clinical application. *Neurol Med Chir (Tokyo).* (2016) 56:110–124. doi: 10.2176/nmc.ra.2015-0340
14. Christian KM, Song H, Ming GL. Functions and dysfunctions of adult hippocampal neurogenesis. *Annu Rev Neurosci.* (2014) 37:243–62. doi: 10.1146/annurev-neuro-071013-014134
15. Vieira MS, Santos AK, Vasconcellos R, Goulart VAM, Parreira RC, Kihara AH, et al. NSC differentiation into mature neurons: Mechanisms of regulation and biotechnological applications. *Biotechnol Adv.* (2018) 36:1946–70. doi: 10.1016/j.biotechadv.2018.08.002
16. Mooney R, Hammad M, Batalla-Covello J, Abdul Majid A, Aboody KS. Concise review: NSC-mediated targeted cancer therapies. *Stem Cells Transl Med.* (2018) 7:740–7. doi: 10.1002/sctm.18-0003
17. Darvishi M, Tiraihi T, Mesbah-Namin SA, Delshad A, Taheri T. Motor neuron transdifferentiation of neural stem cell from adipose-derived stem cell characterized by differential gene expression. *Cell Mol Neurobiol.* (2017) 37:275–89. doi: 10.1007/s10571-016-0368-x
18. Rosati J, Ferrari D, Altieri F, Tardivo S, Ricciolini C, Fusilli C, et al. Establishment of stable iPS-derived human neural stem cell lines suitable for cell therapies. *Cell Death Dis.* (2018) 9:937. doi: 10.1038/s41419-018-0990-2
19. Matsushita T, Kibayashi T, Katayama T, Yamashita Y, Suzuki S, Kawamata J, et al. Mesenchymal stem cells transmigrate across brain microvascular endothelial cell monolayers through transiently formed inter-endothelial gaps. *Neurosci Lett.* (2011) 502:41–5. doi: 10.1016/j.neulet.2011.07.021
20. Reagan MR, Kaplan DL. Concise review: mesenchymal stem cell tumor-homing: detection methods in disease model systems. *Stem Cells.* (2011) 29:920–7. doi: 10.1002/stem.645
21. Paul G, Anisimov SV. The secretome of mesenchymal stem cells: potential implications for neuroregeneration. *Biochimie.* (2013) 95:2246–56. doi: 10.1016/j.biochi.2013.07.013
22. Caplan AI. Mesenchymal stem cells: time to change the name! *Stem Cells Transl Med.* (2017) 6:1445–51. doi: 10.1002/sctm.17-0051
23. Lai RC, Yeo RW, Lim SK. Mesenchymal stem cell exosomes. *Semin Cell Dev Biol.* (2015) 40:82–8. doi: 10.1016/j.semcdb.2015.03.001
24. Aleynik A, Gernavage KM, Mourad YSH, Sherman LS, Liu K, Gubenko YA, et al. Stem cell delivery of therapies for brain disorders. *Clin Transl Med.* (2014) 3:24. doi: 10.1186/2001-1326-3-24
25. Earls RH, Menees KB, Chung J, Gutekunst CA, Lee HJ, Hazim MG, et al. NK cells clear alpha-synuclein and the depletion of NK cells exacerbates synuclein pathology in a mouse model of alpha-synucleinopathy. *Proc Natl Acad Sci U S A.* (2020) 117:1762–71. doi: 10.1073/pnas.1909110117
26. Castriconi R, Daga A, Dondero A, Zona G, Poliani PL, Melotti A, et al. NK cells recognize and kill human glioblastoma cells with stem cell-like properties. *J Immunol.* (2009) 182:3530–9. doi: 10.4049/jimmunol.0802845
27. Fares J, Fares MY, Fares Y. NK cells in the brain tumor microenvironment: defining a new era in neuro-oncology. *Surg Neurol Int.* (2019) 10:43. doi: 10.25259/SNI-97-2019
28. Mehta RS, Rezvani K. Chimeric antigen receptor expressing natural killer cells for the immunotherapy of cancer. *Front Immunol.* (2018) 9:283. doi: 10.3389/fimmu.2018.00283
29. Maude SL, Laetsch TW, Buechner J, Rives S, Boyer M, Bittencourt H, et al. Tisagenlecleucel in children and young adults with B-cell lymphoblastic leukemia. *N Engl J Med.* (2018) 378:439–48. doi: 10.1056/NEJMoa1709866
30. Schuster SJ, Bishop MR, Tam CS, Waller EK, Borchmann P, McGuirk JP, et al. Tisagenlecleucel in adult relapsed or refractory diffuse large B-cell lymphoma. *N Engl J Med.* (2019) 380:45–56. doi: 10.1056/NEJMoa1804980
31. Hersh DS, Wadajkar AS, Roberts N, Perez JG, Connolly NP, Frenkel V, et al. Evolving drug delivery strategies to overcome the blood brain barrier. *Curr Pharm Des.* (2016) 22:1177–93. doi: 10.2174/1381612822666151221150733
32. Chen CC, Hsu PW, Erich Wu TW, Lee ST, Chang CN, Wei KC, et al. Stereotactic brain biopsy: single center retrospective analysis of complications. *Clin Neurol Neurosurg.* (2009) 111:835–9. doi: 10.1016/j.clineuro.2009.08.013
33. Wolak DJ, Thorne RG. Diffusion of macromolecules in the brain: implications for drug delivery. *Mol Pharm.* (2013) 10:1492–504. doi: 10.1021/mp300495e
34. Kapke JT, Schneidewend RJ, Jawa ZA, Huang CC, Connelly JM, Chitambar CR. High-dose intravenous methotrexate in the management of breast cancer with leptomeningeal disease: Case series and review of the literature. *Hematol Oncol Stem Cell Ther.* (2019) 12:189–93. doi: 10.1016/j.hemonc.2019.08.008
35. Penn RD, Savoy SM, Corcos D, Latash M, Gottlieb G, Parke B, et al. Intrathecal baclofen for severe spinal spasticity. *N Engl J Med.* (1989) 320:1517–21. doi: 10.1056/NEJM198906083202303
36. Sugiyama Y, Sato Y, Kitase Y, Suzuki T, Kondo T, Mikrogeorgiou A, et al. Intravenous administration of bone marrow-derived mesenchymal stem cell, but not adipose tissue-derived stem cell, ameliorated the neonatal hypoxic-ischemic brain injury by changing cerebral inflammatory state in rat. *Front Neurol.* (2018) 9:757. doi: 10.3389/fneur.2018.00757
37. Thompson M, Mei SHJ, Wolfe D, Champagne J, Fergusson D, Stewart DJ, et al. Cell therapy with intravascular administration of mesenchymal stromal cells continues to appear safe: an updated systematic review and meta-analysis. *EClinicalMedicine.* (2020) 19:100249. doi: 10.1016/j.eclinm.2019.100249
38. Fischer UM, Harting MT, Jimenez F, Monzon-Posadas WO, Xue H, Savitz SI, et al. Pulmonary passage is a major obstacle for intravenous stem cell delivery: the pulmonary first-pass effect. *Stem Cells Dev.* (2008) 18:683–92. doi: 10.1089/scd.2008.0253
39. Lundberg J, Sodersten E, Sundstrom E, Le Blanc K, Andersson T, Hermanson O, et al. Targeted intra-arterial transplantation of stem cells to the injured CNS is more effective than intravenous administration: engraftment is dependent on cell type and adhesion molecule expression. *Cell Transplant.* (2012) 21:333–43. doi: 10.3727/096368911X576036
40. Gonzales-Portillo GS, Sanberg PR, Franzblau M, Gonzales-Portillo C, Diamandis T, Staples M, et al. Mannitol-enhanced delivery of stem cells and their growth factors across the blood-brain barrier. *Cell Transplant.* (2014) 23:531–9. doi: 10.3727/096368914X678337

41. Bellavance MA, Blanchette M, Fortin D. Recent advances in blood-brain barrier disruption as a CNS delivery strategy. *AAPS J.* (2008) 10:166–77. doi: 10.1208/s12248-008-9018-7
42. Li YH, Feng L, Zhang GX, Ma CG. Intranasal delivery of stem cells as therapy for central nervous system disease. *Exp Mol Pathol.* (2015) 98:145–51. doi: 10.1016/j.yexmp.2015.01.016
43. Erdo F, Bors LA, Farkas D, Bajza A, Gizurarson S. Evaluation of intranasal delivery route of drug administration for brain targeting. *Brain Res Bull.* (2018) 143:155–70. doi: 10.1016/j.brainresbull.2018.10.009
44. Shoichet MS, Winn SR. Cell delivery to the central nervous system. *Adv Drug Delivery Rev.* (2000) 42:81–102. doi: 10.1016/S0169-409X(00)00055-7
45. Zhang G, Li Y, Reuss JL, Liu N, Wu C, Li J, et al. Stable intracerebral transplantation of neural stem cells for the treatment of paralysis due to ischemic stroke. *Stem Cells Transl Med.* (2019) 8:999–1007. doi: 10.1002/sctm.18-0220
46. Harris VK, Stark J, Vyshkina T, Blackshear L, Joo G, Stefanova V, et al. Phase I trial of intrathecal mesenchymal stem cell-derived neural progenitors in progressive multiple sclerosis. *EBioMedicine.* (2018) 29:23–30. doi: 10.1016/j.ebiom.2018.02.002
47. Fauzi AA, Suroto NS, Bajamal AH, Machfoed MH. Intraventricular transplantation of autologous bone marrow mesenchymal stem cells via ommaya reservoir in persistent vegetative state patients after haemorrhagic stroke: report of two cases and review of the literature. *J Stem Cells Regen Med*. (2016) 12:100–4. doi: 10.46582/jsrm.1202014
48. Reitz M, Demestre M, Sedlacik J, Meissner H, Fiehler J, Kim SU, et al. Intranasal delivery of neural stem/progenitor cells: a noninvasive passage to target intracerebral glioma. *Stem Cells Transl Med.* (2012) 1:866–73. doi: 10.5966/sctm.2012-0045
49. Janowski M, Walczak P, Date I. Intravenous route of cell delivery for treatment of neurological disorders: a meta-analysis of preclinical results. *Stem Cells Dev.* (2010) 19:5–16. doi: 10.1089/scd.2009.0271
50. Okuma Y, Wang F, Toyoshima A, Kameda M, Hishikawa T, Tokunaga K, et al. Mannitol enhances therapeutic effects of intra-arterial transplantation of mesenchymal stem cells into the brain after traumatic brain injury. *Neurosci Lett.* (2013) 554:156–61. doi: 10.1016/j.neulet.2013.08.058
51. Harting MT, Jimenez F, Xue H, Fischer UM, Baumgartner J, Dash PK, et al. Intravenous mesenchymal stem cell therapy for traumatic brain injury. *J Neurosurg.* (2009) 110:1189–97. doi: 10.3171/2008.9.JNS08158
52. Miller DB, O'Callaghan JP. New horizons for focused ultrasound (FUS) - therapeutic applications in neurodegenerative diseases. *Metabolism.* (2017) 69S:S3–7. doi: 10.1016/j.metabol.2017.01.012
53. Elias WJ, Lipsman N, Ondo WG, Ghanouni P, Kim YG, Lee W, et al. A randomized trial of focused ultrasound thalamotomy for essential tremor. *N Engl J Med.* (2016) 375:730–9. doi: 10.1056/NEJMc1612210
54. Elias WJ, Huss D, Voss T, Loomba J, Khaled M, Zadicario E, et al. A pilot study of focused ultrasound thalamotomy for essential tremor. *N Engl J Med.* (2013) 369:640–8. doi: 10.1056/NEJMoa1300962
55. Zhu L, Huang Y, Lam D, Gach HM, Zoberi I, Hallahan DE, et al. Targetability of cervical cancer by magnetic resonance-guided high-intensity focused ultrasound (MRgHIFU)-mediated hyperthermia (HT) for patients receiving radiation therapy. *Int J Hyperthermia.* (2021) 38:498–510. doi: 10.1080/02656736.2021.1895330
56. Singh MP, Sethuraman SN, Miller C, Malayer J, Ranjan A. Boiling histotripsy and in-situ CD40 stimulation improve the checkpoint blockade therapy of poorly immunogenic tumors. *Theranostics.* (2021) 11:540–54. doi: 10.7150/thno.49517
57. Sethuraman SN, Singh MP, Patil G, Li S, Fiering S, Hoopes PJ, et al. Novel calreticulin-nanoparticle in combination with focused ultrasound induces immunogenic cell death in melanoma to enhance antitumor immunity. *Theranostics.* (2020) 10:3397–412. doi: 10.7150/thno.42243
58. Mead BP, Mastorakos P, Suk JS, Klibanov AL, Hanes J, Price RJ. Targeted gene transfer to the brain via the delivery of brain-penetrating DNA nanoparticles with focused ultrasound. *J Control Release.* (2016) 223:109–17. doi: 10.1016/j.jconrel.2015.12.034
59. Wei HJ, Upadhyayula PS, Pouliopoulos AN, Englander ZK, Zhang X, Jan CI, et al. Focused ultrasound-mediated blood-brain barrier opening increases delivery and efficacy of etoposide for glioblastoma treatment. *Int J Radiat Oncol Biol Phys*. (2021) 110:539–50. doi: 10.1016/j.ijrobp.2020.12.019
60. McMahon D, Bendayan R, Hynynen K. Acute effects of focused ultrasound-induced increases in blood-brain barrier permeability on rat microvascular transcriptome. *Sci Rep.* (2017) 7:45657. doi: 10.1038/srep45657
61. Kovacs ZI, Kim S, Jikaria N, Qureshi F, Milo B, Lewis BK, et al. Disrupting the blood-brain barrier by focused ultrasound induces sterile inflammation. *Proc Natl Acad Sci U S A.* (2017) 114:E75–84. doi: 10.1073/pnas.1614777114
62. Wang S, Frenkel V, Zderic V. Optimization of pulsed focused ultrasound exposures for hyperthermia applications. *J Acoust Soc Am.* (2011) 130:599–609. doi: 10.1121/1.3598464
63. O'Neill BE, Vo H, Angstadt M, Li KP, Quinn T, Frenkel V. Pulsed high intensity focused ultrasound mediated nanoparticle delivery: mechanisms and efficacy in murine muscle. *Ultrasound Med Biol.* (2009) 35:416–24. doi: 10.1016/j.ultrasmedbio.2008.09.021
64. Frenkel V, Etherington A, Greene M, Quijano J, Xie J, Hunter F, et al. Delivery of liposomal doxorubicin (Doxil) in a breast cancer tumor model: investigation of potential enhancement by pulsed-high intensity focused ultrasound exposure. *Acad Radiol.* (2006) 13:469–79. doi: 10.1016/j.acra.2005.08.024
65. Vykhodtseva NI, Hynynen K, Damianou C. Histologic effects of high intensity pulsed ultrasound exposure with subharmonic emission in rabbit brain *in vivo*. *Ultrasound Med Biol.* (1995) 21:969–79. doi: 10.1016/0301-5629(95)00038-S
66. Hynynen K, McDannold N, Vykhodtseva N, Jolesz FA. Noninvasive MR imaging-guided focal opening of the blood-brain barrier in rabbits. *Radiology.* (2001) 220:640–6. doi: 10.1148/radiol.2202001804
67. Burgess A, Shah K, Hough O, Hynynen K. Focused ultrasound-mediated drug delivery through the blood-brain barrier. *Expert Rev Neurother.* (2015) 15:477–91. doi: 10.1586/14737175.2015.1028369
68. Fishman PS, Frenkel V. Treatment of movement disorders with focused ultrasound. *J Central Nerv Syst Dis.* (2017) 9:117957351770567. doi: 10.1177/1179573517705670
69. Meng Y, Jones RM, Davidson B, Huang Y, Pople CB, Surendrakumar S, et al.Technical principles and clinical workflow of transcranial MR-guided focused ultrasound. *Stereotact Funct Neurosurg.* (2020). doi: 10.1159/000512111. [Epub ahead of print].
70. Huang Y, Alkins R, Schwartz ML, Hynynen K. Opening the blood-brain barrier with MR imaging-guided focused ultrasound: preclinical testing on a trans-human skull porcine model. *Radiology.* (2017) 282:123–30. doi: 10.1148/radiol.2016152154
71. Rivens I, Shaw A, Civale J, Morris H. Treatment monitoring and thermometry for therapeutic focused ultrasound. *Int J Hyperthermia.* (2007) 23:121–39. doi: 10.1080/02656730701207842
72. Treat LH, McDannold N, Vykhodtseva N, Zhang Y, Tam K, Hynynen K. Targeted delivery of doxorubicin to the rat brain at therapeutic levels using MRI-guided focused ultrasound. *Int J Cancer.* (2007) 121:901–7. doi: 10.1002/ijc.22732
73. Mainprize T, Lipsman N, Huang Y, Meng Y, Bethune A, Ironside S, et al. Blood-brain barrier opening in primary brain tumors with non-invasive MR-guided focused ultrasound: a clinical safety and feasibility study. *Sci Rep.* (2019) 9:321. doi: 10.1038/s41598-018-36340-0
74. Lipsman N, Meng Y, Bethune AJ, Huang Y, Lam B, Masellis M, et al. Blood-brain barrier opening in Alzheimer's disease using MR-guided focused ultrasound. *Nat Commun.* (2018) 9:2336. doi: 10.1038/s41467-018-04529-6
75. Abrahao A, Meng Y, Llinas M, Huang Y, Hamani C, Mainprize T, et al. First-in-human trial of blood–brain barrier opening in amyotrophic lateral sclerosis using MR-guided focused ultrasound. *Nat Commun.* (2019) 10:4373. doi: 10.1038/s41467-019-12426-9
76. Jordao JF, Thevenot E, Markham-Coultes K, Scarcelli T, Weng YQ, Xhima K, et al. Amyloid-beta plaque reduction, endogenous antibody delivery and glial activation by brain-targeted, transcranial focused ultrasound. *Exp Neurol.* (2013) 248:16–29. doi: 10.1016/j.expneurol.2013.05.008
77. Burgess A, Ayala-Grosso CA, Ganguly M, Jordão JF, Aubert I, Hynynen K. Targeted delivery of neural stem cells to the brain using MRI-guided focused ultrasound to disrupt the blood-brain barrier. *PLoS ONE.* (2011) 6:e27877. doi: 10.1371/journal.pone.0027877
78. Lee J, Chang WS, Shin J, Seo Y, Kong C, Song BW, et al. Non-invasively enhanced intracranial transplantation of mesenchymal stem cells using

focused ultrasound mediated by overexpression of cell-adhesion molecules. *Stem Cell Res.* (2020) 43:101726. doi: 10.1016/j.scr.2020.101726
79. Alkins R, Burgess A, Ganguly M, Francia G, Kerbel R, Wels WS, et al. Focused ultrasound delivers targeted immune cells to metastatic brain tumors. *Cancer Res.* (2013) 73:1892–99. doi: 10.1158/0008-5472.CAN-12-2609
80. Alkins R, Burgess A, Kerbel R, Wels WS, Hynynen K. Early treatment of HER2-amplified brain tumors with targeted NK-92 cells and focused ultrasound improves survival. *Neuro Oncol.* (2016) 18:974–81. doi: 10.1093/neuonc/nov318
81. Shen WB, Anastasiadis P, Nguyen B, Yarnell D, Yarowsky PJ, Frenkel V, et al. Magnetic enhancement of stem cell-targeted delivery into the brain following MR-guided focused ultrasound for opening the blood-brain barrier. *Cell Transplant.* (2017) 26:1235–46. doi: 10.1177/0963689717715824
82. Liu HL, Hua MY, Yang HW, Huang CY, Chu PC, Wu JS, et al. Magnetic resonance monitoring of focused ultrasound/magnetic nanoparticle targeting delivery of therapeutic agents to the brain. *Proc Natl Acad Sci U S A.* (2010) 107:15205–10. doi: 10.1073/pnas.1003388107
83. Cui H, Zhu Q, Xie Q, Liu Z, Gao Y, He Y, et al. Low intensity ultrasound targeted microbubble destruction assists MSCs delivery and improves neural function in brain ischaemic rats. *J Drug Target.* (2020) 28:320–9. doi: 10.1080/1061186X.2019.1656724
84. Kalkowski L, Malysz-Cymborska I, Golubczyk D, Janowski M, Holak P, Milewska K, et al. MRI-guided intracerebral convection-enhanced injection of gliotoxins to induce focal demyelination in swine. *PLoS ONE.* (2018) 13:e0204650. doi: 10.1371/journal.pone.0204650
85. Ruster B, Gottig S, Ludwig RJ, Bistrian R, Muller S, Seifried E, et al. Mesenchymal stem cells display coordinated rolling and adhesion behavior on endothelial cells. *Blood.* (2006) 108:3938–44. doi: 10.1182/blood-2006-05-025098
86. Prowse AB, Chong F, Gray PP, Munro TP. Stem cell integrins: implications for *ex-vivo* culture and cellular therapies. *Stem Cell Res.* (2011) 6:1–12. doi: 10.1016/j.scr.2010.09.005
87. Ziadloo A, Burks SR, Gold EM, Lewis BK, Chaudhry A, Merino MJ, et al. Enhanced homing permeability and retention of bone marrow stromal cells by noninvasive pulsed focused ultrasound. *Stem Cells.* (2012) 30:1216–27. doi: 10.1002/stem.1099
88. Burks SR, Ziadloo A, Hancock HA, Chaudhry A, Dean DD, Lewis BK, et al. Investigation of cellular and molecular responses to pulsed focused ultrasound in a mouse model. *PLoS ONE.* (2011) 6:e24730. doi: 10.1371/journal.pone.0024730
89. Burks SR, Ziadloo A, Kim SJ, Nguyen BA, Frank JA. Noninvasive pulsed focused ultrasound allows spatiotemporal control of targeted homing for multiple stem cell types in murine skeletal muscle and the magnitude of cell homing can be increased through repeated applications. *Stem Cells.* (2013) 31:2551–60. doi: 10.1002/stem.1495
90. Burks SR, Nguyen BA, Tebebi PA, Kim SJ, Bresler MN, Ziadloo A, et al. Pulsed focused ultrasound pretreatment improves mesenchymal stromal cell efficacy in preventing and rescuing established acute kidney injury in mice. *Stem Cells.* (2015) 33:1241–53. doi: 10.1002/stem.1965
91. Tebebi PA, Kim SJ, Williams RA, Milo B, Frenkel V, Burks SR, et al. Improving the therapeutic efficacy of mesenchymal stromal cells to restore perfusion in critical limb ischemia through pulsed focused ultrasound. *Sci Rep.* (2017) 7:41550. doi: 10.1038/srep41550
92. Jang KW, Tu TW, Rosenblatt RB, Burks SR, Frank JA. MR-guided pulsed focused ultrasound improves mesenchymal stromal cell homing to the myocardium. *J Cell Mol Med.* (2020) 24:13278–88. doi: 10.1111/jcmm.15944
93. Burks SR, Lorsung RM, Nagle ME, Tu TW, Frank JA. Focused ultrasound activates voltage-gated calcium channels through depolarizing TRPC1 sodium currents in kidney and skeletal muscle. *Theranostics.* (2019) 9:5517–31. doi: 10.7150/thno.33876
94. Burks SR, Nguyen BA, Bresler MN, Nagle ME, Kim SJ, Frank JA. Anti-inflammatory drugs suppress ultrasound-mediated mesenchymal stromal cell tropism to kidneys. *Sci Rep.* (2017) 7:8607. doi: 10.1038/s41598-017-08887-x
95. Hancock HA, Smith LH, Cuesta J, Durrani AK, Angstadt M, Palmeri ML, et al. Investigations into pulsed high-intensity focused ultrasound-enhanced delivery: preliminary evidence for a novel mechanism. *Ultrasound Med Biol.* (2009) 35:1722–36. doi: 10.1016/j.ultrasmedbio.2009.04.020
96. Ziadloo A, Xie J, Frenkel V. Pulsed focused ultrasound exposures enhance locally administered gene therapy in a murine solid tumor model. *J Acoust Soc Am.* (2013) 133:1827–34. doi: 10.1121/1.4789390
97. Hersh DS, Anastasiadis P, Mohammadabadi A, Nguyen BA, Guo S, Winkles JA, et al. MR-guided transcranial focused ultrasound safely enhances interstitial dispersion of large polymeric nanoparticles in the living brain. *PLoS ONE.* (2018) 13:e0192240. doi: 10.1371/journal.pone.0192240
98. Tebebi PA, Burks SR, Kim SJ, Williams RA, Nguyen BA, Venkatesh P, et al. Cyclooxygenase-2 or tumor necrosis factor-alpha inhibitors attenuate the mechanotransductive effects of pulsed focused ultrasound to suppress mesenchymal stromal cell homing to healthy and dystrophic muscle. *Stem Cells.* (2015) 33:1173–86. doi: 10.1002/stem.1927
99. Xhima K, Nabbouh F, Hynynen K, Aubert I, Tandon A. Noninvasive delivery of an alpha-synuclein gene silencing vector with magnetic resonance-guided focused ultrasound. *Mov Disord.* (2018) 33:1567–79. doi: 10.1002/mds.101
100. Provenzale JM, Silva GA. Uses of nanoparticles for central nervous system imaging and therapy. *AJNR Am J Neuroradiol.* (2009) 30:1293–301. doi: 10.3174/ajnr.A1590
101. Zheng Y, Huang J, Zhu T, Li R, Wang Z, Ma F, et al. Stem cell tracking technologies for neurological regenerative medicine purposes. *Stem Cells Int.* (2017) 2017:9. doi: 10.1155/2017/2934149
102. Gu E, Chen WY, Gu J, Burridge P, Wu JC. Molecular imaging of stem cells: tracking survival, biodistribution, tumorigenicity, and immunogenicity. *Theranostics.* (2012) 2:335–45. doi: 10.7150/thno.3666
103. Zhu J, Zhou L, XingWu F. Tracking neural stem cells in patients with brain trauma. *N Engl J Med.* (2006) 355:2376–8. doi: 10.1056/NEJMc055304
104. Bulte JWM, Daldrup-Link HE. Clinical tracking of cell transfer and cell transplantation: trials and tribulations. *Radiology.* (2018) 289:604–15. doi: 10.1148/radiol.2018180449
105. Gorelik M, Orukari I, Wang J, Galpoththawela S, Kim H, Levy M, et al. Use of MR cell tracking to evaluate targeting of glial precursor cells to inflammatory tissue by exploiting the very late antigen-4 docking receptor. *Radiology.* (2012) 265:175–85. doi: 10.1148/radiol.12112212
106. Richard J-P, Hussain U, Gross S, Taga A, Kouser M, Almad A, et al. Perfluorocarbon labeling of human glial-restricted progenitors for 19F magnetic resonance imaging. *Stem Cells Transl Med.* (2019) 8:355–65. doi: 10.1002/sctm.18-0094
107. Cheng SH, Yu D, Tsai HM, Morshed RA, Kanojia D, Lo LW, et al. Dynamic *in vivo* SPECT imaging of neural stem cells functionalized with radiolabeled nanoparticles for tracking of glioblastoma. *J Nucl Med.* (2016) 57:279–84. doi: 10.2967/jnumed.115.163006
108. Bulte JW, Walczak P, Janowski M, Krishnan KM, Arami H, Halkola A, et al. Quantitative "hot spot" imaging of transplanted stem cells using superparamagnetic tracers and magnetic particle imaging (MPI). *Tomography.* (2015) 1:91–7. doi: 10.18383/j.tom.2015.00172
109. Kennis BA, Michel KA, Brugmann WB, Laureano A, Tao R-H, Somanchi SS, et al. Monitoring of intracerebellarly-administered natural killer cells with fluorine-19 MRI. *J Neuro Oncol.* (2019) 142:395–407. doi: 10.1007/s11060-019-03091-5
110. Bose RJC, Mattrey RF. Accomplishments and challenges in stem cell imaging *in vivo*. *Drug Discovery Today.* (2019) 24:492–504. doi: 10.1016/j.drudis.2018.10.007
111. Tannous BA, Grimm J, Perry KF, Chen JW, Weissleder R, Breakefield XO. Metabolic biotinylation of cell surface receptors for in vivo imaging. *Nat Methods.* (2006) 3:391–6. doi: 10.1038/nmeth875
112. Bindslev L, Haack-Sørensen M, Bisgaard K, Kragh L, Mortensen S, Hesse B, et al. Labelling of human mesenchymal stem cells with indium-111 for SPECT imaging: effect on cell proliferation and differentiation. *Eur J Nucl Med Mol Imaging.* (2006) 33:1171–7. doi: 10.1007/s00259-006-0093-7
113. Gildehaus FJ, Haasters F, Drosse I, Wagner E, Zach C, Mutschler W, et al. Impact of Indium-111 oxine labelling on viability of human mesenchymal stem cells *in vitro*, and 3D cell-tracking using SPECT/CT *in vivo*. *Mol Imaging Biol.* (2011) 13:1204–14. doi: 10.1007/s11307-010-0439-1
114. Varma NR, Janic B, Iskander AS, Shankar A, Bhuiyan MP, Soltanian-Zadeh H, et al. Endothelial progenitor cells (EPCs) as gene carrier

system for rat model of human glioma. *PLoS ONE.* (2012) 7:e30310. doi: 10.1371/journal.pone.0030310
115. Wolfs E, Struys T, Notelaers T, Roberts SJ, Sohni A, Bormans G, et al. 18F-FDG labeling of mesenchymal stem cells and multipotent adult progenitor cells for PET imaging: effects on ultrastructure and differentiation capacity. *J Nucl Med.* (2013) 54:447–54. doi: 10.2967/jnumed.112.108316
116. Holvoet B, De Waele L, Quattrocelli M, Gheysens O, Sampaolesi M, Verfaillie CM, et al. Increased understanding of stem cell behavior in neurodegenerative and neuromuscular disorders by use of noninvasive cell imaging. *Stem Cells Int.* (2016) 2016:6235687. doi: 10.1155/2016/6235687
117. Ludewig P, Gdaniec N, Sedlacik J, Forkert ND, Szwargulski P, Graeser M, et al. Magnetic particle imaging for real-time perfusion imaging in acute stroke. *ACS Nano.* (2017) 11:10480–8. doi: 10.1021/acsnano.7b05784
118. Nejadnik H, Pandit P, Lenkov O, Lahiji AP, Yerneni K, Daldrup-Link HE. Ferumoxytol can be used for quantitative magnetic particle imaging of transplanted stem cells. *Mol Imaging Biol.* (2019) 21:465–72. doi: 10.1007/s11307-018-1276-x
119. Graeser MFT, Szwargulski P, Werner F, Gdaniec N, Boberg M, Griese F, et al. Human-sized magnetic particle imaging for brain applications. *Nat Commun.* (2019) 10:1936. doi: 10.1038/s41467-019-09704-x
120. Klauer P, Vogel P, Rückert MA, Kullmann WH, Jakob PM, Behr VC. Bimodal TWMPI-MRI hybrid scanner—coil setup and electronics. *IEEE Transac Magnet.* (2015) 51:1–4. doi: 10.1109/TMAG.2014.2324180
121. Dorsey ER, Sherer T, Okun MS, Bloem BR. The emerging evidence of the Parkinson pandemic. *J Parkinsons Dis.* (2018) 8:S3–8. doi: 10.3233/JPD-181474
122. Liu Z, Cheung HH. Stemcell-based therapies for Parkinson disease. *Int J Mol Sci.* (2020) 21. doi: 10.3390/ijms21218060
123. Thomsen GM, Avalos P, Ma AA, Alkaslasi M, Cho N, Wyss L, et al. Transplantation of neural progenitor cells expressing glial cell line-derived neurotrophic factor into the motor cortex as a strategy to treat amyotrophic lateral sclerosis. *Stem Cells.* (2018) 36:1122–31. doi: 10.1002/stem.2825
124. Parmar M, Grealish S, Henchcliffe C. The future of stem cell therapies for Parkinson disease. *Nat Rev Neurosci.* (2020) 21:103–15. doi: 10.1038/s41583-019-0257-7
125. Downs ME, Buch A, Sierra C, Karakatsani ME, Teichert T, Chen S, et al. Long-term safety of repeated blood-brain barrier opening via focused ultrasound with microbubbles in non-human primates performing a cognitive task. *PLoS ONE.* (2015) 10:e0125911. doi: 10.1371/journal.pone.0125911
126. van Linde ME, Brahm CG, de Witt Hamer PC, Reijneveld JC, Bruynzeel AME, Vandertop WP, et al. Treatment outcome of patients with recurrent glioblastoma multiforme: a retrospective multicenter analysis. *J Neurooncol.* (2017) 135:183–92. doi: 10.1007/s11060-017-2564-z
127. Ballabh P, Braun A, Nedergaard M. The blood-brain barrier: an overview: structure, regulation, clinical implications. *Neurobiol Dis.* (2004) 16:1–13. doi: 10.1016/j.nbd.2003.12.016
128. Bago JR, Alfonso-Pecchio A, Okolie O, Dumitru R, Rinkenbaugh A, Baldwin AS, et al. Induced neural stem cells are tumour-homing and inhibit progression of glioblastoma. *Nat Commun.* (2016) 7:10593. doi: 10.1038/ncomms10593
129. Sharif S, Ghahremani MH, Soleimani M. Delivery of exogenous miR-124 to glioblastoma multiform cells by wharton's jelly mesenchymal stem cells decreases cell proliferation and migration, confers chemosensitivity. *Stem Cell Rev Rep.* (2018) 14:236–46. doi: 10.1007/s12015-017-9788-3
130. Portnow J, Synold TW, Badie B, Tirughana R, Lacey SF, D'Apuzzo M, et al. NSC-based anticancer gene therapy: a first-in-human study in recurrent high-grade glioma patients. *Clin Cancer Res.* (2017) 23:2951–60. doi: 10.1158/1078-0432.CCR-16-1518
131. Park SH, Kim MJ, Jung HH, Chang WS, Choi HS, Rachmilevitch I, et al. Safety and feasibility of multiple blood-brain barrier disruptions for the treatment of glioblastoma in patients undergoing standard adjuvant chemotherapy. *J Neurosurg.* (2020) 134:1–9. doi: 10.3171/2019.10.JNS192206
132. Xiao J, Yang R, Biswas S, Zhu Y, Qin X, Zhang M, et al. NSC-based regenerative treatment of multiple sclerosis. *Mol Neurobiol.* (2018) 55:3152–71. doi: 10.1007/s12035-017-0566-7
133. Yousefi F, Lavi Arab F, Saeidi K, Amiri H, Mahmoudi M. Various strategies to improve efficacy of stem cell transplantation in multiple sclerosis: focus on mesenchymal stem cells and neuroprotection. *J Neuroimmunol.* (2019) 328:20–34. doi: 10.1016/j.jneuroim.2018.11.015
134. Kim MJ, Lim JY, Park SA, Park SI, Kim WS, Ryu CH, et al. Effective combination of methylprednisolone and interferon beta-secreting mesenchymal stem cells in a model of multiple sclerosis. *J Neuroimmunol.* (2018) 314:81–8. doi: 10.1016/j.jneuroim.2017.11.010
135. Connick P, Kolappan M, Crawley C, Webber DJ, Patani R, Michell AW, et al. Autologous mesenchymal stem cells for the treatment of secondary progressive multiple sclerosis: an open-label phase 2a proof-of-concept study. *Lancet Neurol.* (2012) 11:150–6. doi: 10.1016/S1474-4422(11)70305-2
136. Riordan NH, Morales I, Fernandez G, Allen N, Fearnot NE, Leckrone ME, et al. Clinical feasibility of umbilical cord tissue-derived mesenchymal stem cells in the treatment of multiple sclerosis. *J Transl Med.* (2018) 16:57. doi: 10.1186/s12967-018-1433-7
137. Dimitrios Karussis M, Karageorgiou C, Vaknin-Dembinsky A,. Safety and Immunological effects of mesenchymal stem cell transplantation in patients with multiple sclerosis and amyotrophic lateral sclerosis. *Arch Neurol.* (2010) 67:1187–94. doi: 10.1001/archneurol.2010.248
138. Leker RR, Shohami E. Cerebral ischemia and trauma—different etiologies yet similar mechanisms: neuroprotective opportunities. *Brain Res Rev.* (2002) 39:55–73. doi: 10.1016/S0165-0173(02)00157-1
139. Steinberg GK, Kondziolka D, Wechsler LR, Lunsford LD, Kim AS, Johnson JN, et al. Two-year safety and clinical outcomes in chronic ischemic stroke patients after implantation of modified bone marrow-derived mesenchymal stem cells (SB623): a phase 1/2a study. *J Neurosurg.* (2018) 131:1–11. doi: 10.3171/2018.5.JNS173147
140. Nikolic B, Faintuch S, Goldberg SN, Kuo MD, Cardella JF. Stem cell therapy: a primer for interventionalists and imagers. *J Vasc Interv Radiol.* (2009) 20:999–1012. doi: 10.1016/j.jvir.2009.04.075
141. Pendharkar AV, Chua JY, Andres RH, Wang N, Gaeta X, Wang H, et al. Biodistribution of NSCs after intravascular therapy for hypoxic-ischemia. *Stroke.* (2010) 41:2064–70. doi: 10.1161/STROKEAHA.109.575993

Conflict of Interest: The authors declare that the research was conducted in the absence of any commercial or financial relationships that could be construed as a potential conflict of interest.

frontiers in Neurology

ORIGINAL RESEARCH
published: 09 July 2021
doi: 10.3389/fneur.2021.673060

Peripheral Nerve Focused Ultrasound Lesioning—Visualization and Assessment Using Diffusion Weighted Imaging

Matthew R. Walker[1,2], *Jidan Zhong*[2], *Adam C. Waspe*[3,4], *Karolina Piorkowska*[3], *Lananh N. Nguyen*[5], *Dimitri J. Anastakis*[1,2,6], *James M. Drake*[1,3,7] *and Mojgan Hodaie*[1,2,8]*

[1] *Institute of Medical Science, University of Toronto, Toronto, ON, Canada,* [2] *Division of Brain, Imaging & Behaviour, Krembil Research Institute, University Health Network, Toronto, ON, Canada,* [3] *Centre for Image Guided Innovation and Therapeutic Intervention, Hospital for Sick Children, Toronto, ON, Canada,* [4] *Department of Medical Imaging, University of Toronto, Toronto, ON, Canada,* [5] *Laboratory Medicine Program, University Health Network and University of Toronto, Toronto, ON, Canada,* [6] *Department of Surgery, Toronto Western Hospital, University Health Network and University of Toronto, Toronto, ON, Canada,* [7] *Department of Neurosurgery, Hospital for Sick Children, Toronto, ON, Canada,* [8] *Department of Neurosurgery, Toronto Western Hospital, University Health Network, Toronto, ON, Canada*

OPEN ACCESS

Edited by:
Vibhor Krishna, The Ohio State University, United States

Reviewed by:
J. Levi Chazen, Cornell University, United States
Rao P. Gullapalli, University of Maryland, United States

***Correspondence:**
Mojgan Hodaie
mojgan.hodaie@uhn.ca

Specialty section:
This article was submitted to Experimental Therapeutics, a section of the journal Frontiers in Neurology

Received: *26 February 2021*
Accepted: *18 June 2021*
Published: *09 July 2021*

Citation:
Walker MR, Zhong J, Waspe AC, Piorkowska K, Nguyen LN, Anastakis DJ, Drake JM and Hodaie M (2021) Peripheral Nerve Focused Ultrasound Lesioning—Visualization and Assessment Using Diffusion Weighted Imaging. Front. Neurol. 12:673060. doi: 10.3389/fneur.2021.673060

Objectives: Magnetic resonance-guided focused ultrasound (MRgFUS) is a non-invasive targeted tissue ablation technique that can be applied to the nervous system. Diffusion weighted imaging (DWI) can visualize and evaluate nervous system microstructure. Tractography algorithms can reconstruct fiber bundles which can be used for treatment navigation and diffusion tensor imaging (DTI) metrics permit the quantitative assessment of nerve microstructure *in vivo*. There is a need for imaging tools to aid in the visualization and quantitative assessment of treatment-related nerve changes in MRgFUS. We present a method of peripheral nerve tract reconstruction and use DTI metrics to evaluate the MRgFUS treatment effect.

Materials and Methods: MRgFUS was applied bilaterally to the sciatic nerves in 6 piglets (12 nerves total). T1-weighted and diffusion images were acquired before and after treatment. Tensor-based and constrained spherical deconvolution (CSD) tractography algorithms were used to reconstruct the nerves. DTI metrics of fractional anisotropy (FA), and mean (MD), axial (AD), and radial diffusivities (RD) were measured to assess acute (<1–2 h) treatment effects. Temperature was measured *in vivo* via MR thermometry. Histological data was collected for lesion assessment.

Results: The sciatic nerves were successfully reconstructed in all subjects. Tract disruption was observed after treatment using both CSD and tensor models. DTI metrics in the targeted nerve segments showed significantly decreased FA and increased MD, AD, and RD. Transducer output power was positively correlated with lesion volume and temperature and negatively correlated with MD, AD, and RD. No correlations were observed between FA and other measured parameters.

Conclusions: DWI and tractography are effective tools for visualizing peripheral nerve segments for targeting in non-invasive surgical methods and for assessing the microstructural changes that occur following MRgFUS treatment.

Keywords: magnetic resonance-guided focused ultrasound, high intensity focused ultrasound, diffusion weighted imaging, diffusion tensor imaging, tractography, peripheral nerves, neuromodulation

INTRODUCTION

Magnetic resonance-guided focused ultrasound (MRgFUS) is a technique to thermally ablate targeted tissue using MR imaging for navigation (1). It is non-invasive and does not involve ionizing radiation. Current clinically approved indications include essential tremor (2), prostate cancer (3), uterine fibroids (4), and bone metastases (5). There is great potential in extending the use of MRgFUS to the peripheral nervous system for treating conditions such as spasticity and chronic pain (6), which is supported by observations of FUS effects on nerve conduction (7). Ablation techniques, of which MRgFUS is a potential alternative, have been studied in peripheral nerve-related conditions including painful stump neuromas (8), peripheral nerve sheath tumors (9), inguinal neuralgia (10), and lumbar degenerative disease (11). Ablation has also been used for cancer pain relief (12, 13) and to treat tumors with proximity to neural structures (14). An understanding of the nerve involvement in these ablation procedures is of great concern whether the nerves are to be targeted directly or to be avoided.

Diffusion weighted imaging (DWI), an imaging technique sensitive to the movement of water in tissue, has the ability to image nerve fibers and measure their microstructural characteristics *in vivo* (15). Tractography algorithms permit the reconstruction of nervous system fiber connectivity based on patterns of restricted water diffusion (16). Modeling the movement of water with tensors, called diffusion tensor imaging (DTI), includes metrics for quantitative evaluation of nerve characteristics. Fractional anisotropy (FA) reflects the directionality of diffusion and has been used as a proxy for nerve integrity (16). Mean diffusivity (MD), an average of all three orthogonal tensor indices, describes the overall magnitude of diffusion and reflects the degree of water diffusion restriction within tissues regardless of fiber orientation (17). Radial diffusivity (RD), a measure of diffusion perpendicular to the primary diffusion direction, is associated with degree of myelination (18). Axial diffusivity (AD), a measure of diffusion parallel to the primary diffusion direction, is sensitive to axonal integrity (18). These DTI metrics can be used as quantitative tools to assess peripheral nerve pathology and measure microstructural changes following treatment.

Accurate imaging is imperative in non-invasive treatments such as MRgFUS as faulty targeting could exacerbate comorbidities or depress treatment outcomes. It is also important that the imaging characteristics are well-understood in order to properly assess treatment response and inform treatment parameters. Conventional MR sequences, such as T1- and T2-weighted imaging, are limited as they cannot selectively visualize peripheral nerves or quantify nerve integrity or injury. Peripheral nerves have been visualized using MR neurography (19) and selective excitation techniques (20), however these approaches do not provide quantitative assessment of nerve changes after treatment. Targeting by atlas or structural images only is also limited in the ability to account for subject variability and specificity in identifying tracts of interest (21). Tractography can remedy these limitations by enhancing navigation in treatments such as transcranial thalamotomy for essential tremor (22, 23) and deep brain stimulation (21, 24, 25), resulting in improved targeting accuracy and patient outcomes.

Early work in DTI suggests its potential to evaluate peripheral nerve injury and regeneration *in vivo* (26, 27). Diffusion imaging permits longitudinal assessment and, in the case of animal studies, obviates the need for large subject numbers to be sacrificed at multiple time points, providing insight into cellular changes in lieu of histological data. Imaging of peripheral nerves has associated technical challenges due to the complexity and variability of the peripheral nervous system and surrounding muscle tissue, which is also fibrous and thus carries an anisotropic diffusion signature. Previous work has shown the importance of employing appropriate diffusion processing and tractography techniques in order to achieve anatomically accurate results (24).

There is a paucity of MRgFUS lesioning studies focusing on peripheral nerves and a greater limitation on the use of DWI to guide treatment. This is primarily due to the technical limitations associated with the accurate anatomical identification of these nerves. In this study, we investigate the use of diffusion tractography for targeting the sciatic nerves of piglets in ablative MRgFUS and DTI metrics for assessing the microstructural changes following treatment. Histological lesion analysis provides insight into cellular changes after treatment and their correlations with imaging and treatment parameters.

MATERIALS AND METHODS

Animal Model

These experiments were approved by the Animal Care Committee and Laboratory Animal Services at the Hospital for Sick Children in Toronto, Ontario, Canada. This study conforms to the policies of the Canadian Council on Animal Care (CCAC).

Six male Yorkshire piglets (average weight 6.7 $\pm$ 1.3 kg, age 24 $\pm$ 4 days) were used. The animals were pre-anesthetized with ketamine solution [10 mg/kg] (Ketalean, CDMV Inc., Quebec, Canada) intramuscularly before being intubated and anesthesia maintained with 2.5% isoflurane and 2 L oxygen via

MR-compatible ventilator. Hair was removed from both thighs of the animal via shaving and commercial depilatory cream to facilitate skin surface coupling with the MRgFUS system, aided by degassed ultrasound gel.

Once prepared, the animals were transported to the MR facilities for pre-treatment imaging on a standard clinical diagnostic table. Heart rate, peripheral capillary oxygen saturation, and body temperature were monitored throughout the experiment. A circulating water blanket was used to help maintain the piglet's core body temperature around 37°C. Upon completion of the experiment, the animals were euthanized while under anesthesia via intravenous injection of sodium pentobarbital [120 mg/kg] (Euthanyl, CDMV Inc., Quebec, Canada).

MR Imaging

DWI and T1-weighted images were acquired before and after treatment using a clinical Philips Achieva 3T MR scanner (Philips Healthcare, Best, Netherlands) and a 32-channel receive-only cardiac coil on a standard diagnostic table. For both imaging and treatment, the animals were placed in lateral decubitus position with thighs perpendicular to the long axis of the body and the leg of interest closest to the tabletop. Separate data sets were acquired for each leg with the lateromedial coverage extending from the outer skin surface to the contralateral spinal nerve roots. This position provided stability to limit potential movement of the animal and a clear path for the ultrasound beam to target the sciatic nerve.

Anatomical images were acquired with a three-dimensional T1 magnetization prepared rapid gradient echo (MPRAGE) sequence. Acquisition parameters included: repetition time (TR) 8.1 ms; echo time (TE) 3.7 ms; flip angle 8°; matrix 224 × 224; field of view (FOV) 224 × 224 mm; slice thickness 1 mm; slice number 70; voxel resolution 1 × 1 × 1 mm; number of signal averages (NSA) 4; SENSE reduction factor 2; acquisition time 14 min 35 s.

Diffusion images were collected with a SENSE-single shot spin-echo echo-planar-imaging (SE-EPI) sequence with a *b*-value of 800 s/mm^2 and 128 diffusion encoding directions. Two additional baseline images with $b = 0$ s/mm^2 were acquired, one each in forward and reverse phase-encode directions, for post-processing EPI-based susceptibility distortion corrections. Other diffusion scanning parameters include: TR 5845 ms; TE 106 ms; flip angle 90°; matrix 128 × 128; FOV 205 × 205 mm; slice thickness 1.6 mm; slice number 38; voxel resolution 1.6 × 1.6 × 1.6 mm; NSA 2; SENSE reduction factor 2; diffusion gradient pulse duration/time interval 15.7/52.9 ms; acquisition time 29 min 33 s.

Image Post-processing and Tractography

Post-processing was carried out with the FSL software library (Analysis Group, FMRIB, Oxford, UK: https://fsl.fmrib.ox.ac.uk/fsl/fslwiki) (28). Corrections were performed to remedy distortions caused by EPI and susceptibility-induced off-resonance fields using the two baseline images with opposing phase-encoding as implemented in FSL "topup" (29, 30). Susceptibility-corrected images were further processed to remove distortions associated with bulk motion and eddy currents in FSL "eddy" (31). Water diffusion was modeled from fully corrected data by fitting tensors to each image voxel (32). Tensors were used to calculate scalar maps of FA, MD, AD, and RD (33). Structural and diffusion images were linearly co-registered using FSL FLIRT and manual adjustment (34). Pre- and post-treatment images within each subject were co-registered with the same method. Image processing time required was ∼40 min for each subject using a moderately powerful workstation with dedicated graphical processing unit.

Fiber tracking was performed with MRtrix (Brain Research Institute, Melbourne, Australia: http://www.brain.org.au/software) (35). The response function for a single fiber population was estimated using the default threshold of FA > 0.2 (36). This response function was then used with a basis of constrained spherical deconvolution (CSD) to estimate the fiber orientation distribution (FOD) (37). CSD has been shown to be an effective tractography method in regions of complex fiber orientations and crossing fibers (38). A deterministic tractography algorithm, "SD-Stream," was used to generate tracks (35). Tracking seeds were delineated manually at the lumbar nerve roots based on structural T1 and FOD maps. Tracts were segmented by placing inclusion regions of interest (ROI) in terminating muscle regions.

DTI metric assessment was performed by manual placement of a 2 × 2 × 1 voxel (3.2 × 3.2 × 1.6 mm^3) ROI on the sciatic nerve overlapped by the post-treatment lesion as identified by tractography and T1 data. Measurements of FA, AD, RD, and MD were pulled from co-registered pre- and post-treatment images using the same ROI mask. Visually distinct lesion zones were manually identified and measured on T1, aided by voxel intensity thresholding, as a region of hyperintensity (zone I) concentrically surrounded by hypointensity (zone II).

MRgFUS Treatment

Treatment was performed with a clinical MRgFUS system (Sonalleve V1, Profound Medical, Toronto, Canada). Animals were positioned on the treatment table housing the ultrasound transducer. The same lateral decubitus position was used in pre- and post-treatment imaging. Degassed ultrasound gel was applied to the skin surface with a 20 mm gel pad (Aquaflex, Parker Laboratories, New Jersey, USA) placed between the animal and treatment table to facilitate acoustic coupling with the transducer.

Imaging during treatment was accomplished using one element of the cardiac coil (16 channels) placed on top of the animal. Skin bubble images were acquired using a three-dimensional spoiled gradient echo (FFE) sequence to confirm that no air bubbles were present which may interfere with acoustic beam propagation. T1-weighted FFE images were acquired for immediate target identification and treatment cell placement using the Sonalleve planning software.

Cells were placed on the sciatic nerve, posterior to the proximal head of the adjacent femur, with guidance from pre-treatment tractography (**Figure 1A**). The sciatic nerves in these piglets are ∼3 mm wide therefore treatment cell diameters of 4 and 8 mm were chosen to cover the whole nerve. Sonication

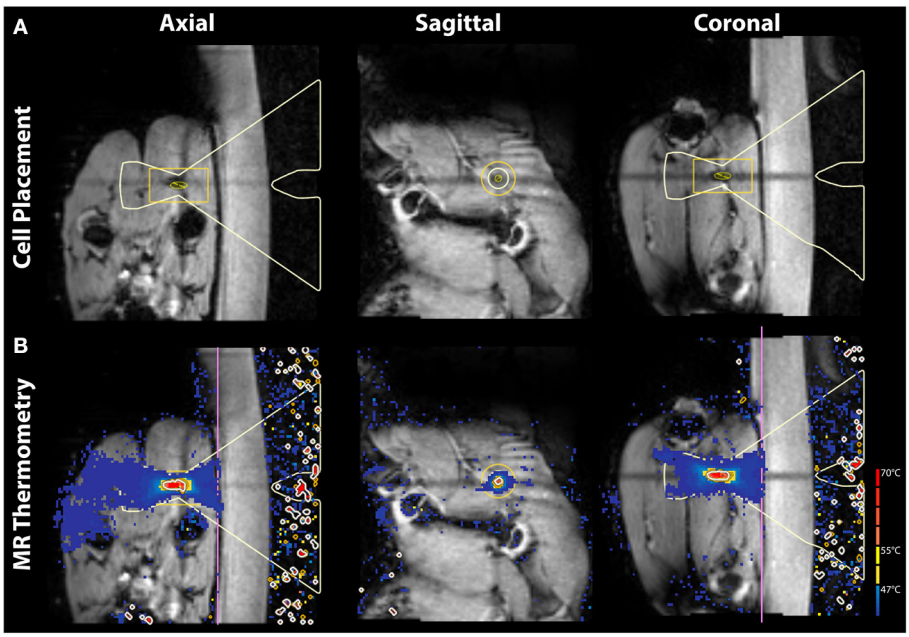

FIGURE 1 | Pre-treatment planning images and in-treatment MR thermometry in axial, sagittal, and coronal view. **(A)** T1-weighted images are shown with the MRgFUS treatment cell placed on the sciatic nerve. **(B)** *In vivo* MR thermometry displaying heat deposition during treatment.

times are fixed based on cell diameter leading to 20 and 27 s treatments for these respective cell sizes. The distance along the beam path from skin surface to treatment cell center was measured. A single sonication was used for each treatment in order to isolate the effect of a given cell size and transducer output power. All ultrasound treatments were delivered with a frequency of 1.2 MHz. Before each therapeutic exposure, one to two test sonications at reduced power of 10 W and 20 s were performed for calibration of beam focus location. Temperature was measured simultaneously with sonication via MR thermometry (**Figure 1B**). Specific treatment parameters for each nerve can be found in **Table 1**. Immediately following treatment in both legs, the animal was repositioned on the diagnostic table for post-treatment imaging (1–2 h after sonication). Identical scanning sequences were used as in pre-treatment imaging.

Histology

Animals were euthanized immediately after post-treatment imaging (<2 h following treatment). The treated area was identified by reflecting the biceps femoris muscle to expose the sciatic nerve and lesion on surrounding muscle tissue. The treated portion of the sciatic nerve and adjacent sections of biceps femoris and semitendinosus muscles were collected. Treated muscle specimens were sampled superficially, deep or mirror to the treated area. Nerve specimens were sampled longitudinally along the axis of the beam path. Internal control specimens of both nerve and muscle were sampled several centimeters away from treated areas, confirmed to free from temperature changes via MR thermometry maps and tissue damage via gross inspection. Samples were immersion fixed with 10% neutral buffered formalin and cooled in a 4°C refrigerator for 48 h before routine histological processing. The tissue was sectioned at a 5-micron thickness at 200-micron levels and stained with hematoxylin and eosin (H&E) and luxol fast blue (LFB). Control samples were exposed to the same conditions and processing as for treated samples except for MRgFUS ablation. Thus, any differences observed between treated and control tissue would be related to MRgFUS treatment. All specimens were evaluated by a neuropathologist who was blinded to the treatment conditions of each specimen.

Statistical Analysis

DTI metric comparisons from pre- and post-treatment lesion ROIs were carried out using paired, two-tailed *t*-tests. Significance was taken as $P < 0.05$. Pearson correlations were performed between maximum temperature, temperature change from baseline, lesion volumes (zones I and II), DTI metrics, and output power (absolute and normalized by skin-to-focus distance). Statistical analysis was performed using SPSS version 23 (IBM, Inc.).

RESULTS

Peripheral Nerve Imaging

On T1-weighted imaging, the sciatic nerve presented as a moderate hyperintensity associated with suppressed signal from nearby blood vessels. Surrounding fat and connective tissue of similar signal intensity to the nerve introduced uncertainty in assessing nerve position at all points in its caudal trajectory from the lumbar plexus. However, the sciatic nerves were successfully reconstructed via both single tensor and CSD tractography in all subjects (**Figure 2**). Tract models were

TABLE 1 | MR-guided focused ultrasound treatment parameters.

Animal #	Target leg	Treatment cell diameter (mm)	Sonication time (s)	Input power (W)	Energy (J)	Maximum temperature (°C)	Temperature difference (°C)	Zone I volume (mm^3)	Zone II volume (mm^3)	Total volume (mm^3)
1	Left	8	27	70	1,890	57.6	18.2	41	140	181
1	Right	8	27	50	1,350	58.7	19.3	53	110	163
2	Left	8	27	110	2,970	82.2	45.7	131	564	695
2	Right	8	27	90	2,430	66.2	29.7	93	340	433
3	Left	8	27	60	1,620	53.2	20.2	59	211	270
3	Right	4	20	80	1,600	56.4	26.4	20	81	101
4	Left	4	20	90	1,800	66.9	35.6	130	410	540
4	Right	8	27	100	2,700	64.2	33.6	274	290	564
5	Left	4	20	100	2,000	65.8	32.4	326	729	1,055
5	Right	4	20	110	2,200	77.6	44.6	392	948	1,340
6	Left	4	20	120	2,400	74.9	39.3	531	809	1,340
6	Right	4	20	130	2,600	112.7	77.3	430	1,270	1,700

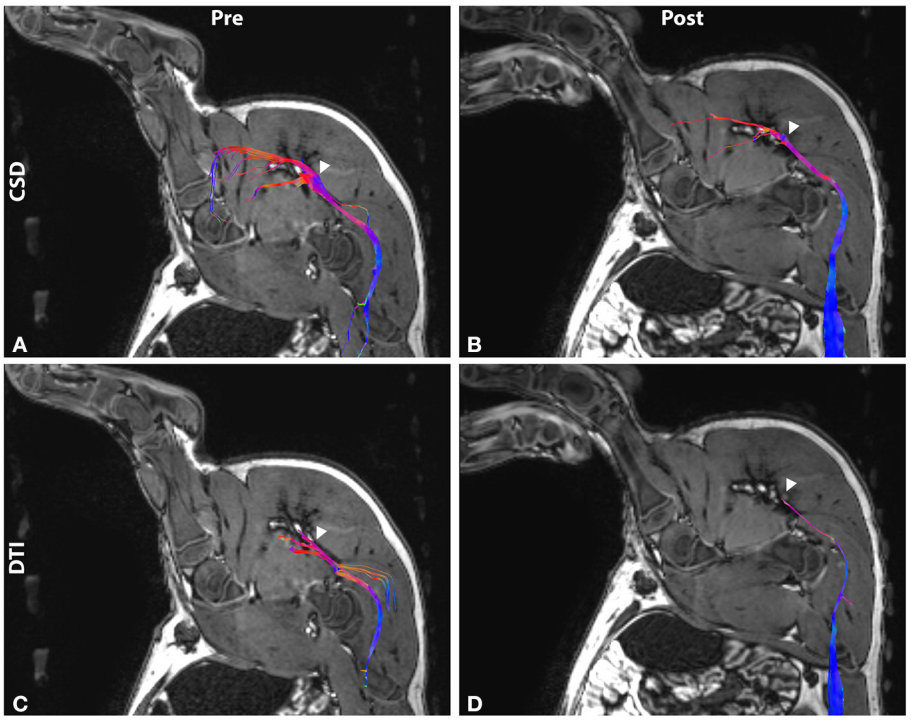

FIGURE 2 | Tractography before and after MRgFUS treatment in sagittal view. Tracts are reconstructed using **(A,B)** constrained spherical deconvolution (CSD) and **(C,D)** diffusion tensor imaging (DTI) methods. Tracts are overlaid on T1-weighted images and colored by orientation: anterior-posterior (blue); superior-inferior (red); left-right (green). Arrowhead indicates treatment target.

observed extending from the vertebral roots, through the lumbar plexus, and terminating in the muscles of the leg posterior to the femur.

MRgFUS Treatment Assessment

Tract abnormalities following MRgFUS treatment were observed in both single tensor and CSD reconstruction models (**Figure 2**). For the tensor model, tracts were discontinuous within the lesion in 8 of the 12 nerves imaged. DTI tracts that did extend into the lesion displayed narrowing and decreased fiber density. In the CSD model, tract continuity was maintained through the lesion in all cases with narrowing and decreased fiber density within the treatment area.

Lesions were identified on T1 images by regions of hyperintensity (zone I) surrounded by hypointensity (zone II) (**Figure 3**). Zone I ranged 20–531 mm^3 with an average of volume of 207 mm^3. Zone II ranged 81 to 1,270 mm^3 with an average of 492 mm^3. Total volume ranged 101–1,700 mm^3 with an average of 699 mm^3. Individual volume measurements and treatment parameters are listed in **Table 1**.

Significant correlations were observed between output power and maximum lesion temperature (correlation coefficient $r = 0.81$, $P = 0.001$), temperature difference ($r = 0.86$, $P = 0.0004$), lesion zone I volume ($r = 0.82$, $P = 0.001$), zone II volume ($r = 0.86$, $P = 0.0003$), and total lesion volume ($r = 0.88$, $P = 0.0001$). Output energy was also correlated with maximum temperature ($r = 0.64$, $P = 0.025$), temperature difference ($r = 0.64$, $P = 0.025$).

DTI metrics measured over the sciatic nerve within the lesion immediately after treatment compared to the pre-treatment baseline revealed significantly decreased FA ($P = 0.00008$), and increased MD ($P = 0.0008$), AD ($P = 0.01$), and RD ($P = 0.0001$). Results are depicted graphically in **Figure 4**.

Significant negative correlations were also observed for output power with diffusivity changes relative to baseline: MD ($r = -0.77$, $P = 0.004$), AD ($r = -0.70$, $P = 0.011$), and RD ($r = -0.70$, $P = 0.011$). No correlations were seen between power and FA.

Maximum temperature and temperature difference were well-correlated with total lesion volume ($r = 0.81$, $P = 0.004$ and $r = 0.80$, $P = 0.005$, respectively) and zone II volume ($r = 0.88$, $P = 0.001$ and $r = 0.89$, $P = 0.001$, respectively) and relatively weakly correlated with zone I volume ($r = 0.65$, $P = 0.023$ and $r = 0.67$, $P = 0.017$, respectively). Temperature difference correlated with MD ($r = -0.68$, $P = 0.016$) and AD ($r = -0.67$, $P = 0.016$) but not significantly with RD ($r = -0.56$, $P = 0.058$) or FA ($r = 0.05$, $P = 0.87$).

Output power normalized by skin-to-focus distance (measured as distance from skin surface to center of treatment cell) was weakly correlated with only maximum temperature ($r = 0.58$, $P = 0.047$) and temperature difference ($r = 0.68$, $P = 0.015$)—less significant than correlations with absolute output power. Selected correlations are shown graphically in **Figure 5**.

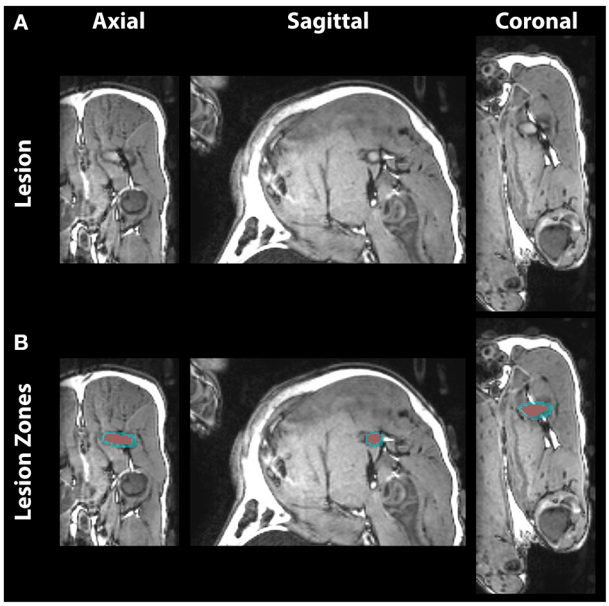

FIGURE 3 | Post-treatment T1-weighted images in axial, sagittal, and coronal view. **(A)** The lesion on the sciatic nerve shows distinct zones of hyperintense necrotic core and surrounding hypointense edema. **(B)** Lesion voxels were segmented into central zone I (red) and surrounding zone II (blue).

Histological Analysis

Gross examination of the dissected tissue revealed pallor of the surrounding muscles and red discoloration of the perineural tissue, further confirming accurate and sufficient delivery of the acoustic energy to the sciatic nerve. Control specimens appeared unremarkable (i.e., no signs tissue damage observed). Microscopic examination of the muscle specimens showed pathologic changes in all areas sampled, superficially, deep or mirror, indicating sensitivity to the acoustic energy regardless of location. All specimens showed changes in a zonal or gradient pattern. **Figures 6A–D** shows a representative zonal pattern where on one end, minimal endomysial edema was present while on the other end, extensive edema and myofiber dropout were present. Nerve specimens (**Figures 6E–H**) showed marked changes. On H&E, specimens showed extensive perineurial and endoneurial edema. LFB stain highlighted loss of myelin while H&E/LFB dual stain highlighted axonal loss. Control specimens for muscle and nerve were unremarkable histologically.

DISCUSSION

In this study, we have demonstrated the feasibility of using diffusion MR tractography to identify and visually reconstruct peripheral nerves and guide their ablative treatment with a clinical MRgFUS system. Further, we have shown the ability of DTI metrics to quantitatively assess the acute changes following treatment. MRgFUS informed by tractography is capable of producing thermal lesions focused on peripheral nerves with minimal damage to surrounding tissue. DTI metrics demonstrate significant microstructural changes to nervous tissue in the form of decreased FA and increased MD, AD, and RD, the latter three of which were found to negatively correlate with transducer output power. Histological analysis verified the damage to the nerves and sharp transition zones from lesions and adjacent untreated tissue.

Experiments of constriction injury in rabbit sciatic nerves have reported microstructural alterations consistent with decreased FA and increased MD and RD (39, 40). However, we observed increased AD while these authors cited significant (40) and non-significant (39) decreases in AD. In constriction injury, it appears that the chronic compression primarily restricts water motion parallel with the nerve and secondarily drives an inflammatory response of axonal swelling and loosening of the myelin sheath. In acute MRgFUS, the thermal ablation results in axonal fragmentation and the accumulation of cell debris which, along with the influx of inflammatory fluid and loosening myelin, contributes to a change toward isotropic diffusion within the nerve. RD, which is associated with degree of fiber myelination, experienced the largest change relative to pre-treatment baseline. Thus, we suspect the myelin disruption and widening of the periaxonal space as seen on histology to be the driving factor behind the results of increased diffusivity and decreased directionality. This is supported by a previous report (7) which

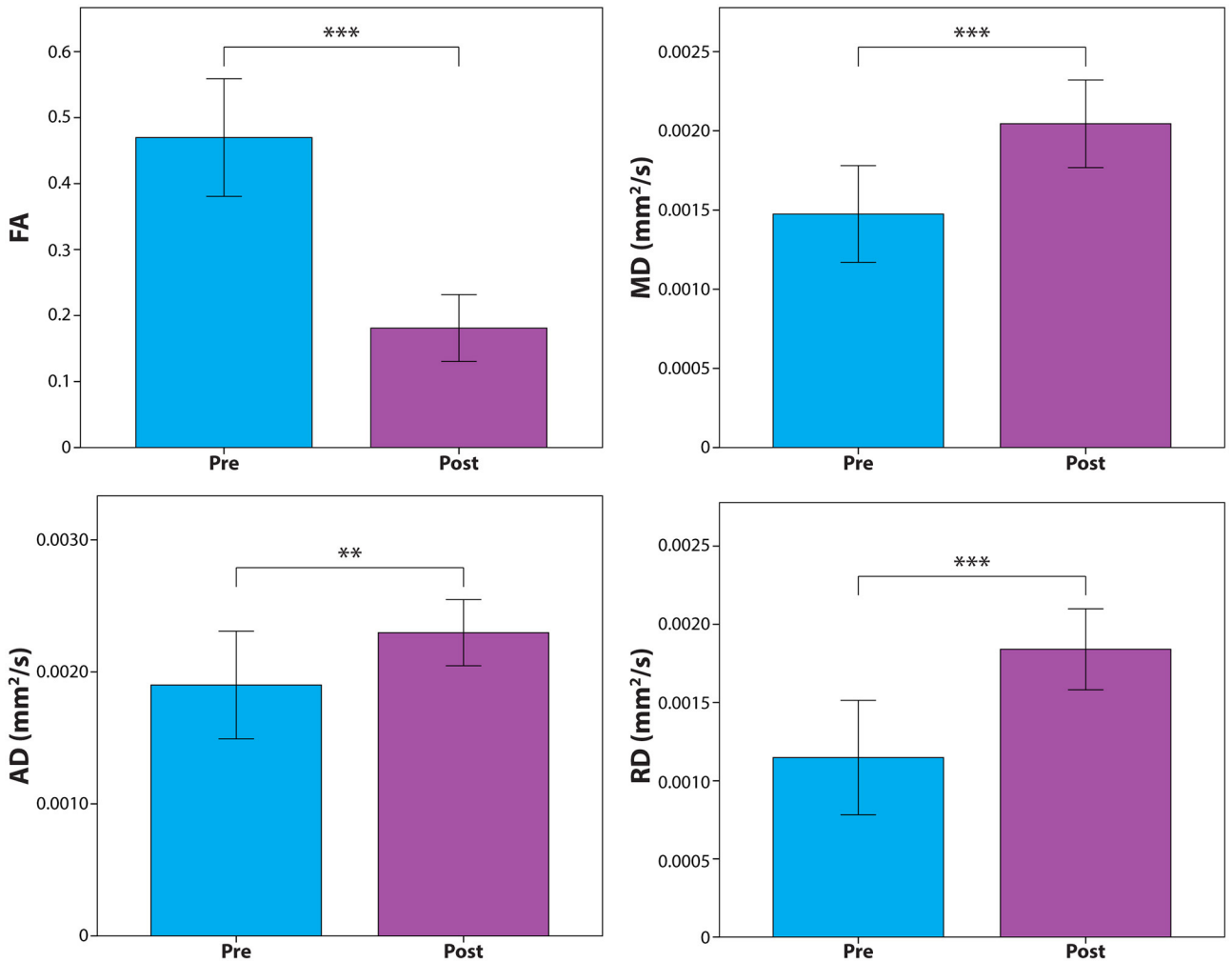

FIGURE 4 | Diffusion tensor metric assessment of the treated sciatic nerve segment before and after MRgFUS. Results show significant changes in fractional anisotropy (FA) and mean (MD), axial (AD), and radial diffusivity (RD). $^{**}P < 0.01$; $^{***}P < 0.001$.

identified axonotmesis, where the axons and myelin sheath are damaged but the gross structure (i.e., epineurium, perineurium, and endoneurium) remains intact, in rat sciatic nerves following FUS exposure. Our tractography results corroborate this further as fiber reconstruction with CSD within the lesion was still possible after treatment. Narrowing of reconstructed fibers and decreased fiber density within the lesion is indicative of some axonal damage and decreased diffusion directionality.

In addition to significant changes in DTI metrics at the group level, negative correlations were observed for MD, AD, and RD with transducer output power. That is, with increasing power more modest alterations to diffusivities were measured. Similar correlations were seen between temperature change from baseline and MD and AD with the RD correlation failing to reach statistical significance ($P = 0.058$). FA changes did not correlate with any other observable. We interpret these FA findings as a possible ceiling effect to the FA decrease in which the nervous tissue has become sufficiently disordered such that further acoustic energy will not further affect diffusion directionality within the nerve. Negative correlations between the diffusivities and both output power and temperature were unexpected, however. We hypothesize that the damage associated with higher sonication intensity and lesion temperature results in increasing damage and accumulation of cellular debris which acts to inhibit the increased motion of water within the nerve. RD exhibited greater relative change with power than both MD and AD. Thus, RD would be the most substantially affected in this regard as myelin disruption-associated RD changes are suspected to be the driving factor behind the diffusivity increases overall.

DWI has been used previously as a monitoring tool immediately after the MRgFUS treatment of bone in *ex vivo* lamb legs (41). Correlations were reported between applied energy, maximum temperature, and lesion volume, which was expected and is confirmed in the present study. Giles et al. also observed a positive correlation between apparent diffusion coefficient (ADC) and applied energy, maximum temperature,

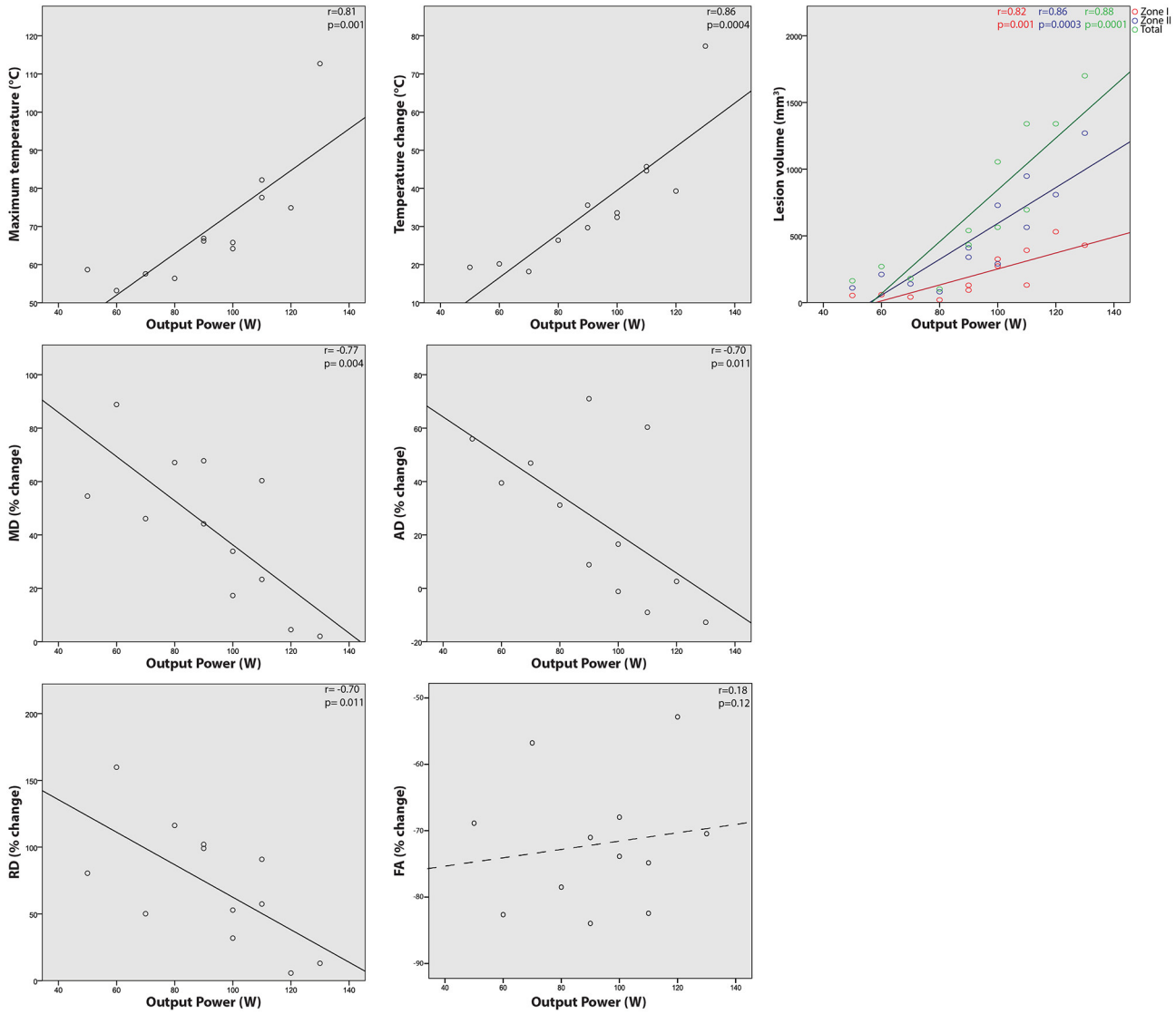

FIGURE 5 | Relationships between single sonication MRgFUS output and treatment results. Correlations are shown between transducer output power and resulting maximum temperature, temperature change from baseline, percent change in fractional anisotropy (FA), mean (MD), axial (AD), and radial diffusivity (RD), and lesion volume (zone I, II, and total).

and lesion volume in muscle tissue adjacent to treated bone at time points ranging from <1–50 min after treatment. While this result differs from the anti-correlation currently presented, several important differences exist between studies: Giles et al. measure only ADC in muscle tissue adjacent to bone in room temperature *ex vivo* subjects at time points <50 min post-treatment. Conversely, we measured multiple DTI metrics in nervous tissue *in vivo* 1–2 h after sonication. The differences in acoustic energy attenuation between bone and soft tissue (42), thermal diffusion dynamics due to blood flow (43), and differing time points complicates direct comparison of the two studies. Further investigation is needed regarding the time evolution of MRgFUS lesions and microstructural dynamics of nerve and muscle tissue.

DTI metrics have been used longitudinally to evaluate sciatic nerve repair following peripheral nerve injury in varying levels of severity where nerve continuity is maintained (26, 27, 39) to complete disruption of axonal and surrounding connective tissue (44, 45). DTI has great potential in this regard as measurements are taken *in vivo*, precluding the need for large numbers of animals to be sacrificed at multiple time points. Due to limitations in data acquisition, these authors were able to reconstruct only small segments of the sciatic nerve and included spurious fibers. We present here robust tractography of the branches of the sciatic nerve from the dorsal root ganglion to their respective terminal muscle destinations, showing that accurate peripheral nerve tractography is achievable with appropriate acquisition

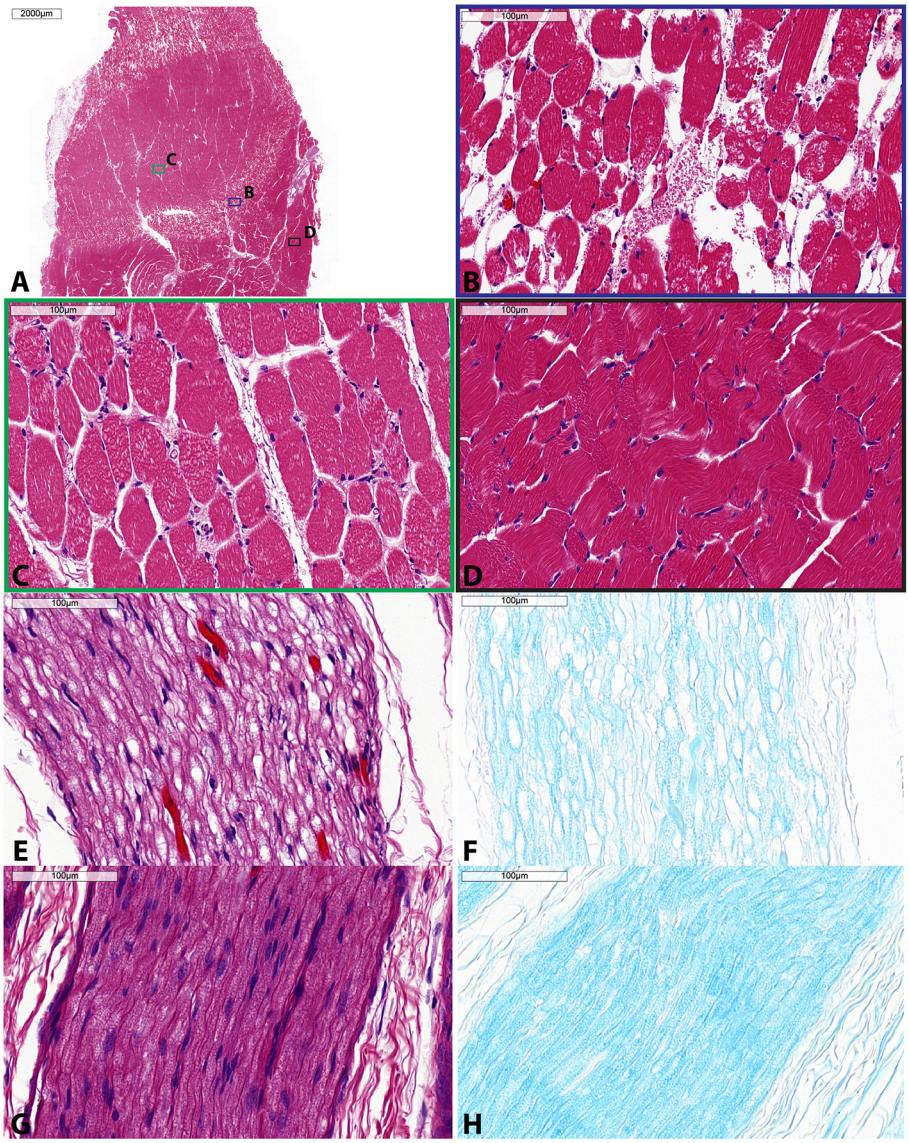

FIGURE 6 | Histologic specimens taken of muscle **(A–D)** and sciatic nerve **(E–H)** following single sonication MRgFUS treatment. **(A)** Low magnification showing zonal changes within the muscle—severe, moderate, and mild. Within this muscle specimen, colored boxes indicate areas of high magnification shown in panels **(B–D)**, each corresponding to these zonal changes. **(B)** High magnification of severe muscle involvement (blue) shows diffuse edema, myofiber vacuolation, and myofiber dropout. **(C)** High magnification of moderate muscle involvement (green) shows perimysial and endomysial edema, myofiber vacuolation, and myofiber necrosis. **(D)** High magnification of mild muscle involvement (black) shows mild myofiber atrophy and endomysial edema. **(E)** High magnification of involved nerve shows endoneurial edema, demyelination, and axonal fragmentation as highlighted by **(F)** LFB stain. **(G)** High magnification of control nerve H&E stain and **(H)** LFB stain. H&E, hematoxylin and eosin; LFB, luxol fast blue. Scale bar is 2,000 µm in **(A)** and 100 µm for **(B–H)**.

parameters and post-processing techniques. Some of the above authors have used track length, normalized to a pre-surgical baseline, as a marker of nerve integrity. This can be problematic as the angle of nerve trajectory is a significant factor in fiber reconstruction and body position is not easily reproduced in repeated imaging sessions and between subjects. Nerve assessment via DTI metrics from a ROI, as we present here, may be a more robust method of evaluating nerve integrity.

The results of this study are consistent with previous experiments who reported similar observations of disrupted myelin and axon swelling in the sciatic nerves of pigs (19, 46) and rats (7) after treatment with FUS. These authors' observations are based on histology but are reinforced by our analysis of both histology and DTI metrics. This important validation of histological analysis by *in vivo* imaging obviates the need to sacrifice animals in order to assess the microstructural response to FUS treatment. DTI has been demonstrated previously as a

useful adjunct to histological analysis (47, 48) and this study extends its application to MRgFUS.

We note that both Huisman et al. and Kaye et al. used large adult pigs (50–75 and 19–40 kg, respectively) with relatively large sciatic nerves (8–10 mm wide) (19, 46). Here we demonstrate the ability to image small animals (5–8 kg) and target small nerves (3–4 mm wide) with similar hardware. These smaller nerves reflect a similar size to potential human clinical MRgFUS targets such as the pudendal nerve (49) or posterior femoral cutaneous nerve (50), as noted by Huisman et al. (19).

Clinically, MRgFUS has potential as a non-invasive alternative to other ablation modalities, including radiofrequency ablation. Peripheral nerve ablation has been studied in a variety of cancerous (8, 9, 12, 13) and non-cancerous conditions (6, 10, 11). Ablation has also been used to treat tumors with close proximity to neural structures (14). For pain relief, a nerve conduction block may be indicated before ablative tract disruption is considered, as suggested by the findings of Foley et al. on FUS-related changes in nerve conduction (7). While conduction block can be successful in reducing pain, the effect can be limited in duration and nerve modulation or ablation may be further considered (51). Whether nerve conduction block or ablation is indicated, an *in vivo* imaging-based understanding of FUS-related nerve changes is important for characterizing treatments and predicting outcomes. This study demonstrates the utility of DWI to visualize and assess nerve changes in these treatments, thus bolstering the potential clinical utility of MRgFUS treatments.

We have demonstrated specificity on segmenting portions of the sciatic nerve based on vertebral origin and terminating muscle innervation (**Supplementary Figure 1**). The same seed ROIs at the nerve roots were used while disparate inclusion ROIs were placed at distal branches of the nerve. Similar techniques have been validated in the central nervous system for segmenting specific tract locations in thalamic nuclei by utilizing anatomically and functionally distinct cortical and subcortical regions in patients with essential tremor (25, 52). This demonstrates the potential to target specific portions of peripheral nerves in non-invasive treatments while avoiding branches of non-interest.

LIMITATIONS

This is an acute study and thus we are not able to determine the longitudinal effect of single-exposure MRgFUS treatment including effects at the lesion site and distal portions of the treated nerve. Previous studies have suggested that Wallerian-type degeneration may cause disruption in nearby white matter and along the length of the lesioned tract (53). Further studies incorporating multiple imaging time points are needed to understand the evolution of MRgFUS lesions and microstructural changes at both the primary injury site and distal tract segments. This study also uses ablative treatments of peripheral nerves, whereas lower intensity, non-ablative sonication may be indicated, as in the case of nerve conduction blocks (7). Future longitudinal studies may thus also incorporate lower power MRgFUS treatments to assess sub-lesional nerve changes and the inflection point between ablative and non-ablative therapies.

Technical challenges limit three-dimensional tractograms from being visualized directly on the MRgFUS targeting software. As such, specific fiber positions must be inferred *in vivo* relative to nearby anatomical structures and with reference to pre-treatment planning images. There exists the potential for targeting errors due to operator bias and positioning reproducibility. This problem is not limited to MRgFUS treatments but with surgical interventions incorporating the visualization of the central and peripheral nervous systems in general. Stereotactic frames in cranial applications can aid target registration but such devices are not generally available for peripheral nerve treatments. Further development in adequate forms of repeatable limb positioning and immobilization is needed for coupling tractography directly with non-invasive surgical approaches to minimize the effect of movement and maximize targeting accuracy.

CONCLUSIONS

This study demonstrates the potential of DWI and tractography for the *in vivo* targeting and assessment of changes following MRgFUS treatment of peripheral nerves. Significant changes in DTI metrics of FA, MD, AD, and RD were observed in the sciatic nerve following single exposure MRgFUS treatment. These DTI metric changes were correlated with sonication parameters. Robust visual reconstruction of the sciatic nerve via tractography was achieved. Diffusion imaging may thus be a valuable tool in optimizing peripheral nerve treatments with MRgFUS and evaluating the effects of treatment.

DATA AVAILABILITY STATEMENT

The raw data supporting the conclusions of this article will be made available by the authors, without undue reservation.

ETHICS STATEMENT

The animal study was reviewed and approved by Animal Care Committee and Laboratory Animal Services at the Hospital for Sick Children, Toronto, Ontario, Canada.

AUTHOR CONTRIBUTIONS

MW, JZ, AW, KP, JD, and MH participated in the experimental design. Data was collected by MW, JZ, AW, and KP. The manuscript was written by MW. Manuscript critique and interpretation was contributed by JZ, AW, KP, LN, DA, JD, and MH. All authors contributed to this work and contributed to the analysis.

FUNDING

MH and JD are supported by a Brain Canada Multi-Investigator Research Initiative and MW by a Mitacs-Accelerate Canada Fellowship (IT05779).

ACKNOWLEDGMENTS

The authors would like to thank Marvin Estrada, Anson Lam, and the rest of the Laboratory Animal Services department at the Hospital for Sick Children for their animal care and handling for these experiments.

SUPPLEMENTARY MATERIAL

The Supplementary Material for this article can be found online at: https://www.frontiersin.org/articles/10.3389/fneur.2021.673060/full#supplementary-material

Supplementary Figure 1 | CSD tractography of the sciatic nerve segmented by fiber bundle vertebral origin and distal termination (individual tracts separated by color). Full reconstructed tracts visible from **(A)** axial, **(B)** sagittal, and **(C)** coronal view. **(D)** Axial views showing only tract segments within the visible slice centered on the MRgFUS lesion. **(E)** Lesion zones I (red) and II (blue) are highlighted. CSD, constrained spherical deconvolution; MRgFUS, magnetic resonance-guided focused ultrasound.

REFERENCES

1. Ghanouni P, Pauly KB, Elias WJ, Henderson J, Sheehan J, Monteith S, et al. Transcranial MRI-Guided Focused Ultrasound: A Review of the Technologic and Neurologic Applications. *Am J Roentgenol*. (2015) 205:150–9. doi: 10.2214/AJR.14.13632
2. Elias WJ, Lipsman N, Ondo WG, Ghanouni P, Kim YG, Lee W, et al. A randomized trial of focused ultrasound thalamotomy for essential tremor. *N Engl J Med*. (2016) 375:730–9. doi: 10.1056/NEJMoa1600159
3. Chaussy CG, Thuroff S. High-intensity focused ultrasound for the treatment of prostate cancer: a review. *J Endourol*. (2017) 31:S-30-S-37. doi: 10.1089/end.2016.0548
4. Hesley GK, Felmlee JP, Gebhart JB, Dunagan KT, Gorny KR, Kesler JB, et al. Noninvasive treatment of uterine fibroids: early Mayo Clinic experience with magnetic resonance imaging-guided focused ultrasound. *Mayo Clin Proc*. (2006) 81:936–42. doi: 10.4065/81.7.936
5. Liberman B, Gianfelice D, Inbar Y, Beck A, Rabin T, Shabshin N, et al. Pain palliation in patients with bone metastases using MR-guided focused ultrasound surgery: a multicenter study. *Ann Surg Oncol*. (2009) 16:140–6. doi: 10.1245/s10434-008-0011-2
6. Foley JL, Little JW, Starr FL, Frantz C, Vaezy S. Image-guided HIFU neurolysis of peripheral nerves to treat spasticity and pain. *Ultrasound Med Biol*. (2004) 30:1199–207. doi: 10.1016/j.ultrasmedbio.2004.07.004
7. Foley JL, Little JW, Vaezy S. Effects of high-intensity focused ultrasound on nerve conduction. *Muscle Nerve*. (2008) 37:241–50. doi: 10.1002/mus.20932
8. Pu S, Wu J, Han Q, Zhang X, Lv Y, Xu Y, et al. Ultrasonography-guided radiofrequency ablation for painful stump neuromas to relieve postamputation pain: a pilot study. *J Pain Res*. (2020) 13:3437–45. doi: 10.2147/JPR.S283986
9. Hirbe AC, Jennings J, Saad N, Giardina JD, Tao Y, Luo J, et al. A Phase II Study of Tumor Ablation in Patients with Metastatic Sarcoma Stable on Chemotherapy. *Oncologist*. (2018) 23:760–e76. doi: 10.1634/theoncologist.2017-0536
10. Kastler A, Aubry S, Barbier-Brion B, Jehl J, Kastler B. Radiofrequency neurolysis in the management of inguinal neuralgia: Preliminary study. *Radiology*. (2012) 262:701–7. doi: 10.1148/radiol.11110727
11. Kim HS, Wu PH, Jang IT. Lumbar degenerative disease part 1: anatomy and pathophysiology of intervertebral discogenic pain and radiofrequency ablation of basivertebral and sinuvertebral nerve treatment for chronic discogenic back pain: a prospective case series and review of lite. *Int J Mol Sci*. (2020) 21:1483. doi: 10.3390/ijms21041483
12. Raslan AM, Cetas JS, Mccartney S, Burchiel KJ. Destructive procedures for control of cancer pain: the case for cordotomy: a review. *J Neurosurg*. (2011) 114:155–70. doi: 10.3171/2010.6.JNS10119
13. Bentley JN, Viswanathan A, Rosenberg WS, Patil PG. Treatment of medically refractory cancer pain with a combination of intrathecal neuromodulation and neurosurgical ablation: Case series and literature review. *Pain Med. (United States)*. (2014) 15:1488–95. doi: 10.1111/pme.12481
14. Kurup AN, Morris JM, Schmit GD, Atwell TD, Weisbrod AJ, Murthy NS, et al. Neuroanatomic considerations in percutaneous tumor ablation. *Radiographics*. (2013) 33:1195–215. doi: 10.1148/rg.334125141
15. Ciccarelli O, Catani M, Johansen-Berg H, Clark C, Thompson A. Diffusion-based tractography in neurological disorders: concepts, applications, and future developments. *Lancet Neurol*. (2008) 7:715–27. doi: 10.1016/S1474-4422(08)70163-7
16. Basser PJ, Pierpaoli C. Microstructural and physiological features of tissues elucidated by quantitative-diffusion-tensor MRI. *J Magn Reson B*. (1996) 111:209–19. doi: 10.1006/jmrb.1996.0086
17. Hagmann P, Jonasson L, Maeder P, Thiran JP, Wedeen VJ, Meuli R. Understanding diffusion MR imaging techniques: from scalar diffusion-weighted imaging to diffusion tensor imaging and beyond. *Radiographics*. (2006) 26(Suppl 1):S205–23. doi: 10.1148/rg.26si065510
18. Song S-K, Sun S-W, Ju W-K, Lin S-J, Cross AH, Neufeld AH. Diffusion tensor imaging detects and differentiates axon and myelin degeneration in mouse optic nerve after retinal ischemia. *Neuroimage*. (2003) 20:1714–22. doi: 10.1016/j.neuroimage.2003.07.005
19. Huisman M, Staruch RM, Ladouceur-Wodzak M, van den Bosch MA, Burns DK, Chhabra A, et al. Non-Invasive Targeted Peripheral Nerve Ablation Using 3D MR Neurography and MRI-Guided High-Intensity Focused Ultrasound. (MR-HIFU): Pilot Study in a Swine Model. *PLoS One*. (2015) 10:e0144742. doi: 10.1371/journal.pone.0144742
20. Budzik J-F, Verclytte S, Lefebvre G, Monnet A, Forzy G, Cotten A. Assessment of reduced field of view in diffusion tensor imaging of the lumbar nerve roots at 3 T. *Eur Radiol*. (2013) 23:1361–6. doi: 10.1007/s00330-012-2710-0
21. Kincses ZT, Szabó N, Valálik I, Kopniczky Z, Dézsi L, Klivényi P, et al. Target identification for stereotactic thalamotomy using diffusion tractography. *PLoS One*. (2012) 7:e29969. doi: 10.1371/journal.pone.0029969
22. Tian Q, Wintermark M, Jeffrey Elias W, Ghanouni P, Halpern CH, Henderson JM, et al. Diffusion MRI tractography for improved transcranial MRI-guided focused ultrasound thalamotomy targeting for essential tremor. *NeuroImage Clin*. (2018) 19:572–80. doi: 10.1016/j.nicl.2018.05.010
23. Chazen JL, Sarva H, Stieg PE, Min RJ, Ballon DJ, Pryor KO, et al. Clinical improvement associated with targeted interruption of the cerebellothalamic tract following MR-guided focused ultrasound for essential tremor. *J Neurosurg*. (2018) 129:1–9. doi: 10.3171/2017.4.JNS162803
24. Sammartino F, Krishna V, King NKK, Lozano AM, Schwartz ML, Huang Y, et al. Tractography-Based Ventral Intermediate Nucleus Targeting: Novel Methodology and Intraoperative Validation. *Mov Disord*. (2016) 31:1217–25. doi: 10.1002/mds.26633
25. Pouratian N, Zheng Z, Bari AA, Behnke E, Elias WJ, DeSalles AAF. Multi-institutional evaluation of deep brain stimulation targeting using probabilistic connectivity-based thalamic segmentation. *J Neurosurg*. (2011) 115:995–1004. doi: 10.3171/2011.7.JNS11250
26. Lehmann HC, Zhang J, Mori S, Sheikh KA. Diffusion tensor imaging to assess axonal regeneration in peripheral nerves. *Exp Neurol*. (2010) 223:238–44. doi: 10.1016/j.expneurol.2009.10.012
27. Takagi T, Nakamura M, Yamada M, Hikishima K, Momoshima S, Fujiyoshi K, et al. Visualization of peripheral nerve degeneration and regeneration:

Monitoring with diffusion tensor tractography. *Neuroimage*. (2009) 44:884–92. doi: 10.1016/j.neuroimage.2008.09.022
28. Jenkinson M, Beckmann CF, Behrens TEJ, Woolrich MW, Smith SM. FSL. *Neuroimage*. (2012) 62:782–90. doi: 10.1016/j.neuroimage.2011.09.015
29. Andersson JLR, Skare S, Ashburner J. How to correct susceptibility distortions in spin-echo echo-planar images: application to diffusion tensor imaging. *Neuroimage*. (2003) 20:870–88. doi: 10.1016/S1053-8119(03)00336-7
30. Smith SM, Jenkinson M, Woolrich MW, Beckmann CF, Behrens TEJ, Johansen-Berg H, et al. Advances in functional and structural MR image analysis and implementation as FSL. *Neuroimage*. (2004) 23 Suppl 1:S208–19. doi: 10.1016/j.neuroimage.2004.07.051
31. Andersson JLR, Sotiropoulos SN. An integrated approach to correction for off-resonance effects and subject movement in diffusion MR imaging. *Neuroimage*. (2016) 125:1063–78. doi: 10.1016/j.neuroimage.2015.10.019
32. Veraart J, Sijbers J, Sunaert S, Leemans A, Jeurissen B. Weighted linear least squares estimation of diffusion MRI parameters: strengths, limitations, and pitfalls. *Neuroimage*. (2013) 81:335–46. doi: 10.1016/j.neuroimage.2013.05.028
33. Westin C-F, Peled S, Gudbjartsson H, Kikinis R, Jolesz F. Geometrical diffusion measures for mri from tensor basis analysis. In: *Proceedings of the 5th Annual Meeting of ISMRM'97*. (2000). p. 1742.
34. Jenkinson M, Bannister P, Brady M, Smith S. Improved optimization for the robust and accurate linear registration and motion correction of brain images. *Neuroimage*. (2002) 17:825–41. doi: 10.1006/nimg.2002.1132
35. Tournier J-D, Calamante F, Connelly A. MRtrix: diffusion tractography in crossing fiber regions. *Int J Imaging Syst Technol*. (2012) 22:53–66. doi: 10.1002/ima.22005
36. Tournier J-D, Calamante F, Connelly A. Determination of the appropriate b value and number of gradient directions for high-angular-resolution diffusion-weighted imaging. *NMR Biomed*. (2013) 26:1775–86. doi: 10.1002/nbm.3017
37. Tournier J-D, Calamante F, Connelly A. Robust determination of the fibre orientation distribution in diffusion MRI: non-negativity constrained super-resolved spherical deconvolution. *Neuroimage*. (2007) 35:1459–72. doi: 10.1016/j.neuroimage.2007.02.016
38. Tournier J-D, Yeh C-H, Calamante F, Cho K-H, Connelly A, Lin C-P. Resolving crossing fibres using constrained spherical deconvolution: Validation using diffusion-weighted imaging phantom data. *Neuroimage*. (2008) 42:617–25. doi: 10.1016/j.neuroimage.2008.05.002
39. Yamasaki T, Fujiwara H, Oda R, Mikami Y, Ikeda T, Nagae M, et al. In vivo evaluation of rabbit sciatic nerve regeneration with diffusion tensor imaging. (DTI): correlations with histology and behavior. *Magn Reson Imaging*. (2015) 33:95–101. doi: 10.1016/j.mri.2014.09.005
40. Wu W, Niu Y, Kong X, Liu D, Long X, Shu S, et al. Application of diffusion tensor imaging in quantitatively monitoring chronic constriction injury of rabbit sciatic nerves: correlation with histological and functional changes. *Br J Radiol*. (2017) 91:1083. doi: 10.1259/bjr.20170414
41. Giles SL, Winfield JM, Collins DJ, Rivens I, Civale J, Ter Haar GR, et al. Value of diffusion-weighted imaging for monitoring tissue change during magnetic resonance-guided high-intensity focused ultrasound therapy in bone applications: an *ex-vivo* study. *Eur Radiol Exp*. (2018) 2:10. doi: 10.1186/s41747-018-0041-x
42. van Rhoon GC, Samaras T, Yarmolenko PS, Dewhirst MW, Neufeld E, Kuster N. CEM43C thermal dose thresholds: a potential guide for magnetic resonance radiofrequency exposure levels? *Eur Radiol*. (2013) 23:2215–27. doi: 10.1007/s00330-013-2825-y
43. Kolios MC, Sherar MD, Hunt JW. Blood flow cooling and ultrasonic lesion formation. *Med Phys*. (1996) 23:1287–98. doi: 10.1118/1.597694
44. Li X, Chen J, Hong G, Sun C, Wu X, Peng MJ, et al. In vivo DTI longitudinal measurements of acute sciatic nerve traction injury and the association with pathological and functional changes. *Eur J Radiol*. (2013) 82:e707–14. doi: 10.1016/j.ejrad.2013.07.018
45. Boyer RB, Kelm ND, Riley DC, Sexton KW, Pollins AC, Shack RB, et al. 4.7-T diffusion tensor imaging of acute traumatic peripheral nerve injury. *Neurosurg Focus*. (2015) 39:E9. doi: 10.3171/2015.6.FOCUS1590
46. Kaye EA, Gutta NB, Monette S, Gulati A, Loh J, Srimathveeravalli G, et al. Feasibility Study on MR-Guided High-Intensity Focused Ultrasound Ablation of Sciatic Nerve in a Swine Model: preliminary results. *Cardiovasc Intervent Radiol*. (2015) 38:985–92. doi: 10.1007/s00270-015-1141-0
47. Schilling KG, Janve V, Gao Y, Stepniewska I, Landman BA, Anderson AW. Histological validation of diffusion MRI fiber orientation distributions and dispersion. *Neuroimage*. (2018) 165:200–21. doi: 10.1016/j.neuroimage.2017.10.046
48. Seehaus A, Roebroeck A, Bastiani M, Fonseca L, Bratzke H, Lori N, et al. Histological validation of high-resolution DTI in human post mortem tissue. *Front Neuroanat*. (2015) 9:98. doi: 10.3389/fnana.2015.00098
49. Rofaeel A, Peng P, Louis I, Chan V. Feasibility of Real-Time Ultrasound for Pudendal Nerve Block in Patients with Chronic Perineal Pain. *Reg Anesth Pain Med*. (2008) 33:139–45. doi: 10.1016/j.rapm.2007.10.004
50. Fritz J, Bizzell C, Kathuria S, Flammang AJ, Williams EH, Belzberg AJ, et al. High-resolution magnetic resonance-guided posterior femoral cutaneous nerve blocks. *Skeletal Radiol*. (2013) 42:579–86. doi: 10.1007/s00256-012-1553-8
51. Choi EJ, Choi YM, Jang EJ, Kim JY, Kim TK, Kim KH. Neural ablation and regeneration in pain practice. *Korean J Pain*. (2016) 29:3–11. doi: 10.3344/kjp.2016.29.1.3
52. Behrens TEJ, Johansen-Berg H, Woolrich MW, Smith SM, Wheeler-Kingshott CAM, Boulby PA, et al. Non-invasive mapping of connections between human thalamus and cortex using diffusion imaging. *Nat Neurosci*. (2003) 6:750–7. doi: 10.1038/nn1075
53. Reginold W, Sam K, Poublanc J, Fisher J, Crawley A, Mikulis DJ. Impact of white matter hyperintensities on surrounding white matter tracts. *Neuroradiology*. (2018) 60:933–44. doi: 10.1007/s00234-018-2053-x

Conflict of Interest: The authors declare that the research was conducted in the absence of any commercial or financial relationships that could be construed as a potential conflict of interest.

frontiers in Neurology

MINI REVIEW
published: 04 November 2021
doi: 10.3389/fneur.2021.749047

Focused Ultrasound Mediated Opening of the Blood-Brain Barrier for Neurodegenerative Diseases

Paul S. Fishman and Johnathan M. Fischell*

Department of Neurology, University of Maryland School of Medicine, Baltimore, MD, United States

The blood brain barrier (BBB) is an obstacle for the delivery of potential molecular therapies for neurodegenerative diseases such as Parkinson's disease (PD), Alzheimer's disease (AD), and amyotrophic lateral sclerosis (ALS). Although there has been a proliferation of potential disease modifying therapies for these progressive conditions, strategies to deliver these large agents remain limited. High intensity MRI guided focused ultrasound has already been FDA approved to lesion brain targets to treat movement disorders, while lower intensity pulsed ultrasound coupled with microbubbles commonly used as contrast agents can create transient safe opening of the BBB. Pre-clinical studies have successfully delivered growth factors, antibodies, genes, viral vectors, and nanoparticles in rodent models of AD and PD. Recent small clinical trials support the safety and feasibility of this strategy in these vulnerable patients. Further study is needed to establish safety as MRI guided BBB opening is used to enhance the delivery of newly developed molecular therapies.

Keywords: FUS, blood-brain barrier, Alzheimer's disease, Parkinson's disease, focused ultrasound (MRgFUS)

OPEN ACCESS

Edited by:
Vibhor Krishna,
The Ohio State University,
United States

Reviewed by:
Fedor Panov,
Mount Sinai Health System,
United States
Bhavya Shah,
University of Texas Southwestern
Medical Center, United States

****Correspondence:***
Paul S. Fishman
pfishman@som.umaryland.edu

Specialty section:
This article was submitted to Experimental Therapeutics, a section of the journal Frontiers in Neurology

Received: *28 July 2021*
Accepted: *27 September 2021*
Published: *04 November 2021*

Citation:
Fishman PS and Fischell JM (2021) Focused Ultrasound Mediated Opening of the Blood-Brain Barrier for Neurodegenerative Diseases. Front. Neurol. 12:749047. doi: 10.3389/fneur.2021.749047

In spite of major gains in the understanding of the biology of neurodegenerative disease such as Alzheimer's disease (AD), Parkinson's disease (PD), amyotrophic lateral sclerosis (ALS), and Huntington's disease, they remain progressively disabling and deadly conditions. Although many agents have provided neuroprotection in cellular and animal models of these conditions, none has resulted in clinically meaningful modification of their progressively worsening natural course. The need for effective disease modifying therapy (DMT) is so dire that agents with likely marginal benefit such as the recently FDA approved aducanumab for AD generate great public interest (1).

Although the factors responsible for the widespread failures of promising agents to translate into clinically effective DMTs are complex, a role for poor brain bioavailability has been suggested (2). This is particularly true for the growing pharmacopeia of molecular therapies including growth factors, enzymes, monoclonal antibodies, and genetic material, all too large to cross the specialized endothelia that compose the blood-brain barrier (BBB). Unfortunately, the intensity of research progress in the development of molecular therapies has greatly outpaced the development of strategies for their delivery to brain.

Contemporary clinical trials of gene therapy for neurodegenerative disease continue to rely on invasive methods such intracerebral infusion (3, 4). The most well-explored strategy to allow large molecules to cross the BBB has been the creation of hybrid molecules that contain a domain the binds to brain endothelial membrane transport receptors such as the transferrin and insulin receptors (5). These "trojan horse" therapeutics have begun to enter clinical trials (6). There has been a resurgence in interest in intra-arterial infusion of hyperosmolar solutions of mannitol to open the BBB, a method initially developed in the 1980's (7, 8).

The newest strategy to enhance delivery of therapeutics from blood to brain is to use focused ultrasound (FUS). The specialized endothelia of the brain have continuous tight junctions that form the BBB, limiting the movement of large molecules from the bloodstream into brain. Studies by Hynynen, McDannold, and colleagues (9–12) initially demonstrated that FUS applied during the circulation of microbubble suspensions (FDA-approved ultrasound contrast agents) can create a transient and safe disruption of the BBB, which can be targeted to a specific brain region using MRI. This allows large therapeutics to enter the brain from the systemic circulation including antibodies, growth factors, nanoparticles, nucleic acids, viral vectors, and even cells (13–19). Using pulsed ultrasound at a much lower intensity than the continuous ultrasound used for brain tissue ablation, the microbubbles undergo oscillations of expansion and contraction that cause transient separation of endothelial tight junctions—the basis for the BBB (20, 21). The procedure can create transient (hours) opening of the BBB, sufficient to allow extravasation of large therapeutics without pathology or entry of blood components (22, 23).

Delivery of large therapeutics across the BBB with any strategy has been limited by the inefficiency of the transfer where accumulation of 1–2% of the total blood injectate in the brain is a true accomplishment (5). Within safe parameters, BBB opening may last only a few hours, and the amount of the therapeutic entering brain is usually much less. Studies of molecular therapies usually find that <0.1% of the injected agent can be detected in the sonicated region of brain after MRgFUS-mediated opening of the BBB (24).

The first application of this strategy was in brain tumor therapy where in preclinical models of brain metastatic breast cancer, FUS-mediated BBB opening substantially improved the efficacy of the antihuman epidermal growth factor 2 monoclonal antibody trastuzumab (24). Clinical trials of FUS opening to enhance chemotherapy of brain tumors are currently in progress (25).

For neurodegenerative diseases, studies using MRI guided FUS (MRgFUS) have enhanced delivery of several potential DMTs including genes in preclinical models of PD. The delivery of glial cell-derived neurotrophic factor (GDNF) and the related factor neurturin from the blood was improved in rodents with the use of this strategy (26, 27). Gene delivery of GDNF has been successful in restoring dopamine metabolism and reversing motor abnormalities in a toxin-induced rat model of PD (28). In an effort to improve the efficiency of delivery (a persistent problem with all blood to brain strategies), the plasmid was preloaded into the microbubbles to enhance its concentration in the region of FUS-mediated BBB opening.

Gene delivery for GDNF has also been successful with enhanced brain distribution using brain penetrant nanoparticles with FUS mediated BBB disruption (D) in the 6-OHDA rodent model of PD (29). Another strategy to improve efficiency of delivery of FUS mediated BBBD has been the use of viral vectors (19, 30). Gene delivery using an adeno associated viral (AAV) vector for GDNF was effective in ameliorating the sub-acute MPTP injection rodent model of PD (31). These studies demonstrate that FUS mediated BBBD can clearly be combined with other delivery methods in the goal of improving the efficiency of brain delivery while still minimizing invasiveness. In a highly novel approach, FUS enhanced the distribution of intranasally delivered BDNF. Although the mechanism of this enhancement is uncertain, this combination successfully improved mice exposed to MPTP (32). Similar mechanism may underlie FUS mediated improvement in distribution of therapeutics after convection-enhanced intracerebral injection, which is the current clinical standard for delivery of protein and gene therapy to the brain (33, 34).

More than 30 years after the initial clinical trials, cell-based therapy has yet to fulfill its promise as a DMT for neurodegenerative disease. As with gene therapy, clinical studies of stem cells for PD still rely on intraparenchymal injection (35, 36). In spite of their large size, rodent studies have demonstrated enhanced delivery of stem cells to brain from the blood, which may involve active mechanism such as chemoattraction and transcytosis across the brain endothelium (37). At this point, however, a beneficial effect of FUS enhanced stem cell delivery has yet to be demonstrated in an animal model of a neurodegenerative disease.

There is also a strong body of evidence from animal studies suggesting the potential benefit of BBBD in AD. These studies explored the possibility that BBBD could be a tool to accelerate the clearance of beta-amyloid from the brain—a major goal of many current AD experimental therapeutics. Studies in mouse models of AD have demonstrated both reduction in brain amyloid burden and behavioral improvement using BBBD coupled with either infused or endogenous anti-amyloid antibodies (18, 38). This reduction in amyloid burden and improved behavior occurred without evidence of brain hemorrhage, a known risk of FUS as well as a clear concern when considering the coexistence of amyloid angiopathy in AD with its significant risk of brain hemorrhage (39). One of the AD/amyloid animal studies demonstrated that moving the target of sonication through the brain (scanning FUS) could be a potential useful strategy for treatment of a large brain volume (40).

As with most antibodies, relatively little of an anti-amyloid antibody enters the brain from an IV injection [0.1% (41)]. However, these antibodies appear to have the capacity to accumulate in the AD brain, likely due to binding to brain amyloid (42). The mechanism by which anti-amyloid antibodies in the blood reduce brain amyloid burden without significant entry into brain remains controversial and how FUS potentiates amyloid clearance is under active investigation (43, 44). There is also concern that compromise of the BBB may also interfere with normal amyloid clearance from the brain (45).

FUS mediated BBB opening also appears to stimulate neurogenesis in the treated region, although once again the mechanism involved is uncertain (46, 47).

In spite of these promising pre-clinical rodent studies, the path to clinical trials of BBBD for neurodegenerative disease is not straightforward. All potential therapeutics utilized in the animal studies are experimental, without full FDA approval. A trial that combines a first of its kind study of an experimental delivery method such as FUS mediated BBBD with an experimental agent such as gene therapy would pose unknown risks to this fragile

patient population that may be additive. This is particularly relevant to the combined use of BBBD for delivery of an anti-amyloid antibody where there is overlap in potential adverse effects and pathology. FUS mediated BBBD carries with it a risk of excessive disruption of the BBB resulting in brain edema and hemorrhage although neither pathology was observed in animal studies with transgenic AD mice or aged dogs with amyloid deposition (48). An increase in multiple inflammatory markers has been described in other animal studies of FUS mediated BBBD (49). Both brain edema and hemorrhage are also risk of treatment with monoclonal antibodies against amyloid for AD (50).

The possibility of additive and unknown risks with the combination of an experimental agent and an experimental delivery method influenced the design of the first clinical trial of FUS mediated BBBD in patients with AD. Supported by the pre-clinical studies, patient with mild to moderate AD underwent BBBD alone, without infusion of an anti-amyloid antibody (51). A frontal cortex location was chosen as the sonication target, reflecting the emphasis on safety in this first of kind study. Although a hippocampal target could be viewed as more clinically important, its deep location was felt to pose a greater risk if significant edema or bleeding were to occur. Patients who tolerated a relatively small volume of BBBD had the procedure repeated later targeting a larger volume. This study supported both the feasibility of opening the BBBD in AD patients (using gadolinium extravasation as an outcome measure) as well as its safety. No significant change in amyloid signal on PET scans or cognitive change was detected, although the study was not powered to assess these efficacy outcomes. There was no significant edema or bleeding among the five treated patients, although transient evidence of possible micro-hemorrhage was observed.

A subsequent study of six patients with AD targeting the hippocampus also supported the safety of FUS mediated BBBD (52). This group of patients also showed a modest reduction of amyloid related signal on 18 F-Florbetaben PET the after three rounds of BBBD over 6 months (53).

It should be noted that this is one of several setting where FUS mediated BBBD will need to be performed on a repeated basis. This will also increase an aspect of brain FUS that reduces patient satisfaction, that of complete shaving of the head, which contemporary neurosurgical procedures tend to avoid. With the recent FDA approval of aducanumab (Aduhelm), it is likely that this agent will be combined with FUS mediated BBBD in the near future. A recent study in an AD transgenic mouse has already assessed the combination of a murine aducanumab analog and BBBD using scanning FUS (54). As expected, FUS substantially increased the distribution and amount of this anti-amyloid antibody in the brain. It is encouraging that a potential safety outcome—brain microhemorrhages—were not increased in any of the treatment groups including combination treatment. Although the effect on clearance of amyloid from the brain varied with brain region (increased clearance with combination treatment of frontal cortex but not in the hippocampus), there was substantial improvement in performance on a spatial memory tasks only with combination treatment. Although the hypothesis is that this combined approach will be more effective than either modality alone for both removal of cerebral amyloid and clinical improvement, safety will remain the primary outcome measure in the initial studies.

A similar approach has been utilized in patients with PD dementia (55). Although PD has predominantly intracellular accumulation of pathologic forms of alpha synuclein, PD dementia is strongly associated with a combination of alpha synuclein and amyloid deposition (56). This recent study of five patients supports the safety of multiple repeated rounds of BBBD of a target region at the parieto-occipito-temporal junction. Although mild improvement in cognition was observed, no significant change in either amyloid or fluorodeoxy glucose by PET scan was observed.

The strategy of combining FUS mediated BBBD with an approved therapeutic is currently underway with a potential DMT for PD. There is a strong association between Gaucher's disease, a lysosomal storage disease caused by mutant forms of the enzyme glucocerebrosidase (GCase) with PD (57). Studies of the interaction of this enzyme with alpha synuclein have also supported GCase as a possible DMT for PD (58). A recombinant form of normal GCase has been an FDA approved therapy for Gaucher's disease for many years (59). As with all forms of enzyme replacement therapy, large molecular size prevents crossing the BBB with limited benefit for CNS forms of diseases associated with detective endogenous enzyme such as Gaucher's. A clinical trial where PD patients are infused intravenously with GCase at the same time as BBBD targeted to the basal ganglia is currently in progress (ClinicalTrials.gov identifier NCT04370665).

The safety of BBBD even in patients where a region with symptomatic neuronal dysfunction is directly targeted is supported by the first study of FUS mediated BBBD in patients with ALS (60). The four volunteers showed no worsening of their motor function after successful BBBD targeted to their motor cortex. The goal of this study as preparation to deliver molecular therapeutics to corticospinal neuronal cell bodies reflects a contemporary review of ALS which emphasizes both the physiologic importance of these "upper motorneurons" in motor symptoms as well as the "dying forward" nature of its pathogenesis that likely begins in the cell soma (61, 62).

These studies illustrate the potential of FUS mediated BBBD to enhance potential DMT for neurodegenerative disease. The initial clinical experience suggests that pulsed FUS coupled with microbubble infusion can result in safe, transient localized opening of the BBBD in patients with AD, PD, and ALS. Pre-clinical studies suggest that this form of BBBD may amplify the efficacy of circulating endogenous and exogenous molecules that are too large to cross the normal BBBD. As the safety of FUS mediated BBBD becomes more established, the opportunities for utilizing it to delivery experimental therapies

show as gene therapies will develop. The combination of effective molecular agents and a safe strategy to enhance their delivery to brain such as FUS mediated BBB opening could accelerate the development of clinical useful disease modifying therapies for the million of patients suffering from progressive neurodegenerative diseases.

AUTHOR CONTRIBUTIONS

PF had primary responsibility for the review of the studies cited and writing of the paper. JF verified the accuracy of the representation of the cited literature. Both authors contributed to the article and approved the submitted version.

REFERENCES

1. de la Torre JC, Gonzalez-Lima F. The FDA approves aducanumab for Alzheimer's disease, raising important scientific questions. *J Alzheimers Dis.* (2021) 2021:210736. doi: 10.3233/JAD-210736
2. Kimura S, Harashima H. Current status and challenges associated with CNS-targeted gene delivery across the BBB. *Pharmaceutics.* (2020) 12:1216. doi: 10.3390/pharmaceutics12121216
3. Hitti FL, Yang AI, Gonzalez-Alegre P, Baltuch GH. Human gene therapy approaches for the treatment of Parkinson's disease: an overview of current andcompleted clinical trials. *Parkinsonism Relat Disord.* (2019) 66:16–24. doi: 10.1016/j.parkreldis.2019.07.018
4. Olanow CW, Bartus RT, Baumann TL, Factor S, Boulis N, Stacy M, et al. Gene delivery of neurturin to putamen and substantia nigra in Parkinson disease: a double-blind, randomized, controlled trial. *Ann Neurol.* (2015) 78:248–57. doi: 10.1002/ana.24436
5. Pardridge WM, Boado RJ. Reengineering biopharmaceuticals for targeted delivery across the blood-brain barrier. *Methods Enzymol.* (2012) 503:269–92. doi: 10.1016/B978-0-12-396962-0.00011-2
6. Giugliani R, Giugliani L, de Oliveira Poswar F, Donis KC, Corte AD, Schmidt M, et al. Neurocognitive and somatic stabilization in pediatric patients with severe Mucopolysaccharidosis Type I after 52 weeks of intravenous brain-penetrating insulin receptor antibody-iduronidase fusion protein (valanafusp alpha): an open label phase 1–2trial. *Orphanet J Rare Dis.* (2018) 13:110. doi: 10.1186/s13023-018-0849-8
7. Gonzales-Portillo GS, Sanberg PR, Franzblau M, Gonzales-Portillo C, Diamandis T, Staples M, et al. Mannitol-enhanced delivery of stem cells and their growth factors across the Blood-Brain barrier. *Cell Transplant.* (2014) 23:531–9. doi: 10.3727/096368914X678337
8. Doolittle ND, Muldoon LL, Culp AY, Neuwelt EA. Delivery of chemotherapeutics across the blood–brain barrier: challenges and advances. *Adv Pharmacol.* (2014) 71:203–43. doi: 10.1016/bs.apha.2014.06.002
9. Sheikov N, McDannold N, Vykhodtseva N, Jolesz F, Hynynen K. Cellular mechanisms of the blood-brain barrier opening induced by ultrasound in presence of microbubbles. *Ultrasound Med Biol.* (2004) 30:979–89. doi: 10.1016/j.ultrasmedbio.2004.04.010
10. McDannold N, Vykhodtseva N, Hynynen K. Use of ultrasound pulses combined with definity for targeted blood-brain barrier disruption: a feasibility study. *Ultrasound Med Biol.* (2007) 33:584–90. doi: 10.1016/j.ultrasmedbio.2006.10.004
11. Hynynen K. Focused ultrasound for blood–brain disruption and delivery of therapeutic molecules into the brain. *Expert Opin Drug Deliv.* (2007) 4:27–35. doi: 10.1517/17425247.4.1.27
12. Hynynen K. Macromolecular delivery across the blood–brain barrier. *Methods Mol Biol.* (2009) 480:175–85. doi: 10.1007/978-1-59745-429-2_13
13. Huang Q, Deng J, Wang F, Chen S, Liu Y, Wang Y, et al. Targeted gene delivery to the mouse brain by MRI-guided focused ultrasound-induced blood–brain barrier disruption. *Exp Neurol.* (2012) 233:350–6. doi: 10.1016/j.expneurol.2011.10.027
14. Fan CH, Ting C, Lin H, Wang C, Liu H, Yen T, et al. SPIO-conjugated, doxorubicin-loaded microbubbles for concurrent MRI and focused-ultrasound enhanced brain-tumor drug delivery. *Biomaterials.* (2013) 34:3706–15. doi: 10.1016/j.biomaterials.2013.01.099
15. Burgess A, Ayala-Grosso CA, Ganguly M, Jordão JF, Aubert I, Hynynen K. Targeted delivery of neural stem cells to the brain using MRI-guided focused ultrasound to disrupt the blood-brain barrier. *PLoS ONE.* (2011) 6:e27877. doi: 10.1371/journal.pone.0027877
16. Burgess A, Huang Y, Querbes W, Sah DW, Hynynen K. Focused ultrasound for targeted delivery of siRNA and efficient knockdown of htt expression. *J Control Release.* (2012) 163:125–9. doi: 10.1016/j.jconrel.2012.08.012
17. Shen WB, Anastasiadis P, Nguyen B, Yarnell D, Yarowsky PJ, Frenkel V, et al. Magnetic enhancement of stem cell-targeted delivery into the brain following MR-guided focused ultrasound for opening the blood-brain barrier. *Cell Transplant.* (2017) 26:1235–46. doi: 10.1177/0963689717715824
18. Jordão JF, Ayala-Grosso CA, Markham K, Huang Y, Chopra R, McLaurin J, et al. Antibodies targeted to the brain with image-guided focused ultrasound reduces amyloid-beta plaque load in the TgCRND8 mouse model of Alzheimer's disease. *PLoS ONE.* (2010) 5:e10549. doi: 10.1371/journal.pone.0010549
19. Thevenot E, Jordao JF, O'Reilly MA, Markham K, Weng YQ, Foust KD, et al. Targeted delivery of self-complementary adeno-associated virus serotype 9 to thebrain, using magnetic resonance imaging-guided focused ultrasound. *Hum Gene Ther.* (2012) 23:1144–55. doi: 10.1089/hum.2012.013
20. Konofagou EE, Tung YS, Choi J, Deffieux T, Baseri B, Vlachos F. Ultrasound-induced blood-brain barrier opening. *Curr Pharm Biotechnol.* (2012) 13:1332–45. doi: 10.2174/138920112800624364
21. Lin CY, Hsieh HY, Chen CM, Wu SR, Tsai CH, Huang CY, et al. Non-invasive, neuron-specific gene therapy by focused ultrasound-induced blood-brain barrier opening in Parkinson's disease mouse model. *J Control Release.* (2016) 235:72–81. doi: 10.1016/j.jconrel.2016.05.052
22. Kobus T, Vykhodtseva N, Pilatou M, Zhang Y, McDannold N. Safety validation of repeated Blood–Brain barrier disruption using focused ultrasound. *Ultrasound Med Biol.* (2016) 42:481–92. doi: 10.1016/j.ultrasmedbio.2015.10.009
23. Jolesz FA, McDannold NJ. Magnetic resonance–guided focused ultrasound: a new technology for clinical neurosciences. *Neurol Clin.* (2014) 32:253–69. doi: 10.1016/j.ncl.2013.07.008
24. Kinoshita M, McDannold N, Jolesz FA, Hynynen K. Noninvasive localized delivery of herceptin to the mouse brain by MRI-guided focused ultrasound-induced blood-brain barrier disruption. *Proc Natl Acad Sci USA.* (2006) 103:11719–23. doi: 10.1073/pnas.0604318103
25. Mainprize T, Lipsman N, Huang Y, Meng Y, Bethune A, Ironside S, et al. Blood-brain barrier openingin primary brain tumors with non-invasive MR-guided focused ultrasound: a clinical safety and feasibility study. *Sci Rep.* (2019) 9:321. doi: 10.1038/s41598-018-36340-0
26. Wang F, Shi Y, Lu L, Liu L, Cai Y, Zheng H, et al. Targeted delivery of GDNF through the blood–brain barrier by MRI-guided focused ultrasound. *PLoS ONE.* (2012) 7:e52925. doi: 10.1371/journal.pone.0052925
27. Samiotaki G, Acosta C, Wang S, Konofagou EE. Enhanced delivery and bioactivity of the neurturin neurotrophic factor through focused ultrasound-mediated blood–brain barrier opening *in vivo*. *J Cereb Blood Flow Metab.* (2015) 35:611–22. doi: 10.1038/jcbfm.2014.236
28. Fan CH, Ting CY, Lin CY, Chan HL, Chang YC, Chen YY, et al. Noninvasive, targeted, and non-viral ultrasound-mediated GDNF-plasmid delivery for treatment of Parkinson's disease. *Sci Rep.* (2016) 6:19579. doi: 10.1038/srep19579
29. Mead BP, Kim N, Miller GW, Hodges D, Mastorakos P, Klibanov AL, et al. Novel focused ultrasound gene therapy approach noninvasively restores dopaminergic neuron function in a rat Parkinson's disease model. *Nano Lett.* (2017) 17:3533–42. doi: 10.1021/acs.nanolett.7b00616
30. Alonso A, Reinz E, Leuchs B, Kleinschmidt J, Fatar M, Geers B, et al. Focal delivery of AAV2/1-transgenes into the rat brain by localized ultrasound-induced BBB opening. *Mol Ther.* (2013) 2:e73. doi: 10.1038/mtna.2012.64
31. Karakatsani ME, Wang S, Samiotaki G, Kugelman T, Olumolade OO, Acosta C, et al. Amelioration of the nigrostriatal pathway facilitated by ultrasound-mediatedneurotrophic delivery in early Parkinson's disease. *J Control Release.* (2019) 303:289–301. doi: 10.1016/j.jconrel.2019.03.030

32. Ji R, Smith M, Niimi Y, Karakatsani ME, Murillo MF, Jackson-Lewis V, et al. Focused ultrasound enhanced intranasal delivery of brain derived neurotrophic factor produces neurorestorative effects in a Parkinson's disease mouse model. *Sci Rep*. (2019) 9:19402. doi: 10.1038/s41598-019-55294-5
33. Fiandaca MS, Lonser RR, Elder JB, Zabek M, Bankiewicz KS. Advancing gene therapies, methods, and technologies for Parkinson's Disease and other neurological disorders. *Neurol Neurochir Pol*. (2020) 54:220–31. doi: 10.5603/PJNNS.a2020.0046
34. Hersh DS, Anastasiadis P, Mohammadabadi A, Nguyen BA, Guo S, Winkles JA, et al. MR-guided transcranial focused ultrasound safely enhances interstitial dispersion of large polymeric nanoparticles in the living brain. *PLoS ONE*. (2018) 13:e0192240. doi: 10.1371/journal.pone.0192240
35. Spencer DD, Robbins RJ, Naftolin F, Marek KL, Vollmer T, Leranth C, et al. Unilateral transplantation of human fetal mesencephalic tissue into the caudate nucleus of patients with Parkinson's disease. *N Engl J Med*. (1992) 327:1541–8. doi: 10.1056/NEJM199211263272201
36. Schweitzer JS, Song B, Herrington TM, Park TY, Lee N, Ko S, et al. Personalized iPSC-derived dopamine progenitor cells for Parkinson's disease. *N Engl J Med*. (2020) 382:1926–32. doi: 10.1056/NEJMoa1915872
37. Ahmed N, Gandhi D, Melhem ER, Frenkel V. MRI guided focused ultrasound-mediated delivery of therapeutic cells to the brain: a review of the state-of-the-art methodology and future applications. *Front Neurol*. (2021) 12:669449. doi: 10.3389/fneur.2021.669449
38. Jordão JF, Thévenot E, Markham-Coultes K, Scarcelli T, Weng YQ, Xhima K, et al. Amyloid-β plaque reduction, endogenous antibody delivery and glial activation by brain-targeted, transcranial focused ultrasound. *Exp Neurol*. (2013) 248:16–29. doi: 10.1016/j.expneurol.2013.05.008
39. Jäkel L, De Kort AM, Klijn CJM, Schreuder FHBM, Verbeek MM. Prevalence of cerebral amyloid angiopathy: a systematic review and meta-analysis. *Alzheimers Dement*. (2021) 2021:alz.12366. doi: 10.1002/alz.12366
40. Leinenga G, Götz J. Safety and efficacy of scanning ultrasound treatment of aged APP23 mice. *Front Neurosci*. (2018) 12:55. doi: 10.3389/fnins.2018.00055
41. Banks WA, Terrell B, Farr SA, Robinson SM, Nonaka N, Morley JE. Passage of amyloid beta protein antibody across the blood-brain barrier in a mouse model of Alzheimer's disease. *Peptides*. (2002) 23:2223–6. doi: 10.1016/S0196-9781(02)00261-9
42. Sevigny J, Chiao P, Bussière T, Weinreb PH, Williams L, Maier M, et al. The antibody aducanumab reduces Aβ plaques in Alzheimer's disease. *Nature*. (2016) 537:50–6. doi: 10.1038/nature19323
43. Levites Y, Smithson LA, Price RW, Dakin RS, Yuan B, Sierks MR, et al. Insights into the mechanisms of action of anti-Abeta antibodies in Alzheimer's disease mouse models. *FASEB J*. (2006) 20:2576–8. doi: 10.1096/fj.06-6463fje
44. Lee Y, Choi Y, Park EJ, Kwon S, Kim H, Lee JY, et al. Improvement of glymphatic-lymphatic drainage of beta-amyloid by focused ultrasound in Alzheimer's disease model. *Sci Rep*. (2020) 10:16144. doi: 10.1038/s41598-020-73151-8
45. Cockerill I, Oliver JA, Xu H, Fu BM, Zhu D. Blood-brain barrier integrity and clearance of amyloid-β from the BBB. *Adv Exp Med Biol*. (2018) 1097:261–78. doi: 10.1007/978-3-319-96445-4_14
46. Burgess A, Dubey S, Yeung S, Hough O, Eterman N, Aubert I, et al. Alzheimer disease in a mouse model: MR imaging-guided focused ultrasound targeted to the hippocampus opens the blood-brain barrier and improves pathologic abnormalities and behavior. *Radiology*. (2014) 273:736–45. doi: 10.1148/radiol.14140245
47. Dubey S, Heinen S, Krantic S, McLaurin J, Branch DR, Hynynen K, et al. Clinically approved IVIg delivered to the hippocampus with focused ultrasound promotes neurogenesis in a model of Alzheimer's disease. *Proc Natl Acad Sci USA*. (2020) 117:32691–700. doi: 10.1073/pnas.1908658117
48. O'Reilly MA, Jones RM, Barrett E, Schwab A, Head E, Hynynen K. Investigation of the safety of focused ultrasound-induced blood-brain barrier opening in a natural canine model of aging. *Theranostics*. (2017) 7:3573–84. doi: 10.7150/thno.20621
49. Kovacs ZI, Kim S, Jikaria N, Qureshi F, Milo B, Lewis BK, et al. Disrupting the blood-brain barrier by focused ultrasound induces sterile inflammation. *Proc Natl Acad Sci USA*. (2017) 114:E75–84. doi: 10.1073/pnas.1614777114
50. Avgerinos KI, Ferrucci L, Kapogiannis D. Effects of monoclonal antibodies against amyloid-β on clinical and biomarker outcomes and adverse event risks: a systematic review and meta-analysis of phase III RCTs in Alzheimer's disease. *Ageing Res Rev*. (2021) 68:101339. doi: 10.1016/j.arr.2021.101339
51. Lipsman N, Meng Y, Bethune AJ, Huang Y, Lam B, Masellis M, et al. Blood-brain barrier opening in Alzheimer's disease using MR-guided focused ultrasound. *Nat Commun*. (2018) 9:2336. doi: 10.1038/s41467-018-04529-6
52. Rezai AR, Ranjan M, D'Haese PF, Haut MW, Carpenter J, Najib U, et al. Noninvasive hippocampal blood-brain barrier opening in Alzheimer's disease with focused ultrasound. *Proc Natl Acad Sci USA*. (2020) 117:9180–2. doi: 10.1073/pnas.2002571117
53. D'Haese PF, Ranjan M, Song A, Haut MW, Carpenter J, Dieb G, et al. β-amyloid plaque reduction in the hippocampus after focused ultrasound-induced blood-brain barrier opening in Alzheimer's disease. *Front Hum Neurosci*. (2020) 14:593672. doi: 10.3389/fnhum.2020.593672
54. Leinenga G, Koh WK, Götz J. A comparative study of the effects of Aducanumab and scanning ultrasound on amyloid plaques and behavior in the APP23 mouse model of Alzheimer disease. *Alzheimers Res Ther*. (2021) 13:76. doi: 10.1186/s13195-021-00809-4
55. Gasca-Salas C, Fernández-Rodríguez B, Pineda-Pardo JA, Rodríguez-Rojas R, Obeso I, Hernández-Fernández F, et al. Blood-brain barrier opening with focused ultrasound in Parkinson's disease dementia. *Nat Commun*. (2021) 12:779. doi: 10.1038/s41467-021-21022-9
56. Irwin DJ, Lee VM, Trojanowski JQ. Parkinson's disease dementia: convergence of α-synuclein, tau and amyloid-β pathologies. *Nat Rev Neurosci*. (2013) 14:626–36. doi: 10.1038/nrn3549
57. Riboldi GM, Di Fonzo AB. *GBA*, Gaucher disease, and Parkinson's disease: from genetic to clinic to new therapeutic approaches. *Cells*. (2019) 8:364. doi: 10.3390/cells8040364
58. Do J, McKinney C, Sharma P, Sidransky E. Glucocerebrosidase and its relevance to Parkinson disease. *Mol Neurodegener*. (2019) 14:36. doi: 10.1186/s13024-019-0336-2
59. Pastores GM, Weinreb NJ, Aerts H, Andria G, Cox TM, Giralt M, et al. Therapeutic goals in the treatment of Gaucher disease. *Semin Hematol*. (2004) 41(4 Suppl.5):4–14. doi: 10.1053/j.seminhematol.2004.07.009
60. Abrahao A, Meng Y, Llinas M, Huang Y, Hamani C, Mainprize T, et al. First-in-human trial of blood-brain barrier opening in amyotrophic lateral sclerosis using MR-guided focused ultrasound. *Nat Commun*. (2019) 10:4373. doi: 10.1038/s41467-019-12426-9
61. Lemon RN. The cortical "Upper Motoneuron" in health and disease. *Brain Sci*. (2021) 11:619. doi: 10.3390/brainsci11050619
62. Eisen A, Braak H, Del Tredici K, Lemon R, Ludolph AC, Kiernan MC. Cortical influences drive amyotrophic lateral sclerosis. *J Neurol Neurosurg Psychiatry*. (2017) 88:917–24. doi: 10.1136/jnnp-2017-315573

Conflict of Interest: PF has received funding from Insightec which has funded some of the clinical studies cited.

The remaining author declares that the research was conducted in the absence of any commercial or financial relationships that could be construed as a potential conflict of interest.

The handling Editor declared a past co-authorship with one of the authors, PF.

Publisher's Note: All claims expressed in this article are solely those of the authors and do not necessarily represent those of their affiliated organizations, or those of the publisher, the editors and the reviewers. Any product that may be evaluated in this article, or claim that may be made by its manufacturer, is not guaranteed or endorsed by the publisher.

frontiers in Neurology

ORIGINAL RESEARCH
published: 12 January 2022
doi: 10.3389/fneur.2021.786734

Resting State Functional Connectivity Signatures of MRgFUS Vim Thalamotomy in Parkinson's Disease: A Preliminary Study

Mario Stanziano[1,2], Nico Golfrè Andreasi[3], Giuseppe Messina[4], Sara Rinaldo[3], Sara Palermo[1,5], Mattia Verri[1], Greta Demichelis[1], Jean Paul Medina[1], Francesco Ghielmetti[6], Salvatore Bonvegna[3], Anna Nigri[1], Giulia Frazzetta[7], Ludovico D'Incerti[1], Giovanni Tringali[4], Francesco DiMeco[8,9,10], Roberto Eleopra[3]* and Maria Grazia Bruzzone[1]*

[1] Neuroradiology Unit, Diagnostic and Technology Department, Fondazione Istituto di Ricovero e Cura a Carattere Scientifico (IRCCS) Istituto Neurologico Carlo Besta, Milan, Italy, [2] Neurosciences Department "Rita Levi Montalcini," University of Turin, Turin, Italy, [3] Parkinson and Movement Disorders Unit, Clinical Neurosciences Department, Fondazione Istituto di Ricovero e Cura a Carattere Scientifico (IRCCS) Istituto Neurologico Carlo Besta, Milan, Italy, [4] Functional Neurosurgery Unit, Neurosurgery Department, Fondazione Istituto di Ricovero e Cura a Carattere Scientifico (IRCCS) Istituto Neurologico Carlo Besta, Milan, Italy, [5] European Innovation Partnership on Active and Healthy Ageing, Brussels, Belgium, [6] Health Department, Fondazione Istituto di Ricovero e Cura a Carattere Scientifico (IRCCS) Istituto Neurologico Carlo Besta, Milan, Italy, [7] InSightec Ltd., Tirat Carmel, Haifa, Israel, [8] Neurosurgery Department, Fondazione Istituto di Ricovero e Cura a Carattere Scientifico (IRCCS) Istituto Neurologico Carlo Besta, Milan, Italy, [9] Pathophysiology and Transplantation Department, University of Milan, Milan, Italy, [10] Neurological Surgery Department, Johns Hopkins Medical School, Baltimore, MD, United States

OPEN ACCESS

Edited by:
Aristide Merola, The Ohio State University, United States

Reviewed by:
Paola Feraco, University of Bologna, Italy
Gaëtan Poulen, Centre Hospitalier Universitaire de Montpellier, France

***Correspondence:**
Sara Palermo
sara.palermo@istituto-besta.it
Roberto Eleopra
roberto.eleopra@istituto-besta.it

Specialty section:
This article was submitted to Experimental Therapeutics, a section of the journal Frontiers in Neurology

Received: *30 September 2021*
Accepted: *02 December 2021*
Published: *12 January 2022*

Citation:
Stanziano M, Golfrè Andreasi N, Messina G, Rinaldo S, Palermo S, Verri M, Demichelis G, Medina JP, Ghielmetti F, Bonvegna S, Nigri A, Frazzetta G, D'Incerti L, Tringali G, DiMeco F, Eleopra R and Bruzzone MG (2022) Resting State Functional Connectivity Signatures of MRgFUS Vim Thalamotomy in Parkinson's Disease: A Preliminary Study. Front. Neurol. 12:786734. doi: 10.3389/fneur.2021.786734

Magnetic Resonance-guided high-intensity Focused Ultrasound (MRgFUS) of the thalamic ventral intermediate nucleus (Vim) for tremor has increasingly gained interest as a new non-invasive alternative to standard neurosurgery. Resting state functional connectivity (rs-FC) correlates of MRgFUS have not been extensively investigated yet. A region of interest (ROI)-to-ROI rs-FC MRI "connectomic" analysis focusing on brain regions relevant for tremor was conducted on 15 tremor-dominant patients with Parkinson's disease who underwent MRgFUS. We tested whether rs-FC between tremor-related areas was modulated by MRgFUS at 1 and 3 months post-operatively, and whether such changes correlated with individual clinical outcomes assessed by the MDS-UPDRS-III sub items for tremor. Significant increase in FC was detected within bilateral primary motor (M1) cortices, as well as between bilateral M1 and crossed primary somatosensory cortices, and also between pallidum and the dentate nucleus of the untreated hemisphere. Correlation between disease duration and FC increase at 3 months was found between the putamen of both cerebral hemispheres and the Lobe VI of both cerebellar hemispheres, as well as between the Lobe VI of untreated cerebellar hemisphere with bilateral supplementary motor area (SMA). Drop-points value of MDS-UPDRS at 3 months correlated with post-treatment decrease in FC, between the anterior cingulate cortex and bilateral SMA, as well as between the Lobe VI of treated cerebellar hemisphere and the interpositus nucleus of untreated cerebellum. Tremor improvement at 3 months, expressed as percentage of intra-subject MDS-UPDRS changes, correlated with FC decrease between bilateral occipital fusiform gyrus and crossed Lobe VI and Vermis VI. Good responders (≥50% of baseline tremor improvement) showed reduced FC between bilateral SMA, between the interpositus nucleus of untreated cerebellum

and the Lobe VI of treated cerebellum, as well as between the untreated SMA and the contralateral putamen. Good responders were characterized at baseline by crossed hypoconnectivity between bilateral putamen and M1, as well as between the putamen of the treated hemisphere and the contralateral SMA. We conclude that MRgFUS can effectively modulate brain FC within the tremor network. Such changes are associated with clinical outcome. The shifting mode of integration among the constituents of this network is, therefore, susceptible to external redirection despite the chronic nature of PD.

Keywords: MRgFUS (magnetic resonance-guided focused ultrasound surgery), tremor, Parkinson's disease, ventral intermediate nucleus (VIM), fMRI, resting state functional connectivity

INTRODUCTION

Patients with Parkinson's disease (PD) have a marked heterogeneity in their clinical features in relation to age of onset, motor presentation/phenotype, neuropsychological profile, and the rate of progression (1, 2). A large body of scientific evidence seems to suggest the existence of four main phenotypes of Parkinson's disease. In addition to the early-onset and late-onset subtypes with rapid disease progression, "motor" subtypes are recognized, particularly the "postural instability and the gait difficulty-dominant," as well as the "tremor-dominant" subtypes (2). Tremor-dominant PD (TD-PD) is classically characterized by the resting tremor of the limbs, with a common re-emergent component after holding sustained postures (3). Tremor affects the quality of life (4). Patients with TD-PD experience intense embarrassment and difficulties due to their tremor that limit social interactions and frequently interferes with their ability to perform the daily living activities and simple tasks both at home and at work (5). Tremor is primarily managed with medications, but both response to tremor and satisfaction with medical therapy are highly variable (5). Moreover, effective medications can be associated with adverse effects (6–8).

The search for increasingly effective therapies drives to a better understanding of the pathophysiology of the disorder and the possible targets for non-pharmacological treatments, such as surgical lesions or neuromodulation. The actual pathophysiology of this disabling phenomenon is still partially undetermined, and the proposed mechanisms are currently under debate. Altered interactions between the cerebello-thalamo-cortical circuitry and the basal ganglia are thought to contribute to parkinsonian tremor (9, 10). In addition, dopamine depletion in the globus pallidus has been historically associated with the severity of clinical tremor (9). These assumptions are echoed by the recent "*finger-switch-dimmer*" hypothesis (11), for which tremor in PD would be: (i) induced by pathological triggering from the dopamine-depleted basal ganglia; (ii) generated by changes in the oscillatory activity within related thalamic nuclei (i.e., from pallidal to cerebellar thalamic recipients); and (iii) modulated by the cerebellum. Efferent copies of tremorigenic thalamic activity would be transmitted to the cerebral sensorimotor cortex, then it will be fed back into the basal ganglia and also propagated to the subthalamic nucleus through thalamo-cortical, thalamo-striatal, cortico-striatal, and cortico-subthalamic pathways (12, 13). Therefore, PD tremor would be mediated by parallel and only apparently segregated trans-cortical and sub-cortical circuits converging to the thalamus (14).

Even though none of the above described "circuital perspectives" is likely to explain definitively how tremor is generated and propagated in TD-PD and similar disorders, such as essential tremor (15), tremorigenic disorders would appear to share a common dysfunctionally distributed tremor-network centered on the thalamus, specifically on the thalamic ventral intermediate nucleus (Vim) (16). Vim is the cerebellum-recipient nucleus of the thalamus and has traditionally been regarded as the preferred target for neuromodulation or lesional neurosurgery to obtain tremor relief (17, 18). Growing recent evidences have shown that effectiveness of interventional procedures for tremor may be related to the proximity between the actual Vim lesion and the white matter tracts extending through the Vim, namely the dentato-rubro-thalamic tract (DRTT) (19–31). Vim ablation would, therefore, interfere with the tremor-sustaining aberrant circuitry (32).

In recent years, promising results have been published on the thalamotomy of the Vim using Magnetic Resonance-guided high-intensity focused ultrasound (MRgFUS). This is a non-invasive procedure performed under MRI guidance which allows to produce a small lesion (i.e., a focal area of coagulative necrosis induced by heat) at the level of selected target (i.e., the Vim) (33). This procedure represents an interesting therapeutic option for parkinsonian tremor that is not responsive to pharmacological therapy in cases where patients do not want to undergo or have contraindications to invasive procedures, such as deep brain stimulation. Subsequently, this technique is increasingly being employed as both safe and effective symptomatic treatment

Abbreviations: BOLD, Blood oxygenation level dependent; CSF, cerebrospinal fluid; dPMC, dorsal premotor cortex; DN, dentate nucleus; DRTT, dentato-rubro-thalamic tract; FC, functional connectivity; FDR, false discovery rate; GM, gray matter; GR, good responder; IN, interpositus nucleus; Lob, lobule; mAC, median anterior cingulate; MDS-UPDRS, Movement Disorder Society Unified Parkinson's Disease Rating Scale; MNI, Montreal Neurological Institute; MRgFUS, Magnetic Resonance-guided high-intensity Focused Ultrasound; OFusG, occipital fusiform gyrus; PaCiG, paracingulate gyrus; PR, poor responder, PreCG, precentral gyrus; PostCG, postcentral gyrus; ROI, region-of-interest; rs-fMRI, Resting state functional MRI; T, tesla; SDR, skull density ratio; SPL, superior parietal lobe; SMA, supplementary motor area; SPM, the Statistical Parametric Mapping; STN, the subthalamic nucleus; TD-PD, tremor-dominant Parkinson's disease; Th, thalamus; TOFusG, temporal-occipital fusiform cortex; TS, treated side; unTS, untreated side; Ver, cerebellum–vermis subdivisions; Vim, thalamic ventral intermediate nucleus; vPMC, ventral premotor cortex; WM, white matter.

for medication-resistant, long-lasting, and disabling tremor in patients suffering from TD-PD.

To the best of our knowledge, there are only a few studies describing functional correlates of Vim ablation, and the potential mechanisms of connectivity reorganization over time after lesional procedures on Vim (mainly based on stereotactic radiosurgical thalamotomy) are yet to be recognized. To date, the literature on PD only includes at most 10 patients (34–42).

Here, we used resting state functional MRI (rs-fMRI) to longitudinally explore the dynamics of functional interactions between different nodes of the above-described *"tremor-network"* before and after the MRgFUS Vim ablation in a cohort of patients with TD-PD (*"Main effect"* of MRgFUS treatment). In particular, our goal was to evaluate if the changes in rs-fMRI interactions were transient and limited over time; for example, occurring only at 1 month after treatment mainly due to early postoperative alterations, or if they were still identifiable at 3 months after the complete postoperative oedema reabsorption.

In addition, we examined whether: (i) disease duration was related to changes in intra-subject FC between the areas that are forming part of the tremor-network (*"treatment by disease duration interaction effect"*); (ii) post-MRgFUS Vim lesion's volume at 24 h influenced the FC changes (*"treatment by lesion volume interaction effect"*); (iii) FC changes correlated with clinical improvement at 3 months after MRgFUS (*"treatment by clinical improvement interaction effect"*); (iv) FC changes differed between clinical outcomes (*"treatment by outcome interaction effect"*). Finally, (v) we attempted to retrospectively identify FC features at baseline that might be predictive of different clinical outcomes (*"pretherapeutic functional profiles of outcomes"*).

MATERIALS AND METHODS

We prospectively enrolled 60 consecutive patients with idiopathic TD-PD [according to clinical diagnostic criteria for Parkinson's disease of the Movement Disorder Society: (43)], with disabling tremor resistant to medication, who were evaluated at our institution from January 2019 to June 2020. All patients were carefully evaluated by a neurologist expert in movement disorders [RE; NGA; SB] and were considered good candidates for MRgFUS unilateral Vim thalamotomy. In particular, patients were examined in "off" (at least 12-h overnight withdrawal of antiparkinsonian therapy) and "on" conditions (90 min after a levodopa loading dose, approximately equal to 150% of the patients' usual morning dose) by the part-III items of the Movement Disorder Society Unified Parkinson's Disease Rating Scale [MDS-UPDRS: (44)].

Main *inclusion criteria* for MRgFUS were: (i) medication-refractory disabling tremor, defined as "disabling in the main activities of daily life despite of all available oral treatments" and confirmed by "acute levodopa challenge response"; (ii) age $>$ 18 years; and (iii) contraindication for deep brain stimulation (DBS) or patients who refused DBS.

Exclusion criteria were as follows: (i) other neurodegenerative diseases than PD; (ii) history of prior stereotactic neurosurgery or DBS; (iii) standard contraindications for MR-imaging or for MRI contrast agent; (iv) patient/s unable to tolerate supine position for long time during treatment (4+ h) or claustrophobia; (v) significant cognitive impairment documented by neuropsychological evaluation (Mini-Mental State Examination $\leq$21); (vi) serious psychiatric pathologies, active drug/alcohol dependency, or prior abuse; (vii) risk factors for bleeding, unstable cardiac status, or medical conditions not allowing anticoagulant/antiplatelet therapy discontinuation; (viii) history of intracranial hemorrhage or stroke within the past 6 months; (ix) history of seizures within the past year; (x) presence of brain tumors; and (xi) a skull density ratio (SDR) (45) $\leq$0.34 as calculated from the head computed tomography screening scan.

Study Design and Outcome Definition

The rs-fMRI data were acquired at baseline (during the screening stage, not exceeding 4 months before MRgFUS treatment), as well as at 1 month (1-mo) and 3 months (3-mo) postoperatively. Clinical assessment was usually performed on the same day of each MRI examination or, at most, the day before or after. For this study, the final clinical outcome was defined by the score variation of the tremor improvement at 3 months (3-mo) post-treatment, regarding the body side contralateral to the thalamotomy, and calculated as absolute drop value (score at 3-mo minus score at baseline of the sub-items 3.15.a, 3.16.a, 3.17.a, and 3.17.c of the MDS-UPDRS scale in the off-state) (39), and also, as percentage of intra-subject value (% = baseline minus 3-mo/baseline score x 100) (20). We adopted a clinical and an rs-MRI evaluation in an off-drug condition because we were interested in the MRgFUS thalamotomy effect on FC without any pharmacological influence. Considering a quartile ranking on the degree of effectiveness (46), improvements of $\geq$50% compared to baseline were considered as therapeutic, while those $<$50% as sub-therapeutic, further defining two outcome subgroups (good vs. poor responders, GR vs. PR).

MRI Data Acquisition and Processing

Transcranial MRgFUS Vim-thalamotomy was performed by the ExAblate 4000 system (InSightec, Haifa, Israel) installed on a 1.5T MR scanner. Screening and follow-up of fMRI data were acquired on a 3T scanner equipped with a 32-channel coil (Achieva TX, Philips Healthcare BV, Best, NL). High resolution volumetric turbo field echo T1-weighted (TR = 8,200 ms; TE = 3,700 ms; flip angle = 8°; voxel = 1 × 1 × 1 mm) and T2-weighted (TR = 2,500 ms; TE = 2,800 ms; flip angle = 90°; voxel = 0.8 × 0.8 × 0.8 mm) images were acquired. The rs-fMRI acquisition consisted of a repeated gradient-echo planar imaging sequence (TR = 3,000 ms, TE = 30 ms, α = 80°, 2.5 mm isotropic voxel size, matrix size = 90 x 95) providing 47 ascending interleaved images per volume, parallel to the anterior commissure-posterior commissure (AC–PC) line and covering the whole brain.

Importantly, the patient habitual pharmacological treatment for tremor was discontinued at least 12 h before the MRI scanning session.

The rs-fMRI data preprocessing and analysis were performed using the Statistical Parametric Mapping (SPM12, http://www.fil.ion.ucl.ac.uk/spm), and the CONN toolbox (release 19.c) (47)

running on MATLAB R2019b (MathWorks, Natick, MA, USA). Scans of patients with right thalamotomy were preliminary flipped so that treatments were all conventionally considered on the left hemisphere. Therefore, we could define a treated side (TS) for the whole study sample, corresponding to the left cerebral hemisphere with contralateral (right) cerebellum, as well as the untreated side (unTS), corresponding to the right cerebral hemisphere with contralateral (left) cerebellum. Functional images were realigned, unwrapped, and slice-time corrected. Gray-matter (GM), white-matter (WM), and cerebrospinal fluid (CSF) were automatically segmented, and the functional data were normalized to the Montreal Neurological Institute (MNI) template. Data were spatially smoothed with a Gaussian kernel set at 6 mm full width at half maximum. The first five principal components from WM and CSF signals, the six motion realignment parameters, and their first-order derivatives, as well as the outlier volumes were detected using the ART-based scrubbing method (48) as implemented in CONN, and were regressed out of the signal. Subjects with excessive head motion in one of the 3 follow-up scans (i.e., $\geq$50% of volumes detected as outliers) were excluded from further analysis. Accepted data were then band-pass filtered (0.008 to 0.1 Hz) and were linearly detrended.

Resting-state functional connectivity was tested with region-to-region ("*connectomic*") analysis. Most region-of-interest (ROI) masks were already in the probabilistic Harvard-Oxford (49) and AAL (50) atlases included in the CONN toolbox. We chose ROIs potential relevance for tremor pathogenesis according to existing literature [in particular see (36)]: precentral (PreCG) and postcentral (PostCG) gyrus; supplementary motor area (SMA); paracingulate gyrus (PaCiG); and median anterior cingulate (mAC), covering the most caudal part of pre-supplementary motor area, as well as the cingulate motor areas; inferior and middle frontal gyrus, encompassing the ventral and dorsal premotor cortex (vPMC and dPMC); superior parietal lobe (SPL); temporal-occipital fusiform cortex (TOFusG); and occipital fusiform gyrus (OFusG) [in particular see (36)]; putamen; pallidum; and all cerebellar lobules (Lob), including vermian subdivisions (Ver). Additional ROI in the thalamus (Th) was initially defined based on patient's lesions and then imported in CONN toolbox; in details, individual MRgFUS thalamic lesions were semi-automatically outlined on the 24-h post-treatment volumetric T2-w images (or, when not available, post-contrast T1-w images) using the ITK-Snap software. Only voxels that were rated by two independent expert observers [MS; GD], as belonging to zones I and II of a particular lesion, were included in the final lesion mask, while the surrounding vasogenic oedema (zone III) (33) was excluded. Lesion masks were normalized to MNI in SPM, and then, were averaged across subjects to create a group thalamic ROI, encompassing all the post-operative Vim (TS Th-Vim). The flipped contralateral ROI was set as the unTS Th-Vim. Moreover, segmented thalamic lesion masks were used to extract individual lesion volumes for further correlation analysis. The masks for deep cerebellar nuclei, dentate nucleus (DN), and interpositus nucleus (IN), were taken from the SPM neuroanatomy toolbox (51) and were imported in the CONN toolbox. All ROIs were thresholded to contain only voxels that were inside each ROI with a probability threshold above 60% (52). Notably, when extracting ROI-level BOLD signal, we opted to use the unsmoothed images to further avoid signal contamination from neighboring voxels of other proximal regions, which was especially important in using cerebellar ROIs that are very close to each other (53).

The ROI-to-ROI analyses consisted of the following steps. Each subject's first-level Fisher-Z transformed connectivity matrices (expressing pairwise correlations between the BOLD time series of each pair of ROIs) were subjected to a second-level within-group and within-subject analysis of variance, testing for FC differences across the three-time points (main contrast analysis, corresponding to the *"main effect of treatment"*: baseline vs. 1-mo vs. 3-mo). In this first analysis, the age and duration of disease were considered as a covariate of no interest to minimize their potential influences. Next, the disease duration, the 24-h individual lesion volume (mm^3), the individual absolute drop points, as well as the % value of tremor improvement at 3-mo were separately fed into a regression model against the main contrast (baseline vs. 1-mo vs. 3-mo) to assess their impact on FC changes (respectively: "*treatment by disease duration,*" "*treatment by lesion volume,*" and "*treatment by clinical improvement*"–interaction effects). Then, a between-subject analysis comparing good vs. poor responders (GR vs. PR) was performed both across the three time points ("*treatment by outcome interaction effect*"), and only at baseline ("*pretherapeutic functional profiles of outcomes*"). All results were corrected at cluster-level by parametric multivariate statistics (cluster-level inferences, functional network connectivity-FNC) (54); with connection threshold set at $p < 0.1$ uncorrected, and cluster threshold set at $p < 0.05$ false discovery rate (FDR) corrected (multi-voxel pattern analysis omnibus test). Statistics outside the CONN toolbox were performed using the OriginPro 2015 (Origin Lab Corporation, Northampton, MA, USA).

RESULTS

Final Sample Definition

Of the initial 60 patients with TD-PD, 20 subjects were found to be eligible for MRgFUS and were admitted to the fMRI longitudinal study. All patients successfully completed the MRgFUS Vim ablation. Four patients did not complete the rs-fMRI follow-up. One patient who completed the rs-fMRI follow-up was excluded from the group-analysis because of excessive head movement, thus, leaving 15 TD-PD in the final study sample. The demographics of the patients, including age, gender, disease duration, side of thalamotomy, and the 1-mo and 3-mo post-treatment tremor improvement for the treated body side relative to baseline, as well as 24-h lesion volumes, are summarized in **Table 1**.

By the 3-mo follow-up of neurological examination, the group of patients were divided based on tremor improvement in: PD-GR ($n = 8$), who differed significantly from PD-PR ($n = 7$) ($t = 5.5$, $p < 0.001$; 69.12 vs. 29.57%). The age, disease duration, and 24-h lesion volumes did not significantly differ between

TABLE 1 | Demographic and clinical data of patients with Parkinson's disease with information on 1-mo and 3-mo post-treatment tremor improvement for the treated body side relative to baseline, as well as 24-h lesion volumes.

	Age (yrs)	Sex	Disease duration (yrs)	Tx side	24 h	Tremor score for treated body side	Drop points (-)	Percentage (%) improvement	Drop points (-)	Percentage (%) improvement
					Lesion vol (mm^3)	At baseline*	1-mo–baseline	At 1-mo	3-mo–baseline	At 3-mo
PD 1	60	M	3	L	241	5	−3	60	−3	60
PD 2	71	M	19	R	280	5	−3	60	−4	80
PD 3	68	M	12	R	159	7	−3	43	−6	86
PD 4	77	M	10	L	456	7	−3	43	−6	86
PD 5	55	M	8	L	318	9	−6	67	−6	67
PD 6	63	M	4	R	337	6	−4	67	−3	50
PD 7	58	M	3	R	117	7	−5	71	−4	57
PD 8	61	F	5	R	230	7	−2	67	−2	67
PD 9	57	M	2	R	179	7	−1	14	−2	29
PD 10	68	M	19	L	380	11	−8	73	−4	36
PD 11	65	F	4	R	216	7	−2	29	−2	29
PD 12	61	M	1	L	392	6	−1	17	−2	33
PD 13	74	M	4	R	287	10	−4	40	−4	40
PD 14	53	M	4	R	231	10	0	0	0	0
PD 15	73	M	5	R	256	5	−2	40	−2	40
Mean	64		6.8		272	7.2	−3.1	46	−3.3	50.6
(±SD; range)	(±7; 53–77)		(±6; 1–19)		(±92.5; 117–456)	(±1.9; 5–11)	[±2.1; (-) 8–0]	(±23; 0–73)	[±1.7; (-) 6–0]	(±24.3; 0–86)

**Scores are referred to tremor sub-items (3.15.a, 3.16.a, 3.17.a, and 3.17.c) of the MDS-UPDRS motor part in off-drug. Yrs, years; Tx, treated; vol, volume; M, male; F, female; L, left; R, right; 1-mo, 1 month after MRgFUS; 3-mo, 3 months after MRgFUS.*

TABLE 2 | Demographic and clinical data of GR- and PR- patients.

	GR-PD	PR-PD	GR-PD vs. PR-PD (unpaired *t*-test)
Age (ysr)	64.13 ± 7.34	64.43 ± 7.34	$t = 0.0771$
Sex (male/female)	7/1	6/1	$P = 0.9397$
Disease duration (yrs)	8.00 ± 5.55	5.57 ± 6.08	$t = 0.8097$
TX side (L/R)	3/5	2/5	$P = 0.4333$
24 h (lesion vol mm^3)	267.25 ± 106.64	277.29 ± 81.48	$t = 0.2023$ $P = 0.8428$
Tremor score for treated body side (baseline)	6.63 ± 1.30	8.00 ± 2.31	$t = 1.4462$ $P = 0.1718$
Drop points (-): 1 mo–baseline	−3.63 ± 1.30	−2.57 ± 2.70	$t = 0.9844$ $P = 0.3429$
Percentage (%) improvement (1 mo)	59.75 ± 10.99	30.43 ± 23.71	**$t = 3.1448$ $P = 0.0077$**
Drop points (-): 3 mo – baseline	−4.25 ± 1.58	−2.29 ± 1.38	$t = 2.5443$ $P = 0.0245$
Percentage (%) improvement (3 mo)	69.13 ± 13.59	29.57 ± 13.82	**$t = 5.5800$ $P = 0.0001$**

All values are expressed as Mean ± SD. significant results are highlighted in bold.

the (Good Responder) GR and the (Poor Responder) PR (see **Table 2**).

Main Effect of MRgFUS Treatment

A significant FC increase at 1-mo and 3-mo (as compared to baseline) was detected between: TS PreCG and unTS PreCG; TS PreCG and TS PostCG; unTS PreCG and TS PostCG; and unTS pallidum and unTS DN (**Figure 1**). No significant FC differences in any pair of connections were detected between post-treatment conditions (i.e., 1-mo vs. 3-mo).

Treatment by Disease Duration Interaction Effect

Significant correlations between disease duration and FC increase at 3-mo (as compared to baseline and 1-mo) were found between: unTS putamen and both TS, unTS Lob VI; TS putamen and both TS, unTS Lob VI; and both TS, unTS SMA and unTS Lob VI (**Figure 2**).

Treatment by Lesion Volume Interaction Effect

No significant interaction effects were found between 24-h lesion volumes and post-treatment FC changes.

Treatment by Clinical Improvement Interaction Effect

Significant correlations between the tremor improvement at 3-mo (expressed as drop score value) and the FC decrease in post-treatment (at 1-mo and 3-mo as compared to baseline) were found between mAC with TS, unTS SMA; and TS Lob VI and unTS IN (**Figure 3A**). Significant correlations between the tremor improvement at 3-mo (expressed as % intra-subject value) and the FC decrease in post-treatment (at 1-mo and 3-mo as compared to baseline) were found between: TS OFusG and unTS Lob VI, Ver VI; and unTS OFusG and unTS Lob VI, Ver VI (**Figure 3B**). When comparing post-treatment conditions (1-mo vs. 3-mo), no significant correlations were found between the measures of tremor improvement and the changes in FC.

Treatment by Outcome Interaction Effect

Good Responder-Parkinson's Disease (GR-PD) showed a significantly reduced post-treatment FC (as compared to PR-PD) between: unTS and TS SMA; unTS IN and TS Lob VI. Conversely, they showed significantly increased FC between unTS SMA and TS putamen (**Figure 4**). The poor responders (PR) did not exhibit post-treatment FC changes in any pair of the ROIs connections.

Pretherapeutic FC Profiles of Outcomes

At baseline, the GR-PD showed significant hypoconnectivity (as compared to PR-PD) between: TS putamen and both TS and unTS PreCG; TS putamen and unTS SMA; and unTS putamen and both TS and unTS PreCG (**Figure 5**).

DISCUSSION

The Magnetic Resonance-guided high-intensity Focused Ultrasound (MRgFUS) is a new non-invasive neurosurgical procedure for improving parkinsonian tremor (55–57). It has been demonstrated to be safe and effective, at least not inferior to unilateral DBS (58), thus, providing clinicians with the choice for different options for a more appropriate intervention based on the features of the individual patients. The procedure is fully executed in the MRI setting, which allows real-time monitoring of the location and size of the lesion. Moreover, clinical effect, as well as any potential adverse event, can be promptly assessed. This aspect differentiates the MRgFUS from surgical lesional thalamotomy or radiotherapy. However, as the MRgFUS is a relatively recent technique, follow-up data and randomized clinical trials are quite limited (56).

There is only one report investigating the impact of MRgFUS Vim thalamotomy on the neuronal activity in a whole-brain level (42). In particular, the authors measured fractional amplitude of low-frequency fluctuations (fALFF) on nine medication-refractory of patients with TD-PD, finding significant changes in visual areas at 12 months after the treatment compared to baseline (42). On a different note, in our study, we assessed the effect on the brain FC of unilateral MRgFUS thalamotomy according to the commonly accepted pathogenic structure functional hypothesis of tremor, which is based on the cerebello-thalamo-cortical circuitries converging on the Vim. We conducted a hypothesis-driven ROI-to-ROI rs-fMRI analysis, exclusively focusing on tremor-related brain areas, to accomplish a "*single network*"-based description (59) of medium-term effects (i.e., at 1 and 3 months postoperatively) of the MRgFUS treatment. Therefore, this is the first study to explore the rs-FC changes after the MRgFUS selective thalamotomy adopting a "*classic*" ROI-based approach. Previous studies have investigated longitudinal MRgFUS modulation of both the *topological* brain

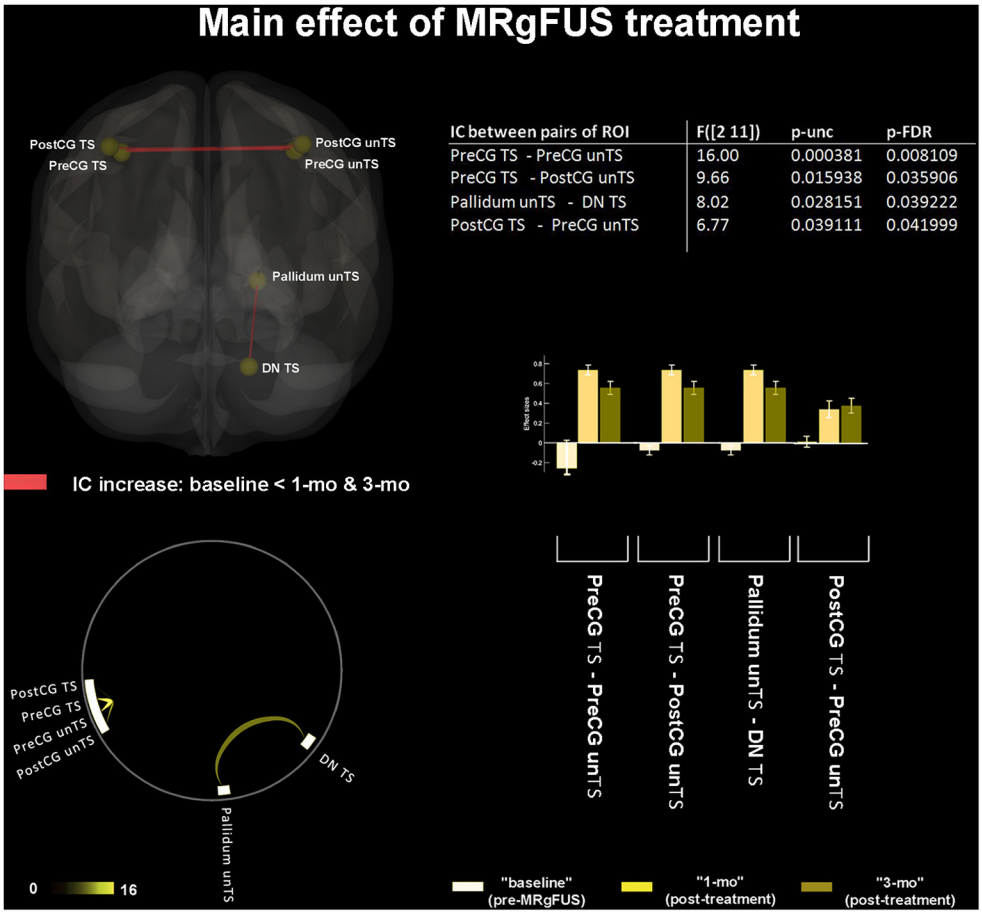

FIGURE 1 | "Main effect" of MRgFUS treatment. The 3D brain rendering and circle connectome graph illustrate statistically significant results. Statistics between each pair of regions of interest (ROI) are detailed within the table and by the corresponding bar plot; IC, Interconnectivity.

networks properties and the *effective connectivity* by employing graph analysis (34) or spectral dynamic causal modeling (35) only in an ET population. Of note, all the previous works included have no more than 10 patients in their study sample, while we could achieve a larger sample of 15 TD-PD subjects.

We would like to emphasize that the investigation of the FC changes after MRgFUS for tremor offers a unique opportunity to identify the neural correlates of this symptom quite univocally, by dissociating it from the overall disease phenotype on a lesional (iatrogenic) basis. Although the MRgFUS effects are immediate, an extended time for the clinical follow-up has been arranged to observe the enduring FC changes associated with the sustained tremor relief, rather than with transient clinical effects that were potentially induced by vasogenic oedema surrounding the lesion (33).

We found that the rs-FC, between tremor-related brain areas, was effectively modulated by MRgFUS. Selective Vim lesion had remote effects, modifying the balance of FC between ROIs far from the site of the lesion. Therefore, we believe that the "whole" tremor-network should be considered as the ultimate target of MRgFUS thalamotomy in PD (59).

The FC increase between TS and unTS PreCG; TS PreCG and unTS PostCG; and unTS PreCG and TS PostCG was one of the main effects of the treatment. It may reflect interhemispheric reorganization within bilateral primary motor (M1) cortices, as well as between bilateral M1 with crossed primary somatosensory (S1) cortices, with a probable enhanced synchronicity in homotopic brain regions underlying coherent sensorimotor behavior. The importance of integrating and cooperating bilateral sensorimotor systems for appropriate motor performance has been highlighted in healthy subjects (60), as well as in post-stroke patients (61). However, the interhemispheric coordination in PD is still under investigation, with little shreds of evidence showing an inverse relationship between the degree of motor impairment and the functional coordination in sensorimotor regions (62), along with optimal interhemispheric neural synchronization of motor cortices after DBS (63). We found that tremor suppression after MRgFUS in patients with TD-PD was paralleled by a greater synchronization of intra-cortical sensorimotor functions. A remodulation of pathological cortico-strial and/or cortico-thalamic interactions caused by Vim ablation could explain this phenomenon. We

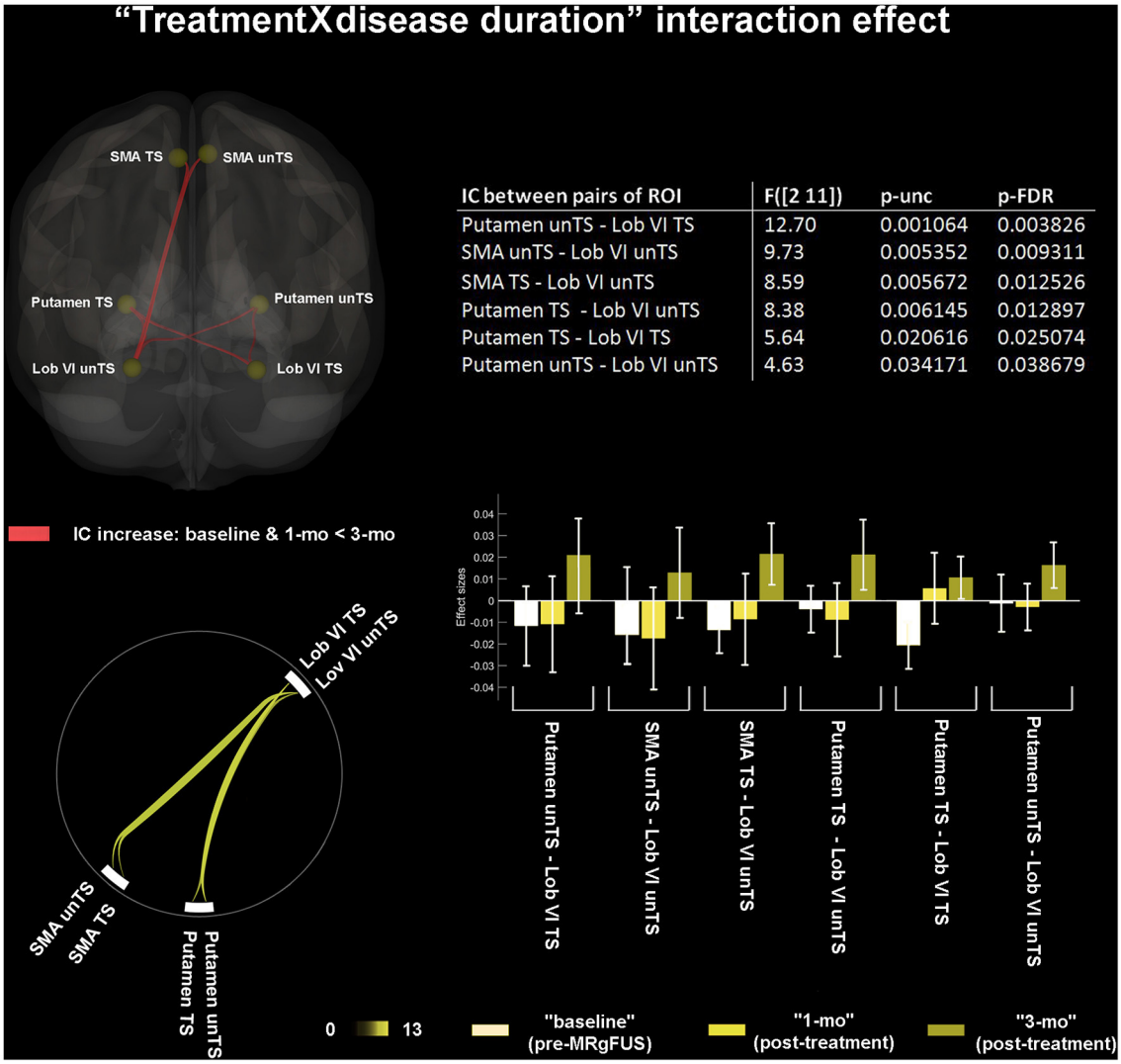

FIGURE 2 | "Treatment by disease duration" interaction effect. 3D brain rendering and circle connectome graph illustrate statistical significant results of functional connectivity (FC) changes. Statistics between each pairs of ROI are detailed within the table and by the corresponding bar plot; IC, interconnectivity.

could suppose that the MRgFUS thalamotomy was able to shift the system toward a more segregated functional state (64).

Another main effect of thalamotomy in PD was the increased FC between TS DN and unTS pallidum. Interactions between the cerebellum and the basal ganglia have been traditionally interpreted as indirectly occurring, *via* discrete multi-synaptic loops, primarily at the level of the cerebral cortex (65). However, recent research in primates using viral tracers has demonstrated bidirectional, disynaptic, and subcortical communication between the basal ganglia and the DN *via* the thalamus (66, 67). Our finding of an enhanced FC between an output stage of cerebellar processing (i.e., the DN), with an in-line station of basal ganglia processing (i.e., the pallidum), supports the existence of direct and reciprocal influences between these subcortical structures. Indeed, basal ganglia and cerebellum work synergistically to produce an efficient motor functioning, being both implicated in reinforcement learning, motor planning, and action understanding, as well as in sensorimotor prediction and control (68). Notwithstanding, the altered activity in cerebellar pathways has only recently been recognized as potentially important in PD tremorigenesis (69). The currently prevailing views emphasize that the cerebellar node of the tremor circuit (i.e., "the dimmer") drives the tremor by manipulating its amplitude (11). Ma et al. (70) reported a higher dentato-cerebellar FC in TD-PD, interpreted as a compensatory mechanism overcoming the basal ganglia impairment, but ultimately favoring the tremor onset. By contrast, Liu et al. (71) found lower FC between the DN and the posterior cerebellum in TD-PD. Our finding of an increased dentate-pallidal FC, associated with a tremor relapse improvement after Vim thalamotomy, might suggest a pre-surgical thalamic interference between these two structures with increasing connectivity after treatment, according to Liu's hypothesis. Vim interference could result in their functional

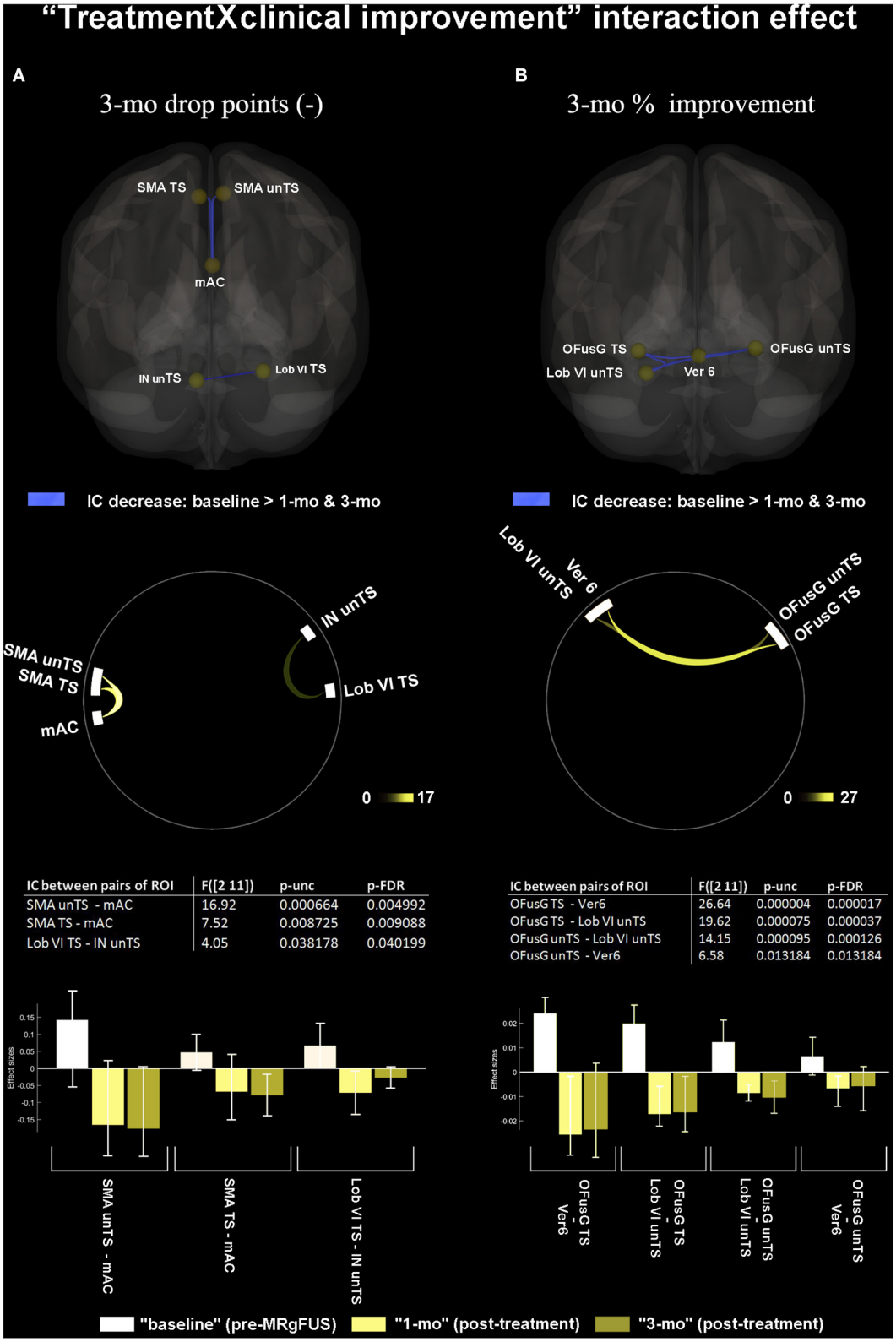

FIGURE 3 | "Treatment by clinical improvement" interaction effect. **(A)** shows significant correlations between FC changes and tremor improvement at 3-mo, expressed as 3 months "absolute drop points" of MDS-UPDRS sub-items for tremor (3.15.a, 3.16.a, 3.17.a, and 3.17.c). **(B)** shows significant correlations between FC changes and tremor improvement at 3-mo, expressed as intra-subject "percentage of improvement." The 3D brain rendering and circle connectome graph illustrate statistically significant results. Statistics between each pair of ROI are detailed within the table and by the corresponding bar plot; IC, Interconnectivity.

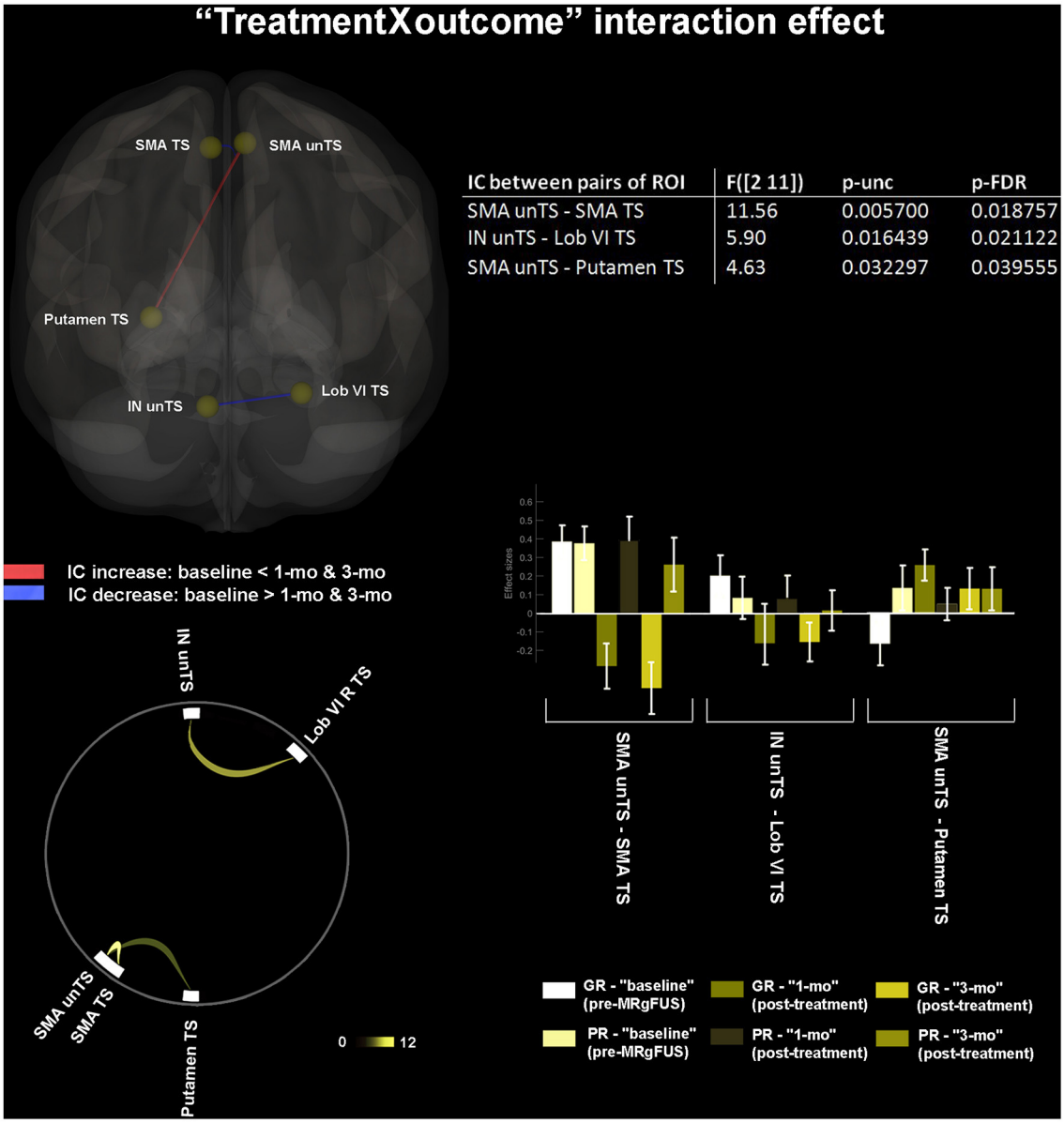

FIGURE 4 | "Treatment by outcome" interaction effect. Within-subject longitudinal changes of FC selectively associated with the clinical outcome (good vs. poor response to treatment) are shown. The 3D brain rendering and circle connectomic graph illustrate statistically significant results. Statistics between each pair of ROI are detailed within the table and by the corresponding bar plot; IC, Interconnectivity.

uncoupling, in terms of delay, asynchrony, or excessive local synchrony, causing a tremor-prone instability.

We also showed that the thalamotomy-induced FC increased between bilateral Lob VI of cerebellum with bilateral putamen and SMA. These effects correlated with a longer disease duration and were delayed, occurring only at 3-mo after the procedure. They were also distributed, involving both hemispheres regardless of treatment side. The Lob VI is associated with primary sensorimotor body representation in the cerebellum (72), has strong functional connections with premotor cortex (i.e. the SMA) (73), and plays a role in the temporal control of action sequences, as well as in sensorimotor processing of errors prediction (74). Functional impairment of the SMA is associated with the pathophysiology of PD, as it is directly implicated in motor planning (75). The SMA and the putamen are mutually connected and constitute the "readiness potential" of self-initiated actions, which is typically less prominent in PD (76). The post-treatment increase in functional synchrony between the SMA, putamen, and Lob VI would indicate a gain of function in this multicomponent cognitive-motor system, composed of discrete processes, occurring simultaneously, and aimed at effective motor performance.

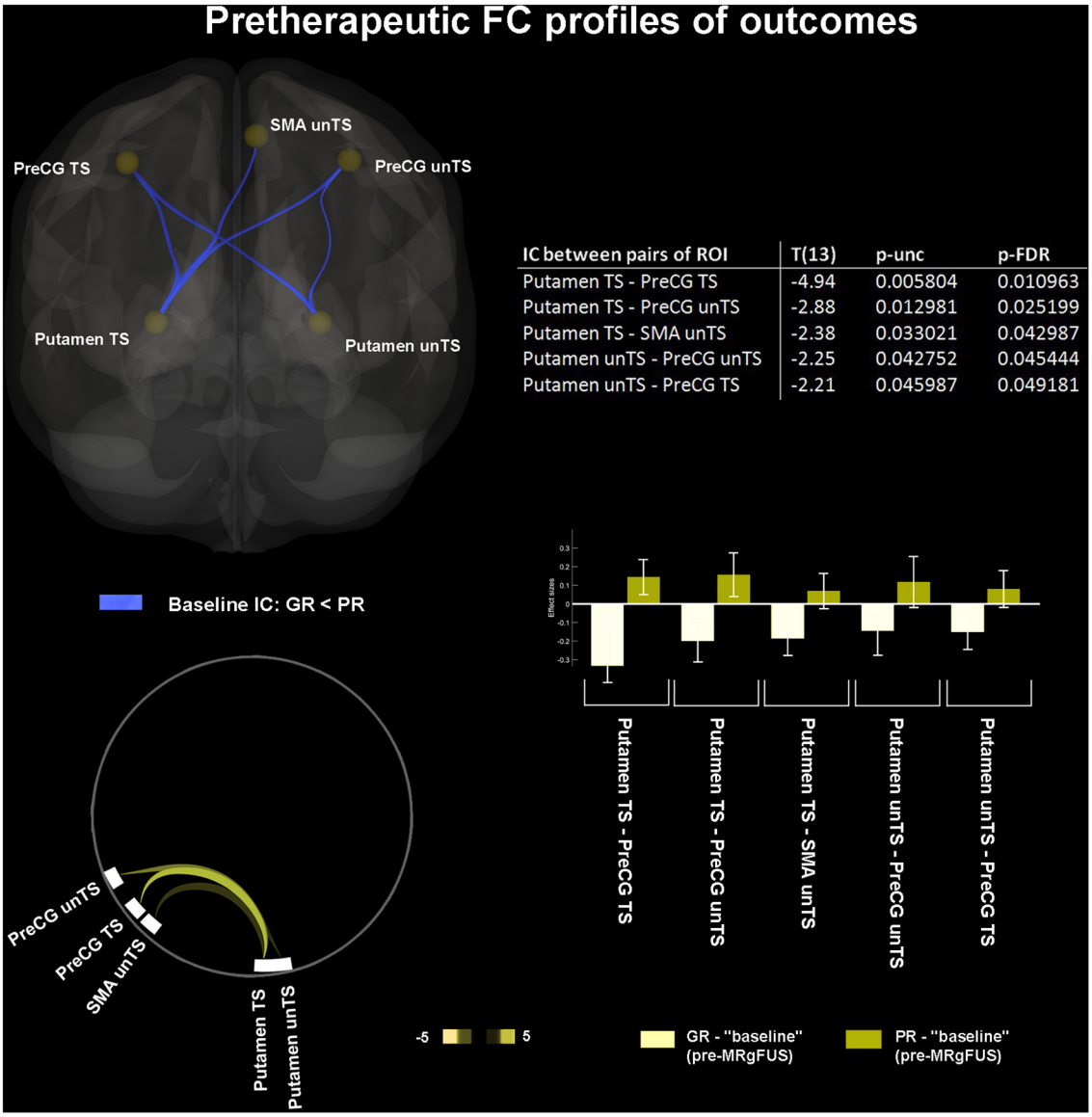

FIGURE 5 | "Pretherapeutic functional profiles of outcomes." Retrospectively identified baseline FC features associated with different clinical outcome (good vs. poor response to treatment). The 3D brain rendering and circle connectomic graph illustrate statistically significant results. Statistics between each pair of ROI are detailed within the table and by the corresponding bar plot; IC, Interconnectivity.

The central role played by the altered patterns of FC, involving the SMA, putamen, and Lob VI, also emerged from other findings.

First, the clinical improvement on the treated body-side (expressed as 3-mo drop points at the MDS-UPDRS tremor sub items) was associated with decreased FC between bilateral SMA and mAC. The mAC is part of the so-called "cingulate motor areas" (77), which, in turn, belongs to the wider "supplementary motor complex" of the medial prefrontal cortex. Similar to the proximal pre-SMA, these areas contribute to second-order aspects of motor function (78–80).We couldn't topographically disentangle the involvement of the different cingulate motor areas along their rostro-caudal axis (77) due to inherent methodological limitations. This would have allowed a more accurate definition of the role of the mAC in the PD tremor. We can only suppose that Vim ablation induced functional reorganization within the supplementary motor complex, particularly between the anterior cingulate and the bilateral SMA, and that this effect, among others, best reflected the patient's clinical improvement. Speculatively, we could assume the presence of a previous aberrant functional recruitment among premotor areas of both the medial hemispheric was potentially related to tremor. However, we cannot definitively determine whether this

mechanism was pathological in nature, or rather represented a maladaptive chronic process (8, 81).

Second, MRgFUS resulted in a significant increase of FC between unTS SMA and TS putamen only in good responders, who were also retrospectively characterized at baseline by reduced FC between these two areas–unlike poor responders who were not.

This pre-treatment hypoconnectivity pattern could be considered a potential FC predictor of MRgFUS response. Since the two prognostic sub-groups were not clinically different at baseline, such FC feature did not correspond to more severe symptoms. We could therefore hypothesize that either *clinical* and corresponding *functional* phenotypes matched quite inaccurately in our sample, or the observed *functional* feature reflected a greater susceptibility to thalamotomy efficacy. This latter hypothesis may rely on a greater predisposition to pathological functional decoupling between the SMA and the putamen. Perhaps, this predisposition may also occur on a structural basis, which needs to be addressed in future works. We should, however, emphasize that the proposed "decoupled" functional status of the SMA-putamen connection is an *indirect inference* of our "ablative iatrogenic study model." In fact, the tremor relief after the FC increase between these two nodes does not necessarily demonstrate restoration of a specific circuit but could, eventually, simply implicate iatrogenic interference within a complex maladaptive loop on which the other remote masked amplifying mechanisms can chronically act upon. Hence, we cannot definitively determine whether the interaction between the two nodes works; *causing*, *sharing,* or simply *mediating* tremor mechanisms.

Nonetheless, our result underlines the importance of the "putamen-SMA" connection in the pathogenesis of TD-PD. Previous observations were quite inconsistent as to whether PD is characterized by stronger or by weaker putamen-SMA FC, compared with healthy subjects. For example, Wu et al. (82) reported a reduced FC, whereas Kwak et al. (83) and Yu et al. (84) reported an enhanced FC. Furthermore, none of these studies specifically accounted for tremor. The present findings support a critical role of putamen-SMA interaction in TD-PD by showing that a better response to treatment paralleled the reorganization of their connectivity, which consisted of an increased cross-functional coupling. In this context, the concomitant post-treatment decrease in inter-hemispheric connectivity between the SMA on both sides should be interpreted as a complementary regulation, perhaps, even reflecting reallocation of functional resources.

Third, good responders retrospectively exhibited limited pre-treatment connectivity between TS, unTS putamen, with both ipsilateral and contralateral PreCG. These results further corroborate the evidence that patterns of altered connectivity in the cortico-striatal loop in TD-PD primarily involves M1 (85, 86), the most critical area in motor execution. Notably, our results are in accordance with previous studies showing a reduced rs-FC between M1 and putamen in PD (87, 88). One might assume that such FC feature might correlate with the clinical picture of tremor before treatment. However, this feature did not correspond to more severe symptoms in our sample, since good and poor responders did not differ in tremor severity at baseline (see **Table 2**). We could, therefore, hypothesize that the *clinical* and the corresponding *functional* phenotypes do not always match accurately.

Fourth, we found that tremor improvement was also associated with post-treatment decrease of FC between the unTS Lob VI/Ver VI of cerebellum and the bilateral OFusG. These FC changes were correlated with clinical improvement of tremor. In line with Xiong et al. (42) we observed the involvement of the second-order, functionally highly-specialized, visual area in the pathogenesis of tremor in PD. Also, such contribution was already evidenced in ET (37, 40, 41, 89). Our finding of a reduced interaction between specific subareas of the occipital lobe and the cerebellar hemisphere supports the evidence that the remote influence between structurally segregated regions with distinct functional profiles may exist even in the absence of direct anatomical projections, through indirect polysynaptic pathways of connection (41, 90). Although the precise function of the OFusG has not been fully revealed yet, it has been implicated in high-level visual processing, such as categorical recognition of visual stimuli (91, 92), and in those processes characterized by high recurrence of perceptual ambiguity (93). It is noteworthy that the PD motor performance is prone to deterioration with increasing ambiguous visual stimuli. This may be due to the peculiar dysfunction of cerebellar forward models used to mitigate the effect of sensory uncertainty on motor performance (94), which would make patients with PD particularly sensitive to visual feedback (95). Therefore, a compensatory pre-treatment increase of FC between the OFusG and the Lob VI/Ver VI of cerebellum–areas that are preferentially activated in the visual guidance of complex limb movement (96)–could be plausible. Conversely, the fact that the greater tremor relief paralleled the reduced FC between these areas would suggest an adaptive and reversible nature of this functional coupling.

Finally, a reduction in good responders between TS Lob VI and unTS IN was observed, following MRgFUS. This effect correlated with clinical improvement (expressed as absolute value of drop in MDS-UPDRS III sum score for contralateral tremor sub items). This finding supports the hypothesis that the tremor in PD would be associated with an increased activity within the cerebellum (97). The IN is part of the olivo-cortico-nuclear kinematic microcircuit, which is responsible for appropriate timing signals for movement coordination during ongoing motor performance. It also participates in the development of internal models for dynamic motor regulation in response to the external environment (98). The finding of the reduced FC between Lob VI and IN in patients who relieved more would suggest possible remodulation of intra-cerebellar functional resources associated with effective treatment.

Limitations

Some limitations need to be mentioned. First, the small sample size ($n = 15$) may have limited statistical power to identify

a less robust effect. This could eventually explain the absence of results in poor responders. Otherwise, it could suggest that ineffective treatments did not determine appreciable FC changes, as well as that characteristic pre-therapeutic profiles might not be recognizable in poor responders. We look forward to multi-center studies sharing data from advanced imaging techniques, which would allow for a wider patient recruitment and longer follow-up with, consequently, more robust results.

Second, although patients were always examined in a pharmacological washout, we cannot rule out the prolonged effect of chronic therapy on brain FC (99). It would be advisable for future studies to explore potential FC changes induced by Vim thalamotomy in PD, while controlling for "off" and "on" states. We are currently proceeding toward this purpose.

Third, the interhemispheric connections *via* the corpus callosum explain quite exhaustively the "crossed" pattern of many of our results between cerebral hemispheres. However, the presence of "uncrossed" functional interactions between supratentorial structures and cerebellum might be not immediately justifiable. We suggest that they may be explained either anatomically–by the presence of the non-decussating cerebellar pathways (100)–or functionally–by the intrinsic nature of endogenous BOLD signal fluctuations, which reflect the spontaneous correlation between distant brain regions as long as they are, somehow, functionally related (101).

Fourth, the rs-FC is a correlational technique, expressing temporal synchrony among BOLD fluctuations at rest between different couple of ROIs. Our analysis is solely correlational. Therefore, we did not provide information about the directed causal influences among involved brain regions (the so-called "effective connectivity"), nor could rule out moderation-mediation effects due to third parts (the so-called "partial correlation" analysis). We can interpret our network-based description of FC changes following MRgFUS only in terms of re-modulation and spatial re-allocation of functional resources. Moreover, we cannot definitively determine if these effects were reactive rather than causative, nor if they corresponded to the restoration of a *"normal old function"* or to a *"treatment specific signature"* superimposed on maladaptive adjustments of a chronically disrupted system.

Last, we found no association between the 24-h MRgFUS lesion volume and clinically relevant post-treatment FC changes. Previous radiological studies on MRgFUS (mainly based on morphological data) suffer from some inconsistency, with most authors reporting fewer symptom recurrences with larger lesions (46, 102–106), while others were focusing more on lesion location (20, 107) or topography (27, 108–110), rather than the lesion volume. Indeed, we observed some heterogeneity in the size and shape of Vim lesions in our sample, whereas lesion volumes did not differ significantly between GR and PR. Therefore, the absence of a correlation between FC changes and the lesion volumes did not particularly surprise us. Future studies on larger samples of patients need to investigate potential interference of lesion volume on FC, which may not have emerged in our study.

Conclusions

We demonstrated for the first time with a ROI-to-ROI connectomic approach how MRgFUS VIM thalamotomy modulates rs-FC of the tremor network in patients with TD-PD. We showed that treatment-mediated changes of FC between specific sub-regions of this diffuse network correlated with the tremor clinical improvement. Taken together, our results demonstrated a shifting mode of cooperation among the constituents of the tremor network that is susceptible to external redirection despite the chronic nature of disease. Finally, we identified the pre-surgical FC interactions that are potentially associated with greater tremor improvement after thalamotomy, suggesting their possible "predictive" use. Future studies in larger samples of PD subjects are mandatory to validate the utility of rs-FC as a quantifiable biomarker of tremor improvement after MRgFUS.

DATA AVAILABILITY STATEMENT

The datasets presented in this article are not readily available because the files cannot be deposited in an accessible repository online in compliance with the regulations on the processing and dissemination of personal data in the health sector (application of the EU Regulation 2016/679 (GDPR) and the Privacy Italian Law as updated by Legislative Decree 101/2018). Requests to access the datasets should be directed to the corresponding author.

ETHICS STATEMENT

The study was reviewed and approved by Scientific Direction-Ethics Committee Fondazione IRCCS Istituto Neurologico Carlo Besta (protocol n°74). The patients/participants provided their written informed consent to participate in this study.

AUTHOR CONTRIBUTIONS

MS conceived the study, executed MRgFUS procedures as neuroradiologist, collected and referred radiological data, analyzed rs-fMRI data and drew inferences, and wrote the first and latest version of the manuscript. NG and SB carried out the neurological assessment, supported the selection of patients for intervention, executed MRgFUS procedures as neurologist, monitored clinical outcomes, and contributed to the interpretation of the results. SR carried out the neurophysiopathological examination, assisted MRgFUS procedures, and defined organizational and procedural aspects of patients' selection for intervention. SP performed descriptive statistics, contributed to the interpretation of the results, and wrote the second and current version of the manuscript. AN contributed to the interpretation of the results. FG, GD, and JM pre-processed and segmented anatomical data. GM and GT executed MRgFUS as neurosurgeons, monitored clinical outcomes, and contributed to the interpretation of the results. LD'I collected and referred radiological data, executed MRgFUS procedures as neuroradiologist, and contributed to the interpretation of the results. FDM contributed to the

conception of the study and to the interpretation of the results. RE contributed to the conception of the study, carried out the neurological assessment, supported the selection of patients for intervention, executed MRgFUS procedures as neurologist, monitored clinical outcomes, contributed to the interpretation of the results, and supervised all stages of work. MGB contributed to the conception of the study, executed MRgFUS procedures as neuroradiologist, collected and referred radiological data, and supervised all stages of work. All authors contributed to the article and approved the submitted version.

REFERENCES

1. Foltynie T, Brayne C, Barker RA. The heterogeneity of idiopathic Parkinson's disease. *J Neurol.* (2002) 249:138–45. doi: 10.1007/PL00007856
2. Thenganatt MA, Jankovic J. Parkinson disease subtypes. *JAMA Neurol.* (2014) 71:499–504. doi: 10.1001/jamaneurol.2013.6233
3. Helmich RC, Dirkx MF. Pathophysiology and management of Parkinsonian tremor. *Semin Neurol.* (2017) 37:127–34. doi: 10.1055/s-0037-1601558
4. Louis ED, Machado DG. Tremor-related quality of life: a comparison of essential tremor vs. Parkinson's disease patients. *Parkinsonism Relat Disord.* (2015) 21:729–35. doi: 10.1016/j.parkreldis.2015.04.019
5. Heusinkveld LE, Hacker ML, Turchan M, Davis TL, Charles D. Impact of tremor on patients with early stage Parkinson's disease. *Front Neurol.* (2018) 9:628. doi: 10.3389/fneur.2018.00628
6. Palermo S, Lopiano L, Zibetti M, Rosato R, Leotta D, Amanzio M, et al. novel framework for understanding reduced awareness of dyskinesias in Parkinson's Disease. *Parkinsonism Relat Disord.* (2017) 39:58–63. doi: 10.1016/j.parkreldis.2017.03.009
7. Palermo S, Morese R, Zibetti M, Dematteis F, Sirgiovanni S, Stanziano M, et al. Impulse control disorder and response-inhibition alterations in Parkinson's disease. A rare case of totally absent functionality of the medial-prefrontal cortex and review of literature. *J Adv Res.* (2017) 8:713–6. doi: 10.1016/j.jare.2017.09.004
8. Palermo S, Stanziano M, Morese R. Commentary: anterior cingulate cortex and response conflict: effects of frequency, inhibition and errors. *Front Behav Neurosci.* (2018) 12:171. doi: 10.3389/fnbeh.2018.00171
9. Helmich RC, Janssen MJ, Oyen WJ, Bloem BR, Toni I. Pallidal dysfunction drives a cerebellothalamic circuit into Parkinson tremor. *Ann Neurol.* (2011) 69:269–81. doi: 10.1002/ana.22361
10. Helmich RC. The cerebral basis of Parkinsonian tremor: a network perspective. *Movement Disorders.* (2018) 33:219–31. doi: 10.1002/mds.27224
11. Duval C, Daneault JF, Hutchison WD, Sadikot AF. A brain network model explaining tremor in Parkinson's disease. *Neurobiol Dis.* (2016) 85:49–59. doi: 10.1016/j.nbd.2015.10.009
12. Guan X, Xuan M, Gu Q, Xu X, Huang P, Wang N, et al. Influence of regional iron on the motor impairments of Parkinson's disease: a quantitative susceptibility mapping study. *J Magn Reson Imaging.* (2017) 45:1335–42. doi: 10.1002/jmri.25434
13. van Nuland A, den Ouden H, Zach H, Dirkx M, van Asten J, Scheenen T, et al. GABAergic changes in the thalamocortical circuit in Parkinson's disease. *Hum Brain Mapp.* (2020) 41:1017–29. doi: 10.1002/hbm.24857
14. Helmich RC, Hallett M, Deuschl G, Toni I, Bloem BR. Cerebral causes and consequences of parkinsonian resting tremor: a tale of two circuits? *Brain.* (2012) 135(Pt 11):3206–26. doi: 10.1093/brain/aws023
15. Cagnan H, Little S, Foltynie T, Limousin P, Zrinzo L, Hariz M, et al. The nature of tremor circuits in parkinsonian and essential tremor. *Brain.* (2014) 137(Pt 12):3223–34. doi: 10.1093/brain/awu250
16. Fiechter M, Nowacki A, Oertel MF, Fichtner J, Debove I, Lachenmayer ML, et al. Deep brain stimulation for tremor: is there a common structure? *Stereotact Funct Neurosurg.* (2017) 95:243–50. doi: 10.1159/000478270
17. Hamani C, Dostrovsky JO, Lozano AM. The motor thalamus in neurosurgery. *Neurosurgery.* (2006) 58:146–58; discussion 58. doi: 10.1227/01.NEU.0000192166.62017.C1
18. Walters H, Shah BB. Focused ultrasound and other lesioning therapies in movement disorders. *Curr Neurol Neurosci Rep.* (2019) 19:66. doi: 10.1007/s11910-019-0975-2
19. King NKK, Krishna V, Sammartino F, Bari A, Reddy GD, Hodaie M, et al. Anatomic targeting of the optimal location for thalamic deep brain stimulation in patients with essential tremor. *World Neurosurg.* (2017) 107:168–74. doi: 10.1016/j.wneu.2017.07.136
20. Boutet A, Ranjan M, Zhong J, Germann J, Xu D, Schwartz ML, et al. Focused ultrasound thalamotomy location determines clinical benefits in patients with essential tremor. *Brain.* (2018) 141:3405–14. doi: 10.1093/brain/awy278
21. Chazen JL, Sarva H, Stieg PE, Min RJ, Ballon DJ, Pryor KO, et al. Clinical improvement associated with targeted interruption of the cerebellothalamic tract following MR-guided focused ultrasound for essential tremor. *J Neurosurg.* (2018) 129:315–23. doi: 10.3171/2017.4.JNS162803
22. Coenen VA, Sajonz B, Prokop T, Reisert M, Piroth T, Urbach H, et al. The dentato-rubro-thalamic tract as the potential common deep brain stimulation target for tremor of various origin: an observational case series. *Acta Neurochir.* (2020) 162:1053–66. doi: 10.1007/s00701-020-04248-2
23. Lehman VT, Lee KH, Klassen BT, Blezek DJ, Goyal A, Shah BR, et al. MRI and tractography techniques to localize the ventral intermediate nucleus and dentatorubrothalamic tract for deep brain stimulation and MR-guided focused ultrasound: a narrative review and update. *Neurosurg Focus.* (2020) 49:E8. doi: 10.3171/2020.4.FOCUS20170
24. Saluja S, Barbosa DAN, Parker JJ, Huang Y, Jensen MR, Ngo V, et al. Case report on deep brain stimulation rescue after suboptimal mr-guided focused ultrasound thalamotomy for essential tremor: a tractography-based investigation. *Front Hum Neurosci.* (2020) 14:191. doi: 10.3389/fnhum.2020.00191
25. Gallay MN, Moser D, Jeanmonod D. MR-guided focused ultrasound cerebellothalamic tractotomy for chronic therapy-resistant essential tremor: anatomical target reappraisal and clinical results. *J Neurosurg.* (2020) 2020:1–10. doi: 10.3171/2019.12.JNS192219
26. Gallay MN, Moser D, Rossi F, Pourtehrani P, Magara AE, Kowalski M, et al. Incisionless transcranial MR-guided focused ultrasound in essential tremor: cerebellothalamic tractotomy. *J Ther Ultrasound.* (2016) 4:5. doi: 10.1186/s40349-016-0049-8
27. Pineda-Pardo JA, Martinez-Fernandez R, Rodriguez-Rojas R, Del-Alamo M, Hernandez F, Foffani G, et al. Microstructural changes of the dentato-rubro-thalamic tract after transcranial MR guided focused ultrasound ablation of the posteroventral VIM in essential tremor. *Hum Brain Mapp.* (2019) 40:2933–42. doi: 10.1002/hbm.24569
28. Miller T, Zhuo J, Eisenberg H, Fishman P, Melhem E, Gullapalli R, et al. Targeting of the dentato-rubro-thalamic tract for MR-guided focused ultrasound treatment of essential tremor. *Neuroradiol J.* (2019) 32:401–7. doi: 10.1177/1971400919870180
29. Buijink AW, Caan MW, Contarino MF, Schuurman PR, van den Munckhof P, de Bie RM, et al. Structural changes in cerebellar outflow tracts after thalamotomy in essential tremor. *Parkinsonism Relat Disord.* (2014) 20:554–7. doi: 10.1016/j.parkreldis.2014.02.020
30. Listik C, Santiago N, Reis PR, Godinho F, Duarte K, Teixeira MJ, et al. Targeting the hot spot in a patient with essential tremor and Parkinson's disease: tractography matters. *Clin Neurol Neurosurg.* (2018) 174:230–2. doi: 10.1016/j.clineuro.2018.09.037
31. Su JH, Choi EY, Tourdias T, Saranathan M, Halpern CH, Henderson JM, et al. Improved Vim targeting for focused ultrasound ablation treatment of essential tremor: a probabilistic and patient-specific approach. *Hum Brain Mapp.* (2020) 41:4769–88. doi: 10.1002/hbm.25157
32. Meng F, Zhang J, Kao C, Klein J, Hilker R. The tremor network targeted by successful VIM deep brain stimulation in humans. *Neurology.* (2012) 79:787–95. doi: 10.1212/01.wnl.0000419345.94406.07
33. Wintermark M, Druzgal J, Huss DS, Khaled MA, Monteith S, Raghavan P, et al. Imaging findings in MR imaging-guided focused ultrasound treatment for patients with essential tremor. *AJNR Am J Neuroradiol.* (2014) 35:891–6. doi: 10.3174/ajnr.A3808

34. Jang C, Park HJ, Chang WS, Pae C, Chang JW. Immediate and longitudinal alterations of functional networks after thalamotomy in essential tremor. *Front Neurol.* (2016) 7:184. doi: 10.3389/fneur.2016.00184
35. Park HJ, Pae C, Friston K, Jang C, Razi A, Zeidman P, et al. Hierarchical dynamic causal modeling of resting-state fMRI reveals longitudinal changes in effective connectivity in the motor system after thalamotomy for essential tremor. *Front Neurol.* (2017) 8:346. doi: 10.3389/fneur.2017.00346
36. Tuleasca C, Najdenovska E, Regis J, Witjas T, Girard N, Champoudry J, et al. Clinical response to Vim's thalamic stereotactic radiosurgery for essential tremor is associated with distinctive functional connectivity patterns. *Acta Neurochir.* (2018) 160:611–24. doi: 10.1007/s00701-017-3456-x
37. Tuleasca C, Najdenovska E, Regis J, Witjas T, Girard N, Champoudry J, et al. Ventrolateral motor thalamus abnormal connectivity in essential tremor before and after thalamotomy: a resting-state functional magnetic resonance imaging study. *World Neurosurg.* (2018) 113:e453–e64. doi: 10.1016/j.wneu.2018.02.055
38. Tuleasca C, Regis J, Najdenovska E, Witjas T, Girard N, Bolton T, et al. Pretherapeutic resting-state fMRI profiles are associated with MR signature volumes after stereotactic radiosurgical thalamotomy for essential tremor. *J Neurosurg.* (2018) 129(Suppl1):63–71. doi: 10.3171/2018.7.GKS18752
39. Tuleasca C, Regis J, Najdenovska E, Witjas T, Girard N, Champoudry J, et al. Pretherapeutic functional imaging allows prediction of head tremor arrest after thalamotomy for essential tremor: the role of altered interconnectivity between thalamolimbic and supplementary motor circuits. *World Neurosurg.* (2018) 112:e479–e88. doi: 10.1016/j.wneu.2018.01.063
40. Tuleasca C, Bolton T, Regis J, Najdenovska E, Witjas T, Girard N, et al. Thalamotomy for tremor normalizes aberrant pre-therapeutic visual cortex functional connectivity. *Brain.* (2019) 142:e57. doi: 10.1093/brain/awz299
41. Tuleasca C, Bolton TAW, Regis J, Najdenovska E, Witjas T, Girard N, et al. Normalization of aberrant pretherapeutic dynamic functional connectivity of extrastriate visual system in patients who underwent thalamotomy with stereotactic radiosurgery for essential tremor: a resting-state functional MRI study. *J Neurosurg.* (2019) 132:1792–801. doi: 10.3171/2019.2.JNS183454
42. Xiong Y, Han D, He J, Zong R, Bian X, Duan C, et al. Correlation of visual area with tremor improvement after MRgFUS thalamotomy in Parkinson's disease. *J Neurosurg.* (2021) 2021:1–8. doi: 10.3171/2021.3.JNS204329
43. Postuma RB, Poewe W, Litvan I, Lewis S, Lang AE, Halliday G, et al. Validation of the MDS clinical diagnostic criteria for Parkinson's disease. *Mov Disord.* (2018) 33:1601–8. doi: 10.1002/mds.27362
44. Goetz CG, Tilley BC, Shaftman SR, Stebbins GT, Fahn S, Martinez-Martin P, et al. Movement disorder society-sponsored revision of the unified Parkinson's disease rating scale (MDS-UPDRS): scale presentation and clinimetric testing results. *Mov Disord.* (2008) 23:2129–70. doi: 10.1002/mds.22340
45. Boutet A, Gwun D, Gramer R, Ranjan M, Elias GJB, Tilden D, et al. The relevance of skull density ratio in selecting candidates for transcranial MR-guided focused ultrasound. *J Neurosurg.* (2019) 132:1785–91. doi: 10.3171/2019.2.JNS182571
46. Keil VC, Borger V, Purrer V, Groetz SF, Scheef L, Boecker H, et al. MRI follow-up after magnetic resonance-guided focused ultrasound for non-invasive thalamotomy: the neuroradiologist's perspective. *Neuroradiology.* (2020) 62:1111–22. doi: 10.1007/s00234-020-02433-9
47. Whitfield-Gabrieli S, Nieto-Castanon A. Conn: a functional connectivity toolbox for correlated and anticorrelated brain networks. *Brain Connect.* (2012) 2:125–41. doi: 10.1089/brain.2012.0073
48. Power JD, Mitra A, Laumann TO, Snyder AZ, Schlaggar BL, Petersen SE. Methods to detect, characterize, and remove motion artifact in resting state fMRI. *Neuroimage.* (2014) 84:320–41. doi: 10.1016/j.neuroimage.2013.08.048
49. Desikan RS, Segonne F, Fischl B, Quinn BT, Dickerson BC, Blacker D, et al. An automated labeling system for subdividing the human cerebral cortex on MRI scans into gyral based regions of interest. *Neuroimage.* (2006) 31:968–80. doi: 10.1016/j.neuroimage.2006.01.021
50. Tzourio-Mazoyer N, Landeau B, Papathanassiou D, Crivello F, Etard O, Delcroix N, et al. Automated anatomical labeling of activations in SPM using a macroscopic anatomical parcellation of the MNI MRI single-subject brain. *Neuroimage.* (2002) 15:273–89. doi: 10.1006/nimg.2001.0978
51. Eickhoff SB, Stephan KE, Mohlberg H, Grefkes C, Fink GR, Amunts K, et al. A new SPM toolbox for combining probabilistic cytoarchitectonic maps and functional imaging data. *Neuroimage.* (2005) 25:1325–35. doi: 10.1016/j.neuroimage.2004.12.034
52. Lee KH, Oh H, Suh JS, Cho KIK, Yoon YB, Shin WG, et al. Functional and structural connectivity of the cerebellar nuclei with the striatum and cerebral cortex in first-episode psychosis. *J Neuropsychiatry Clin Neurosci.* (2019) 31:143–51. doi: 10.1176/appi.neuropsych.17110276
53. Mishra A, Rogers BP, Chen LM, Gore JC. Functional connectivity-based parcellation of amygdala using self-organized mapping: a data driven approach. *Hum Brain Mapp.* (2014) 35:1247–60. doi: 10.1002/hbm.22249
54. Jafri MJ, Pearlson GD, Stevens M, Calhoun VD, A. method for functional network connectivity among spatially independent resting-state components in schizophrenia. *Neuroimage.* (2008) 39:1666–81. doi: 10.1016/j.neuroimage.2007.11.001
55. Gallay MN, Moser D, Magara AE, Haufler F, Jeanmonod D. Bilateral MR-Guided Focused Ultrasound Pallidothalamic Tractotomy for Parkinson's Disease With 1-Year Follow-Up. *Front Neurol.* (2021) 12:601153. doi: 10.3389/fneur.2021.601153
56. Ge Y, Wang Z, Gu F, Yang X, Chen Z, Dong W, et al. Clinical application of magnetic resonance-guided focused ultrasound in Parkinson's disease: a meta-analysis of randomized clinical trials. *Neurol Sci.* (2021) 42:3595–604. doi: 10.1007/s10072-021-05443-4
57. Yamamoto K, Ito H, Fukutake S, Odo T, Kamei T, Yamaguchi T, et al. Focused ultrasound thalamotomy for tremor-dominant Parkinson's disease: a prospective 1-year follow-up study. *Neurol Med Chir.* (2021) 61:414–21. doi: 10.2176/nmc.oa.2020-0370
58. Lin F, Wu D, Yu J, Weng H, Chen L, Meng F, et al. Comparison of efficacy of deep brain stimulation and focused ultrasound in parkinsonian tremor: a systematic review and network meta-analysis. *J Neurol Neurosurg Psychiatry.* (2021). doi: 10.1136/jnnp-2020-323656. [Epub ahead of print].
59. Permezel F. Brain MRI-guided focused ultrasound conceptualised as a tool for brain network intervention. *J Clin Neurosci.* (2021) 90:370–9. doi: 10.1016/j.jocn.2021.05.062
60. Bressler SL, Kelso JAS. Cortical coordination dynamics and cognition. *Trends Cogn Sci.* (2001) 5:26–36. doi: 10.1016/S1364-6613(00)01564-3
61. van Meer MP, van der Marel K, Wang K, Otte WM, El Bouazati S, Roeling TA, et al. Recovery of sensorimotor function after experimental stroke correlates with restoration of resting-state interhemispheric functional connectivity. *J Neurosci.* (2010) 30:3964–72. doi: 10.1523/JNEUROSCI.5709-09.2010
62. Luo C, Guo X, Song W, Zhao B, Cao B, Yang J, et al. Decreased resting-state interhemispheric functional connectivity in Parkinson's disease. *Biomed Res Int.* (2015) 2015:692684. doi: 10.1155/2015/692684
63. Mamun KA, Mace M, Lutman ME, Stein J, Liu X, Aziz T, et al. Movement decoding using neural synchronization and inter-hemispheric connectivity from deep brain local field potentials. *J Neural Eng.* (2015) 12:056011. doi: 10.1088/1741-2560/12/5/056011
64. Nigro S, Bordier C, Cerasa A, Nistico R, Olivadese G, Vescio B, et al. Apomorphine-induced reorganization of striato-frontal connectivity in patients with tremor-dominant Parkinson's disease. *Parkinsonism Relat Disord.* (2019) 67:14–20. doi: 10.1016/j.parkreldis.2019.09.006
65. Percheron G, Francois C, Talbi B, Yelnik J, Fenelon G. The primate motor thalamus. *Brain Res Rev.* (1996) 22:93–181. doi: 10.1016/0165-0173(96)00003-3
66. Bostan AC, Strick PL. The cerebellum and basal ganglia are interconnected. *Neuropsychol Rev.* (2010) 20:261–70. doi: 10.1007/s11065-010-9143-9
67. Bostan AC, Strick PL. The basal ganglia and the cerebellum: nodes in an integrated network. *Nat Rev Neurosci.* (2018) 19:338–50. doi: 10.1038/s41583-018-0002-7
68. Caligiore D, Pezzulo G, Miall RC, Baldassarre G. The contribution of brain sub-cortical loops in the expression and acquisition of action understanding abilities. *Neurosci Biobehav Rev.* (2013) 37:2504–15. doi: 10.1016/j.neubiorev.2013.07.016
69. Wu T, Hallett M. The cerebellum in Parkinson's disease. *Brain.* (2013) 136(Pt 3):696–709. doi: 10.1093/brain/aws360

70. Ma H, Chen H, Fang J, Gao L, Ma L, Wu T, et al. Resting-state functional connectivity of dentate nucleus is associated with tremor in Parkinson's disease. *J Neurol.* (2015) 262:2247–56. doi: 10.1007/s00415-015-7835-z
71. Liu H, Edmiston EK, Fan G, Xu K, Zhao B, Shang X, et al. Altered resting-state functional connectivity of the dentate nucleus in Parkinson's disease. *Psychiatry Res.* (2013) 211:64–71. doi: 10.1016/j.pscychresns.2012.10.007
72. Balsters JH, Laird AR, Fox PT, Eickhoff SB. Bridging the gap between functional and anatomical features of cortico-cerebellar circuits using meta-analytic connectivity modeling. *Hum Brain Mapp.* (2014) 35:3152–69. doi: 10.1002/hbm.22392
73. Buckner RL, Krienen FM, Castellanos A, Diaz JC, Yeo BT. The organization of the human cerebellum estimated by intrinsic functional connectivity. *J Neurophysiol.* (2011) 106:2322–45. doi: 10.1152/jn.00339.2011
74. Schlerf J, Ivry RB, Diedrichsen J. Encoding of sensory prediction errors in the human cerebellum. *J Neurosci.* (2012) 32:4913–22. doi: 10.1523/JNEUROSCI.4504-11.2012
75. Grafton ST. Contributions of functional imaging to understanding parkinsonian symptoms. *Curr Opin Neurobiol.* (2004) 14:715–9. doi: 10.1016/j.conb.2004.10.010
76. Nachev P, Kennard C, Husain M. Functional role of the supplementary and pre-supplementary motor areas. *Nat Rev Neurosci.* (2008) 9:856–69. doi: 10.1038/nrn2478
77. Loh KK, Hadj-Bouziane F, Petrides M, Procyk E, Amiez C. Rostro-Caudal Organization of Connectivity between Cingulate Motor Areas and Lateral Frontal Regions. *Front Neurosci.* (2017) 11:753. doi: 10.3389/fnins.2017.00753
78. Picard N, Strick PL. Motor areas of the medial wall: a review of their location and functional activation. *Cereb Cortex.* (1996) 6:342–53. doi: 10.1093/cercor/6.3.342
79. Maier MA, Armand J, Kirkwood PA, Yang H-W, Davis JN, Lemon RN. Differences in the corticospinal projection from primary motor cortex and supplementary motor area to macaque upper limb motoneurons: an anatomical and electrophysiological study. *Cereb Cortex.* (2002) 12:281–96. doi: 10.1093/cercor/12.3.281
80. Chouinard PA, Paus T. What have we learned from "Perturbing" the human cortical motor system with transcranial magnetic stimulation? *Front Hum Neurosci.* (2010) 4:173. doi: 10.3389/fnhum.2010.00173
81. Palermo S, Lopiano L, Morese R, Zibetti M, Romagnolo A, Stanziano M, et al. Role of the cingulate cortex in dyskinesias-reduced-self-awareness: an fMRI study on Parkinson's disease patients. *Front Psychol.* (2018) 9:1765. doi: 10.3389/fpsyg.2018.01765
82. Wu T, Wang L, Chen Y, Zhao C, Li K, Chan P. Changes of functional connectivity of the motor network in the resting state in Parkinson's disease. *Neurosci Lett.* (2009) 460:6–10. doi: 10.1016/j.neulet.2009.05.046
83. Kwak Y, Peltier S, Bohnen NI, Muller ML, Dayalu P, Seidler RD. Altered resting state cortico-striatal connectivity in mild to moderate stage Parkinson's disease. *Front Syst Neurosci.* (2010) 4:143. doi: 10.3389/fnsys.2010.00143
84. Yu R, Liu B, Wang L, Chen J, Liu X. Enhanced functional connectivity between putamen and supplementary motor area in Parkinson's disease patients. *PLoS ONE.* (2013) 8:e59717. doi: 10.1371/journal.pone.0059717
85. Wu T, Long X, Wang L, Hallett M, Zang Y, Li K, et al. Functional connectivity of cortical motor areas in the resting state in Parkinson's disease. *Hum Brain Mapp.* (2011) 32:1443–57. doi: 10.1002/hbm.21118
86. Burciu RG, Vaillancourt DE. Imaging of motor cortex physiology in Parkinson's disease. *Mov Disord.* (2018) 33:1688–99. doi: 10.1002/mds.102
87. Helmich RC, Derikx LC, Bakker M, Scheeringa R, Bloem BR, Toni I. Spatial remapping of cortico-striatal connectivity in Parkinson's disease. *Cereb Cortex.* (2010) 20:1175–86. doi: 10.1093/cercor/bhp178
88. Luo C, Song W, Chen Q, Zheng Z, Chen K, Cao B, et al. Reduced functional connectivity in early-stage drug-naive Parkinson's disease: a resting-state fMRI study. *Neurobiol Aging.* (2014) 35:431–41. doi: 10.1016/j.neurobiolaging.2013.08.018
89. Archer DB, Coombes SA, Chu WT, Chung JW, Burciu RG, Okun MS, et al. A widespread visually-sensitive functional network relates to symptoms in essential tremor. *Brain.* (2018) 141:472–85. doi: 10.1093/brain/awx338
90. Tuleasca C, Witjas T, Van de Ville D, Najdenovska E, Verger A, Girard N, et al. Right Brodmann area 18 predicts tremor arrest after Vim radiosurgery: a voxel-based morphometry study. *Acta Neurochir.* (2018) 160:603–9. doi: 10.1007/s00701-017-3391-x
91. Palejwala AH, O'Connor KP, Milton CK, Anderson C, Pelargos P, Briggs RG, et al. Anatomy and white matter connections of the fusiform gyrus. *Sci Rep.* (2020) 10:13489. doi: 10.1038/s41598-020-70410-6
92. Zhang W, Wang J, Fan L, Zhang Y, Fox PT, Eickhoff SB, et al. Functional organization of the fusiform gyrus revealed with connectivity profiles. *Hum Brain Mapp.* (2016) 37:3003–16. doi: 10.1002/hbm.23222
93. Andrews TJ, Schluppeck D, Homfray D, Matthews P, Blakemore C. Activity in the fusiform gyrus predicts conscious perception of rubin's vase–face illusion. *Neuroimage.* (2002) 17:890–901. doi: 10.1006/nimg.2002.1243
94. van Beers RJ, Baraduc P, Wolpert DM. Role of uncertainty in sensorimotor control. *Philos Trans R Soc Lond B Biol Sci.* (2002) 357:1137–45. doi: 10.1098/rstb.2002.1101
95. Stevenson JK, Oishi MM, Farajian S, Cretu E, Ty E, McKeown MJ. Response to sensory uncertainty in Parkinson's disease: a marker of cerebellar dysfunction? *Eur J Neurosci.* (2011) 33:298–305. doi: 10.1111/j.1460-9568.2010.07501.x
96. Vaillancourt DE, Mayka MA, Corcos DM. Intermittent visuomotor processing in the human cerebellum, parietal cortex, and premotor cortex. *J Neurophysiol.* (2006) 95:922–31. doi: 10.1152/jn.00718.2005
97. Lewis MM, Galley S, Johnson S, Stevenson J, Huang X, McKeown MJ. The role of the cerebellum in the pathophysiology of Parkinson's disease. *Can J Neurol Sci.* (2013) 40:299–306. doi: 10.1017/S0317167100014232
98. Perciavalle V, Apps R, Bracha V, Delgado-Garcia JM, Gibson AR, Leggio M, et al. Consensus paper: current views on the role of cerebellar interpositus nucleus in movement control and emotion. *Cerebellum.* (2013) 12:738–57. doi: 10.1007/s12311-013-0464-0
99. Amanzio M, Palermo S, Zibetti M, Leotta D, Rosato R, Geminiani G, et al. Self-unawareness of levodopa induced dyskinesias in patients with Parkinson's disease. *Brain Cogn.* (2014) 90:135–41. doi: 10.1016/j.bandc.2014.06.014
100. Meola A, Comert A, Yeh FC, Sivakanthan S, Fernandez-Miranda JC. The nondecussating pathway of the dentatorubrothalamic tract in humans: human connectome-based tractographic study and microdissection validation. *J Neurosurg.* (2016) 124:1406–12. doi: 10.3171/2015.4.JNS142741
101. Fox MD, Raichle ME. Spontaneous fluctuations in brain activity observed with functional magnetic resonance imaging. *Nat Rev Neurosci.* (2007) 8:700–11. doi: 10.1038/nrn2201
102. Chang WS, Jung HH, Kweon EJ, Zadicario E, Rachmilevitch I, Chang JW. Unilateral magnetic resonance guided focused ultrasound thalamotomy for essential tremor: practices and clinicoradiological outcomes. *J Neurol Neurosurg Psychiatry.* (2015) 86:257–64. doi: 10.1136/jnnp-2014-307642
103. Chang WS, Jung HH, Zadicario E, Rachmilevitch I, Tlusty T, Vitek S, et al. Factors associated with successful magnetic resonance-guided focused ultrasound treatment: efficiency of acoustic energy delivery through the skull. *J Neurosurg.* (2016) 124:411–6. doi: 10.3171/2015.3.JNS142592
104. Federau C, Goubran M, Rosenberg J, Henderson J, Halpern CH, Santini V, et al. Transcranial MRI-guided high-intensity focused ultrasound for treatment of essential tremor: A pilot study on the correlation between lesion size, lesion location, thermal dose, and clinical outcome. *J Magn Reson Imaging.* (2018) 48:58–65. doi: 10.1002/jmri.25878
105. Harary M, Essayed WI, Valdes PA, McDannold N, Cosgrove GR. Volumetric analysis of magnetic resonance-guided focused ultrasound thalamotomy lesions. *Neurosurg Focus.* (2018) 44:E6. doi: 10.3171/2017.11.FOCUS17587
106. Park YS, Jung NY, Na YC, Chang JW. Four-year follow-up results of magnetic resonance-guided focused ultrasound thalamotomy for essential tremor. *Mov Disord.* (2019) 34:727–34. doi: 10.1002/mds.27637
107. Kapadia AN, Elias GJB, Boutet A, Germann J, Pancholi A, Chu P, et al. Multimodal MRI for MRgFUS in essential tremor: post- treatment radiological markers of clinical outcome. *J Neurol Neurosurg Psychiatry.* (2020) 91:921–7. doi: 10.1136/jnnp-2020-322745
108. Nowackia A, Bogdanovic M, Sarangmat N, Fitzgerald J, Green A, Aziz TZ. Revisiting the rules for anatomical targeting of ventralis intermediate nucleus. *J Clin Neurosci.* (2019) 68:97–100. doi: 10.1016/j.jocn.2019.07.027
109. Martinez-Fernandez R, Pineda-Pardo JA. Magnetic resonance-guided focused ultrasound for movement disorders: clinical

and neuroimaging advances. *Curr Opin Neurol.* (2020) 33:488–97. doi: 10.1097/WCO.0000000000000840

110. Rodriguez-Rojas R, Pineda-Pardo JA, Martinez-Fernandez R, Kogan RV, Sanchez-Catasus CA, Del Alamo M, et al. Functional impact of subthalamotomy by magnetic resonance-guided focused ultrasound in Parkinson's disease: a hybrid PET/MR study of resting-state brain metabolism. *Eur J Nucl Med Mol Imaging.* (2020) 47:425–36. doi: 10.1007/s00259-019-04497-z

Conflict of Interest: GF was employed by company InSightec Ltd.

The remaining authors declare that the research was conducted in the absence of any commercial or financial relationships that could be construed as a potential conflict of interest.

Publisher's Note: All claims expressed in this article are solely those of the authors and do not necessarily represent those of their affiliated organizations, or those of the publisher, the editors and the reviewers. Any product that may be evaluated in this article, or claim that may be made by its manufacturer, is not guaranteed or endorsed by the publisher.

frontiers in Neurology

ORIGINAL RESEARCH
published: 21 January 2022
doi: 10.3389/fneur.2021.808810

Technical Comparison of Treatment Efficiency of Magnetic Resonance-Guided Focused Ultrasound Thalamotomy and Pallidotomy in Skull Density Ratio-Matched Patient Cohorts

Abdul-Kareem Ahmed[1], Sijia Guo[2], Nathaniel Kelm[3], Ryan Clanton[3], Elias R. Melhem[2], Rao P. Gullapalli[2], Alexander Ksendzovsky[1], Howard M. Eisenberg[1], Timothy R. Miller[1,2] and Dheeraj Gandhi[1,2]*

[1] Department of Neurosurgery, University of Maryland School of Medicine, Baltimore, MD, United States, [2] Department of Diagnostic Radiology and Nuclear Medicine, University of Maryland School of Medicine, Baltimore, MD, United States, [3] Insightec, Tirat Carmel, Israel

OPEN ACCESS

Edited by:
J. Levi Chazen, Cornell University, United States

Reviewed by:
Jurgen Germann, University Health Network (UHN), Canada
Michael Schwartz, Sunnybrook Health Science Centre, Canada
Ausaf Bari, University of California, Los Angeles, United States

***Correspondence:**
Abdul-Kareem Ahmed
akahmed@som.umaryland.edu

Specialty section:
This article was submitted to Experimental Therapeutics, a section of the journal Frontiers in Neurology

Received: *04 November 2021*
Accepted: *17 December 2021*
Published: *21 January 2022*

Citation:
Ahmed A-K, Guo S, Kelm N, Clanton R, Melhem ER, Gullapalli RP, Ksendzovsky A, Eisenberg HM, Miller TR and Gandhi D (2022) Technical Comparison of Treatment Efficiency of Magnetic Resonance-Guided Focused Ultrasound Thalamotomy and Pallidotomy in Skull Density Ratio-Matched Patient Cohorts. Front. Neurol. 12:808810. doi: 10.3389/fneur.2021.808810

Objective: MR-guided focused ultrasound (MRgFUS) is increasingly being used to treat patients with essential tremor (ET) and Parkinson's disease (PD) with thalamotomy and pallidotomy, respectively. Pallidotomy is performed off-center within the cranium compared to thalamotomy and may present challenges to therapeutic lesioning due to this location. However, the impact of target location on treatment efficiency and ability to create therapeutic lesions has not been studied. This study aimed to compare the physical efficiency of MRgFUS thalamotomy and pallidotomy.

Methods: Treatment characteristics were compared between patients treated with thalamotomy ($n = 20$) or pallidotomy ($n = 20$), matched by skull density ratios (SDR). Aspects of treatment efficiency were compared between these groups. Demographic and comparative statistics were conducted to assess these differences. Acoustic field simulations were performed to compare and validate the simulated temperature profile for VIM and GPi ablation.

Results: Lower SDR values were associated with greater energy requirement for thalamotomy ($R^2 = 0.197$, $p = 0.049$) and pallidotomy ($R^2 = 0.342$, $p = 0.007$). The impact of low SDR on efficiency reduction was greater for pallidotomy, approaching significance ($p = 0.061$). A nearly two-fold increase in energy was needed to reach 50°C in pallidotomy (10.9kJ) than in thalamotomy (5.7kJ), ($p = 0.002$). Despite lower energy requirement, the maximum average temperature reached was higher in thalamotomy (56.7°C) than in pallidotomy (55.0°C), ($p = 0.017$). Mean incident angle of acoustic beams was lesser in thalamotomy (12.7°) than in pallidotomy (18.6°), ($p<0.001$). For all patients, a lesser mean incident angle correlated with a higher maximum average temperature reached ($R^2 = 0.124$, $p = 0.026$), and less energy needed to reach 50°C ($R^2 = 0.134$, $p = 0.020$). Greater skull thickness was associated with a higher maximum energy for a

single sonication for thalamotomy ($R^2 = 0.206$, $p = 0.045$) and pallidotomy ($R^2 = 0.403$, $p = 0.003$). An acoustic and temperature field simulation validated similar findings for thalamotomy and pallidotomy in a single patient.

Conclusion: The centrally located VIM offers a more efficient location for therapeutic lesioning compared to GPi pallidotomy in SDR matched cohort of patients. The impact on therapeutic lesioning with lower SDR may be greater for pallidotomy patients. As newer off-center targets are investigated, these findings can inform patient selection and treatment requirements for lesion production.

Keywords: focused ultrasound (MRgFUS), thalamotomy pallidotomy, movement disorders, stereotactic ablation, skull density ratio

INTRODUCTION

Magnetic resonance imaging-guided focused ultrasound (MRgFUS) is a promising, non-invasive technology that is being increasingly applied to treat various neurological disorders, including essential tremor and Parkinson's disease (1). However, all focused ultrasound neurological applications must overcome the physical limitations of the human skull, which historically required a craniectomy to enable ultrasound beams to reach the target (2–4). In 2002, Clement and Hynynen introduced an approach utilizing computer tomography data of the subject's calvarium to focus individual ultrasound beams through the intact skull (5). This transcranial technique works by registering CT data with MR imaging to predict the phase aberration and beam attenuation occurring at the calvarial-soft tissue interface, which is then corrected for by steering of individual transducer elements (6).

However, the efficiency of transcranial ablation using a hemispherical array of transducers is known to vary by target location, with a small treatment envelope being present in the center of the brain. In this envelope, the incident angles of individual transducer elements at the calvarium are optimal for current mid-frequency systems (7). As one targets locations farther from the brain's center, the incident angles increase, resulting in more beam deformity and overall lower treatment efficiency (7, 8). The efficiency of acoustic penetration through the intact cranium also varies by the skull density ratio (SDR). SDR is the median ratio at element points of cancellous to cortical bone in the calvarium, and ranges from 0 to 1, with a cutoff of around 0.4 considered to be more efficacious and used in the United States (9, 10). Unfortunately, in a review of 163 patients presenting to a single emergency room, 37 percent have an SDR below 0.4 and so are ineligible for treatment (10). Though it is known that a treatment envelope exists, that targets at the center of the brain are easier to lesion, the magnitude of variation in treatment efficiency between different locations within the treatment envelope and beyond, with different SDRs, has not been well delineated (11). This variation could have implications for new targets and for patients with low SDRs.

We therefore elected to compare the physical efficiency of MRgFUS ablation of the near-center thalamic ventral intermediate (VIM) nucleus for treatment of essential tremor (ET) to that of ablation of the more laterally and anteriorly located globus pallidus internus (GPi) for dyskinesias or motor fluctuations of Parkinson's disease (PD). Data were collected from individual cases performed at our institution, and partnering institutions, and matched by patients' skull density ratio (SDR), as SDR is the most significant determinant of treatment efficiency (9, 10). Acoustic and thermal simulations were performed to compare temperature profiles of each lesion target.

METHODS

Patient Selection

To compare treatment characteristics, 20 patients treated with MRgFUS unilateral VIM thalamotomy for ET and 20 patients treated with unilateral GPi pallidotomy for PD were selected in pairs with matching SDRs, defined as values within 0.02 of each other. All 20 of 20 PD patients with available data were included, and 20 ET patients with similar SDRs were manually selected from a larger repository of treated patients. Patients were treated using the ExAblate 4,000 mid-frequency (670 kHz) head transducer system (InSightec, Haifa, Israel). All thalamotomies and 13 of the pallidotomies were performed in an identical fashion with the same neurosurgeon (H.M.E.), with low-level sonications to start for correction and alignment of the focal spot, followed by a relatively rapid rises in power to achieve ablative temperatures. The remaining pallidotomies were performed at partnering institutions. Parkinson's disease patients were treated in a prospective, open-label, multicenter trial of unilateral MRgFUS ablation of globus pallidus interna (NCT02263885). Institutional review board (IRB) approval was obtained at respective institutions and anonymized data were available in accordance with a prior data sharing agreement (NCT03100474). ET patients were all treated at the University of Maryland, Baltimore, and their data were entered into a prospectively maintained IRB-approved database (NCT01827904; NCT02289560). All data were anonymized.

Data Collection

Data on patient disease, age, and sex were collected. SDR, mean skull thickness, and skull surface are data were downloaded from respective ultrasound systems. To evaluate aspects of

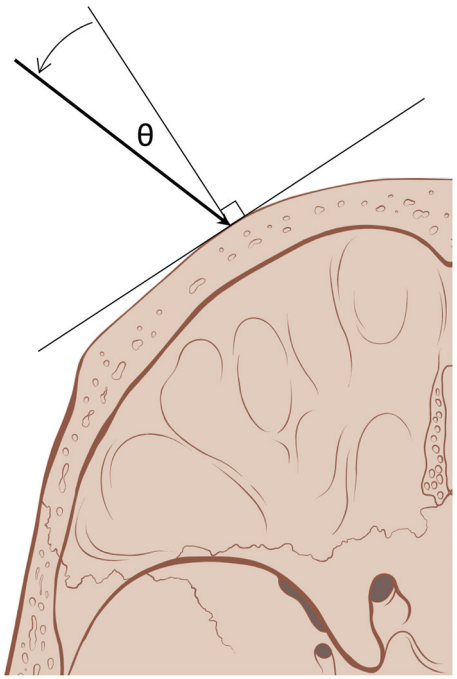

FIGURE 1 | Incident angle (θ) measures the degree from normal, orthogonal, at which acoustic beams (arrow) emitted by ultrasound elements reach the outer table of the skull. With a smaller incident angle, a greater proportion of the beam's energy traverses the skull (skull art reused with permission from Patrick J. Lynch and C. Carl Jaffe, MD).

treatment efficiency, the incident angles of acoustic beams (θ) on the outer table of the skull emitted by ultrasound elements, the number of sonications for treatment, the sonication time (minutes), the maximum average temperature reached (°C, T_{max}), the maximum energy for a single sonication (kilojoules, kJ), and the energy required to reach a temperature of 50 °C (kJ) were recorded (**Figure 1**). These were compared between thalamotomy and pallidotomy. Given that the treatment efficiency and not clinical efficacy was the objective of this study, and the fact that clinical outcomes for the two treatment populations would not be congruent, we did not collect or compare clinical outcomes. However, the clinical outcomes for the PD cohort has been published and this data is available (12).

Statistical Analysis

Demographic and comparative statistics were conducted to assess differences between the treatment groups and to develop regression models to assess relationships between different parameters (independent samples *t*-test, Mann–Whitney *U* test, and Pearson's χ^2 coefficient) (13). Energy to reach 50°C was calculated using logarithmic fit curves of input energy compared to temperature rise to account for differences in treatment approaches between patients and operators. A univariate linear regression model of SDR and energy required to reach 50°C was developed for each treatment group and compared, and additional linear regression models were developed. A benchmark of 50°C was used as all treatments reached or exceeded this temperature. Normal distributions were assumed for variables, however not for skull thickness (10, 14). The alpha level was set to 0.05. All statistical tests were computed with IBM SPSS Statistics software, version 23.0 (Armonk, NY, *IBM Corp*).

Acoustic and Temperature Field Simulation

To better understand the differences of lesion formation between MRgFUS thalamotomy and pallidotomy, acoustic field simulations were performed to evaluate the resulting acoustic profile. The acoustic fields within the head were simulated using a 3-D finite differences algorithm, which aims to solve the full Westervelt equation, a method to estimate temperature rise through heterogenous tissues (15). The acoustic properties of the skull were modeled based on CT images of one treated ET patient (16). Temperature simulation was estimated using the inhomogeneous Pennes equation of heat conduction (17). By solving the bio-heat equation with the calculated acoustic intensity field as the input, peak tissue temperature distribution was calculated. Both acoustic and temperature simulations were done at a resolution of 1×1×3 millimeters, to match the resolution of MR thermometry images obtained during treatment. The resulting simulated temperature profile for VIM and GPi ablation was compared on the same patient, particularly, the VIM temperature profile was compared with the MR thermometry data acquired during the treatment.

RESULTS

Data on 40 patients were collected and analyzed (**Table 1**). Patients treated with thalamotomy ($n = 20$) were older than patients treated with pallidotomy ($n = 20$) ($p < 0.001$). The proportions of patients in each treatment group did not differ by sex ($p = 0.490$). The mean SDR for thalamotomy was 0.54 (SD: 0.071) and for pallidotomy was 0.55 (SD: 0.067), (t-test, $p = 0.584$). The mean of absolute differences in SDR between treatment groups was 0.013 (SD: 0.0092). The mean skull thickness, an average of thickness calculated at every element point across the skull area treated, was 6.1 mm (SD: 1.1) for thalamotomy and 6.4 mm (SD: 1.1) for pallidotomy. The distribution of skull thickness between these groups was not different (Mann-Whitney *U* test, $p = 0.327$). There was no difference in mean skull surface area between thalamotomy, 340.3 cm^2 (SD: 30.2), and pallidotomy, 336.7 cm^2 (SD: 22.9), (*t*-test, $p = 0.678$).

The mean incident angle of acoustic beams was less in thalamotomy (12.7°, SD: 1.1) than in pallidotomy (18.6°, SD: 1.5), (*t*-test, $p < 0.001$). The mean number of elements of 1,024 maximum elements that emitted beams with incident angles <25 degrees, previously shown to be an optimal incident angle, was greater for thalamotomy (982.4, SD: 21.9) than for pallidotomy (791.7, SD: 89.0) (*t*-test, $p < 0.001$) (**Figure 2**) (1, 18).

Treatment groups did not differ in the mean number of sonications ($p = 0.233$) or the mean sonication time ($p = 0.679$). The mean maximum average temperatures reached was higher in the thalamotomy group (56.7°C, SD: 2.2) than in the pallidotomy (55.0°C, SD: 2.1), (*t*-test, $p = 0.017$). Mean maximum energy for

TABLE 1 | Demographics, skull parameters, and treatment characteristics of magnetic resonance-guided focused ultrasound unilateral thalamotomy and pallidotomy.

	Thalamotomy	Pallidotomy	*p*
Demographics			
Patients (*n*)	20	20	n/a
Mean age, years (SD)	70.4 (8.4)	56.3 (11.2)	<0.001
Sex ratio (M:F)	15:5	13:7	0.490
Skull parameters, mean			
Skull density ratio (SD)	0.54 (0.071)	0.55 (0.067)	0.584
Skull thickness, mm (SD)	6.1 (1.1)	6.4 (1.1)	0.327[a]
Skull surface area, cm^2 (SD)	340.3 (30.2)	336.7 (22.9)	0.678
Treatment characteristics, mean			
Incident angle, θ, (SD)	12.7 (1.1)	18.6 (1.5)	<0.001
Elements with incident angles <25° (SD)	982.4 (21.9)	791.7 (89.0)	<0.001
Sonications (SD)	18.0 (7.3)	15.8 (3.0)	0.233
Sonication time, min, (SD)	110.4 (53.5)	104.9 (26.1)	0.679
Maximum average temperature, °C, (SD)	56.7 (2.2)	55.0 (2.1)	0.017
Maximum energy, kJ (SD)	12.4 (6.3)	16.6 (7.8)	0.069
Energy, kJ, to 50°C (SD)	5.7 (2.8)	10.9 (6.5)	0.002

mm, millimeters; min, minutes; SD, standard deviation; kJ, kilojoules; M, male; F, female; R, right; L, left.
p-value: independent samples t-test. Mann–Whitney U test, or Pearson's χ^2 coefficient.
[a]*Mann–Whitney U test, reflects comparison of populations, not means.*

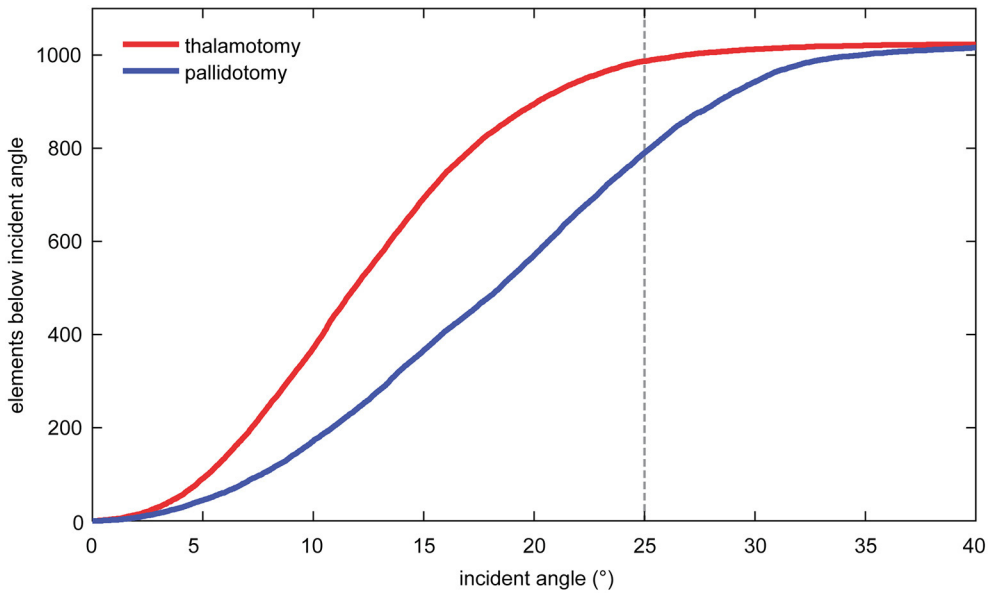

FIGURE 2 | The mean number of elements that emitted beams with incident angles <25 degrees was greater for thalamotomy of the ventral intermediate nucleus (VIM) than for pallidotomy of the globus pallidus internus (GPi).

a single sonication was higher in pallidotomy (16.6 kJ, SD: 7.8) than in thalamotomy (12.4 kJ, SD: 6.3), approaching significance (*t*-test, $p = 0.069$). The mean energy needed to reach 50 °C was nearly two-fold higher in pallidotomy (10.9 kJ, SD: 6.5) than in thalamotomy (5.7 kJ, SD: 2.8), (*t*-test, $p = 0.002$).

Univariate linear regression models were developed to determine the relationships between mean incident angle and treatment characteristics, and SDR and treatment characteristics. For all patients, a lesser mean incident angle was associated with a higher maximum average temperature reached (slope $= -0.250$, $R^2 = 0.124$, $p = 0.026$), and less energy needed to reach 50 °C (slope $= 0.632$, $R^2 = 0.134$, $p = 0.020$) (**Figures 3A,B**). A lower SDR was correlated with more energy needed to reach 50 °C, more strongly for thalamotomy (slope $= -17.8$, $R^2 = 0.197$, $p = 0.049$) than for pallidotomy (slope $= -56.3$, $R^2 = 0.342$, $p = 0.007$). The slope of this relationship

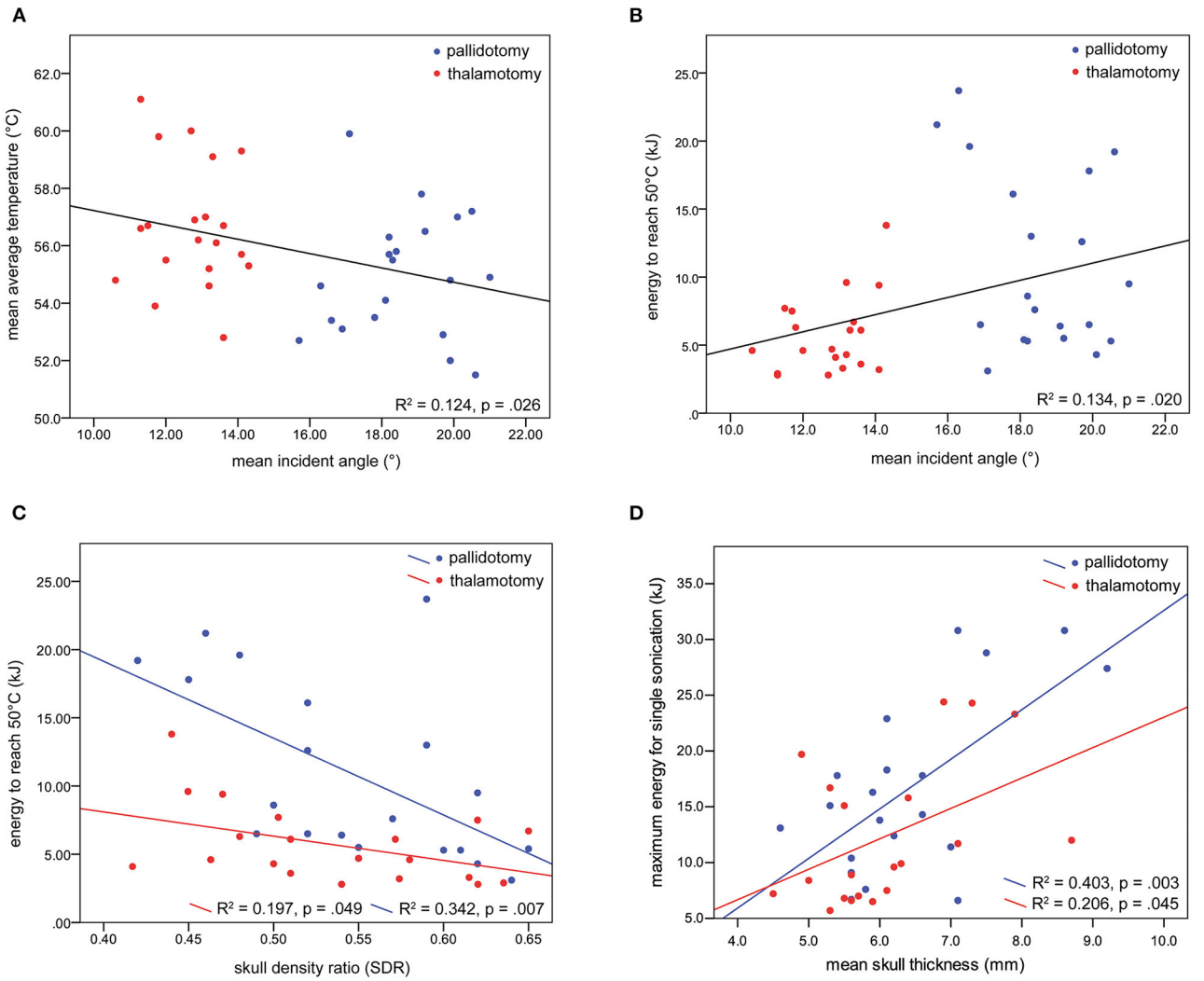

FIGURE 3 | Univariate regression models were developed. A lesser mean incident angle was associated with a higher maximum average temperature reached **(A)**, and less energy needed to reach 50 °C **(B)**. A lower SDR was correlated with more energy needed to reach 50 °C, for thalamotomy and for pallidotomy, nearly to a greater degree for pallidotomy **(C)**. Greater skull thickness was associated with greater energy for a single sonication **(D)**.

was steeper for pallidotomy, approaching significance on comparison between thalamotomy and pallidotomy ($p = 0.061$) (**Figure 3C**).

A greater skull thickness was associated with more energy needed to reach 50°C among all patients, however analysis by treatment revealed this held true for pallidotomy, not for thalamotomy, (slope = 3.3, $R^2 = 0.324$, $p = 0.009$). Additionally, a greater skull thickness was associated with a higher maximum energy for a single sonication for thalamotomy (slope = 2.7, $R^2 = 0.206$, $p = 0.045$) and pallidotomy (slope = 4.4, $R^2 = 0.403$, $p = 0.003$), but the slopes of these relationships did not differ ($p = 0.345$) (**Figure 3D**). Skull thickness was not associated with maximum average temperature reached. Skull surface area was not associated with any measure of treatment efficiency. In a multiple regression model, incident angle (slope = 0.688, $p = 0.002$), SDR (slope = −29.4, $p = 0.004$), and skull thickness (slope = 2.4, $p < 0.001$) correlated with energy needed to reach 50 °C ($F(3, 36) = 12.719$, $p < 0.001$, $R^2 = 0.515$). Age and sex did not correlate with each other, or with SDR, incident angle, maximum average temperature reached, or energy needed to reach 50 °C.

Simulated temperature maps for both VIM (**Figure 4B**) and GPi (**Figure 4C**) ablation on a single ET patient with the same sonication duration and power were rendered. The estimated peak temperature was 59.8 °C and 57.8 °C at the VIM and GPi targets, respectively. On the VIM target, the simulated peak temperature was quite close to the peak temperature (59.8 °C) recorded by MR thermometry (**Figure 4A**) during the treatment under the same conditions.

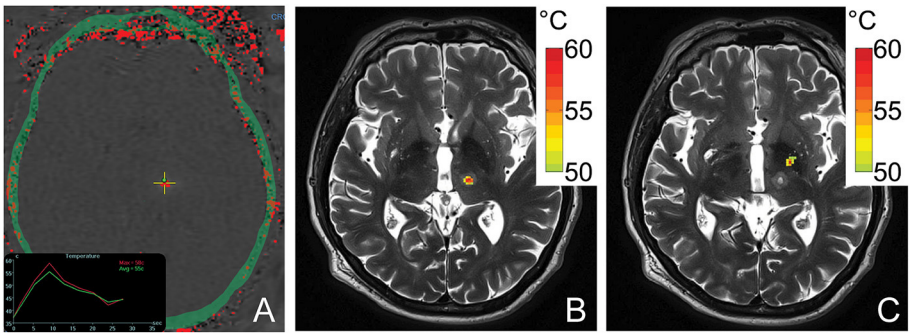

FIGURE 4 | An MR thermometry image acquired during the treatment of ET with focused ultrasound thalamotomy showing 58°C was achieved as the maximum temperature on this patient **(A)**. An example of temperature simulation results is shown when targeting VIM **(B)** and GPi **(C)** on the same patient. The temperature fields were registered to the post 1-day T2-weighted images. The globus pallidus internus lies antero-lateral compared to the ventral intermediate nucleus.

DISCUSSION

Our results demonstrate that MRgFUS ablation of the GPi is less efficient than ablation of the thalamic VIM nucleus in patient populations with matched skull density ratios. The energy required to reach 50 °C during pallidotomy was nearly twice that of thalamotomy. This is likely due to the greater incident angles of individual ultrasound elements when targeting the more antero-laterally located GPi, which in turn results in decreased transmission and greater reflection of acoustic energy at the skull outer table (**Figure 4**) (1, 18, 19). This reduced transmission of acoustic energy also likely explains the lower maximum average temperature achieved during GPi ablation although, in this present cohort of patients, definitive evidence of successful lesioning was always observed and confirmed on post-operative MRI.

Similar to prior studies, SDR and skull thickness significantly influenced treatment efficiency at both targets in our cohort, SDR more so than skull thickness (9, 10, 19). However, there was a strong trend toward a greater influence of lower SDR on pallidotomy efficiency. Greater skull thickness also uniquely reduced efficiency in pallidotomy patients. This again may be due to the location of the GPi in relation to the cranium. While prior authors have demonstrated that VIM ablation may still be successfully performed in low-SDR candidates, our results suggest that operators should be more cautious when proceeding with pallidotomy in this patient population (10, 20). Yet, it is important to note that although lower SDRs have been correlated with a greater energy requirements for MRgFUS ablation, they have not been shown to impact clinical outcomes (10, 21). Further investigation regarding the feasibility of MRgFUS pallidotomy in low SDR patients is warranted. Future innovations in treatment algorithms could focus on selectively turning off elements with extreme beam angles to increase or modify treatment efficiency, especially in patients with low SDR. Other therapeutic strategies in low SDR patients may rely on either repeated prolonged exposures of the intended target to lower than ideal temperatures to accomplish ablative lesioning or alternatively steeper ramp up of temperatures during treatment since repeated sonications with smaller energy increments may result in reduction in skull efficiency (22).

An acoustic and temperature field simulation demonstrated a higher peak temperature for thalamotomy than pallidotomy in the same ET patient, an internal control. The close estimated peak temperature by simulation compared with the treatment data indicated the accuracy of the simulation model. The simulated thermal profiles also closely resemble those observed in ET and PD treatment cases (22, 23). GPi lesions assume an elongated, ellipsoid shape extending in the inferolateral to superomedial direction due to the off-center target location which results a larger mean incident angle and therefore, an uneven energy distribution (22). These same factors result in an overall reduced peak acoustic intensity generated at the GPi compared to VIM, with resulting lower achievable peak ablation temperatures. In contradistinction, the near-center location of the VIM results in spherical lesions as well as, on average, a higher peak temperature under the same sonication conditions.

Although it was beyond the scope of the current study, there was no evidence to suggest that the lower treatment efficiency of pallidotomy impacted the ability to generate a lesion at the GPi in our cohort. Specifically, all Parkinson's patients included in the current investigation underwent successful GPi ablation with evidence of the expected T2 hyperintense, diffusion restricting lesion on post-procedure MRI (12). One potential explanation for how GPi ablation was achieved despite the significantly reduced treatment efficiency was our prior observation that pallidotomy may be accomplished using repetitive lower maximum average temperature sonications (22). Consequently, the peak temperature achieved in GPi ablation may be less important than the accumulative thermal dose delivered at this target. Moreover, GPi ablations were performed in the setting of a trial, with a cut-off SDR value of 0.4 (12). Therefore, although our data predicts that GPi of the patients with SDR <0.4 may be much more difficult to lesion compared to VIM, this is a speculation since we did not have any patients lower than 0.4 SDR in the trial.

In one attempt to perform MRgFUS lesioning of the hippocampus for mesial temporal lobe epilepsy, adequate

temperatures could not be reached, likely secondary to the peripherality of the target (24). There are multiple efforts aimed at improving the treatment envelope in MRgFUS systems, as more lateral and peripheral targets are investigated for epilepsy, tumor ablation, and psychiatric diseases (24–27). Cadaveric phantom models treated with MRgFUS thermal ablation provide a method to test new target sites, and corresponding treatment requirements (28). In patients who undergo a craniotomy for initial treatment of a tumor, cranial prostheses optimized for acoustic penetration can be implanted instead of native bone to facilitate future MRgFUS treatment (29). Additionally, a cadaveric simulation study tested a patient-specific conformal array that uses concave ultrasound elements and pulsed ultrasound to improve energy delivery to peripheral targets (30). Furthermore, for targets near the skull base, a blocking algorithm to selectively exclude ultrasound elements can prevent heating of the skull and neurovascular damage (31, 32). Lastly, optimization of transcranial focusing, such as with echo-focusing, may further expand the treatment envelope and improve the treatment efficiency for MRgFUS, even in low SDR patients (33, 34).

This study has several important limitations, including its retrospective design and smaller cohort size; the latter was due to the limited number of pallidotomy patients with data available for analysis. Also, SDRs are specific between individuals, and were unable to be matched exactly between cohort groups, which may have influenced our results. Our data was not granular enough to determine the effect of local SDR on treatment efficiency, so we used average SDR as prior studies have done. Although most of our patients were treated at a single institution, differences in treatment practices between institutions can be difficult to parse out when grouping individuals treated for the same disease. Similarly, treatment practices and strategies can vary between teams affecting treatment duration. Finally, we did not include any patients with lower SDRs (i.e. < 0.4), which would pose a significantly greater challenge for successful MRgFUS lesioning due to reduced treatment efficiency. Future studies should focus on this cohort of patients to understand the true impact of larger incident angles while treating off-center locations.

CONCLUSION

MRgFUS thalamotomy of the VIM for essential tremor has higher treatment efficiency characteristics than pallidotomy of the GPi for Parkinson's disease. This is likely due to the central location of the VIM. As new off-center targets within the skull are investigated for MRgFUS thermal ablation and treatments are considered in low SDR subjects, these findings can inform appropriate patient selection and physical treatment requirements (35).

DATA AVAILABILITY STATEMENT

The raw data supporting the conclusions of this article will be made available by the authors, without undue reservation.

ETHICS STATEMENT

The studies involving human participants were reviewed and approved by University of Maryland, Baltimore Institutional Review Board (Exemption HP-00093725). Written informed consent for participation was not required for this study in accordance with the national legislation and the institutional requirements.

AUTHOR CONTRIBUTIONS

A-KA organized the database. A-KA and TM performed the statistical analysis. A-KA, DG, and TM wrote the first draft of the manuscript. SG and AK wrote sections of the manuscript. All authors contributed to manuscript revision, conception, read, design of the study, and approved the submitted version.

REFERENCES

1. Krishna V, Sammartino F, Rezai A. A review of the current therapies, challenges, and future directions of transcranial focused ultrasound technology: advances in diagnosis and treatment. *JAMA Neurol.* (2018) 75:246–54. doi: 10.1001/jamaneurol.2017.3129
2. Fry WJ, Mosberg WHJr, Barnard JW, Fry FJ. Production of focal destructive lesions in the central nervous system with ultrasound. *J Neurosurg.* (1954) 11:471–8. doi: 10.3171/jns.1954.11.5.0471
3. Fry FJ. Precision high intensity focusing ultrasonic machines for surgery. *Am J Phys Med.* (1958) 37:152–6. doi: 10.1097/00002060-195806000-00011
4. Jagannathan J, Sanghvi NT, Crum LA, Yen CP, Medel R, Dumont AS, et al. High-intensity focused ultrasound surgery of the brain: part 1–A historical perspective with modern applications. *Neurosurgery.* (2009) 64:201–210. doi: 10.1227/01.NEU.0000336766.18197.8E
5. Clement GT, Hynynen K. A non-invasive method for focusing ultrasound through the human skull. *Phys Med Biol.* (2002) 47:1219–36. doi: 10.1088/0031-9155/47/8/301
6. Khanna N, Gandhi D, Steven A, Frenkel V, Melhem ER. Intracranial applications of MR imaging-guided focused ultrasound. *AJNR Am J Neuroradiol.* (2017) 38:426–31. doi: 10.3174/ajnr.A4902
7. Franzini A, Moosa S, Prada F, Elias WJ. Ultrasound ablation in neurosurgery: current clinical applications and future perspectives. *Neurosurgery.* (2020) 87:1–10. doi: 10.1093/neuros/nyz407
8. Pulkkinen A, Huang Y, Song J, Hynynen K. Simulations and measurements of transcranial low-frequency ultrasound therapy: skull-base heating and effective area of treatment. *Phys Med Biol.* (2011) 56:4661–83. doi: 10.1088/0031-9155/56/15/003
9. Chang WS, Jung HH, Zadicario E, Rachmilevitch I, Tlusty T, Vitek S, et al. Factors associated with successful magnetic resonance-guided focused ultrasound treatment: efficiency of acoustic energy delivery through the skull. *J Neurosurg.* (2016) 124:411–6. doi: 10.3171/2015.3.JNS142592
10. Boutet A, Gwun D, Gramer R, Ranjan M, Elias GJB, Tilden D, et al. The relevance of skull density ratio in selecting candidates for transcranial MR-guided focused ultrasound. *J Neurosurg.* (2019) 132:1785–91. doi: 10.3171/2019.2.JNS182571
11. Ghanouni P, Pauly KB, Elias WJ, Henderson J, Sheehan J, Monteith S, et al. Transcranial MRI-guided focused ultrasound: a review of the technologic and neurologic applications. *AJR Am J Roentgenol.* (2015) 205:150–9. doi: 10.2214/AJR.14.13632

12. Eisenberg HM, Krishna V, Elias WJ, Cosgrove GR, Gandhi D, Aldrich CE, et al. MR-guided focused ultrasound pallidotomy for Parkinson's disease: safety and feasibility. *J Neurosurg.* (2020) 1–7. doi: 10.3171/2020.6.JNS192773
13. Lachin JM. Nonparametric statistical analysis. *JAMA.* (2020) 323:2080–1. doi: 10.1001/jama.2020.5874
14. Li H, Ruan J, Xie Z, Wang H, Liu W. Investigation of the critical geometric characteristics of living human skulls utilising medical image analysis techniques. *Int J Veh Saf.* (2007) 2:345–67. doi: 10.1504/IJVS.2007.016747
15. Hamilton MF, Blackstock DT. *Nonlinear acoustics*. San Diego, CA: Academic Press. (1998).
16. Aubry J-F, Tanter M, Pernot M, Thomas J-L, Fink M. Experimental demonstration of noninvasive transskull adaptive focusing based on prior computed tomography scans. *J Acoust Soc.* (2003) 113:84–93. doi: 10.1121/1.1529663
17. Pennes HH. Analysis of tissue and arterial blood temperatures in the resting human forearm. *J Appl Physiol.* (1948) 1:93–122. doi: 10.1152/jappl.1948.1.2.93
18. White PJ, Clement GT, Hynynen K. Longitudinal and shear mode ultrasound propagation in human skull bone. *Ultrasound Med Biol.* (2006) 32:1085–96. doi: 10.1016/j.ultrasmedbio.2006.03.015
19. Jung NY, Rachmilevitch I, Sibiger O, Amar T, Zadicario E, Chang JW. Factors related to successful energy transmission of focused ultrasound through a skull: a study in human cadavers and its comparison with clinical experiences. *J Korean Neurosurg Soc.* (2019) 62:712–22. doi: 10.3340/jkns.2018.0226
20. D'souza M, Chen KS, Rosenberg J, Elias WJ, Eisenberg HM, Gwinn R, et al. Impact of skull density ratio on efficacy and safety of magnetic resonance-guided focused ultrasound treatment of essential tremor. *J Neurosurg.* (2019) 132:1392–7. doi: 10.3171/2019.2.JNS183517
21. Gagliardo C, Marrale M, D'angelo C, Cannella R, Collura G, Iacopino G, et al. Transcranial magnetic resonance imaging-guided focused ultrasound treatment at 1.5 T: A retrospective study on treatment- and patient-related parameters obtained from 52 procedures. *Front Phy*. (2020) 7. doi: 10.3389/fphy.2019.00223
22. Miller TR, Guo S, Melhem ER, Eisenberg HM, Zhuo J, Kelm N, et al. Predicting final lesion characteristics during MR-guided focused ultrasound pallidotomy for treatment of Parkinson's disease. *J Neurosurg.* (2020) 134:1083–90. doi: 10.3171/2020.2.JNS192590
23. Wintermark M, Druzgal J, Huss DS, Khaled MA, Monteith S, Raghavan P, et al. Imaging findings in MR imaging-guided focused ultrasound treatment for patients with essential tremor. *AJNR Am J Neuroradiol.* (2014) 35:891–6. doi: 10.3174/ajnr.A3808
24. Abe K, Yamaguchi T, Hori H, Sumi M, Horisawa S, Taira T, et al. Magnetic resonance-guided focused ultrasound for mesial temporal lobe epilepsy: a case report. *BMC Neurol.* (2020) 20:160. doi: 10.1186/s12883-020-01744-x
25. Fountain N, Tseng P, Quigg M, Dallapiazza R, Elias J. Potential of focused ultrasound in epilepsy surgery. *J Ther Ultrasound.* (2015) 3:O29–O29. doi: 10.1186/2050-5736-3-S1-O29
26. Hersh DS, Kim AJ, Winkles JA, Eisenberg HM, Woodworth GF, Frenkel V. Emerging applications of therapeutic ultrasound in neuro-oncology: moving beyond tumor ablation. *Neurosurgery*. (2016) 79:643–54. doi: 10.1227/NEU.0000000000001399
27. Davidson B, Hamani C, Rabin JS, Goubran M, Meng Y, Huang Y, et al. Magnetic resonance-guided focused ultrasound capsulotomy for refractory obsessive compulsive disorder and major depressive disorder: clinical and imaging results from two phase I trials. *Mol Psychiatry.* (2020) 25:1946–57. doi: 10.1038/s41380-020-0737-1
28. Eames MD, Farnum M, Khaled M, Elias WJ, Hananel A, Snell JW, et al. Head phantoms for transcranial focused ultrasound. *Med Phys.* (2015) 42:1518–27. doi: 10.1118/1.4907959
29. Prada F, Franzini A, Moosa S, Padilla F, Moore D, Solbiati L, et al. In vitro and in vivo characterization of a cranial window prosthesis for diagnostic and therapeutic cerebral ultrasound. *J Neurosurg.* (2020) 1–13. doi: 10.3171/2019.10.JNS191674
30. Hughes A, Hynynen K. Design of patient-specific focused ultrasound arrays for non-invasive brain therapy with increased trans-skull transmission and steering range. *Phys Med Biol.* (2017) 62:L9–L19. doi: 10.1088/1361-6560/aa7cd5
31. Monteith SJ, Medel R, Kassell NF, Wintermark M, Eames M, Snell J, et al. Transcranial magnetic resonance-guided focused ultrasound surgery for trigeminal neuralgia: a cadaveric and laboratory feasibility study. *J Neurosurg.* (2013) 118:319–28. doi: 10.3171/2012.10.JNS12186
32. Monteith S, Snell J, Eames M, Kassell NF, Kelly E, Gwinn R. Transcranial magnetic resonance-guided focused ultrasound for temporal lobe epilepsy: a laboratory feasibility study. *J Neurosurg.* (2016) 125:1557–64. doi: 10.3171/2015.10.JNS1542
33. Jones RM, Huang Y, Meng Y, Scantlebury N, Schwartz ML, Lipsman N, et al. Echo-focusing in transcranial focused ultrasound thalamotomy for essential tremor: a feasibility study. *Movement Disorders*. (2020) 1–6. doi: 10.1002/mds.28226
34. Chang KW, Rachmilevitch I, Chang WS, Jung HH, Zadicario E, Prus O, et al. Safety and efficacy of magnetic resonance-guided focused ultrasound surgery with autofocusing. *Echo Imaging.* (2021) 14. doi: 10.3389/fnins.2020.592763
35. Davidson B, Mithani K, Huang Y, Jones RM, Goubran M, Meng Y, et al. Technical and radiographic considerations for magnetic resonance imaging–guided focused ultrasound capsulotomy. *J Neurosurg.* (2020) 1–9. doi: 10.3171/2020.6.JNS201302

Conflict of Interest: Authors NK and RC were employed by company Insightec. HE and DG were on the advisory board of Insightec.

The remaining authors declare that the research was conducted in the absence of any commercial or financial relationships that could be construed as a potential conflict of interest.

frontiers in Neurology

ORIGINAL RESEARCH
published: 18 February 2022
doi: 10.3389/fneur.2022.743649

Magnetic Resonance Image Guided Focused Ultrasound Thalamotomy. A Single Center Experience With 160 Procedures

Asad M. Lak[1], *David J. Segar*[1], *Nathan McDannold*[2], *Phillip Jason White*[2,3] *and Garth Rees Cosgrove*[1]*

[1] Department of Neurosurgery, Brigham and Women's Hospital and Harvard Medical School, Boston, MA, United States,
[2] Department of Radiology, Brigham and Women's Hospital and Harvard Medical School, Boston, MA, United States,
[3] Department of Chemistry and Physics, Simmons University, Boston, MA, United States

OPEN ACCESS

Edited by:
Vibhor Krishna,
The Ohio State University,
United States

Reviewed by:
Rushna Ali,
Spectrum Health, United States
Mojgan Hodaie,
University of Toronto, Canada
Michael Kaplitt,
Weill Cornell Medicine, United States

***Correspondence:**
Garth Rees Cosgrove
rcosgrove2@bwh.harvard.edu

Specialty section:
This article was submitted to Experimental Therapeutics, a section of the journal Frontiers in Neurology

Received: 19 July 2021
Accepted: 24 January 2022
Published: 18 February 2022

Citation:
Lak AM, Segar DJ, McDannold N, White PJ and Cosgrove GR (2022) Magnetic Resonance Image Guided Focused Ultrasound Thalamotomy. A Single Center Experience With 160 Procedures. Front. Neurol. 13:743649. doi: 10.3389/fneur.2022.743649

Introduction: MRgFUS thalamotomy has gained popularity as an FDA approved, non-invasive treatment for patients with Essential Tremor and tremor predominant Parkinson's Disease. We present our initial clinical experience with 160 consecutive cases of MRgFUS thalamotomy and describe the clinical outcomes with long term follow-up.

Methods: A retrospective chart review of all patients who underwent MRgFUS thalamotomy at our institution was performed. CRST Part A tremor scores were obtained pre-operatively and at each follow-up visit along with an assessment of side effects (SE). All patients had a post-operative MRI within 24 h to determine the location, size, and extent of the MRgFUS lesion.

Results: One hundred and sixty unilateral MRgFUS Thalamotomies (Left, $n = 128$; Right, $n = 32$) were performed for medically refractory essential Tremor ($n = 150$) or tremor predominant Parkinson's disease ($n = 10$). Mean age at surgery was 75 Years (range: 48-93) and the mean skull density ratio (SDR) was 0.48 (range: 0.32-0.75; median: 0.46). In ET patients, both rest and postural tremor was abolished acutely and remained so at follow-up whereas intention tremor was reduced acutely by 93% below baseline, 87% at 3 months, 83.0% at 1-year, and 78% at 2 years. On post-operative day 1, the most common SE's included imbalance (57%), sensory disturbances (25%), and dysmetria (11%). All adverse events were rated as mild on the Clavien-Dindo Scale and improved over time. At 2-years follow-up, imbalance was seen in 18%, sensory disturbance in 10% and dysmetria in 8% patients. Mean clinical follow-up for all patients was 14 months (range: 1-48 months).

Conclusion: MRgFUS thalamotomy is a safe and effective procedure for long term improvement of unilateral tremor symptoms, with the most common side-effects being imbalance and sensory disturbance.

Keywords: focused ultrasound (FUS), thalamotomy, tremor, essential tremor (ET), Parkinson's disease (PD)

INTRODUCTION

Magnetic Resonance Image guided Focused Ultrasound (MRgFUS) thalamotomy has emerged as a novel treatment option for medically refractory tremor. The ability to ablate the intracranial target non-invasively, during an awake outpatient procedure, has made MRgFUS a reasonable treatment option for patients who are not suitable for or choose not to undergo an invasive surgical procedure. Since publication of the landmark randomized controlled trial (RCT) demonstrating the safety and efficacy of MRgFUS thalamotomy in unilateral Essential Tremor (ET) (1), reports from several centers have documented sustained benefit from the procedure at long term follow-up (2–5). Recent publications have attempted to identify key factors that may improve clinical outcomes following MRgFUS thalamotomy (4, 6–9). Skull Density Ratio (SDR), lesion location and lesion volume have all been reported as important factors that determine tremor outcomes and the adverse event profile (7, 10, 11). SDR has also been reported as a key factor in achieving therapeutic temperature at target site (8). Despite several publications reporting outcomes following MRgFUS, the current literature is limited by small sample size, heterogeneity in institutional protocols and studies involving multiple surgeons (2–4, 6).

In this retrospective observational study, we report our institution's experience with MRgFUS thalamotomy performed by the senior author (G.R.C) over a period of 4 years. We believe this represents a "real-world" clinical experience in a large number of patients undergoing this procedure and identifies areas for future advances in the field.

METHODS

After obtaining institutional review board approval, a retrospective chart review of all patients who underwent unilateral Magnetic Resonance Image guided Focused Ultrasound (MRgFUS) thalamotomy for medically refractory Essential tremor (ET) or tremor predominant Parkinson's disease from March 2016 to January 2021 was performed.

Disease Characteristics

A detailed chart review was performed to extract demographics (age, gender), disease characteristics (family history, duration, tremor severity), treatment parameters [lesion location, sonication parameters (i.e., mean maximum temperature, mean maximum power, mean maximum energy, number of sonications), skull density ratio] and follow-up information (tremor scores in treated extremity, adverse events). Tremor scores in the treated extremity were documented using CRST Part A which rates tremor severity from 0 to 4, with 0 being no tremor and 4 being severe tremor (12). Tremor scores were documented at baseline, post-operative day 1, 3 months, 1 year, and later at annual follow-up. A systematic questionnaire for adverse events was documented at the same post-operative follow-up intervals.

Surgical Procedure

Details of the surgical procedure have been published elsewhere (13). Briefly, on the day of the procedure, the patient's head was shaved, and a modified stereotactic frame was affixed low on the patient's skull after infiltration with local anesthetic. A flexible rubber gasket was placed over the frame posts and the patient's head firmly fixed to the MRI table. The space between the patient's head and the FUS transducer was then filled with circulating, degassed water and heavily T2-weighted images were obtained in sagittal, coronal, and axial planes. Standard stereotactic coordinates were used to locate the Ventral Intermediate Nucleus (Vim) of thalamus: 11 mm from the lateral wall of third ventricle, ¼ distance of the anterior commissure-posterior commissure (AC-PC) distance in front of PC and 1-2 mm above the intercommissural plane. Minor corrections to this initial target were made to adjust for individual patient anatomy. A baseline neurological examination was performed to assess speech, motor and sensory function, coordination and the magnitude of tremor with posture and intentional tasks (spiral, line drawing, and drinking from a bottle). Test sonications using lower temperatures were then performed to verify target alignment and determine the optimal lesion location. Once confirmed, higher temperature sonications were performed sequentially to ablate the Vim. Serial neurological examinations were performed after each sonication to assess for tremor improvement and side effects. No major change in methodology of FUS thalamotomy was undertaken except for altering the initial targeting to 1.5-2 mm above the intercommissural plane instead of at the intercommissural plane after the first few cases.

Outcome Assessment

Change in tremor scores were documented as percentage improvement from baseline and adverse events were recorded at each follow-up interval. An immediate MRI was obtained within 24 h post-operatively. Thin cut (2 mm) axial and coronal T2 slices were used for image analysis in this study (**Figure 1**). The center of the lesion was estimated on axial T2 images at the AC-PC plane and lesion volumes were then calculated by measuring the maximal distance from the center of the lesion along axial, coronal and sagittal axes. Wintermark zones 1 and 2 which represent coagulative necrosis and cytotoxic edema, respectively, and have been shown to correlate with permanent lesion were used for analysis of lesion volume (14). Wintermark zone 3 which represents vasogenic edema and is apparent on 24-h and 1-week MRI scans but resolves later was not used for calculation of lesion volume. In order to analyze the impact of SDR on tremor outcomes, the overall cohort was divided into two groups based on SDR. SDR < 0.45 was called "low SDR" group and SDR ≥ 0.45 was called "high SDR" group. With only 10 patients treated for tremor predominant PD, only the subset of patients with a diagnosis of ET were included in the analysis of tremor outcomes. The entire cohort was however analyzed for the adverse events analysis.

Statistical Analysis

Continuous variables are reported as mean $\pm$ standard deviation (range) and categorical variables as frequency (%). Comparison

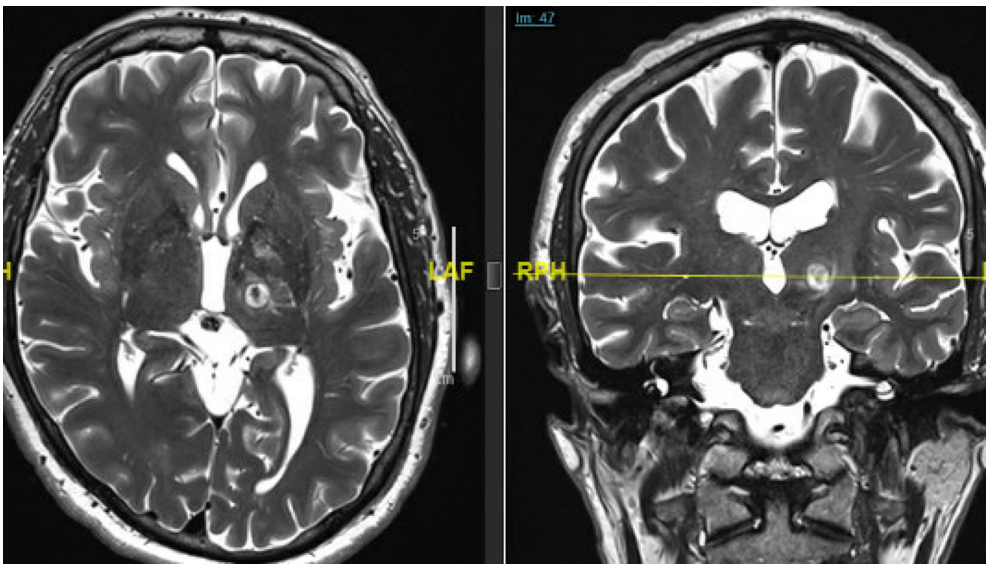

FIGURE 1 | Immediate (24 h post-op) T2-weighted axial (left) and coronal (right) MRI scans demonstrating the size, shape, and location of a typical left Vim FUS thalamotomy. Note the edema extending around the lesion into the surrounding thalamus and the internal capsule.

of tremor scores at each follow-up was performed using paired *t*-test. Comparison of percentage improvement in tremor scores in low SDR and high SDR groups was also performed using paired *t*-test.

RESULTS

Demographics

A total of 160 cases were included in the study (**Table 1**). Treatment was aborted in one case due to a technical failure and inability to raise temperature, and one patient did not return after day 1 follow up, hence 158 patients were available for analysis of tremor outcomes. The mean patient age was 75 (range 55-93 years) and 68% were male. The overwhelming majority of patients had a diagnosis of ET ($n = 150$) whereas the rest had tremor predominant Parkinson's disease ($n = 10$). A positive family history was present in 68.75% patients and the mean duration of disease was 27.5 years. The mean SDR of entire cohort was 0.48 (median: 0.46; range 0.32-0.75).

TABLE 1 | Demographics and clinical data of included patients ($n = 160$).

Age (years)	75.0 ± 7.50 (48-93)
Percentage males (%)	68.0% ($n = 109$)
Essential tremor	93.75% ($n = 150$)
Tremor-dominant Parkinson's	6.25% ($n = 10$)
Family history of tremor	68.75% ($n = 110$)
Mean duration from diagnosis (years)	27.5 ± 18.0 (2-70)
Laterality of Thalamotomy	
Left	80.0% ($n = 128$)
Right	20.0% ($n = 32$)
FTM intention tremor at follow up (ET)	Significant difference from preop baseline ($p < 0.0001$)
Preop Baseline ($n = 149$)	3.39 ± 0.60 (2-4)
Day 1 ($n = 148$)	0.29 + 0.48 (0 – 2) (92.6%)
3 months ($n = 110$)	0.50 + 0.95 (0 – 4) (87.2%)
1 year follow-up ($n = 101$)	0.66 ± 1.08 (0 – 4) (83.1%)
2 year follow-up ($n = 49$)	0.87 ± 0.90 (0-3) (78.0%)
Treatment parameters	
Skull density ratio	0.48 ± 0.08 (0.32-0.75)
Lesion volume	335.45 ± 174.4 mm^{-3}

Tremor Scores

Left sided thalamotomy was most commonly performed (80%). The mean tremor score at baseline in ET patients was rest: 0.23 ± 0.55; posture: 2.72 ± 0.81; intention: 3.39 ± 0.60. The mean tremor score at baseline in tremor predominant PD was rest: 3.5 ± 0.52; posture: 2.8 ± 0.78; intention: 1.5 ± 1.18. Immediately following treatment, tremor scores in ET patients reduced sharply such that both rest and postural tremor scores declined to zero and remained so at long term follow-up. In addition, intention tremor was completely abolished in 107 patients on the first post-operative day. Intention tremor scores on post-operative day 1 ($n = 148$) were 0.29 ± 0.48, 0.50 ± 0.95 at 3 months ($n = 110$), 0.66 ± 1.08 at 1 year ($n = 101$), 0.87 ± 0.90 at 2 years ($n = 49$), 1.25 ± 0.57 at 3 years ($n = 8$) and 1 ± 0.63 at 4 years ($n = 6$) follow-up. At 1-year follow-up, nine patients had lost > 50% of their treatment benefit and at 2 years follow-up, five additional patients developed recurrence of tremor. In patients with tremor predominant PD, tremor scores also declined to zero and remained so till 3-months follow-up. At 1 year follow up ($n = 4$), mean rest tremor scores in PD patients were 0.75 and at 2 years ($n = 2$) it was 1.00.

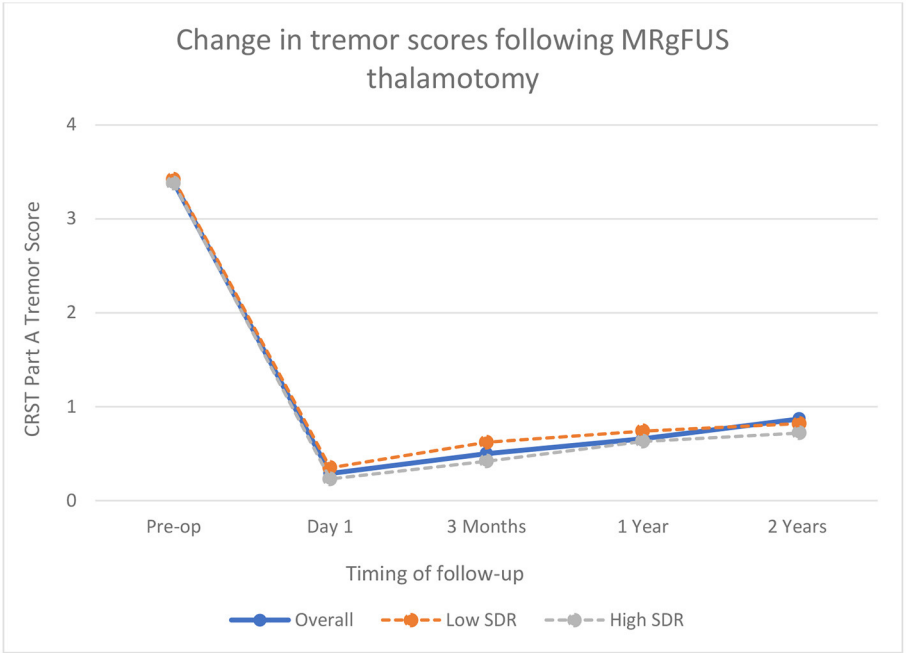

FIGURE 2 | Change in tremor scores following MRgFUS thalamotomy in Essential Tremor patients.

High SDR vs. Low SDR Group

In comparing ET patients based on SDR, the percentage improvement in tremor scores was slightly higher in high SDR group at each follow-up interval [93% on day 1, 87% at 3 months, 81.5% at 1 year and 79% at 2 years as compared to 90% on day 1, 82% at 3 months, 78.5% at 1 year and 76% at 2-years] but this finding was statistically non-significant (**Figure 2**). The high SDR group had on average larger lesions than the low SDR group [310.5 vs. 262.0 mm^3], lower mean maximum energy [17242.0 vs. 26253.5 J], lower mean maximum power [936.0 vs. 1048.5 Watts] and higher mean maximum temperature [61.0vs. 57.5°C]. At 1-year follow-up, there were five patients in each group who had lost treatment benefit and were back to baseline tremor scores.

Adverse Events

Adverse events following treatment were common (**Table 2**). On post-operative day 1 ($n = 160$), the most common adverse events were gait imbalance (56.8%) followed by sensory deficits (25%), dysarthria (18.75%), dysmetria (11.25%), motor weakness (8.75%), headache (3.12%), dysgeusia (0.62%), and others (2.5%). The majority of adverse events were transient (**Figure 3**) such that at 3-months follow up ($n = 116$), gait imbalance was seen in 25.8% patients, sensory deficits in 24.15%, dysarthria in 7.75%, dysmetria in 10.34%, motor weakness in 5.17%, and dysgeusia in 7.75% cases. At 1 year follow up ($n = 105$), most common adverse events were sensory deficits (16.2%) followed by gait imbalance (14.28%), dysmetria (6.66%), dysarthria (5.71%), motor weakness (2.85%), and dysgeusia (2.85%). The similar trend continued at 2 years follow-up ($n = 51$) where the most common adverse events were gait imbalance (17.5%), sensory deficits (10.0%), dysmetria (8.0%), dysgeusia (4.0%), and motor weakness (2.0%).

DISCUSSION

In this retrospective study of 160 patients undergoing unilateral MRgFUS thalamotomy for severe, intractable essential tremor, we have demonstrated marked improvement in tremor scores of the treated arm in >90% of patients. This improvement was sustained at long-term follow-up as highlighted by sustained ∼80% improvement in tremor scores at 2-years follow-up. Although adverse events were common, the majority were transient and had resolved or improved substantially at long-term follow-up. We also demonstrated that patients with SDR < 0.45, i.e., "low SDR" group had comparable improvements in tremor scores as the patients with SDR ≥ 0.45. Another reassuring finding in our study is the sustained improvement in tremor scores at long-term follow-up. Notably, our long-term tremor outcomes are slightly better than what is currently reported in the literature (3, 4, 15).

SDR has been found to correlate with the ability to achieve therapeutic temperatures at target site and current recommendations suggest an SDR ≥ 0.45 for successful ablation (16). Many centers feel this recommendation is somewhat arbitrary and offer MRgFUS to patients with an SDR < 0.45. A recently published trial in a Japanese population demonstrated positive outcomes in a population with lower average SDR than other studies (2). This study highlighted that patients with lower SDR had lower maximum temperature than the high SDR group, but the temperature achieved was still sufficient

to provide clinical benefit. Two additional studies have also concluded that SDR does not affect clinical outcome despite being correlated with a lower maximum temperature at target site (16, 17). Our results align with the previously reported studies and highlight that percentage improvement in tremor scores at long-term follow-up was comparable between the two groups.

TABLE 2 | Adverse events.

Adverse events	1-day post-op (n = 160)	3-months post-op (n = 116)	1-year post-op (n = 105)	2-years post-op (n = 51)
Motor weakness	14 (8.75%)	6 (5.17%)	3 (2.85%)	1 (2.0%)
Face	5 (3.12%)	-	-	-
Limb	7 (4.37%)	6 (5.17%)	3 (2.85%)	1 (2.0%)
Face and limb	2 (1.25%)	-	-	-
Dysarthria	30 (18.75%)	9 (7.75%)	6 (5.71%)	1 (2.0%)
Sensory deficits (Paresthesia/Numbness)	40 (25.0%)	28 (24.15%)	17 (16.2%)	5 (10.0%)
Orofacial	27 (16.87%)	20 (17.25%)	11 (10.5%)	1 (2.0%)
Orofacial and finger	10 (6.25%)	5 (4.30%)	6 (5.71%)	3 (6.0%)
Fingers	3 (1.87%)	3 (2.5%)	-	1 (2.0%)
Gait imbalance	91 (56.87%)	30 (25.8%)	15 (14.28%)	9 (17.5%)
Dysgeusia	1 (0.62%)	9 (7.75%)	3 (2.85%)	2 (4.0%)
Dysmetria	18 (11.25%)	12 (10.34%)	7 (6.66%)	4 (8.0%)
Headache	5 (3.12%)	-	-	
Others (hypotension/ lightheadedness, somnolence, new onset LE tremor)	4 (2.5%)	-	-	

Due to the proximity of MRgFUS lesion to key adjacent thalamic nuclei and the internal capsule, adverse events following MRgFUS thalamotomy are frequent with the incidence of adverse events ranging from 10 to 60% (18). In our experience, the most commonly encountered adverse events were gait imbalance and sensory deficits which is consistent with earlier studies. Notably, all the adverse events following MRgFUS thalamotomy in our study were mild and classified as Clavien-Dindo Grade I (19). Previous studies like ours have identified several key factors related to the occurrence of complications. Lesion location, volume and extent have all been identified as important factors determining the occurrence of complications (7, 11). In a previously published study, we demonstrated that patients with any adverse event had significantly larger lesion (300 vs. 229mm^3) and had more inferior and lateral lesion margins (11). Extension of the lesion laterally into the internal capsule can lead to contralateral weakness or dysarthria. Posterior extension can lead to sensory deficits in the face or fingers. Inferior extension can lead to imbalance and dysmetria (11, 13). Lesion location and volume are important considerations for both enduring therapeutic benefit and the occurrence of complications. Our lesions were consistently located on our specified target but were significantly larger than previously reported at other centers. Some studies have suggested a particular lesion volume threshold to achieve maximum tremor benefit while avoiding complications (7). A thalamic lesion volume of at least 40 mm^3 is necessary to achieve tremor benefit (20). However, larger lesion volumes have been suggested to achieve better tremor control (21). Notably, larger lesions volumes have also been found to be associated with higher risk of adverse events (7, 11). Other studies have suggested using a tractography based approach to localize the optimal target which can optimize clinical outcomes although these techniques were not used in any of our cases (22). Despite our larger average treatment volume, our complication rates were consistent with all previously reported

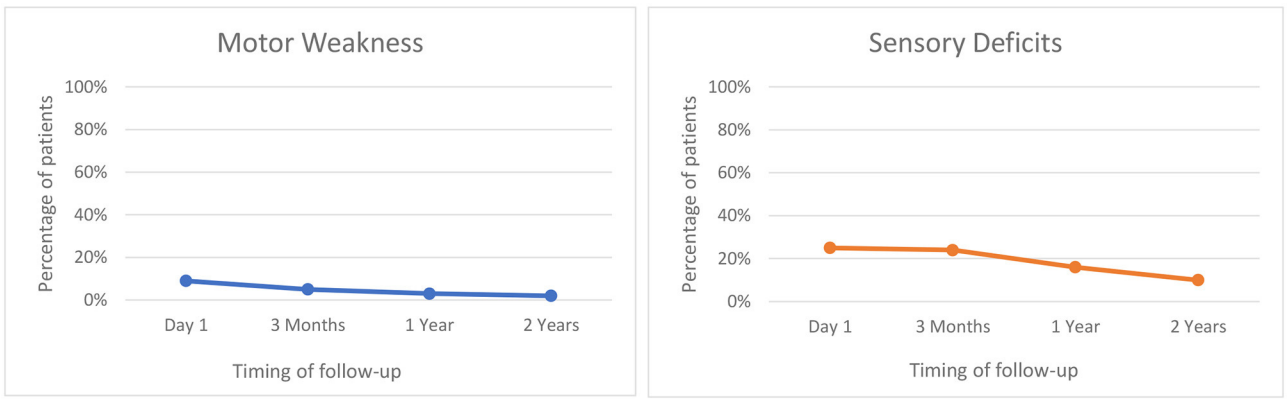

FIGURE 3 | Evolution of adverse events following MRgFUS thalamotomy.

studies. Moreover, every patient was questioned for adverse events in a standardized fashion at each follow-up interview to more accurately reflect the incidence of complications in our series. Nevertheless, future efforts should explore detailed post-operative MRI lesional analysis to help determine the optimal lesion location and volume to maximize long term therapeutic outcomes and minimize complications. Advances in MRI tractography and imaging may optimize targeting of Vim in the future as well.

Limitations

The major limitations of this study are due to its' retrospective nature and the fact that post-operative evaluations were performed by an unblinded observer which could have led to a risk of positive reporting bias. Since the goal of the study was to present a "real-world" clinical experience hence standardized tremor scales were not utilized during routine follow-up evaluations. Moreover, the small number of PD patients in our series limited our ability to perform meaningful tremor outcomes analysis in this subset of patients.

CONCLUSION

MRgFUS thalamotomy is a safe and effective procedure for unilateral tremor symptoms. Adverse events following the procedure are common but generally mild and transient in the majority of cases. Future work should explore the optimal MRgFUS lesion location, volume and extent in order to maximize long term tremor control and minimize complications.

DATA AVAILABILITY STATEMENT

The raw data supporting the conclusions of this article will be made available by the authors, without undue reservation.

ETHICS STATEMENT

The studies involving human participants were reviewed and approved by Brigham and Women's Hospital IRB. Written informed consent for participation was not required for this study in accordance with the national legislation and the institutional requirements.

AUTHOR CONTRIBUTIONS

AL and DS performed the retrospective analysis of clinical material and initial formulation of manuscript under the direction of GC. GC performed all procedures assisted by magnetic resonance physicists, NM and PW. All authors contributed to the writing and editing of the manuscript.

FUNDING

GC has received clinical research support from Insightec.

REFERENCES

1. Elias WJ, Lipsman N, Ondo WG, Ghanouni P, Kim YG, Lee W, et al. A randomized trial of focused ultrasound thalamotomy for essential tremor. *N Engl J Med.* (2016) 375:730–9. doi: 10.1056/NEJMoa1600159
2. Abe K, Horisawa S, Yamaguchi T, Hori H, Yamada K, Kondo K, et al. Focused ultrasound thalamotomy for refractory essential tremor: a Japanese multicenter single-arm study. *Neurosurgery.* (2021) 88:751–7. doi: 10.1093/neuros/nyaa536
3. Park YS, Jung NY, Na YC, Chang JW. Four-year follow-up results of magnetic resonance-guided focused ultrasound thalamotomy for essential tremor. *Movement Disord.* (2019) 34:727–34. doi: 10.1002/mds.27637
4. Sinai A, Nassar M, Eran A, Constantinescu M, Zaaroor M, Sprecher E, et al. Magnetic resonance–guided focused ultrasound thalamotomy for essential tremor: a 5-year single-center experience. *J Neurosurg.* (2019) 133:417–24. doi: 10.3171/2019.3.JNS19466
5. Halpern CH, Santini V, Lipsman N, Lozanao AM, Schwartz ML, Shah BB, et al. Three-year follow-up of prospective trial of focused ultrasound thalamotomy for essential tremor. *Neurology.* (2019) 93:e2284–93. doi: 10.1212/WNL.0000000000008561
6. Fukutome K, Kuga Y, Ohnishi H, Hirabayashi H, Nakase H. What factors impact the clinical outcome of magnetic resonance imaging–guided focused ultrasound thalamotomy for essential tremor? *J Neurosurg.* (2020) 1:1–6. doi: 10.1159/000518662
7. Boutet A, Ranjan M, Zhong J, Germann J, Xu D, Schwartz ML, et al. Focused ultrasound thalamotomy location determines clinical benefits in patients with essential tremor. *Brain.* (2018) 141:3405–14. doi: 10.1093/brain/awy278
8. Chang WS, Jung HH, Zadicario E, Rachmilevitch I, Tlusty T, Vitek S, et al. Factors associated with successful magnetic resonance-guided focused ultrasound treatment: efficiency of acoustic energy delivery through the skull. *J Neurosurg.* (2016) 124:411–6. doi: 10.3171/2015.3.JNS142592
9. Krishna V, Sammartino F, Cosgrove R, Ghanouni P, Schwartz M, Gwinn R, et al. Predictors of outcomes after focused ultrasound thalamotomy. *Neurosurgery.* (2020) 87:229–37. doi: 10.1093/neuros/nyz417
10. Federau C, Goubran M, Rosenberg J, Henderson J, Halpern CH, Santini V, et al. Transcranial MRI-guided high-intensity focused ultrasound for treatment of essential tremor: a pilot study on the correlation between lesion size, lesion location, thermal dose, and clinical outcome. *J Magn Reson Imaging.* (2018) 48:58–65. doi: 10.1002/jmri.25878
11. Segar DJ, Lak AM, Lee S, Hararay M, Chavakula V, Lauro P, et al. Lesion location and lesion creation affect outcomes after focused ultrasound thalamotomy. *Brain.* (2021) 144:3089–100. doi: 10.1093/brain/awab176
12. Fahn S, Tolosa E, Marín C. Clinical rating scale for tremor. In: Jankovic J TJ, editor. *Parkinson's Disease and Movement Disorders.* Vol 2. Baltimore, MD: Williams and Wilkins (1993). p. 271–80.
13. Harary M, Essayed WI, Valdes PA, McDannold N, Cosgrove GR. Volumetric analysis of magnetic resonance–guided focused ultrasound thalamotomy lesions. *Neurosurg Focus.* (2018) 44:E6. doi: 10.3171/2017.11.FOCUS17587
14. Wintermark M, Druzgal J, Huss D, Khaled MA, Monteith S, Raghavan P, et al. Imaging findings in MR imaging–guided focused ultrasound treatment for patients with essential tremor. *Am J Neuroradiol.* (2014) 35:891–6. doi: 10.3174/ajnr.A3808
15. Chang JW, Park CK, Lipsman N, Schwartz ML, Ghanouni P, Henderson JM, et al. A prospective trial of magnetic resonance–guided focused ultrasound thalamotomy for essential tremor: results at the 2-year follow-up. *Ann Neurol.* (2018) 83:107–14. doi: 10.1002/ana.25126
16. D'Souza M, Chen KS, Rosenberg J, Elias WJ, Eisenberg HM, Gwinn R, et al. Impact of skull density ratio on efficacy and safety of magnetic resonance–guided focused ultrasound treatment of essential tremor. *J Neurosurg.* (2019) 132:1392–7. doi: 10.3171/2019.2.JNS183517
17. Boutet A, Gwun D, Gramer R, Ranjan M, Elias GJB, Tilden D, et al. The relevance of skull density ratio in selecting candidates for transcranial MR-guided focused ultrasound. *J Neurosurg.* (2019) 132:1785–91. doi: 10.3171/2019.2.JNS182571

18. Mohammed N, Patra D, Nanda A. A meta-analysis of outcomes and complications of magnetic resonance–guided focused ultrasound in the treatment of essential tremor. *Neurosurg Focus.* (2018) 44:E4. doi: 10.3171/2017.11.FOCUS17628
19. Dindo D. The Clavien–Dindo classification of surgical complications. In: Cuesta MBH, editor. *Treatment of Postoperative Complications After Digestive Surgery.* London: Springer (2014). p. 13–17.
20. Hirai T, Miyazaki M, Nakajima H, Shibazaki T, Ohye C. The correlation between tremor characteristics and the predicted volume of effective lesions in stereotaxic nucleus ventralis intermedius thalamotomy. *Brain.* (1983) 106:1001–18. doi: 10.1093/brain/106.4.1001
21. Young RF, Li F, Vermeulen S, Meier R. Gamma Knife thalamotomy for treatment of essential tremor: long-term results. *J Neurosurg.* (2010) 112:1311–7. doi: 10.3171/2009.10.JNS09332
22. Krishna V, Sammartino F, Agrawal P, Changizi BK, Bourekas E, Knoop MV, et al. Prospective tractography-based targeting for improved safety of focused ultrasound thalamotomy. *Neurosurgery.* (2019) 84:160–8. doi: 10.1093/neuros/nyy020

Conflict of Interest: The authors declare that the research was conducted in the absence of any commercial or financial relationships that could be construed as a potential conflict of interest.

frontiers | Frontiers in Neurology

ORIGINAL RESEARCH
published: 25 April 2022
doi: 10.3389/fneur.2022.791092

Somatotopic Organization of Hyperdirect Pathway Projections From the Primary Motor Cortex in the Human Brain

Sonia Pujol[1]*, *Ryan P. Cabeen*[2], *Jérôme Yelnik*[3,4], *Chantal François*[3,4], *Sara Fernandez Vidal*[3,4], *Carine Karachi*[3,4,5], *Eric Bardinet*[3,4], *G. Rees Cosgrove*[6†] and *Ron Kikinis*[1†]

[1] Surgical Planning Laboratory, Department of Radiology, Brigham and Women's Hospital, Harvard Medical School, Boston, MA, United States, [2] Laboratory of Neuro Imaging, Stevens Institute for Neuroimaging and Informatics, Keck School of Medicine of the USC, University of Southern California, Los Angeles, CA, United States, [3] Sorbonne Université, CNRS, INSERM, APHP GH Pitié-Salpêtriére, Paris Brain Institute - Institut du Cerveau (ICM), Paris, France, [4] CENIR Platform, Institut du Cerveau (ICM), Paris, France, [5] Department of Neurosurgery, APHP, Hôpitaux Universitaires Piti9-Salpêtriére/Charles Foix, Paris, France, [6] Department of Neurosurgery, Brigham and Women's Hospital, Harvard Medical School, Boston, MA, United States

OPEN ACCESS

Edited by:
Vibhor Krishna, The Ohio State University, United States

Reviewed by:
Benito de Celis Alonso, Meritorious Autonomous University of Puebla, Mexico
Francesco Sammartino, The Ohio State University, United States

***Correspondence:**
Sonia Pujol
spujol@bwh.harvard.edu

[†]*These authors share senior authorship*

Specialty section:
This article was submitted to Experimental Therapeutics, a section of the journal Frontiers in Neurology

Received: *07 October 2021*
Accepted: *04 March 2022*
Published: *25 April 2022*

Citation:
Pujol S, Cabeen RP, Yelnik J, François C, Fernandez Vidal S, Karachi C, Bardinet E, Cosgrove GR and Kikinis R (2022) Somatotopic Organization of Hyperdirect Pathway Projections From the Primary Motor Cortex in the Human Brain. Front. Neurol. 13:791092. doi: 10.3389/fneur.2022.791092

Background: The subthalamic nucleus (STN) is an effective neurosurgical target to improve motor symptoms in Parkinson's Disease (PD) patients. MR-guided Focused Ultrasound (MRgFUS) subthalamotomy is being explored as a therapeutic alternative to Deep Brain Stimulation (DBS) of the STN. The hyperdirect pathway provides a direct connection between the cortex and the STN and is likely to play a key role in the therapeutic effects of MRgFUS intervention in PD patients.

Objective: This study aims to investigate the topography and somatotopy of hyperdirect pathway projections from the primary motor cortex (M1).

Methods: We used advanced multi-fiber tractography and high-resolution diffusion MRI data acquired on five subjects of the Human Connectome Project (HCP) to reconstruct hyperdirect pathway projections from M1. Two neuroanatomy experts reviewed the anatomical accuracy of the tracts. We extracted the fascicles arising from the trunk, arm, hand, face and tongue area from the reconstructed pathways. We assessed the variability among subjects based on the fractional anisotropy (FA) and mean diffusivity (MD) of the fibers. We evaluated the spatial arrangement of the different fascicles using the Dice Similarity Coefficient (DSC) of spatial overlap and the centroids of the bundles.

Results: We successfully reconstructed hyperdirect pathway projections from M1 in all five subjects. The tracts were in agreement with the expected anatomy. We identified hyperdirect pathway fascicles projecting from the trunk, arm, hand, face and tongue area in all subjects. Tract-derived measurements showed low variability among subjects, and similar distributions of FA and MD values among the fascicles projecting from different M1 areas. We found an anterolateral somatotopic arrangement of the fascicles in the corona radiata, and an average overlap of 0.63 in the internal capsule and 0.65 in the zona incerta.

Conclusion: Multi-fiber tractography combined with high-resolution diffusion MRI data enables the identification of the somatotopic organization of the hyperdirect pathway. Our preliminary results suggest that the subdivisions of the hyperdirect pathway projecting from the trunk, arm, hand, face, and tongue motor area are intermixed at the level of the zona incerta and posterior limb of the internal capsule, with a predominantly overlapping topographical organization in both regions. Subject-specific knowledge of the hyperdirect pathway somatotopy could help optimize target definition in MRgFUS intervention.

Keywords: somatotopy, diffusion MRI, tractography, stereotactic surgery, neuroanatomy

INTRODUCTION

The hyperdirect cortico-subthalamic pathway is a set of white matter fibers sending direct inputs from the cortex to the subthalamic nucleus (STN) (1, 2). Hyperdirect pathway projections are sought to play a key role in the clinical outcomes of Deep Brain Stimulation (DBS) of the STN in Parkinson's disease (PD) patients (3–5). Several studies have demonstrated that direct stimulation of hyperdirect pathway fibers is involved in DBS therapeutic effects (4, 6–10). In particular, hyperdirect pathway projections from motor and premotor cortical areas are sought to be a major neural substrate modulated by STN DBS in addition to the STN itself (11). Recently, Magnetic Resonance guided Focused Ultrasound (MRgFUS) subthalamotomy has shown potential for improving motor symptoms and dyskinesias in PD patients (12–14). In that context, patient-specific knowledge of the topography of hyperdirect pathway fibers could help optimize target definition during planning of DBS and MRgFUS intervention. The anatomy of the hyperdirect pathway has been investigated in non-human primates (2, 15, 16). Animal experiments using anterograde tracers in monkeys have shown that the STN receives somatotopically organized projections from the primary motor cortex, and that these projections are arranged from medial to lateral in the order of hindlimb, forelimb and orofacial part (2, 3, 16). In rats, retrograde and anterograde tracing studies indicate that a subset of projections from the motor cortex innervate the STN and the striatum (17–19). In addition, anterograde tracing studies have shown that projections from the motor cortex are topographically organized with the rostral part of the lateral motor cortex projecting to the lateral portion of the rostral two-thirds of STN and the caudal part projecting to the ventral aspect of the middle third of STN (20).

Still, such neural tract-tracing techniques cannot be used to study brain connectivity on human subjects. User-defined holographic reconstructions of hyperdirect pathway fibers from structural MRI scans and histological data have been proposed to provide novel anatomical priors for human connectomic analysis (21). However, the reconstructed hyperdirect pathway fibers were defined based on scientific studies generated in the macaque brain, thus the approach presents the same limitations as other studies mapping results of non-human primates into human subjects (22). Diffusion MRI tractography enables the non-invasive exploration of white matter fibers at the individual patient scale. Recent advances in neuroimaging techniques have enabled identification of the trajectory of the hyperdirect pathway *in vivo* in individual subjects using single tensor deterministic tractography (10, 23–28), single tensor probabilistic tractography (29), multi-fiber probabilistic tractography (8, 10, 26, 27, 30–37) and generalized q-sampling imaging (38). Still, the internal organization of the hyperdirect pathway in the human brain remains unexplored. In this study, we seek to reconstruct hyperdirect pathways fibers projecting from the primary motor cortex using multi-fiber deterministic tractography and to investigate the internal organization of hyperdirect fascicles projecting from the trunk, arm, hand, face, and tongue area. We used MRI datasets from the Human Connectome Project as they offer the highest quality diffusion MRI data currently available to investigate brain connectivity. To the best of our knowledge, this is the first study of the somatotopy of the hyperdirect pathway in the human brain.

MATERIALS AND METHODS

MRI Data Acquisition

We used high-resolution structural and diffusion MRI data from five healthy subjects (100307, 100408, 101915, 103414, 106016) of the Washington University, University of Minnesota, and Oxford University Human Connectome Project (WU- Minn HCP) consortium (39). The WU-Minn HCP scans were acquired on young healthy subjects (age 21–35) and represent the best neuroimaging data available for investigating the topography of the white matter in the human brain. The subjects were scanned on a customized Siemens 3.0 Tesla Skyra scanner using a 32-channel head coil and a customized gradient. The structural MRI data included T1-weighted and T2-weighted volumes acquired with the following parameters: T1-weighted: TE = 2.14 ms, TR = 2,400 ms, voxel size = 0.7 mm; T2-weighted: TE = 565 ms, TR = 3,200 ms, voxel size = 0.7 mm. The diffusion-weighted images were acquired using a single-shot 2D spin-echo multiband Echo Planar Imaging sequence with 90 gradient directions, 3 b-values (b1 = 1,000 s/mm^2, b2 = 2,000 s/mm^2, b3 = 3,000 s/mm^2), 1.25 mm slice thickness and 1.25 mm image resolution (40, 41). The diffusion-weighted images used in this study had been processed for intensity normalization, eddy-current, patient-motion and EPI distortion correction and co-registered to the anatomical scans (42–44).

MRI Data Analysis Workflow

Our data analysis workflow consisted of three steps: first, the segmentation of anatomical regions of interest, second the tractography reconstruction of hyperdirect pathway fibers, and third the analysis of the somatotopic organization of the hyperdirect pathway.

Segmentation of the Regions of Interest

We defined three sets of anatomical regions of interest (ROIs) in the primary motor cortex (M1), internal capsule (IC) and subthalamic nucleus (STN) using the 3D Slicer open-source platform for medical research (45). In the first set of ROIs, we outlined the precentral gyrus in a volume-rendered image of the T1-weighted scan. In the second set of ROIs, we generated a fractional anisotropy (FA) map and a diffusion-encoded color (DEC) map from the diffusion-weighted images using the SlicerDMRI extension of 3D Slicer (46, 47). We manually segmented the posterior limb of the IC in axial cross-sections of the FA map overlaid on the DEC map using the Segment Editor module of 3D Slicer. In the third set of ROIs, as the contours of the STN were not directly visible in the T1-weighted images, we used the automated atlas-based segmentation approach of the pyDBS software implemented in 3D Slicer (48). The method uses a 3D histological and deformable atlas of the basal ganglia that comprises 3D meshes of 80 structures identified on histological stainings from a post-mortem specimen (49). We deformed the Yeb atlas using a global-to-local registration approach to generate 3D meshes of the STN from the T1-weighted images (50). The meshes were subsequently voxelized in 3D Slicer to create isotropic ROIs with 0.3 mm voxel size.

Tractography Reconstruction

We applied a combination of diffusion MRI analysis tools that arose from the specific experience of our team. We used a multi-fiber ball-and-stick modeling to estimate the orientation of white matter fibers at each voxel from the diffusion-weighted MRI data. The ball-and-stick model is a multi-compartment approach constrained to include an isotropic "ball" compartment and multiple anisotropic "sticks" compartments (51). The model was fitted to the diffusion-weighted MRI data using a Bayesian estimation procedure to robustly estimate fiber orientations and volume fractions, as well as their total count (52). Parameter settings included the continuous exponential approach for multi-shell data and a maximum of three fiber compartments per voxel.

To reconstruct the hyperdirect pathway fibers using the ROIs described above, we used a multi-fiber streamline tractography algorithm with a model-based interpolation framework (53, 54) from the Quantitative Imaging Toolkit (QIT) (55). The ball-and-stick models were interpolated during bundle tracking using a data-adaptative kernel regression framework with a spatial bandwidth of 1.0 mm, model selection parameter $\lambda = 0.9999$, and up to three fiber compartments (54). Fiber tracking was performed using a step size of 0.5 mm, and 25 seeds per voxel in a one-voxel neighborhood surrounding the M1 and STN ROIs. Hyperdirect pathway fibers were retained only if they intersected the M1, IC and STN ROIs. Tracts were terminated upon reaching the STN or M1 ROIs, when the angle changed more than 55 degrees, or when a compartment's volume fraction dropped below 0.05. We stopped the fibers at the STN surface as the image resolution was not sufficient to follow the tracts inside the nucleus. Thus, by design this aspect of the hyperdirect pathway termination is not covered in this study.

Evaluation by Neuroanatomy Experts

Two expert neuroanatomists (J.Y. and C.F.) with over 30 years of experience performed qualitative evaluation of the anatomical accuracy of the hyperdirect pathway. For each subject, the tractography reconstructions were loaded in 3D Slicer along with the structural MRI scans, diffusion-weighted MRI scans, and 3D models of the subthalamic nucleus. The anatomical accuracy of the tracts was evaluated based on the similarity between the tractography reconstructions and known neuroanatomy using three criteria: the topographical localization of each tract; the start and end region of the fascicles, and the specific shape of the bundles. The experts assigned a score ranging from 5 (excellent) to 1 (poor) averaged on the criteria used for the review of each tract.

Somatotopic Organization

To investigate the internal organization of the reconstructed pathways, we defined five primary motor cortex ROIs in a 3D volume-rendered image of the T1-weighted scan. The ROIs were placed in the trunk, arm, hand, face, and tongue motor homunculus in the precentral gyrus of each hemisphere using the Markups module of 3D Slicer. First, we identified the "hand-knob" sign in the precentral gyrus to place the hand motor ROI (56). Second, we positioned the arm ROI medial to the hand ROI. Third, the trunk ROI was placed medial to the arm ROI and close to the midline of the brain. Fourth, we placed the face ROI lateral to the hand ROI in the lower portion of the precentral gyrus in the section of the top of the lateral ventricles (57). Fifth, the tongue ROI was positioned in the most lateral portion of the precentral gyrus in the section just above the Sylvian fissure (57). We used the SlicerDMRI extension of 3D Slicer to extract the fascicles arising from the trunk, arm, hand, face, and tongue ROIs from the reconstructed hyperdirect pathway.

Tract-Derived Measurements

To assess the variability among subjects, we calculated the fractional anisotropy (FA) and mean diffusivity (MD) of the envelope of the trunk, arm, hand, face and tongue hyperdirect pathway fascicles. We computed the envelope of the fascicles by converting the streamlines into voxel wise binary label maps with label = 1 when a tract was detected in a voxel and label = 0 when no tract was detected. The envelope, FA volume, and MD volume for each fascicle were calculated using the SlicerDMRI extension of 3D Slicer. In addition, to investigate the segregation of hyperdirect pathway fascicles, we segmented the contour of each fascicle in two axial slices at the level of the internal capsule and zona incerta superior to the subthalamic nucleus, and we computed the centroid of each contour.

Quantitative Analysis

We performed a statistical analysis of the scores given by the neuroanatomy experts and the tract-derived measurements. We evaluated the degree of agreement between the experts using the intraclass correlation coefficient (ICC) and we computed the internal consistency of the scores using Cronbach's alpha reliability analysis (58). To evaluate the variability among subjects, we computed the average, maximum and standard deviation of FA and MD values for the fascicles associated with the trunk, arm, hand, face, and tongue M1 areas. Finally, to investigate the segregation of hyperdirect pathway fibers, we computed the Dice Similarity Coefficient (DSC) of overlap between the contours of the trunk, arm, hand, face, and tongue fascicles segmented in the axial slices at the level of the internal capsule and zona incerta. We compared the relative anterior-posterior orientation of the centroids of the contours to assess the spatial arrangement of the fascicles.

RESULTS

We successfully reconstructed hyperdirect cortico-subthalamic fibers connecting the primary motor cortex to the ipsilateral STN in all five subjects. The hyperdirect pathway fibers presented a fan shape configuration with fibers arising from the whole extend of the precentral gyrus, converging into the corona radiata, descending through the posterior limb of the internal capsule, and terminating in a compact stem entering the subthalamic nucleus. **Figure 1** shows the 3D tractography reconstruction in a single subject. The use of an advanced fiber models enables the partial identification of complex fibers crossings of the hyperdirect pathway with the superior longitudinal fasciculus (**Figure 1C**).

The evaluation of the hyperdirect pathway fibers by two neuroanatomical experts demonstrated that the tractography reconstructions were in agreement with the expected anatomy with an average score of 3.7 ± 0.92. The ICC score was 0.44 and the Cronbach's alpha score was 0.91 with 95% confidence interval of [0.67, 0.98] which showed a good level of agreement between the experts.

We identified fascicles projecting from trunk, arm, hand, face, and tongue M1 area in all subjects. **Figure 2** shows the somatotopic organization of hyperdirect pathway fibers in a single subject. The spatial arrangement of hyperdirect pathway fascicles was anterolateral in the corona radiata and predominantly overlapping at the level of the internal capsule and zona incerta. Tract-derived measurements showed low variability among subjects, and similar distributions of FA and MD values among the tracts projecting from the different motor regions (**Figure 3**).

Table 1 summarizes the Dice Similarity Coefficient (DSC) of spatial of overlap values between the trunk, arm, hand, face and tongue fascicles in the internal capsule and zona incerta. Overall, the tracts in the internal capsule showed an average overlap of 0.63 with a maximum average overlap of 0.83 for the fascicles projecting from the arm and hand area, and a minimum average overlap of 0.47 for the fascicles projecting from the trunk and tongue area. In the zona incerta, the tracts showed an average overlap of 0.65 with a maximum average overlap of 0.81 for the fascicles projecting from the arm and hand area, and a minimum average overlap of 0.50 for the fascicles projecting from the hand and tongue area. The analysis of the position of the centroid of the tracts in the internal capsule showed that the most anterior position was occupied by tracts projecting from the tongue (30%) and face (30%) area, while the most posterior position was occupied by tracts projecting from trunk (70%) and tongue (20%) area. In the zona incerta, the most anterior position was occupied by tracts projecting from the hand (40%) and face (40%) area; the most posterior position was occupied by tracts projecting from the tongue (50%) and trunk (30%) area.

DISCUSSION

Our exploratory study investigated the somatotopic organization of hyperdirect pathway projections from the primary motor cortex to the subthalamic nucleus (STN) on healthy subjects of the Human Connectome Project. We have shown that multi-fiber tractography and high-resolution multi-shell diffusion-weighted MRI data enable the identification of white matter fascicles connecting the trunk, arm, face, hand, and tongue primary motor cortex area to the subthalamic nucleus. We demonstrated that the use of an advanced fiber model enables the identification of lateral projections of the hyperdirect pathway from the face and tongue motor area, as well as some complex fibers crossings with the superior longitudinal fasciculus. The evaluation of the anatomical accuracy by neuroanatomy experts demonstrated that the topography of the reconstructed tracts was in agreement with known neuroanatomy. The analysis of tract-derived measurements demonstrated a low level of variability among subjects. We found an anterolateral somatotopic arrangement in the most superior section of the hyperdirect pathway. In the internal capsule, hyperdirect pathway fibers projecting from different motor areas showed an average overlap of 0.63, with the most anterior position occupied by tongue and face fibers and the most posterior position occupied by trunk and tongue tracts. In the zona incerta, the average overlap was 0.65 with the most anterior position occupied by hand and face fibers and the most posterior position occupied by tongue and trunk fibers. Our preliminary tractography results suggest that the subdivisions of the hyperdirect pathway are intermingled in the zona incerta and posterior limb of the internal capsule, with a predominantly overlapping topographical organization in both regions. Tract-tracing experiments in monkeys have previously reported anatomical overlap of projections from the frontal cortex in subcortical structures: Selemon et al. observed topographical overlap and interdigitation of corticostriatal projections in the ventromedial striatum (59); in the pedunculopontine nucleus, Matsumara et al. have shown that the somatotopic representations of projections from motor-related areas are intermingled rather than segregated (60).

Our tractography findings in the hyperdirect pathway are consistent with observations from two previous experimental studies on the structure and function of the STN in the human

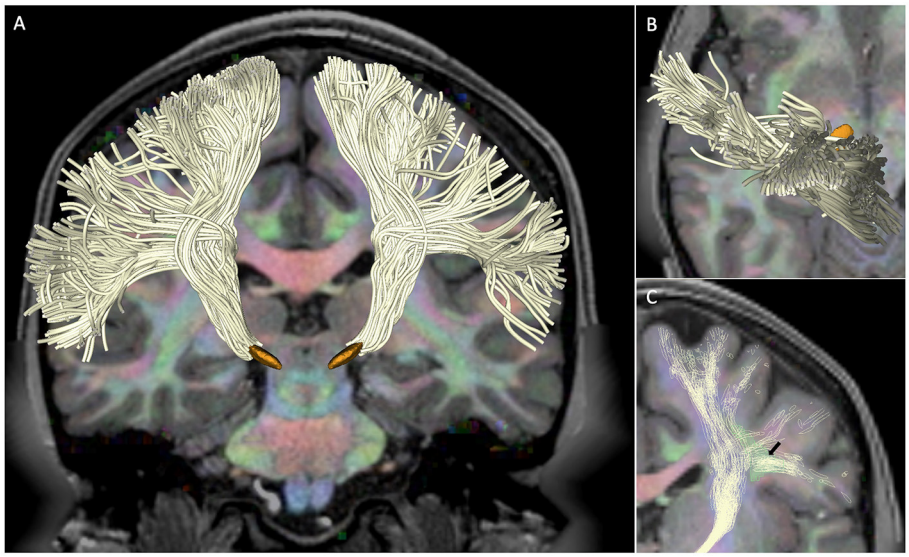

FIGURE 1 | Hyperdirect pathway in subject 100307. The figure shows the tractography reconstruction of hyperdirect pathway fibers projecting from the primary motor cortex to the subthalamic nucleus. The tracts (white) are displayed on a diffusion encoded color map overlaid on a T1-weighted image with 3D models of the subthalamic nucleus (orange) for anatomical reference. **(A)** Anterior 3D view of the hyperdirect pathway. **(B)** Superior 3D view of hyperdirect pathway fibers descending from the primary motor cortex. **(C)** Anterior 3D view of the crossings of hyperdirect pathway fibers with the superior longitudinal fasciculus. The arrow points at the intersection of lateral projections of the hyperdirect pathway with a cross-section of the superior longitudinal fasciculus (green).

brain. In 2002, an anatomical study using calbindin labeling demonstrated that the subdivisions of the STN are separated by functional gradients, not by sharp boundaries (61). In 2007, a DBS study on PD patients suggested that the STN serves as a nexus for the integration of motor, cognitive and emotional components of behavior and that these functional modalities are not processed in a segregated manner (62). These two studies on the lack of anatomical and functional segregation of components of the STN are in agreement with our observations on the overlap of hyperdirect pathway fibers projecting from different cortical regions. Furthermore, a cytoarchitectural study of STN neurons in the human brain has shown that the dendrites of STN neurons extend up to 1,200 μm to neighboring territories, which suggests a convergence of inputs from different cortical areas on individual neurons of the nucleus (63). This convergence has been used in the model of focused selection and inhibition of competing motor programs by the basal ganglia (64). In this model, when voluntary movement is generated, the motor cortex uses the hyperdirect pathway to send a short-latency signal to the whole STN, which causes a fast and widespread excitation of the globus pallidus pars interna (GPi) and substantia nigra pars reticulata (SNpr) resulting in an inhibition of competing motor mechanisms that would interfere with the desired movement (64). Simultaneously, the motor cortex creates a focused excitation of the striatum through the direct pathway, which causes a focused inhibition of specific GPi and SNpr neurons, followed by a focused excitation of neurons in the thalamus and cortex allowing the desired movement to proceed (64). The convergence of inputs from different cortical areas suggests that the STN might not be topographically organized to preserve the somatotopy of the motor cortex (62), which is in agreement with our findings on the topography of corticosubthalamic fibers.

To the best of our knowledge, this is the first study of the somatotopy of the hyperdirect pathway in the human brain. Tractography studies have investigated the somatotopy of the pyramidal pathway using single-tensor deterministic tractography (65–69), single-tensor probabilistic tractography (70–73), and two-tensor probabilistic tractography (74). These studies have reported a segregation of corticospinal tract fibers (65–74) and an overlap of corticobulbar tract fibers (74). While the pyramidal tract is adjacent to the hyperdirect pathway, the two white matter bundles are anatomically different. Pyramidal projections from the primary motor cortex are composed of corticospinal projections to the spine and corticobulbar projections to motor nuclei of cranial nerves, whereas hyperdirect pathway projections from the primary motor cortex terminate in the subthalamic nucleus. In addition, the hyperdirect pathway and the pyramidal pathway have opposite roles in DBS outcomes: direct stimulation of the hyperdirect pathway is involved in DBS therapeutic effects (4, 6–10), whereas the spread of current to the pyramidal tract can trigger pyramidal tract side effect (75). These anatomical and functional differences are a potential explanation of the differences between the somatotopy we observed in our study and the somatotopies reported in pyramidal tract studies.

The somatotopic organization of the STN has been described in healthy monkeys using invasive neural tracing techniques. These studies have shown that the primary motor cortex projects to the whole extend of the STN (1, 16), and neural

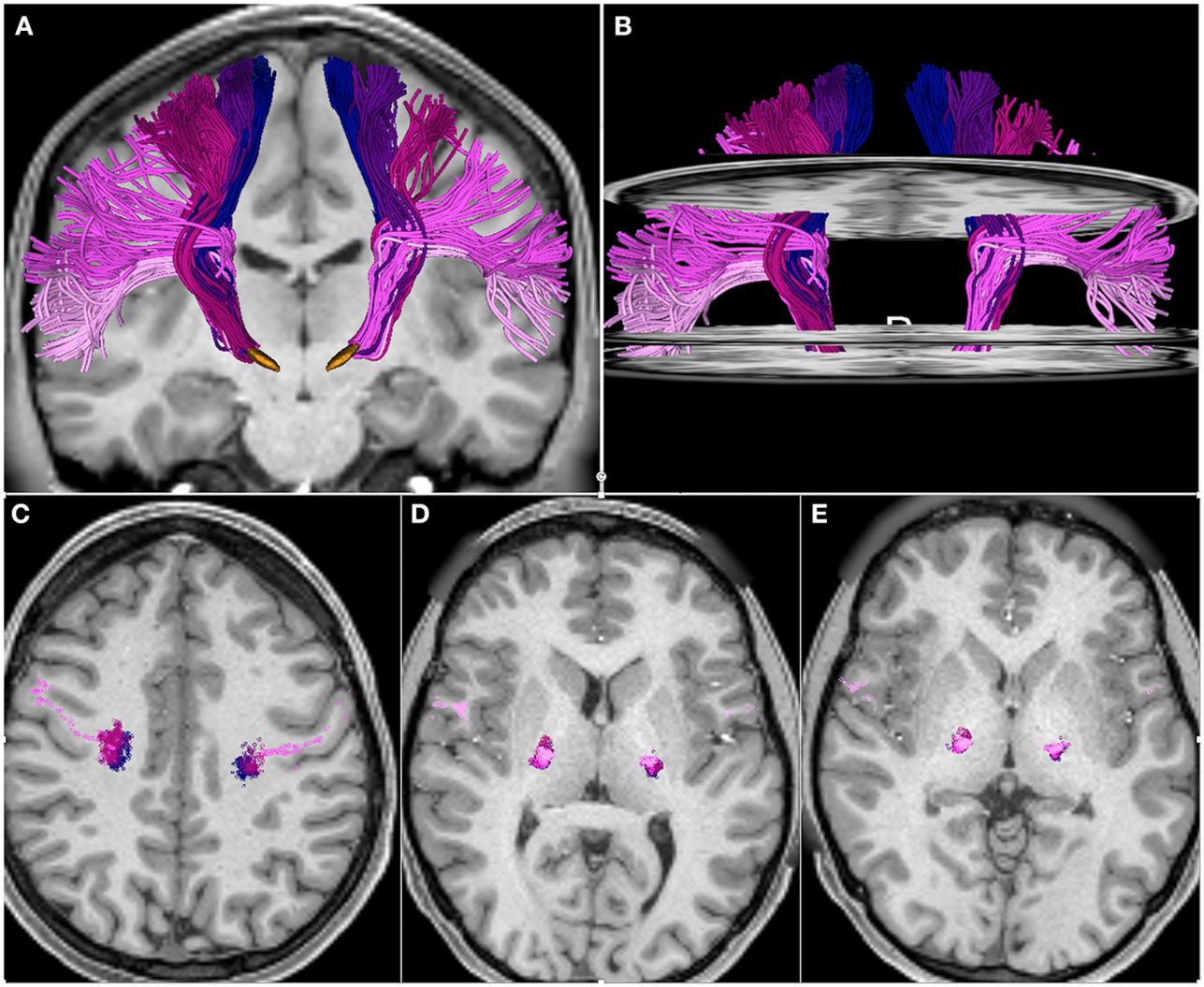

FIGURE 2 | Somatotopic organization of hyperdirect pathway fibers projecting from the primary motor cortex trunk, arm, hand, face, and tongue area. The tracts are displayed on axial and coronal T1-weighted images. **(A)** 3D anterior view of hyperdirect pathway fibers with 3D models of the subthalamic nucleus (orange). **(B)** 3D anterior view of hyperdirect pathway fibers with axial T1-weighted images at the level of the coronal radiata, internal capsule and zona incerta. **(C–E)** Intersection of hyperdirect pathway fibers with an axial T1-weighted image at the level of the corona radiata **(C)**, posterior limb of the internal capsule **(D)**, and zona incerta **(E)**. The three axial slices in **(B)** correspond to the axial images displayed in **(C–E)**. The fibers are colored according to the motor regions: trunk (blue), arm (dark purple), hand (dark pink), face (light purple), tongue (light pink).

tracers have revealed a somatotopic arrangement with lower-limb cells located medially to upper-limb cells, and the face area located in the most lateral zone of the nucleus (1, 76, 77). Several groups have investigated the somatotopic organization of the STN in Parkinson's disease patients using microelectrode recordings (MERs) to identify movement related cells (MRCs) during DBS surgery (78–82). In these studies, most MRCs were detected in the dorsolateral portion of the STN. Rodriguez-Oroz et al. identified a somatotopic distribution similar to the distribution in healthy monkeys, with cells associated in the lower limb located in the upper dorsal third and centromedian portion, and cells associated with the upper limb located in the dorsal two-thirds and lateral region of the STN (78). Abosch et al. found movement-related neurons located throughout the STN, including the ventral portion of the nucleus despite a rostrodorsal clustering of the cells, and reported an absence of clear somatotopic relationship of limb representation (79). Theodosopoulos et al. reported arm-related cells located laterally and at the rostral and caudal poles of the STN, and leg-related cells located medially and centrally (80). Romanelli et al. found that lower extremity–related cells were located medial and ventral to upper extremity–related cells (81). Sasaki et al. showed that cells responding to the upper limbs were more commonly observed in the lateral, anterior, and superior regions of the STN, and that cells associated with the distal joints were located above those associated with

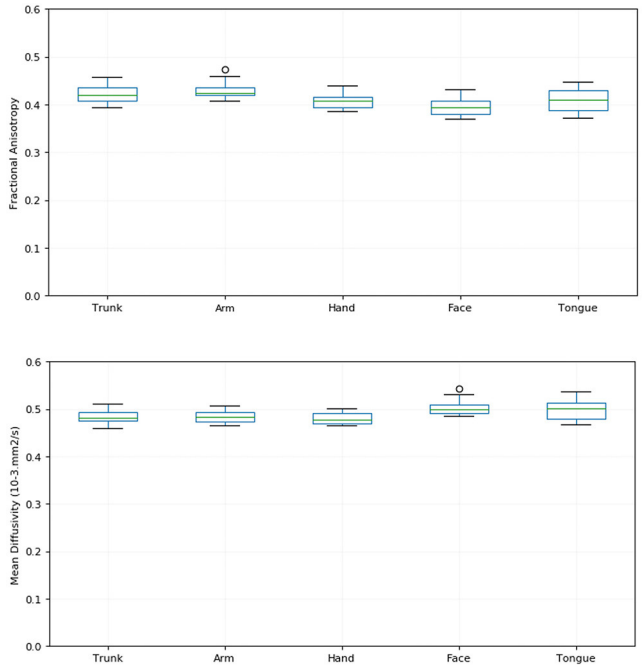

FIGURE 3 | Tract-derived measurements across subjects. The figure shows box plots of the fractional anisotropy (FA) **(top)** and mean diffusivity (MD) **(bottom)** of hyperdirect pathway fascicles projecting from the trunk, arm, hand, face, and tongue motor area for all subjects. The lines in each box correspond to the median (green), interquartile range (blue), minimum and maximum (black) values of the tract-derived measurements.

TABLE 1 | Dice Similarity Coefficient of overlap of hyperdirect pathway fascicles in the internal capsule and zona incerta.

DSC		Tr-A	Tr-H	Tr-F	Tr-To	A-H	A-F	A-To	H-F	H-To	F-To
IC	Mean	0.8	0.74	0.63	0.47	0.83	0.7	0.49	0.68	0.48	0.49
	Std	0.07	0.03	0.09	0.21	0.08	0.13	0.18	0.14	0.12	0.18
ZI	Mean	0.76	0.71	0.67	0.54	0.81	0.73	0.53	0.68	0.50	0.57
	Std	0.09	0.09	0.13	0.21	0.09	0.14	0.20	0.10	0.21	0.20

*The table shows the mean and standard deviation (std) of the Dice Similarity Coefficient (DSC) of spatial overlap of the fascicles projecting from the trunk (Tr), arm (A), hand (H), face (F), and tongue (To) motor area displayed in **Figure 2**. Results show that the fascicles predominantly overlap with a minimum DSC average of 0.47 in the internal capsule (IC) and 0.50 in the zona incerta (ZI).*

the proximal joints, in both upper and lower limbs (82). While somatotopic findings in Parkinson's disease patients may not be generalized to healthy subjects, these electrophysiology results in the STN contrast with our tractography findings. Although we did not investigate the somatotopy of the fibers inside the STN due to the presence of multiple fiber crossings that pose technical limitations to tractography algorithms, our results in the zona incerta immediately superior to the STN show a predominant overlap of hyperdirect fascicles projecting from different motor regions without any clear segregation of the fibers. These discrepancies between MERs findings and tractography results might arise from the difference in scale between the two techniques: the 10 μm diameter of the tip of a microelectrode enables single neuronal response recordings whereas the 1.25 mm voxel size of a diffusion-weighted MRI dataset contains over 100,000 axons. In addition, hyperdirect pathway fibers projecting from large regions of the primary motor cortex homunculus are compacted into a relatively small space at the level of the internal capsule and zona incerta. The use of smaller voxel size may help further establish whether homunculus organization observed in the primary motor cortex is maintained as hyperdirect pathway fibers descend to subcortical areas, as suggested by electrophysiology studies of the STN, or whether intermingling of fibers occurs.

Our study presents several limitations. First, we used a small number of subjects as our goal was to explore the feasibility of identifying the somatotopic organization of the hyperdirect pathway using multi-fiber tractography and the highest quality neuroimaging data available. We showed that white matter bundles projecting from the trunk, arm, hand, face and tongue motor areas could be consistently identified in all subjects. Future work using a larger cohort will enable us to investigate the anatomical variability of hyperdirect pathway projections from the primary motor cortex. Second, we used voxelized tracts to evaluate the variability of tract-derived measurements across subjects. Converting streamlines into a voxel grid can introduce small inaccuracies due to partial volume effects. Third, while we used an advanced multi-fiber model and high-resolution diffusion-weighed data, our tractography results include false-negative tracts in the hand and face fascicles as seen in **Figure 2A**. These false-negative tracts are likely due to complex fiber crossings with the dorsal superior longitudinal fasciculus which interconnects the frontal and parietal lobe (83). While our multi-fiber model enabled the resolution of some of the crossings of hyperdirect fibers with the superior longitudinal fasciculus, the large extent of the pathway still poses technical challenges to fiber tracking. We conducted our analysis using HCP diffusion MRI data which are the best neuroimaging data currently available to study the connectivity of the human brain. The 1.25 mm-voxels of the diffusion-weighted images nevertheless contain a large number of axons belonging to different white matter bundles. Future work with a higher number of compartments will enable us to refine the tractography reconstruction of complex fiber crossings of the hyperdirect pathway with the superior longitudinal fasciculus. Further developments also include the exploration of other advanced tractography methods such as multi-fiber unscented Kalman Filter tractography (47). Finally, a comparison of histological data with our tractography findings would help investigate the topography of hyperdirect pathway fibers in the internal capsule and in the zona incerta.

Diffusion MRI tractography provides a non-invasive window on the architecture of the human brain white matter. While tractography reconstructions enable 3D visualization of the location and trajectory of white matter pathways, the technique still presents limitations for neurosurgical decision-making (84). As mathematical models of diffusion and fiber tracking algorithms are continuously refined by the medical image computing research community, diffusion MRI tractography

has the potential to become part of the apparatus of brain mapping tools to help understand the clinical effects of electrical stimulation and focused ultrasound lesioning in motor disorders patients. Tractography reconstructions of the pyramidal tract, medial lemniscus and dentatorubrothalamic tract have provided innovative tractography-based approaches for targeting the ventral intermediate nucleus during MRgFUS intervention in Essential Tremor patients (85–89). Recent studies using tractography reconstructions of the hyperdirect pathway on motor disorder patients have revealed the potential of the technique to assist with Deep Brain Stimulation intervention in Parkinson's Disease patients (8, 25–28, 34, 35, 37, 38). The HCP diffusion MRI scans represent the state-of-the-art data for characterizing structural human brain connectivity. As transcranial focused ultrasound subthalamotomy is being investigated for unilateral treatment of motor symptoms and dyskinesias in Parkinson's Disease patients (12–14), our study aimed at investigating tractography reconstructions of the hyperdirect pathway that could become available to assist with target definition during MRgFUS intervention in the near future.

CONCLUSION

Our study shows that advanced multi-fiber tractography techniques combined with high-resolution diffusion MRI data enable 3D reconstruction of the whole extent of hyperdirect projections from the primary motor cortex to the STN and the identification of cortico-subthalamic fascicles arising from the trunk, arm, hand, face, and tongue area. Our preliminary tractography results suggest that the subdivisions of the hyperdirect pathway are intermingled in the zona incerta and posterior limb of the internal capsule, with a predominantly overlapping topographical organization in both regions. Diffusion MRI tractography is a clinical research tool that holds promise for identifying the location and trajectory of white matter pathways during stereotactic surgery. Knowledge of the somatotopic organization of the hyperdirect pathway at the individual patient scale could provide clinically relevant information for planning stereotactic surgery of the STN, and contribute to advancing the understanding of the therapeutic mechanisms of action of MRgFUS and DBS. White matter maps of the hyperdirect pathway in healthy subjects could help evaluate potential alterations of the somatotopy of different body parts in Parkinson's disease patients, and thus expand our understanding of the pathophysiology of the disease.

DATA AVAILABILITY STATEMENT

The raw data supporting the conclusions of this article will be made available by the authors, without undue reservation.

ETHICS STATEMENT

The study used publicly available data from the Human Connectome Project. Ethical review and approval was not required for the study on human participants in accordance with the local legislation and institutional requirements. Written informed consent for participation was not required for this study in accordance with the national legislation and the institutional requirements.

AUTHOR CONTRIBUTIONS

SP, RC, JY, CF, EB, GC, and RK: substantial contributions to the conception or design of the work. SP, RC, SFV, EB, and RK: substantial contributions to the data analysis. SP, JY, CF, GC, CK, and RK: substantial contributions to the interpretation of data with anatomical expertise. SP, RC, GC, and RK: substantial contributions to drafting the work. SP, RC, JY, EB, CF, CK, GC, and RK: substantial contributions to revising the work. All authors agreement to be accountable for all aspects of the work in ensuring that questions related to the accuracy or integrity of any part of the work are appropriately investigated and resolved.

FUNDING

This work was partially funded by the Neuroimage Analysis Center (NIH P41EB015902 to SP and RK) and the National Center for Image-Guided Therapy (NIH P41EB015898 to RK). SP was supported in part by grant number 2021-237549(5022) from the Chan Zuckerberg Initiative DAF, an advised fund of Silicon Valley Community Foundation. SP and RK were supported in part by the Lymph Node Quantification System for Multisite Clinical Trials (NIH R01CA235589). RC was supported in part by grant number 2020-225670 from the Chan Zuckerberg Initiative DAF, an advised fund of Silicon Valley Community Foundation.

REFERENCES

1. Nambu A, Takada M, Inase M, Tokuno H. Dual somatotopical representations in the primate subthalamic nucleus: evidence for ordered but reversed body-map transformations from the primary motor cortex and the supplementary motor area. *J Neurosci.* (1996) 16:2671–83. doi: 10.1523/JNEUROSCI.16-08-02671.1996
2. Nambu A, Tokuno H, Takada M. Functional significance of the cortico-subthalamo-pallidal 'hyperdirect' pathway. *Neurosci Res.* (2002) 43:111–7. doi: 10.1016/S0168-0102(02)00027-5
3. Fasano A, Lozano AM. Deep brain stimulation for movement disorders: 2015 and beyond. *Curr Opin Neurol.* (2015) 28:423–36. doi: 10.1097/WCO.0000000000000226
4. Miocinovc S, de Hemptinne C, Chen W, Isbaine F, Willie JT, Ostrem JL, et al. Cortical potentials evoked by subthalamic stimulation demonstrate a short latency hyperdirect pathway in humans. *J Neurosci.* (2018) 38:9129–41. doi: 10.1523/JNEUROSCI.1327-18.2018
5. Lozano AM, Lipsman N, Bergman H, Brown P, Chabardes S, Chang JW, et al. Deep brain stimulation: current challenges and future directions. *Nat Rev Neurol.* (2019) 15:148–60. doi: 10.1038/s41582-018-0128-2
6. Walker HC, Huang H, Gonzalez CL, Bryant JE, Killen J, Cutter GR, et al. Short latency activation of cortex during clinically effective subthalamic deep brain stimulation for Parkinson's disease. *Mov Disord.* (2012) 27:864–73. doi: 10.1002/mds.25025
7. Li S, Arbuthnott GW, Jutras MJ, Goldberg JA, Jaeger D. Resonant antidromic cortical circuit activation as a consequence of high-frequency

subthalamic deep-brain stimulation. *J Neurophysiol.* (2007) 98:3525–7. doi: 10.1152/jn.00808.2007
8. Gunalan K, Chaturvedi A, Howell B, Duchin Y, Lempka SF, Patriat R, et al. Creating and parameterizing patient-specific deep brain stimulation pathway-activation models using the hyperdirect pathway as an example. *PloS ONE.* (2017) 12:e0176132. doi: 10.1371/journal.pone.0176132
9. Anderson RW, Farokhniaee A, Gunalan K, Howell B, McIntyre CC. Action potential initiation, propagation, and cortical invasion in the hyperdirect pathway during subthalamic deep brain stimulation. *Brain Stimul.* (2018) 11:1140–50. doi: 10.1016/j.brs.2018.05.008
10. Howell B, Gunalan K, McIntyre CC. A driving-force predictor for estimating pathway activation in patient-specific models of deep brain stimulation. *Neuromodulation.* (2019) 22:403–15. doi: 10.1111/ner.12929
11. Hamani C, Florence G, Heinsen H, Plantinga BR, Temel Y, Uludag K, et al. Subthalamic nucleus deep brain stimulation: basic concepts and novel perspectives. *eNeuro.* (2017) 4. doi: 10.1523/ENEURO.0140-17.2017
12. Martínez-Fernández R, Rodríguez-Rojas R, Del Álamo M, Hernández-Fernández F, Pineda-Pardo JA, Dileone M, et al. Focused ultrasound subthalamotomy in patients with asymmetric Parkinson's disease: a pilot study. *Lancet Neurol.* (2018) 17:54–63. doi: 10.1016/S1474-4422(17)30403-9
13. Moosa S, Martínez-Fernández R, Elias WJ, Del Alamo M, Eisenberg HM, Fishman PS. The role of high-intensity focused ultrasound as a symptomatic treatment for Parkinson's disease. *Mov Disord.* (2019) 34:1243–51. doi: 10.1002/mds.27779
14. Martínez-Fernández R, Máñez-Miró JU, Rodríguez-Rojas R, Del Álamo M, Shah BB, Hernández-Fernández F, et al. Randomized trial of focused ultrasound subthalamotomy for Parkinson's disease. *N Engl J Med.* (2020) 383:2501–13. doi: 10.1056/NEJMoa2016311
15. Monakow KH, Akert K, Künzle H. Projections of the precentral motor cortex and other cortical areas of the frontal lobe to the subthalamic nucleus in the monkey. *Exp Brain Res.* (1978) 33:395–403. doi: 10.1007/BF00235561
16. Nambu A, Tokuno H, Inase M, Takada M. Corticosubthalamic input zones from forelimb representations of the dorsal and ventral divisions of the premotor cortex in the macaque monkey: comparison with the input zones from the primarymotor cortex and the supplementary motor area. *Neurosci Lett.* (1997) 239:13-6 doi: 10.1016/S0304-3940(97)00877-X
17. Canteras NS, Shammah-Lagnado SJ, Silva BA, Ricardo JA. Afferent connections of the subthalamic nucleus: a combined retrograde and anterograde horseradish peroxidase study in the rat. *Brain Res.* (1990) 513:43–59. doi: 10.1016/0006-8993(90)91087-W
18. Kita T, Kita H. The subthalamic nucleus is one of multiple innervation sites for long-range corticofugal axons: a single-axon tracing study in the rat. *J Neurosci.* (2012) 32:5990–9. doi: 10.1523/JNEUROSCI.5717-11.2012
19. Feger J, Bevan M, Crossman AR. The projections from the parafascicular thalamic nucleus to the subthalamic nucleus and the striatum arise from separate neuronal populations: a com- parison with the corticostriatal and corticosubthalamic efferents in a retrograde fluorescent double-labelling study. *Neuroscience.* (1994) 60:125–32. doi: 10.1016/0306-4522(94)90208-9
20. Afsharpour S. Topographical projections of the cerebral cortex to the subthalamic nucleus. *J Comp Neurol.* (1985) 236:14–28. doi: 10.1002/cne.902360103
21. Petersen MV, Mlakar J, Haber SN, Parent M, Smith Y, Strick PL, et al. Holographic reconstruction of axonal pathways in the human brain. *Neuron.* (2019) 104:1056–64.e3. doi: 10.1016/j.neuron.2019.09.030
22. Rushmore RJ, Bouix S, Kubicki M, Rathi Y, Yeterian EH, Makris N. How human is human connectional neuroanatomy? *Front Neuroanat.* (2020) 14:18. doi: 10.3389/fnana.2020.00018
23. Whitmer D, de Solages C, Hill B, Yu H, Henderson JM, Bronte-Stewart H. High frequency deep brain stimulation attenuates subthalamic and cortical rhythms in Parkinson's disease. *Front Hum Neurosci.* (2012) 6:155. doi: 10.3389/fnhum.2012.00155
24. Avecillas-Chasin JM, Alonso-Frech F, Parras O, Del Prado N, Barcia, JA. Assessment of a method to determine deep brain stimulation targets using deterministic tractography in a navigation system. *Neurosurg Rev.* (2015) 38:739–5. doi: 10.1007/s10143-015-0643-1
25. Avecillas-Chasin JM, Rascón-Ramírez F, Barcia JA. Tractographical model of the cortico-basal ganglia and corticothalamic connections: improving our understanding of Deep Brain Stimulation. *Clin Anat.* (2016) 29:481–92. doi: 10.1002/ca.22689
26. Petersen MV, Lund TE, Sunde N, Frandsen J, Rosendal F, Juul N, et al. Probabilistic versus deterministic tractography for delineation of the cortico-subthalamic hyperdirect pathway in patients with Parkinson's disease selected for deep brain stimulation. *J Neurosurg.* (2017) 126:1657–68. doi: 10.3171/2016.4.JNS1624
27. Chen Y, Ge S, Li Y, Li N, Wang J, Wang X, et al. The role of the cortico-subthalamic hyperdirect pathway in deep brain stimulation for the treatment of Parkinson's disease: a diffusion tensor imaging study. *World Neurosurg.* (2018) 114:e1079–85. doi: 10.1016/j.wneu.2018.03.149
28. Avecillas-Chasin JM, Alonso-Frech F, Nombela C, Villanueva C, Barcia JA. Stimulation of the tractography-defined subthalamic nucleus regions correlates with clinical outcomes. *Neurosurgery.* (2019) 85:E294–303. doi: 10.1093/neuros/nyy633
29. Aravamuthan BR, Muthusamy KA, Stein JF, Aziz TZ, Johansen-Berg H. Topography of cortical and subcortical connections of the human pedunculopontine and subthalamic nuclei. *Neuroimage.* (2007) 37:694–705. doi: 10.1016/j.neuroimage.2007.05.050
30. Aron AR, Behrens TE, Smith S, Frank MJ, Poldrack RA. Triangulating a cognitive control network using diffusion-weighted magnetic resonance imaging (MRI) and functional MRI. *J Neurosci.* (2007) 27:3743–52. doi: 10.1523/JNEUROSCI.0519-07.2007
31. Lambert C, Zrinzo L, Nagy Z, Lutti A, Hariz M, Foltynie T, et al. Confirmation of functional zones within the human subthalamic nucleus: patterns of connectivity and sub-parcellation using diffusion weighted imaging. *Neuroimage.* (2012) 60:83–94. doi: 10.1016/j.neuroimage.2011.11.082
32. Brunenberg EJ, Moeskops P, Backes WH, Pollo C, Cammoun L, Vilanova A, et al. Structural and resting state functional connectivity of the subthalamic nucleus: identification of motor STN parts and the hyperdirect pathway. *PLoS ONE.* (2012) 7:e39061. doi: 10.1371/journal.pone.0039061
33. Milardi D, Gaeta M, Marino S, Arrigo A, Vaccarino G, Mormina E. Basal ganglia network by constrained spherical deconvolution: a possible cortico-pallidal pathway? *Mov Disord.* (2015) 30:342–9. doi: 10.1002/mds.25995
34. Akram H, Sotiropoulos SN, Jbabdi S, Georgiev D, Mahlknecht P, Hyam J, et al. Subthalamic deep brain stimulation sweet spots and hyperdirect cortical connectivity in Parkinson's disease. *Neuroimage.* (2017) 158:332–45. doi: 10.1016/j.neuroimage.2017.07.012
35. Gunalan K, Howell B, McIntyre CC. Quantifying axonal responses in patient-specific models of subthalamic deep brain stimulation. *Neuroimage.* (2018) 172:263–77. doi: 10.1016/j.neuroimage.2018.01.015
36. Temiz G, Sébille SB, Francois C, Bardinet E, Karachi C. The anatomo-functional organization of the hyperdirect cortical pathway to the subthalamic area using *in vivo* structural connectivity imaging in humans. *Brain Struct Funct.* (2020) 225:551–65. doi: 10.1007/s00429-019-02012-6
37. Weaver KE, Caldwell DJ, Cronin JA, Kuo CH, Kogan M, Houston B, et al. Concurrent deep brain stimulation reduces the direct cortical stimulation necessary for motor output. *Mov Disord.* (2020) 35:2348–53. doi: 10.1002/mds.28255
38. Oswal A, Cao C, Yeh CH, Neumann WJ, Gratwicke J, Akram H, et al. Neural signatures of hyperdirect pathway activity in Parkinson's disease. *Nat Commun.* (2021) 12:5185. doi: 10.1038/s41467-021-25366-0
39. Van Essen DC, Smith SM, Barch DM, Behrens TE, Yacoub E, Ugurbil K, et al. The WU-Minn Human Connectome Project: an overview. *Neuroimage.* (2013) 80:62–79. doi: 10.1016/j.neuroimage.2013.05.041
40. Sotiropoulos SN, Jbabdi S, Xu J, Andersson JL, Moeller S, Auerbach EJ, et al. Advances in diffusion MRI acquisition and processing in the Human Connectome Project. *Neuroimage.* (2013) 80:125–43. doi: 10.1016/j.neuroimage.2013.05.057
41. Ugurbil K, Xu J, Auerbach EJ, Moeller S, Vu AT, Duarte-Carvajalino JM, et al. Pushing spatial and temporal resolution for functional and diffusion MRI in the Human Connectome Project. *Neuroimage.* (2013) 80:80–104. doi: 10.1016/j.neuroimage.2013.05.012
42. Glasser MF, Sotiropoulos SN, Wilson JA, Coalson TS, Fischl B, Andersson JL. The minimal preprocessing pipelines for the Human Connectome Project. *Neuroimage.* (2013) 80:105–124. doi: 10.1016/j.neuroimage.2013.04.127
43. Andersson JL, Sotiropoulos SN. Non-parametric representation and prediction of single- and multi-shell diffusion-weighted

MRI data using Gaussian processes. *Neuroimage.* (2015) 15:166–76. doi: 10.1016/j.neuroimage.2015.07.067
44. Andersson JL, Sotiropoulos SN. An integrated approach to correction for off-resonance effects and subject movement in diffusion MR imaging. *Neuroimage.* (2015) 125:1063–78. doi: 10.1016/j.neuroimage.2015.10.019
45. Fedorov A, Beichel R, Kalpathy-Cramer J, Finet J, Fillion-Robin JC, Pujol S, et al. 3D Slicer as an image computing platform for the Quantitative Imaging Network. *Magn Reson Imaging.* (2012) 30:1323–41. doi: 10.1016/j.mri.2012.05.001
46. Norton I, Essayed W, Zhang F, Pujol S, Yarmarkovich A, Golby AJ, et al. SlicerDMRI: open source diffusion MRI software for brain cancer research. *Cancer Res.* (2017) 77:e101–3. doi: 10.1158/0008-5472.CAN-17-0332
47. Zhang F, Noh T, Juvekar P, Frisken SF, Rigolo L, Norton I, et al. SlicerDMRI: diffusion MRI and tractography research software for brain cancer surgery planning and visualization. *JCO Clin Cancer Informatic.* (2020) 4:299–309. doi: 10.1200/CCI.19.00141
48. D'Albis T, Haegelen C, Essert C, Fernández-Vidal S, Lalys F, Jannin P. PyDBS: an automated image processing workflow for deep brain stimulation surgery. *Int J Comput Assist Radiol Surg.* (2015) 10:117–28. doi: 10.1007/s11548-014-1007-y
49. Yelnik J, Bardinet E, Dormont D, Malandain G, Ourselin S, Tandé D. A three-dimensional, histological and deformable atlas of the human basal ganglia. I. Atlas construction based on immunohistochemical and MRI data. *Neuroimage.* (2007) 34:618–38. doi: 10.1016/j.neuroimage.2006.09.026
50. Bardinet E, Bhattacharjee M, Dormont D, Pidoux B, Malandain G, Schüpbach M. A three-dimensional histological atlas of the human basal ganglia. II. Atlas deformation strategy and evaluation in deep brain stimulation for Parkinson disease. *J Neurosurg.* (2009) 110:208–19. doi: 10.3171/2008.3.17469
51. Behrens TE, Berg HJ, Jbabdi S, Rushworth MF, Woolrich MW. Probabilistic diffusion tractography with multiple fibre orientations: what can we gain? *Neuroimage.* (2007) 34.1:144–55. doi: 10.1016/j.neuroimage.2006.09.018
52. Jenkinson M, Beckmann CF, Behrens TE, Woolrich MW, Smith SM. FSL. *Neuroimage.* (2012) 62:782–90. doi: 10.1016/j.neuroimage.2011.09.015
53. Cabeen RP, Bastin ME, Laidlaw DH. Estimating constrained multi-fiber diffusion MR volumes by orientation clustering. *Med Image Comput Comput Assist Interv.* (2013) 16(Pt. 1):82–9. doi: 10.1007/978-3-642-40811-3_11
54. Cabeen RP, Bastin ME, Laidlaw DH. Kernel regression estimation of fiber orientation mixtures in diffusion MRI. *Neuroimage.* (2016) 127:158–72. doi: 10.1016/j.neuroimage.2015.11.061
55. Cabeen RP, Laidlaw DH, Toga AW. Quantitative imaging toolkit: software for interactive 3D visualization, data exploration, and computational analysis of neuroimaging datasets. In: *ISMRM-ESMRMB Abstracts.* Paris (2018). p. 12–14.
56. Yousry TA, Schmid UD, Alkadhi H, Schmidt D, Peraud A, Buettner A, et al. Localization of the motor hand area to a knob on the precentral gyrus. A new landmark. *Brain.* (1997) 120(Pt. 1):141–57. doi: 10.1093/brain/120.1.141
57. Jenabi M, Peck KK, Young RJ, Brennan N, Holodny AI. Identification of the corticobulbar tracts of the tongue and face using deterministic and probabilistic DTI fiber tracking in patients with brain tumor. *AJNR Am J Neuroradiol.* (2015) 36:2036–41. doi: 10.3174/ajnr.A4430
58. Cronbach LJ. Coefficient alpha and the internal structure of tests. *Psychometrika.* (1951) 16:297–334. doi: 10.1007/BF023 10555
59. Selemon LD, Goldman-Rakic PS. Longitudinal topography and interdigitation of corticostriatal projections in the rhesus monkey. *J Neurosci.* (1985) 5:776–94. doi: 10.1523/JNEUROSCI.05-03-00776.1985
60. Matsumura M, Nambu A, Yamaji Y, Watanabe K, Imai H, Inase M, et al. Organization of somatic motor inputs from the frontal lobe to the pedunculopontine tegmental nucleus in the macaque monkey. *Neuroscience.* (2000) 98:97–110. doi: 10.1016/S0306-4522(00)00099-3
61. Karachi C, François C, Parain K, Bardinet E, Tandé D, Hirsch E, et al. Three-dimensional cartography of functional territories in the human striatopallidal complex by using calbindin immunoreactivity. *J Comp Neurol.* (2002) 450:122–34. doi: 10.1002/cne.10312
62. Mallet L, Schüpbach M, N'Diaye K, Remy P, Bardinet E, Czernecki V, et al. Stimulation of subterritories of the subthalamic nucleus reveals its role in the integration of the emotional and motor aspects of behavior. *Proc Natl Acad Sci USA.* (2007) 104:10661–6. doi: 10.1073/pnas.0610849104
63. Yelnik J, Percheron G. Subthalamic neurons in primates: a quantitative and comparative analysis. *Neuroscience.* (1979) 4:1717–43. doi: 10.1016/0306-4522(79)90030-7
64. Mink JW. The basal ganglia: focused selection and inhibition of competing motor programs. *Prog Neurobiol.* (1996) 50:381–425. doi: 10.1016/S0301-0082(96)00042-1
65. Holodny AI, Gor DM, Watts R, Gutin PH, Ulug AM. Diffusion-tensor MR tractography of somatotopic organization of corticospinal tracts in the internal capsule: initial anatomic results in contradistinction to prior reports. *Radiology.* (2005) 234:649–53. doi: 10.1148/radiol.2343032087
66. Smits M, Vernooij MW, Wielopolski PA, Vincent AJ, Houston GC, van der Lugt A. Incorporating functional MR imaging into diffusion tensor tractography in the preoperative assessment of the corticospinal tract in patients with brain tumors. *AJNR Am J Neuroradiol.* (2007) 28:1354–61. doi: 10.3174/ajnr.A0538
67. Ino T, Nakai R, Azuma T, Yamamoto T, Tsutsumi S, Fukuyama H. Somatotopy of corticospinal tract in the internal capsule shown by functional MRI and diffusion tensor images. *Neuroreport.* (2007) 18:665–8. doi: 10.1097/WNR.0b013e3280d943e1
68. Park JK, Kim BS, Choi G, Kim SH, Choi JC, Khang H. Evaluation of the somatotopic organization of corticospinal tracts in the internal capsule and cerebral peduncle: results of diffusion-tensor MR tractography. *Korean J Radiol.* (2008) 9:191–5. doi: 10.3348/kjr.2008.9.3.191
69. Conti A, Raffa G, Granata F, Rizzo V, Germanò A, Tomasello F. Navigated transcranial magnetic stimulation for "somatotopic" tractography of the corticospinal tract. *Neurosurgery.* (2014) 10(Suppl. 4):542–54; discussion 554. doi: 10.1227/NEU.0000000000000502
70. Lee DH, Kwon YH, Hwang YT, Kim JH, Park JW. Somatotopic location of corticospinal tracts in the internal capsule with MR tractography. *Eur Neurol.* (2012) 67:69–73. doi: 10.1159/000334097
71. Lee DH, Lee DW, Han BS. Topographic organization of motor fibre tracts in the human brain: findings in multiple locations using magnetic resonance diffusion tensor tractography. *Eur Radiol.* (2016) 26:1751–9. doi: 10.1007/s00330-015-3989-4
72. Kwon HG, Hong JH, Jang SH. Anatomic location and somatotopic arrangement of the corticospinal tract at the cerebral peduncle in the human brain. *AJNR Am J Neuroradiol.* (2011) 32:2116–9. doi: 10.3174/ajnr.A2660
73. Pan C, Peck KK, Young RJ, Holodny AI. Somatotopic organization of motor pathways in the internal capsule: a probabilistic diffusion tractography study. *AJNR Am J Neuroradiol.* (2012) 33:1274–80. doi: 10.3174/ajnr.A2952
74. Hazzaa NM, Mancini L, Thornton J, Yousry TA. Somatotopic organization of corticospinal/corticobulbar motor tracts in controls and patients with tumours: A combined fMRI-DTI study. *Neuroimage Clin.* (2019) 23:101910. doi: 10.1016/j.nicl.2019.101910
75. Tommasi G, Krack P, Fraix V, Le Bas JF, Chabardes S, Benabid AL, et al. Pyramidal tract side effects induced by deep brain stimulation of the subthalamic nucleus. *J Neurol Neurosurg Psychiatry.* (2008) 79:813–9. doi: 10.1136/jnnp.2007.117507
76. DeLong MR, Crutcher MD, Georgopoulos AP. Primate globus pallidus and subthalamic nucleus: functional organization. *J Neurophysiol.* (1985) 53:530–43. doi: 10.1152/jn.1985.53.2.530
77. Wichmann T, Bergman H, DeLong MR. The primate subthalamic nucleus. I. Functional properties in intact animals. *J Neurophysiol.* (1994) 72:494–506. doi: 10.1152/jn.1994.72.2.494
78. Rodriguez-Oroz MC, Rodriguez M, Guridi J, Mewes K, Chockkman V, Vitek J, et al. The subthalamic nucleus in Parkinson's disease: somatotopic organization and physiological characteristics. *Brain.* (2001) 124(Pt. 9):1777–90. doi: 10.1093/brain/124.9.1777
79. Abosch A, Hutchison WD, Saint-Cyr JA, Dostrovsky JO, Lozano AM. Movement-related neurons of the subthalamic nucleus in patients with Parkinson disease. *J Neurosurg.* (2002) 97:1167–72. doi: 10.3171/jns.2002.97.5.1167
80. Theodosopoulos PV, Marks WJ Jr, Christine C, Starr PA. Locations of movement-related cells in the human subthalamic nucleus in Parkinson's disease. *Mov Disord.* (2003) 18:791–8. doi: 10.1002/mds .10446
81. Romanelli P, Heit G, Hill BC, Kraus A, Hastie T, Brontë-Stewart HM. Microelectrode recording revealing a somatotopic body map in the

subthalamic nucleus in humans with Parkinson disease. *J Neurosurg.* (2004) 100:611–8. doi: 10.3171/jns.2004.100.4.0611
82. Sasaki T, Kuwahara K, Kin I, Okazaki M, Sasada S, Shinko A, et al. Identification of somatotopic organization and optimal stimulation site within the subthalamic nucleus for Parkinson's disease. *Oper Neurosurg.* (2019) 17:239–46. doi: 10.1093/ons/opy351
83. Nakajima R, Kinoshita M, Shinohara H, Nakada M. The superior longitudinal fascicle: reconsidering the fronto-parietal neural network based on anatomy and function. *Brain Imaging Behav.* (2020) 14:2817–30. doi: 10.1007/s11682-019-00187-4
84. Pujol S, Wells W, Pierpaoli C, Brun C, Gee J, Cheng G, et al. The DTI challenge: toward standardized evaluation of diffusion tensor imaging tractography for neurosurgery. *J Neuroimaging.* (2015) 25:875–82. doi: 10.1111/jon.12283
85. Sammartino F, Krishna V, King NK, Lozano AM, Schwartz ML, Huang Y, et al. Tractography-based ventral intermediate nucleus targeting: novel methodology and intraoperative validation. *Mov Disord.* (2016) 31:1217–25. doi: 10.1002/mds.26633
86. Chazen JL, Sarva H, Stieg PE, Min RJ, Ballon DJ, Pryor KO, et al. Clinical improvement associated with targeted interruption of the cerebellothalamic tract following MR-guided focused ultrasound for essential tremor. *J Neurosurg.* (2018) 129:315–23. doi: 10.3171/2017.4.JNS162803
87. King NKK, Krishna V, Basha D, Elias G, Sammartino F, Hodaie M, et al. Microelectrode recording findings within the tractography-defined ventral intermediate nucleus. *J Neurosurg.* (2017) 126:1669–75. doi: 10.3171/2016.3.JNS151992
88. Krishna V, Sammartino F, Agrawal P, Changizi BK, Bourekas E, Knopp MV, et al. Prospective tractography-based targeting for improved safety of focused ultrasound thalamotomy. *Neurosurgery.* (2019) 84:160–8. doi: 10.1093/neuros/nyy020
89. Bruno F, Catalucci A, Varrassi M, Arrigoni F, Sucapane P, Cerone D, et al. Comparative evaluation of tractography-based direct targeting and atlas-based indirect targeting of the ventral intermediate (Vim) nucleus in MRgFUS thalamotomy. *Sci Rep.* (2021) 11:13538. doi: 10.1038/s41598-021-93058-2

Conflict of Interest: The authors declare that the research was conducted in the absence of any commercial or financial relationships that could be construed as a potential conflict of interest.

The handling editor declared a past collaboration with one of the authors GC.

frontiers | Frontiers in Neurology

TYPE Original Research
PUBLISHED 05 September 2022
DOI 10.3389/fneur.2022.926027

OPEN ACCESS

EDITED BY
Paul Fishman,
University of Maryland, Baltimore, United States

REVIEWED BY
George Wittenberg,
University of Pittsburgh, United States
Victor Frenkel,
University of Maryland, Baltimore, United States

*CORRESPONDENCE
Zhi-Ming Tang
tangzhm3@mail.sysu.edu.cn

SPECIALTY SECTION
This article was submitted to Experimental Therapeutics, a section of the journal Frontiers in Neurology

RECEIVED 04 May 2022
ACCEPTED 25 July 2022
PUBLISHED 05 September 2022

CITATION
Zhang M-F, Chen W-Z, Huang F-B, Peng Z-Y, Quan Y-C and Tang Z-M (2022) Low-intensity transcranial ultrasound stimulation facilitates hand motor function and cortical excitability: A crossover, randomized, double blind study.
Front. Neurol. 13:926027.
doi: 10.3389/fneur.2022.926027

Low-intensity transcranial ultrasound stimulation facilitates hand motor function and cortical excitability: A crossover, randomized, double blind study

Meng-Fei Zhang[1], Wei-Zhou Chen[1], Fub-Biao Huang[2], Zhi-Yong Peng[1], Ying-Chan Quan[1] and Zhi-Ming Tang[1,3]*

[1]Department of Rehabilitation Medicine, Yuedong Hospital, The Third Affiliated Hospital of Sun Yat-sen University, Meizhou, China, [2]Department of Occupational Therapy, China Rehabilitation Research Center, Beijing, China, [3]Department of Rehabilitation Medicine, The Third Affiliated Hospital of Sun Yat-Sen University, Guangzhou, China

Objective: Transcranial ultrasound stimulation (TUS) is a new form of non-invasive brain stimulation. Low-intensity TUS is considered highly safe. We aimed to investigate the effect of low-intensity TUS on hand reaction responses and cortical excitability in healthy adults.

Methods: This study used a crossover, randomized, and double-blind design. A total of 20 healthy participants were recruited for the study. All the participants received TUS and sham stimulation on separate days in random order. The finger tapping test (tapping score by using a tablet) and motor evoked potential (MEP) were assessed before and after stimulation, and discomfort levels were assessed using a visual analog scale (VAS) score.

Results: No significant differences in tapping score or MEP amplitude between the two experimental conditions were registered before stimulation. After stimulation, tapping scores were increased regardless of the specific treatment, and the real stimulation condition receiving TUS (90.4 ± 11.0 points) outperformed the sham stimulation condition (86.1 ± 8.4 points) ($p = 0.002$). The MEP latency of real TUS (21.85 ± 1.33 ms) was shorter than that of sham TUS (22.42 ± 1.43 ms) ($p < 0.001$). MEP amplitude of real TUS (132.18 ± 23.28 μV) was higher than that of sham TUS (114.74 ± 25.5 μV, $p = 0.005$). There was no significant difference in the discomfort score between the two conditions ($p = 0.163$).

Conclusion: Transcranial ultrasound stimulation (TUS) can decrease the hand reaction response time and latency of the MEP, enhance the excitability of the motor cortex, and improve hand motor function in healthy individuals without obvious discomfort.

KEYWORDS

transcranial ultrasound, hand function, neuromodulation, motor evoked potential, motor cortex

Introduction

Neuromodulation techniques, which can change central excitability and induce neuroplasticity, have been successfully used for rehabilitation after central neural system injury or function disorder (1, 2). Transcranial magnetic stimulation (TMS) and transcranial direct current stimulation (tDCS) have been widely studied in the past (3, 4). Transcranial Ultrasound stimulation (TUS), which can pass through the skull and influence central nervous function mechanically, has become a research focus for research in recent years (5). As a novel neuromodulation technique, TUS has the advantages of being non-invasive and providing high spatial resolution and greater penetration depth. Preliminary studies suggest that TUS can locally regulate sensory induction and cortical function (6).

Ultrasound can be classified into high, medium, or low intensities according to the power applied. High-intensity ultrasound (>200 W/cm^2) mainly inhibits neuronal activity through nerve ablation, while medium-intensity ultrasound (100–200 W/cm^2) is normally used to disrupt the blood-brain barrier non-invasively. Low-intensity ultrasound (<100 W/cm^2), on the other hand, does not involve a significant accumulation of thermal energy, which may cause DNA fragmentation, coagulative necrosis, and cell death (7, 8), relying instead on a direct mechanical effect (9).

Previous studies mostly focused on animal experiments-very few studies discussed the effect of TUS on the human cortex (10, 11). The animal studies reported both excitation and inhibition effects of low-intensity TUS on the central neural system (12, 13). One human study reported intervention in the right prefrontal gyrus in healthy individuals and found an inhibitory effect on the cortex but a positive effect on mood (14). The therapeutic effect of TUS on the cortex may be related to parameters, such as focused or non-focused, intensity, frequency, and stimulation location (15, 16). Focused TUS and non-focused TUS can lead to a differential stimulation effect according to the volume of the brain tissue impacted (17). Frequency and intensity may cause different physiological effects (8). In humans, TUS delivered to the M1 region at 0.50 MHz, 6.16 W/cm² inhibited neuronal excitability (11). Diagnostic imaging ultrasound (unfocused TUS) stimulation with a frequency of 2.32 MHz and intensity of 34.96 W/cm² increased neuronal excitability (10). Using multiple Focused TUS transducers to stimulate the primary sensory cortex elicited various tactile sensations in the absence of any external sensory stimuli (18). Sanguinetti reported a focused TUS study with a randomized, placebo-controlled, double-blind design, in which participants received 30 s of 500 kHz focused TUS or a placebo control. They found that focused TUS can be used to modulate mood and emotional regulation networks in the prefrontal cortex when targeting the right inferior frontal gyrus in healthy human volunteers (14).

In this study, we used the tapping action and motor evoked potentials (MEPs) (19) to investigate the effect of low-intensity TUS on hand motor function and cortical excitability in healthy adults.

Materials and methods

Participants

According to the data collected from our preliminary experiment, a total of 20 healthy individuals were recruited for the study voluntarily (Table 1) [mean age (32.8 ± 13.4), the age range: 21–59, women: 12, men: 8]. The inclusion criteria were: (1) being between 20 and 60 years of age, and (2) being right-handed. The exclusion criteria were: (1) having poor cooperation due to cognitive or hearing impairment, and (2) having a history of hand trauma. All participants were informed about the study design and objectives and signed informed consent. The study was approved by the Ethics Committee of Yue Dong Hospital of the Third Affiliated Hospital of Sun Yat-sen University (project 8, 2021).

Study design

A double-blind randomized crossover control design was used in this study. Random numbers were generated and recorded by a designated person who did not participate in any other operation or assessment. Each participant received real TUS and sham TUS with an interval of more than 24 h between each intervention to avoid potential residual effects, and the stimulation sequence was determined at random. The evaluator did not participate in the stimulation procedure (Figure 1).

Experimental conditions

Transcranial ultrasound stimulation (TUS) stimulation (UE860A, Beijing Ruao Medical Technology Co., LTD., China) was provided once to each participant for a total duration of 10 min using a power of 1.2 W/cm² and a frequency of 0.8 MHz, stimulation duration was 1 s and rest 2 s on-off ratio of 1:2 (20–22). The center of the probe (diameter = 20 mm) was placed on the "hotspot" determined by TMS as explained in the next section (2.4 evaluation). Participants were seated comfortably, and the surrounding environment was kept comfortable and quiet throughout the treatment session. For the sham stimulations, the ultrasound probe was placed in reverse. The TUS instrument was still in "turn on" state and all the other conditions were kept identical.

TABLE 1 General information on subjects and stimulation methods.

Subjects	Age	Gender	Stimulation methods	
			First stimulus	Second stimulus
1	20	M	Sham TUS	Real TUS
2	21	M	Real TUS	Sham TUS
3	21	M	Real TUS	Sham TUS
4	23	M	Sham TUS	Real TUS
5	22	W	Real TUS	Sham TUS
6	29	M	Real TUS	Sham TUS
7	43	W	Sham TUS	Real TUS
8	29	W	Real TUS	Sham TUS
9	22	M	Sham TUS	Real TUS
10	46	W	Real TUS	Sham TUS
11	32	M	Real TUS	Sham TUS
12	23	W	Sham TUS	Real TUS
13	51	W	Real TUS	ShamTUS
14	58	M	Sham TUS	Real TUS
15	25	W	Real TUS	Sham TUS
16	39	W	Real TUS	Sham TUS
17	59	W	Real TUS	Sham TUS
18	49	W	Sham TUS	Real TUS
19	23	W	Sham TUS	Real TUS
20	22	W	Real TUS	Sham TUS

M, Men; W, Women.

Evaluation

The tapping score and MEP parameters of each participant were measured before and after the stimulation session, and the discomfort of the subjects during the stimulation was assessed. A tapping test based on the Quiq 2.0 APP software was used to quantify hand motor response (23). During the test, participants were required to tap on the moving point displayed on the screen of a tablet as quickly and as accurately as possible within 30 s. One point was awarded for each on-target tap and two points when the participant tapped in the inner circle. Three tests were performed before and after stimulation, and the average value was recorded in each case.

The TMS instrument and supporting MEP monitoring module (Wuhan Yiruide Medical Equipment New Technology Co., LTD., China) were used for measuring MEPs. The recording and reference electrodes were placed on the muscle belly and the tendon of the right abductor pollicis brevis, respectively, and the ground electrode was placed on the left wrist. The location for the stimulation was determined using the EEG 10-20 system, and the C3 position was marked on the head. Stimulation was provided around the C3 position range at 70% intensity using the 8-shaped coil. The coil was then moved until the best location to record the MEP was found ("hotspot"), the intensity was reduced, and the handle was positioned at a 45° angle to the middle line of the body. The resting motor threshold (rMT) was set at an intensity capable of inducing MEPs higher than 50 μV in at least five out of ten trials (19). The latency and amplitude of the hand MEPs before and after stimulation were recorded using a 120% rMT intensity. Ten independent measurements were recorded before and after stimulation, and the average value was considered for the analysis (24–26). The interval of each MEP measurement was 5–10 s.

A visual analog scale (VAS) was used to evaluate the degree of discomfort during the session, with zero considered as very comfortable and ten as extremely uncomfortable.

Statistical analysis

We used G Power Statistics (3.1.9.2 version) to calculate the sample size of this study according to the results of pre-experiment. To achieve 80% power and 5% statistical significance, a sample size of 20 cases was required for this study. The SPSS 23.0 statistical software (IBM corporation, USA) was used for data analysis. Shapiro–Wilk test was used to confirm if the data were normally distributed. Levene statistic method to test if the variance was equal. Tapping score, MEP latency, and MEP amplitude were expressed as mean ± standard deviation. Two-factor repeated measurement ANOVA was used to test the main effect and interaction of conditions (real and sham) and time points (before and after stimulation). Paired *t*-test was used as a post pairwise comparison to determine differences between the two conditions. Also, paired *t*-test was used

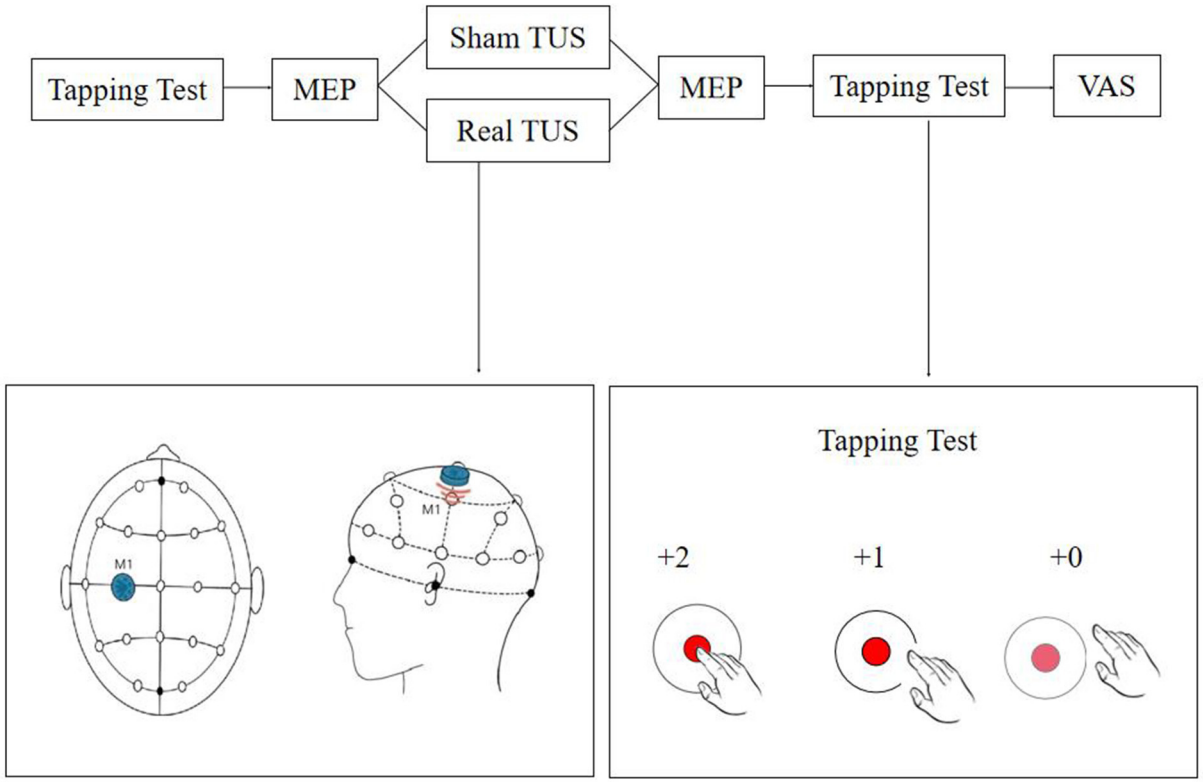

FIGURE 1
Flow diagram of the study. The tapping test and motor evoked potentials (MEPs) were recorded before and after stimulation, and discomfort levels were assessed using a visual analog scale (VAS) score.

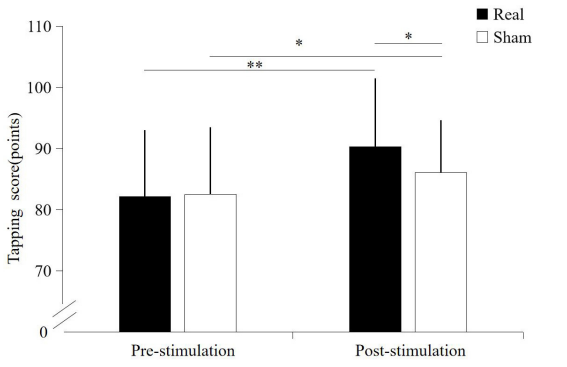

FIGURE 2
The results of the tapping score under both stimulation conditions. *$p < 0.05$, **$p < 0.01$.

to determine the differences between before and after stimulation. VAS was presented as median (P25, P75), Wilcoxon signed ranks test was used to compare the difference between the two conditions. $p < 0.05$ was considered statistically significant.

Results

Tapping score

A significant interaction effect was found between the condition and time point ($F = 16.156$, $p < 0.001$). Significantly main effect was found on condition ($F = 8.120$, $p = 0.010$) and time point ($F = 59.323$, $p < 0.001$). Before stimulation, there was no significant difference in tapping score between the real TUS condition (82.2 ± 10.75 points) and sham TUS conditions (82.5 ± 10.8 points, $t = -0.758$, $p = 0.458$). Moreover, the tapping score after real TUS (90.4 ± 11.02 points) was significantly higher than that obtained after the sham TUS (86.1 ± 8.4 points, $t = 3.556$, $p = 0.002$) (Figure 2). Tapping score became significantly higher after stimulation compared to before stimulation in both real TUS conditions ($t = 11.2$, $p < 0.001$) and sham TUS ($t = 3.153$, $p = 0.005$).

Motor evoked potential latency

A significant interaction effect was found between the condition and time point ($F = 29.188$, $p < 0.001$). No

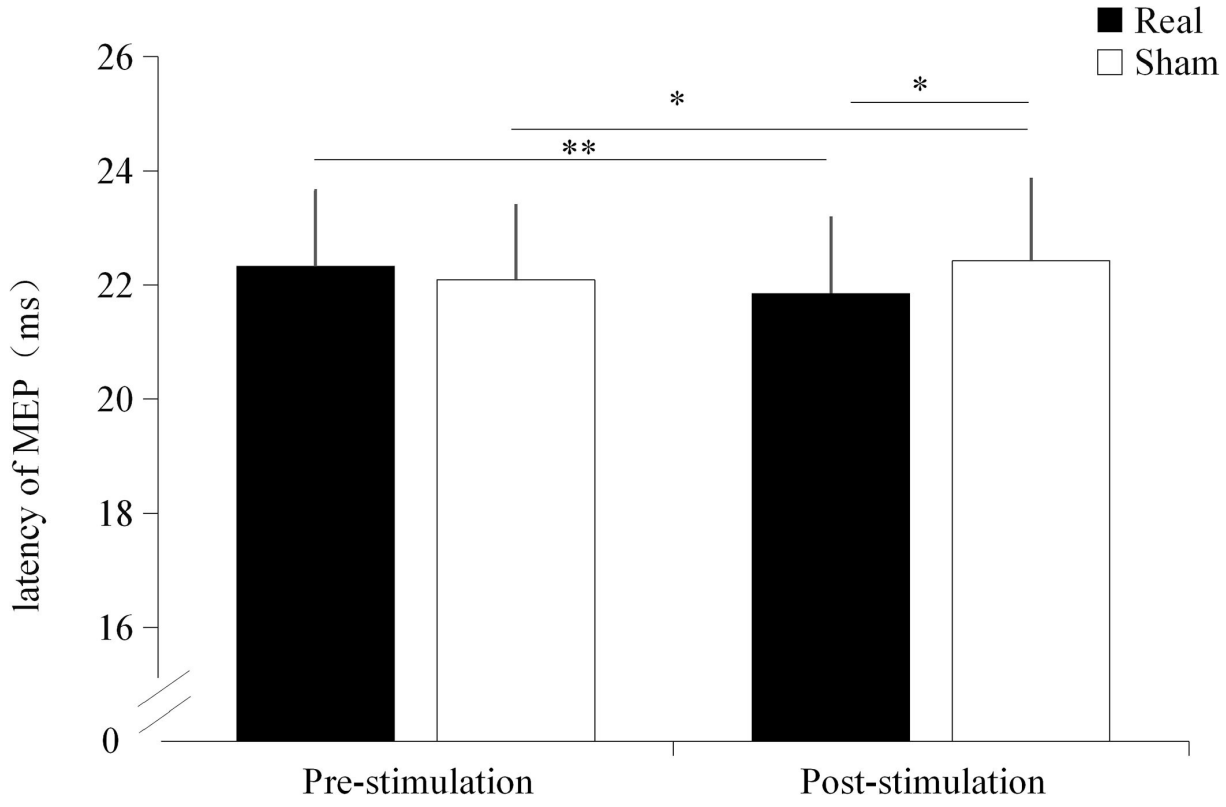

FIGURE 3
The latency of motor evoked potentials (MEPs) under both stimulation conditions. *$p < 0.05$, **$p < 0.01$.

significantly main effect were found on condition ($F = 1.314$, $p = 0.266$) and time point ($F = 0.869$, $p = 0.363$). There was no significant difference in MEP latency before the stimulation between the real TUS condition (22.33 ± 1.32 ms) and sham TUS conditions (22.09 ± 1.30 ms, $t = 1.295$, $p = 0.211$). Moreover, the MEP latency after real TUS (21.85 ± 1.33 ms) was significantly shorter than those obtained after the sham TUS (22.42 ± 1.43 ms, $t = -4.119$, $p < 0.001$, Figure 3). MEPs became significantly shorter after stimulation compared to before stimulation in real TUS conditions ($t = -7.889$, $p < 0.001$), however they were longer under the sham TUS ($t = 2.184$, $p = 0.042$, Figure 3).

Motor evoked potential amplitude

Significant interaction effect was found between the condition and time point ($F = 15.822$, $p < 0.001$). No significant main effect were found on condition ($F = 2.312$, $p = 0.145$) and time point ($F = 1.336$, $p = 0.262$). Before stimulation, there was no significant difference in MEP amplitude between the real TUS condition (115.02 ± 21.7 μV) and the sham TUS condition (122.1 ± 24.23 μV, $t = -2.012$, $p = 0.059$). Moreover, the MEP amplitude after real TUS (132 ± 23.28 μV) was significantly higher than that obtained after the sham TUS (114.74 ± 25.5 μV, $t = 3.193$, $p = 0.005$, Figure 4). MEP amplitude significantly increased after stimulation compared to before stimulation in real TUS condition ($t = 5.140$, $p < 0.001$), however, there were no significant changes in MEP amplitude after stimulation on sham TUS condition ($t = 1.111$, $p = 0.280$, Figure 4).

Comparison of discomfort

There were no significant differences between the discomfort scores associated with real TUS 5(5,5) and sham TUS 5(5,5) stimulation conditions ($z = 1.414$, $p = 0.157$).

Discussion

Transcranial ultrasound stimulation (TUS) is a novel neuromodulation technique that has not yet been widely adopted in clinical practice (8, 13). In this study, TUS was used to stimulate the motor area of the brain in healthy adults, and it could enhance hand responsiveness, shorten the transmission time of MEPs, and enhance motor cortex excitability, indicating that low-frequency and low-intensity TUS has a positive effect on central excitability and hand function.

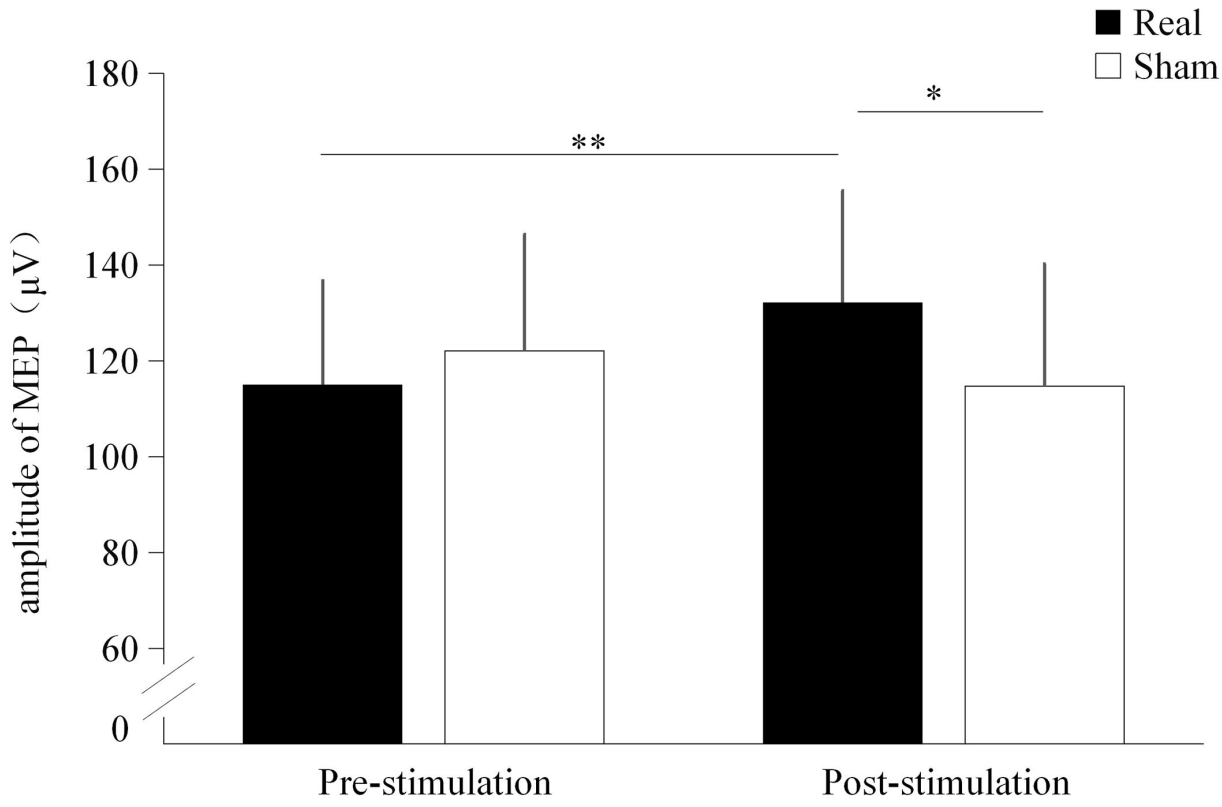

FIGURE 4
The amplitude of the motor evoked potentials (MEPs) under both stimulation conditions. *$p < 0.05$, **$p < 0.01$.

Some previous studies reported that TUS can regulate neuronal activity (8). The short-term neuronal activity involves inhibition or activation, while in the long term it may involve the reorganization of neural circuits (neuroplasticity), which could potentially improve brain function (7). A previous study has shown that transcranial-focused ultrasound increased cortical blood flow in the activated area of the motor cortex (27). Most researchers consider that the non-thermal effects of ultrasound play a role in the regulation of neuronal activity, including the opening of mechanically-gated ion channels and changes in membrane permeability caused by cavitation effects (13, 28). Due to the plasticity of the human cortex, low-intensity TUS can increase the excitability of the target brain circuit within a short time, suggesting that endogenous motor cortex activity can be enhanced by regulating excitability (29).

Our tapping score measurement included a comprehensive evaluation of speed and accuracy like the score calculation of archery. The results indicated that TUS could shorten the reaction time and improve the reaction ability of the hand by direct stimulation of the brain. Ichijo et al. found that low-intensity TUS improved the ability of mice affected by stroke to walk on a wire rope and navigate a maze. Few previous studies have focused on the effects of TUS on human behavior (30).

The results of this study show that the MEP latency was shortened, and the amplitude of the MEP was increased after TUS stimulation, suggesting that low-intensity TUS could enhance the excitability of the motor cortex. When TMS is applied to the primary motor cortex, corticospinal neurons are activated, and an MEP is generated in the target muscle (31). MEP latency reflects the conduction capacity of the corticospinal tract, and MEP amplitude can be used to determine changes in cortical excitability. In agreement with our results, Gibson et al. used diagnostic TUS applied to the cortical area for 2 min and found that the MEP amplitude was increased after stimulation (10). Using self-made ultrasound equipment, Legon et al. also showed that focused TUS (0.5 MHz, 6.16 W/cm^2) can regulate central excitability (11). However, in their case, the MEP amplitude decreased after stimulation, suggesting inhibition of the motor cortex. These result differences may be related to the specific parameter setting of TUS. In the present study, we used non-focused ultrasound, while Legon et al. employed transcranial-focused ultrasound; also, the intensity we used was lower than that used in Legon's study. Nevertheless, both results provide evidence that TUS can regulate the excitability of the human motor cortex.

In the present study, VAS was used as a tool to monitor the discomfort of subjects, reflecting their subjective feelings

about the treatment. Because the low-intensity TUS we used is commercially available and does not have any thermal effects, we expected the participants to not experience any noticeable sensation during the treatment session, and indeed there were no significant differences in the VAS scores between the two conditions. Liu et al. suggested based on animal experiments that the heat generated by low-intensity TUS is extremely weak, far below the temperature threshold capable of causing biological effects (32). This means that the local temperature in the target area may remain almost unchanged, and there is no danger of thermal damage to normal tissues (33). As a non-invasive form of brain stimulation, low-intensity TUS does not involve the opening of the blood–brain barrier, nor does it produce morphological changes in the brain (7), and therefore, it can be considered safe. During the course of our study, a single participant experienced mild dizziness after TUS treatment, which disappeared spontaneously within 5 min.

Our study has several limitations. First, we focused exclusively on the effect of a single TUS stimulus, even though it has a statistically significant difference in MEP latency between the real and sham conditions after stimulation, the changes in mean value were small. Further research is needed to determine the potential effects of a different stimulus schedule on excitability. Second, we observed the regulatory effect of TUS on the brains of healthy adults, and it is not clear whether the same changes would also occur in pathological conditions. Third, this study was restricted to the effects of TUS on hand motor function and central regulation, but the relevance of this effect to behavioral training remains unclear. Finally, the assessment method employed in this study is relatively limited, and therefore, it would be necessary to conduct further research on the impact of TUS on neural networks through methods involving neuroimaging in the future.

In conclusion, low-intensity TUS can improve hand motor function in healthy adults by shortening the latency of MEP and enhancing the excitability of the motor cortex.

Data availability statement

The data that support the findings of this study are available from the corresponding author upon reasonable request.

Ethics statement

The studies involving human participants were reviewed and approved by the Ethics Committee of Yue dong Hospital of the Third Affiliated Hospital of Sun Yat-sen University. The patients/participants provided their written informed consent to participate in this study.

Author contributions

Z-MT and F-BH: conceptualization. M-FZ and Z-MT: methodology. W-ZC: assessment. M-FZ: TUS operator and writing—original draft preparation. Z-YP: formal analysis and investigation. Z-MT: writing—review and editing and funding acquisition. All authors contributed to the study conception and design. All authors contributed to the article and approved the submitted version.

Funding

This work was supported by the National Natural Science Foundation of China (Grant Number: 81401872).

Conflict of interest

The authors declare that the research was conducted in the absence of any commercial or financial relationships that could be construed as a potential conflict of interest.

Publisher's note

All claims expressed in this article are solely those of the authors and do not necessarily represent those of their affiliated organizations, or those of the publisher, the editors and the reviewers. Any product that may be evaluated in this article, or claim that may be made by its manufacturer, is not guaranteed or endorsed by the publisher.

References

1. Lefaucheur JP, André-Obadia N, Antal A, Ayache SS, Baeken C, Benninger DH, et al. Evidence-based guidelines on the therapeutic use of repetitive transcranial magnetic stimulation (rTMS). *Clin Neurophysiol.* (2014) 125:2150–206. doi: 10.1016/j.clinph.2014.05.021

2. Wagner T, Valero-Cabre A, Pascual-Leone A. Noninvasive human brain stimulation. *Annu Rev Biomed Eng.* (2007) 9:527–65. doi: 10.1146/annurev.bioeng.9.061206.133100

3. Lefaucheur JP, Aleman A, Baeken C, Benninger DH, Brunelin J, Di Lazzaro V, et al. Evidence-based guidelines on the therapeutic use of repetitive transcranial magnetic stimulation (rTMS): an update (2014-2018). *Clin Neurophysiol.* (2020) 131:474–528. doi: 10.1016/j.clinph.2019.11.002

4. Bolognini N, Souza Carneiro MI, Russo C, Vallar G. Transcranial direct current stimulation in stroke rehabilitation: ready to move to randomized clinical

trials and clinical practice? The issue of safety guidelines. *Eur J Neurol.* (2017) 24:e78. doi: 10.1111/ene.13396

5. Folloni D, Verhagen L, Mars RB, Fouragnan E, Constans C, Aubry JF, et al. Manipulation of subcortical and deep cortical activity in the primate brain using transcranial focused ultrasound stimulation. *Neuron.* (2019) 101:1109–16.e1105. doi: 10.1016/j.neuron.2019.01.019

6. Legon W, Sato TF, Opitz A, Mueller J, Barbour A, Williams A, et al. Transcranial focused ultrasound modulates the activity of primary somatosensory cortex in humans. *Nat Neurosci.* (2014) 17:322–9. doi: 10.1038/nn.3620

7. Beisteiner R, Lozano AM. Transcranial ultrasound innovations ready for broad clinical application. *Adv Sci.* (2020) 7:2002026. doi: 10.1002/advs.202002026

8. Kim T, Park C, Chhatbar PY, Feld J, Mac Grory B, Nam CS, et al. Effect of low intensity transcranial ultrasound stimulation on neuromodulation in animals and humans: an updated systematic review. *Front Neurosci.* (2021) 15:620863. doi: 10.3389/fnins.2021.620863

9. Wang P, Zhang J, Yu J, Smith C, Feng W. Brain modulatory effects by low-intensity transcranial ultrasound stimulation (TUS): a systematic review on both animal and human studies. *Front Neurosci.* (2019) 13:696. doi: 10.3389/fnins.2019.00696

10. Gibson BC, Sanguinetti JL, Badran BW, Yu AB, Klein EP, Abbott CC, et al. Increased excitability induced in the primary motor cortex by transcranial ultrasound stimulation. *Front Neurol.* (2018) 9:1007. doi: 10.3389/fneur.2018.01007

11. Legon W, Bansal P, Tyshynsky R, Ai L, Mueller JK. Transcranial focused ultrasound neuromodulation of the human primary motor cortex. *Sci Rep.* (2018) 8:10007. doi: 10.1038/s41598-018-28320-1

12. Fini M, Tyler WJ. Transcranial focused ultrasound: a new tool for non-invasive neuromodulation. *Int Rev Psychiatry.* (2017) 29:168–177. doi: 10.1080/09540261.2017.1302924

13. Blackmore J, Shrivastava S, Sallet J, Butler CR, Cleveland RO. Ultrasound neuromodulation: a review of results, mechanisms and safety. *Ultrasound Med Biol.* (2019) 45:1509–36. doi: 10.1016/j.ultrasmedbio.2018.12.015

14. Sanguinetti JL, Hameroff S, Smith EE, Sato T, Daft CMW, Tyler WJ, et al. Transcranial focused ultrasound to the right prefrontal cortex improves mood and alters functional connectivity in humans. *Front Hum Neurosci.* (2020) 14:52. doi: 10.3389/fnhum.2020.00052

15. Yoon K, Lee W, Lee JE, Xu L, Croce P, Foley L, et al. Effects of sonication parameters on transcranial focused ultrasound brain stimulation in an ovine model. *PLoS ONE.* (2019) 14:e0224311. doi: 10.1371/journal.pone.0224311

16. Kim HC, Lee W, Kunes J, Yoon K, Lee JE, Foley L, et al. Transcranial focused ultrasound modulates cortical and thalamic motor activity in awake sheep. *Sci Rep.* (2021) 11:19274. doi: 10.1038/s41598-021-98920-x

17. di Biase L, Falato E, Di Lazzaro V. Transcranial focused ultrasound (tFUS) and transcranial unfocused ultrasound (tUS) neuromodulation: from theoretical principles to stimulation practices. *Front Neurol.* (2019) 10:549. doi: 10.3389/fneur.2019.00549

18. Lee W, Chung YA, Jung Y, Song IU, Yoo SS. Simultaneous acoustic stimulation of human primary and secondary somatosensory cortices using transcranial focused ultrasound. *BMC Neurosci.* (2016) 17:68. doi: 10.1186/s12868-016-0303-6

19. Tang ZM, Xuan CY, Li X, Dou ZL, Lan YJ, Wen HM. Effect of different pulse numbers of transcranial magnetic stimulation on motor cortex excitability: single-blind, randomized cross-over design. *CNS Neurosci Ther.* (2019) 25:1277–81. doi: 10.1111/cns.13248

20. Hao G, Ting C, Xiaojuan X. Effects of transcranial ultrasonic-neuromuscular stimulation therapy combined with edaravone on mood disorders in patients with acute cerebral infarction (Chinese). *Neural Injury Funct Reconst.* (2020) 15:116–7. doi: 10.16780/j.cnki.sjssgncj.2020.02.015

21. Rui H, Lili W. Effects of transcranial ultrasonic-neuromuscular stimulation on negative cognitive bias, neurological function and neurotransmitter levels in PSD patients (Chinese). *Huaxia Med.* (2022) 35:71–5. doi: 10.19296/j.cnki.1008-2409.2022-01-016

22. Huihui W, Yana L, Ying X, Xiaoli L, Yutao J. Effects of motor imagery combined with transcranial ultrasound neuromuscular electrical stimulation on upper limb and daily living ability in patients with stroke (Chinese). *J Mod Med Health.* (2020) 36:1642–4. doi: 10.3969/j.issn.1009-5519.2020.11.012

23. Masaharu T. *Reaction Time Test Gamee [EB/OL]*. Available online at: https://apps.apple.com/cn/app/reaction-time-test -gam/id1141314478?l=en (accessed June 28, 2021).

24. Takamatsu Y, Koganemaru S, Watanabe T, Shibata S, Yukawa Y, Minakuchi M, et al. Transcranial static magnetic stimulation over the motor cortex can facilitate the contralateral cortical excitability in human. *Sci Rep.* (2021) 11:5370. doi: 10.1038/s41598-021-84823-4

25. Davila-Perez P, Pascual-Leone A, Cudeiro J. Effects of transcranial static magnetic stimulation on motor cortex evaluated by different tms waveforms and current directions. *Neuroscience.* (2019) 413:22–30. doi: 10.1016/j.neuroscience.2019.05.065

26. Sun ZG, Pi YL, Zhang J, Wang M, Zou J, Wu W. Effect of acupuncture at ST36 on motor cortical excitation and inhibition. *Brain Behav.* (2019) 9:e01370. doi: 10.1002/brb3.1370

27. Ai L, Bansal P, Mueller JK, Legon W. Effects of transcranial focused ultrasound on human primary motor cortex using 7T fMRI: a pilot study. *BMC Neurosci.* (2018) 19:56. doi: 10.1186/s12868-018-0456-6

28. Darrow DP. Focused ultrasound for neuromodulation. *Neurotherapeutics.* (2019) 16:88–99. doi: 10.1007/s13311-018-00691-3

29. Yu K, Liu C, Niu X, He B. Transcranial focused ultrasound neuromodulation of voluntary movement-related cortical activity in humans. *IEEE Trans Biomed Eng.* (2021) 68:1923–31. doi: 10.1109/TBME.2020.3030892

30. Ichijo S, Shindo T, Eguchi K, Monma Y, Nakata T, Morisue Y, et al. Low-intensity pulsed ultrasound therapy promotes recovery from stroke by enhancing angio-neurogenesis in mice in vivo. *Sci Rep.* (2021) 11:4958. doi: 10.1038/s41598-021-84473-6

31. Ni Z, Udupa K, Hallett M, Chen R. Effects of deep brain stimulation on the primary motor cortex: insights from transcranial magnetic stimulation studies. *Clin Neurophysiol.* (2019) 130:558–67. doi: 10.1016/j.clinph.2018.10.020

32. Liu L, Du J, Zheng T, Hu S, Dong Y, Du D, et al. Protective effect of low-intensity transcranial ultrasound stimulation after differing delay following an acute ischemic stroke. *Brain Res Bull.* (2019) 146:22–7. doi: 10.1016/j.brainresbull.2018.12.004

33. Xie P, Zhou S, Wang X, Wang Y, Yuan Y. Effect of pulsed transcranial ultrasound stimulation at different number of tone-burst on cortico-muscular coupling. *BMC Neurosci.* (2018) 19:60. doi: 10.1186/s12868-018-0462-8

Advantages of publishing in Frontiers

OPEN ACCESS
Articles are free to read for greatest visibility and readership

FAST PUBLICATION
Around 90 days from submission to decision

HIGH QUALITY PEER-REVIEW
Rigorous, collaborative, and constructive peer-review

TRANSPARENT PEER-REVIEW
Editors and reviewers acknowledged by name on published articles

Frontiers
Avenue du Tribunal-Fédéral 34
1005 Lausanne | Switzerland

Visit us: www.frontiersin.org
Contact us: frontiersin.org/about/contact

REPRODUCIBILITY OF RESEARCH
Support open data and methods to enhance research reproducibility

DIGITAL PUBLISHING
Articles designed for optimal readership across devices

FOLLOW US
@frontiersin

IMPACT METRICS
Advanced article metrics track visibility across digital media

EXTENSIVE PROMOTION
Marketing and promotion of impactful research

LOOP RESEARCH NETWORK
Our network increases your article's readership